Terrestrial planet formation in exoplanetary systems

Martyn John Fogg

Thesis submitted for the degree of
Doctor of Philosophy (PhD)
of the University of London

Queen Mary, University of London

2008

Declaration

The results presented in this thesis were produced by myself under the supervision of, and in collaboration with, Prof. Richard P. Nelson. The computer programs used here were either written by myself, or developed on top of the *Mercury* N-body code, originally created by John Chambers. Much of the material presented in Chapters 1–5 has appeared in the peer-reviewed literature as the following papers:

- Fogg, M.J. & Nelson, R.P., "Can Terrestrial Planets Form in Hot-Jupiter Systems?" in Extreme Solar Systems, eds. D. Fischer et al., *ASP Conf. Ser.*, **398**, 525-528 (2008).
- Fogg, M.J. & Nelson, R.P., "The Effect of Type I Migration on the Formation of Terrestrial Planets in Hot-Jupiter Systems," *Astron. Astrophys.*, **472**, 1003-1015 (2007).
- Fogg, M.J. & Nelson, R.P., "On the Formation of Terrestrial Planets in Hot-Jupiter Systems," *Astron. Astrophys.*, **461**, 1195-1208 (2007).
- Fogg, M.J. & Nelson, R.P., "On the Possibility of Terrestrial Planet Formation in Hot-Jupiter Systems," *Intnl. J. Astrobiol.*, **5(3)**, 199-209 (2006).
- Fogg, M.J. & Nelson, R.P., "Oligarchic and Giant Impact Growth of Terrestrial Planets in the Presence of Gas Giant Planet Migration," *Astron. Astrophys.*, **441**, 791-806 (2005).

I declare that the work presented in this thesis is my own.

Martyn John Fogg.

Abstract

Many giant exoplanets are thought to have formed in the outer regions of a protoplanetary disk, and to have then migrated close to the central star. Hence, it is uncertain whether terrestrial planets can grow and be retained in these 'hot-Jupiter' systems. Previous speculations, based on the assumption that migrating giant planets will clear planet-forming material from their swept zone, have concluded that such systems should lack terrestrial planets.

This thesis presents a succession of four planet formation models, of increasing sophistication, aimed at examining how an inner system of solid bodies, undergoing terrestrial planet formation, evolves under the influence of a giant planet undergoing inward type II migration. Protoplanetary growth is handled by an N+N'-body code, capable of simulating the accretion of a two-phase protoplanet–planetesimal population, and tracking their volatiles content. Gas dynamics and related dissipative processes are calculated with a linked viscous gas disk algorithm capable of simulating: gas accretion onto the central star and photoevaporation; type II migration of the giant planet; type I migration of protoplanets; and the effect of gas drag on planetesimals.

In all simulations, a large fraction of the inner system material survives the passage of the giant, either by accreting into massive planets shepherded inward of the giant (reminiscent of the short-period 'hot-Earths' discovered recently), or by being scattered into external orbits. Typically, sufficient mass is scattered outward to provide for the eventual accretion of a set of terrestrial planets in external orbits.

The results of this thesis lead to the prediction that hot-Jupiter systems are likely to harbor water-rich terrestrial planets in their habitable zones and hot-Earths may also be present. These planets may be detected by future planet search missions.

Acknowledgements

I thank Richard Nelson for his intellectual and moral support; for the fruits of his knowledge and wisdom; and for his respect and forbearance. He allowed me a long leash, with enough rope to climb a mountain or descend into a deep hole. His trust in me to use this freedom to climb, and to climb hard, made it a point of honour not to fail.

I thank John Papaloizou for taking a chance on somebody with my unusual academic background and supporting my entry into the PhD programme. I left that first interview with an iron determination not to let the side down.

I thank Richard Taylor for his past years of mentoring: for broadening my horizons, stiffening my spine and encouraging my ambition. None of this could have happened without him. I must phone him more often.

I thank my parents, William and Audrey Fogg, for their devoted support and backing through every phase of my life. Their love is the solid ground beneath my feet and the home I shall always have waiting for me.

I would also like to thank Carl Murray, Iwan Williams, Doug McNeil, Paul Cresswell, Gareth Williams, Daniel Jones, Moritz Fragner and other staff and students of the Astronomy Unit for numerous, often brief but stimulating, conversations that have all contributed to pushing me forward. The same appreciation is extended to the managers of the QMUL computer network for prompt advice and technical support.

The quotations from Lucretius's great didactic poem *De Rerum Natura* are from the translation by W.H.D. Rouse, Loeb Classical Library, Harvard University Press, 1924. The delights of the Loeb editions of the classics are always compounded by the challenge of having the original Greek or Latin on every facing page.

For the term of my studies I was supported by a PPARC/STFC studentship.

Contents

List of Figures

List of Tables

Chapter 1

Introduction

> Now since there is illimitable space empty in every direction, and since seeds innumerable in number in the unfathomable universe are flying about in many ways driven in everlasting movement, it cannot by any means be thought likely that this is the only round earth and sky that has been made...
>
> Lucretius, *De Rerum Natura*, 2, 1052-1058, c.60 BC.

1.1 Thirteen years of exoplanetary discovery

A long-standing question with deep historical and cultural roots concerns the existence of other worlds, especially worlds akin to our own "round earth and sky" that teem with life. It is an issue which, since the Copernican revolution, has been refined into the question of the existence of planets around other stars (van der Kamp, 1963; Dole, 1964; Sagan, 1980; Dick, 1982, 1996; Grinspoon, 2004; Sullivan and Carney, 2007). Astronomers have long suspected that planetary systems are abundant, and perhaps an inevitable by-product of star formation, but proof of this has been difficult to obtain. The direct imaging of extrasolar planets is at present very challenging due to the great distances involved and the huge contrast in brightness between a star and its attendant planets. Nevertheless, it has become possible to indirectly infer the existence of large extrasolar planets, including such details as their minimum masses and orbital characteristics, by observing the Doppler shift of lines in a stellar spectrum which reveals the reflex motion of the star in response to an orbiting planet. This radial velocity technique was used to discover the first known exoplanetary companion to a main sequence star, 51 Pegasi b, in 1995 (Mayor and Queloz, 1995) and since that time has been used to detect over 250 more exoplanets, including some in multiple systems. Alternative techniques such as photometric transit observations and microlensing have identified further exoplanet candidates and discoveries across the board continue to roll in (Butler *et al.*, 2006). Our ignorance is gradually giving way before a picture that, whilst confirming that planets are commonplace, is showing that planetary systems (as characterized by the masses and orbital arrangements of their most massive members) exhibit a wide and exotic variety that was unexpected and has yet to be fully explained (Marcy *et al.*, 2005; Udry and Santos, 2007). Measurements that pose more questions than they answer are one of the drivers of scientific progress, so these past thirteen years of discovery have not just been a triumphant affirmation of the astronomer's art, but also a great opportunity for astrophysicists to advance the understanding of the origin of planetary systems (Bodenheimer and Lin, 2002).

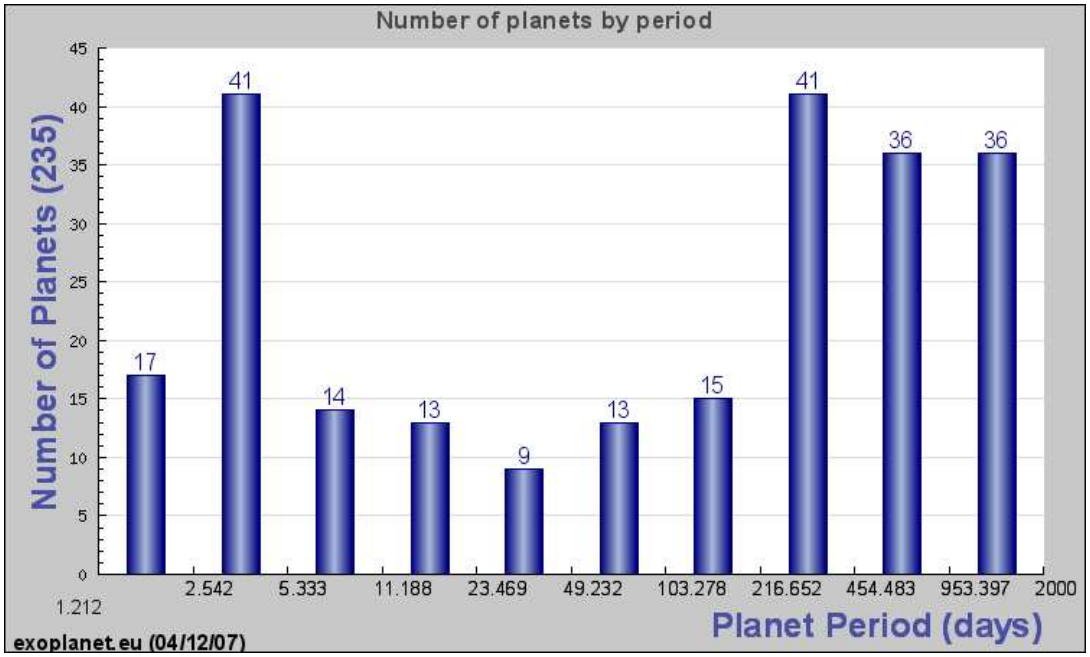

Figure 1.1: Exoplanet frequency versus orbital period up to 2000 days, showing a short period 'pile-up' of hot-Jupiters. Data plotted using the correlation diagrams tool at the Extrasolar Planets Encyclopedia: http://exoplanet.eu.

The exoplanets discovered so far are mostly giant planets of roughly a Saturn-mass or greater, orbiting well within the position of Jupiter in our solar system, with semi-major axes distributed throughout the full range of distances from ~ 5 AU right down to just a few stellar radii (see Figs. 1.1 & 1.2). Although the radial velocity technique, and the limited duration of observational baselines, has an inherent bias towards the detection of high-mass, short-period, planets it was nevertheless a major surprise to find so many giant planets located much closer to their stellar primaries than they are thought to form. The present estimate is that $\sim \ 7\%$ of F/G/K class stars host at least one giant planet within ~ 5 AU, but since their number distribution increases with period, it is strongly suspected that a substantial additional population of giant exoplanets may exist between $\sim \ 3 - 20$ AU that awaits discovery in the future (Udry and Santos, 2007), and it is possible to argue that giant planets are not uncommon, at least around Sun-like stars (Lineweaver and Grether, 2003). Giant exoplanets are observed to be more abundant around stars that are more metal-rich than the Sun, which may be a clue as to their mechanism of formation (Santos *et al.*, 2003; Fischer and Valenti, 2005).

Other surprises have been found in the details of exoplanetary orbits. Many exoplanets with orbital periods greater than 6 days have high orbital eccentricities with a median value for the population of $e \approx 0.3$, much higher than exhibited by the plan-

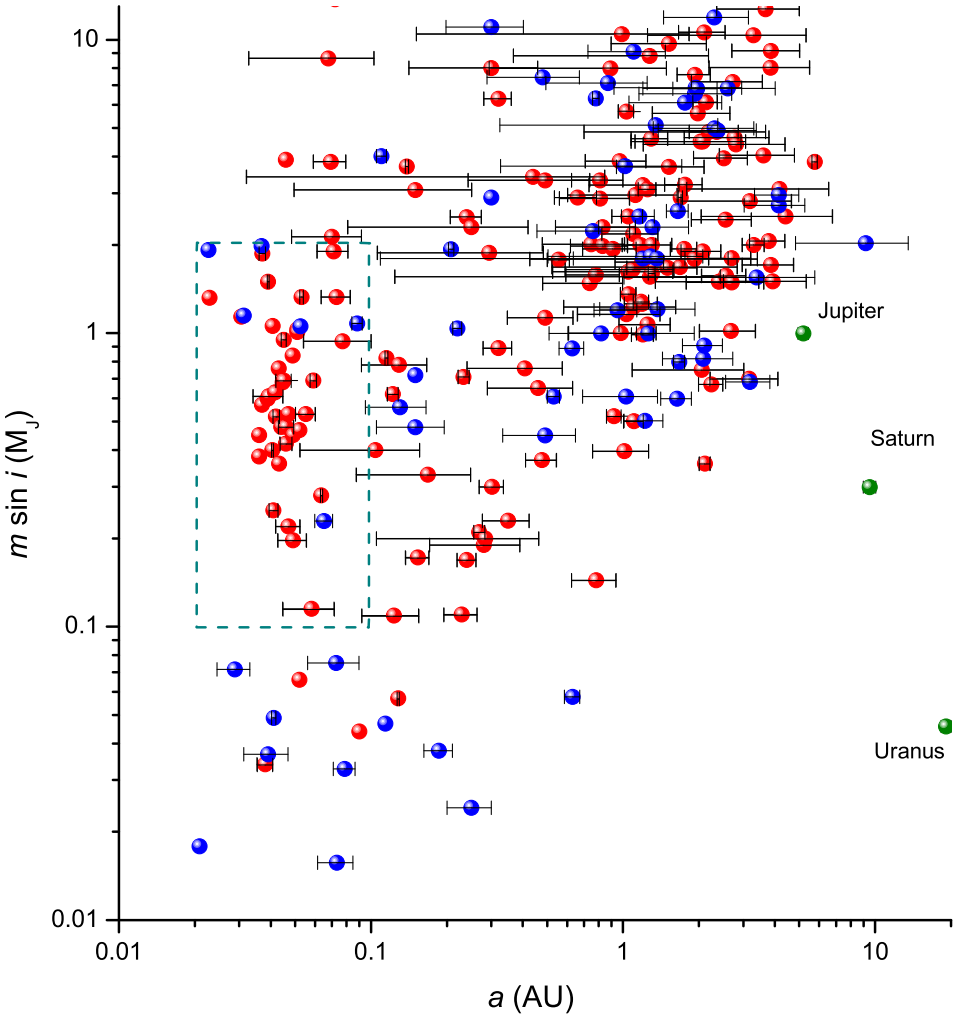

Figure 1.2: Extrasolar planet data plotted as projected mass versus semi-major axis; radial excursions due to orbital eccentricities are plotted as horizontal bars; super- or sub-solar metallicities are indicated by red and blue symbols respectively. Hot-Jupiters around single stars are outlined in the cyan box and are a population with a lower average mass and eccentricity and a higher average metallicity than the overall giant planet sample.

ets of the solar system. Multiple planet systems have been found with some of their orbits locked in mean motion resonances, and perhaps most strangely of all, there exists a peak in the number distribution of exoplanets at a period of ~ 3 days that has identified a distinct population of giant planets, the so-called 'hot-Jupiters' that appear to have accumulated close to the central star (see Fig. 1.1). Typical hot-Jupiters orbiting single stars, of which 51 Pegasi b is an example, have masses $\lesssim\ 2\ \mathrm{M_J}$[1], semi-major axes $a < 0.1$ AU, and low eccentricities consistent with tidal circularization of their orbits. Systems containing hot-Jupiters occur around $\sim\ 1\%$ of F/G/K class stars and represent the most extreme observed rearrangement of planetary mass when compared with the solar system (see Fig. 1.2). It is the question of the existence of terrestrial planets in such 'extreme solar systems' that is the primary focus of this thesis.

1.2 The origin of hot-Jupiters

The mechanism by which giant planets form is not well understood and at present there are two distinct hypotheses competing to explain the process. The *core nucleated accretion* hypothesis is an extension of the classical accretion theory of the formation of the terrestrial planets (Safronov, 1969) and proposes that a giant planet's core grows first from the accretion of much smaller solid bodies in a protoplanetary disk and acquires its gaseous envelope later, once the core has grown sufficiently massive ($\gtrsim\ 10\ \mathrm{M_\oplus}$) to accumulate large quantities of nebular gas (e.g. Pollack *et al.*, 1996; Ida and Lin, 2004a; Hubickyj *et al.*, 2005; Papaloizou and Nelson, 2005; Lissauer and Stevenson, 2007). The core accretion model suffers the greatest difficulties over its timing, as the whole process must be completed before the loss of the nebular gas which is observed to occur just a few Myr after star formation (Haisch *et al.*, 2001; Greaves, 2005). To achieve a sufficiently early growth of a massive core, a high abundance of solid building blocks may be needed in the formation region, enhanced by a factor of ~ 3 – 10 over that of a minimum mass solar nebula model (Lissauer, 1987; Thommes *et al.*, 2003; Ida and Lin, 2004a,b). However, although the core formation problem is yet to be fully understood, this requirement does correspond with observations that giant planets are more common around metal-rich stars (Fischer and Valenti, 2005) which presumably possessed protoplanetary disks in which there was a high content of condensed material. In contrast, the *disk instability* hypothesis

[1] All hot-Jupiters around single stars have masses less than this and are the subject of this thesis. The small number of heavier hot-Jupiters observed in binary star systems may have a different origin that is not considered further here (Wu *et al.*, 2007).

proposes a direct formation of giant planets via the gravitational collapse of gaseous fragments of a massive protoplanetary disk, which could occur very rapidly, in thousands rather than millions of years (e.g. Boss, 2000; Mayer *et al.*, 2002; Durisen *et al.*, 2007). Disk instability however suffers doubts over the capability of self-gravitating disk fragments to last long enough to collapse to planetary dimensions in the face of disruptive processes such as shear and tidal stresses, and accounting for heavy element enrichment in giant planets, the presence of their cores, and intermediate objects such as Uranus and Neptune. It is possible that both mechanisms are valid but operate under different physical circumstances (Matsuo *et al.*, 2007), or that giant planets may form by some hybrid process (e.g. Durisen *et al.*, 2005). Currently however, the majority of astrophysical opinion favors the direction of the core nucleated accretion model.

The core accretion and disk instability hypotheses are polar opposites in the sense that their growth mechanisms can be loosely described as 'bottom-up' and 'top-down' respectively, but both mechanisms agree that giant planets are expected to originate in the cooler, outer, regions of a protoplanetary disk. Cores massive enough to accumulate large quantities of gas require accretion to occur within a wide feeding zone from abundant solid material and optimum conditions for this are thought to exist beyond the nebular 'snowline' (~ 2 – 5 AU for a $1\ \mathrm{M}_{\odot}$ star) where the condensation of ices boosts the quantity of solid material. The generation of self-gravitating clumps of gas with the potential to contract into giant planets requires a cold and massive disk with rapid cooling and low shear stresses: a pre-requisite that must also occur some considerable distance from the central star. Hot-Jupiters, in contrast, lie deep within the potential wells of their primary stars, where ambient temperatures are ~ 1000 K: conditions completely at odds with those thought necessary for their formation.

How then do we explain the existence of hot-Jupiters? Three hypotheses have been the most prominent.

1.2.1 Core nucleated accretion at their present location

The physical environment close to stars is not a favorable place for massive planets to form in situ. In the innermost regions, temperatures may be too high for solid particles to condense; the high Kepler shear regime restricts the feeding zone of a growing core; and there may not be enough mass available locally to form a giant planet. Nevertheless Bodenheimer *et al.* (2000) have investigated the possibility that giant planets might actually form close to their primaries in the context of the core accretion hypothesis. Their model, previously used to grow giant planets similar

to Jupiter at ~ 5 AU, did succeed in forming a 51 Pegasi b analogue, but only by assuming an extreme abundance of solid material with which to form the core and highly efficient accretion. The authors' conclusion was that, although accretion of close orbiting giant planets *in situ* cannot not be ruled out, formation at a greater distance from the star and inward migration seems to be a more likely explanation for the existence of hot-Jupiters.

1.2.2 Inward scattering of giant planets followed by tidal circularization of their orbits

It is thought that in the early stages of giant planet formation growing cores would have near-circular orbits, maintained by strong collisional damping, tidal interactions with the nebular gas, and dynamical friction due to continuous gravitational interactions with smaller bodies. Giant exoplanets however commonly exhibit a high orbital eccentricity (see Fig. 1.2) and the leading explanation for this is that a system of giant planets, growing in close proximity may become dynamically unstable. Mutual perturbations increase as their masses grow, resulting in orbit crossing, repeated close encounters and an end result where some bodies are ejected from the system, leaving the survivors scattered into eccentric orbits both closer to and further away from the central star. Planets scattered inward, with their periastra very close to the central star would be subject to a tidal interaction with the outer envelope of the star and a tidal dissipation in the planet itself which would be expected to reduce both orbital eccentricity and semi-major axis (Rasio *et al.*, 1996), perhaps explaining the presence of hot-Jupiters.

This hypothesis has been studied in detail by a number of authors who have used N-body codes to simulate the evolution of dynamically unstable systems of giant planets, formed originally within the outer regions of a protoplanetary disk (Rasio and Ford, 1996; Weidenschilling and Marzari, 1996; Ford *et al.*, 2001; Papaloizou and Terquem, 2001; Marzari and Weidenschilling, 2002; Terquem and Papaloizou, 2002; Adams and Laughlin, 2003; Ford *et al.*, 2003; Chatterjee *et al.*, 2008; Juric and Tremaine, 2008). However, whilst these models succeed reasonably well at reproducing the observed eccentricity distribution of exoplanets situated at $\gtrsim 0.1$ AU, the 'star-grazing' orbits required for subsequent production of a hot-Jupiter via tidal evolution tend to be a rare outcome of simulations. Thus, whilst some hot-Jupiters could well be produced by this mechanism (note that not all close orbiting giant planets have $e \approx 0$), the observed frequency of hot-Jupiters appears to be much higher than is predicted by the planet-planet scattering scenario.

1.2.3 Planetary migration

The most popular hypothesis of the origin of hot-Jupiters is that of planetary migration, where giant planets, or their cores, form as conventionally conceived in the outer regions of a protoplanetary disk and then migrate inward to small orbital radii via gravitational interactions with the nebular gas (for a recent review see Papaloizou *et al.*, 2007). Planets orbiting within disks will perturb adjacent material such that slower moving particles exterior to its orbit gain angular momentum and interior, faster moving, particles lose angular momentum. Back reaction torques are exerted on the planet which, if not symmetrical, can cause the planet's orbital radius to drift. Calculations suggest that such migration can occur in three distinct ways.

Type I migration

If the perturbations from a planet are small (for masses $\lesssim\ 30 - 100\ \mathrm{M}_{\oplus}$), density waves are launched into the disk at interior and exterior Lindblad resonances, which exert compensating disk torques on the planet. Since the inner resonances are slightly further from the planet because of pressure support in the disk, the outer disk torques dominate: the planet loses angular momentum and spirals inward, whilst remaining embedded in the gas and moving relative to it (Ward, 1997). Since standard theory suggests that type I migration forces are proportional to both planetary mass and gas surface density (Papaloizou and Larwood, 2000; Tanaka *et al.*, 2002; Tanaka and Ward, 2004), giant planet cores should be strongly influenced by this process and Papaloizou and Terquem (1999) have suggested that hot-Jupiters could have formed via the type I migration of a core down to a small orbital radius, followed by a local accretion of its gaseous envelope. However, the realism of type I migration has long been controversial as theoretically predicted spiral-in times ($\sim\ 10^4 - 10^5$ yr for a $\gtrsim\ \mathrm{M}_{\oplus}$ body) can be so short as to threaten protoplanetary survival and to render an explanation of the solar system's architecture particularly difficult. In general, such migration timescales are less than those thought to be required for a giant planet to acquire its gaseous envelope which suggests that giant planets should not form at all before being swept into the inner system and possibly lost to the central star. Many giant planet formation models therefore ignore type I migration entirely, or include it with a greatly reduced effect (e.g. Alibert *et al.*, 2005; Ida and Lin, 2008). It might be that type I migration does not operate as rapidly as predicted: one proposal being that stochastic torques from density fluctuations in a turbulent disk could superimpose a random walk in semi-major axis over the smooth inward drift predicted by theory (Nelson and Papaloizou, 2004; Nelson, 2005). Type I migration might halt altogether

at a surface density transition brought about at a transition between turbulent and dead zones in a disk (Masset *et al.*, 2006), or could be slowed, halted, or even directed outward, if the disk is radiatively inefficient (Paardekooper and Mellema, 2006, 2008). Alternatively, core survival could be a matter of fortunate timing if it occurs late in the lifetime of the protoplanetary disk when gas densities are lower and accretion and migration timescales become comparable (Thommes and Murray, 2006; Thommes *et al.*, 2007).

Type II migration

When the mass of a planet embedded in a protoplanetary disk becomes sufficiently large ($\gtrsim$ 100 $\mathrm{M}_{\oplus}$), the gravitational torques its exerts on the neighboring gas start to exceed the intrinsic viscous torques of the gas. This repels gas from the vicinity of the giant planet's orbit, opening a gap in the disk, of width roughly a disk scale height, which is controlled by a balance between gravitational and viscous torques. The planet therefore no longer migrates relative to the gas, but instead migrates with it, the migration rate being controlled by the disk viscous evolution timescale (Goldreich and Tremaine, 1980; Lin and Papaloizou, 1986; Ward, 1997; Bryden *et al.*, 1999; Nelson *et al.*, 2000). For expected disk viscosities, migration times of $\sim$ 10^5 yr are predicted, which are longer than those typical of giant planet cores undergoing type I migration, but still an order of magnitude less than a disk lifetime. However, if the mass of the planet exceeds that of the gas with which it gravitationally interacts, migration will be significantly opposed by the planet's inertia, a scenario that is expected late in the disk's lifetime. It has been proposed therefore that hot-Jupiters might originally form as fully fledged giant planets in the outer regions of protoplanetary disks and arrived at their present locations via type II migration (e.g. Lin *et al.*, 1996; Ida and Lin, 2004a). In multiple giant planet systems, hot-Jupiters might also originate via a hybrid type II migration/planet-planet scattering mechanism (Moorhead and Adams, 2005). Possible evidence for this is the fact that hot-Jupiters are less massive on average than the overall exoplanet sample (see Fig. 1.2) and hence would have been less resistant to the disk forces that drive type II migration.

Type III migration

Recent work has identified an additional migration regime that could occur between the transition from type I to type II migration in thin and massive protoplanetary disks (Masset and Papaloizou, 2003; Papaloizou, 2005). This type III migration might effect $\sim$ Saturn-mass planets that have opened a partial gap in the gas, creating a local

mass deficit roughly equal to the mass of the planet. In such circumstances, material flowing past the planet, and making one pass between the interior and exterior disk, would generate an inward co-rotation torque that is larger than the drag of the remaining gas in the co-rotation region that migrates with the planet. This torque is found to be proportional to the rate at which the planet moves through the gas, and if the co-orbital mass deficit and the surrounding disk mass are both larger than the planet mass, can drive a fast migration which can vary the semi-major axis of the planet by a large factor in < 100 orbits. Such 'runaway migration' episodes are predicted to run out of steam close to the central star with planets of lower mass attaining shorter periods. It is possible that some of the lighter hot-Jupiters might be better explained by type III migration, rather than type II, as their masses may have been too small to have opened sufficiently wide and clean gaps in their disks. However, type III migration is less well studied at the present time due to the numerical challenges involved in high resolution simulation of gas flows close to partially embedded planets. The effect of gas accretion onto the planet has yet to be included in models and it is unclear how long runaway migration episodes last for and under what conditions they stall (Papaloizou *et al.*, 2007). There is also the difficulty of explaining how planets which undergo such a rapid orbital decay survive accretion by the central star – a problem that appears to be even more severe than the case of type I migration.

Migration halting mechanisms

If, as is generally believed, most hot-Jupiters can be explained as the result of disk-planet interactions, a mechanism that terminates migration and strands exoplanets at their present orbital radii may be required. Migration-halting mechanisms that might work when the planet ventures close to the central star include tidal recession forces exerted by the star's rotation or roche lobe overflow and mass loss to the star (Trilling *et al.*, 1998), or intrusion by the planet into a central cavity or surface density transition in the disk, decoupling it from the evolution of the gas (Lin *et al.*, 1996; Kuchner and Lecar, 2002; Masset *et al.*, 2006; Papaloizou, 2007). Halting migration further out, beyond the $\lesssim 0.1$ AU hot-Jupiter region, may require that giant planets form late in the lifetime of the gas disk and hence only have time for a partial inward migration before stranding at an intermediate distance when the gas is lost (Trilling *et al.*, 1998). Disks around T Tauri stars are observed to last for ~ 1 – 10 Myr (Haisch *et al.*, 2001) but disperse over a much shorter $\sim 10^5$ year timescale (Simon and Prato, 1995; Wolk and Walter, 1996): a behaviour that may result primarily by accretion of gas onto the central star combined with photoevaporative gas loss driven by the stellar UV output (Clarke *et al.*, 2001; Alexander *et al.*, 2006). Models of this

stranding mechanism (Armitage *et al.*, 2002; Armitage, 2007), which can roughly reproduce the exoplanet semi-major axis statistics, have raised the possibility that fortuitous disk dispersal might also explain the presence of the hot-Jupiter population and imply that earlier formed giant planets could have been consumed by the cental star.

Assumptions pertinent to this thesis

For the purposes of this thesis it is necessary to assume a predominant, but not necessarily exclusive, mechanism to account for the origin of hot-Jupiters. The following three assumptions are therefore made in the remainder of this work, all of which could be regarded as reasonable in the light of current knowledge and understanding.

1. Giant planets form via the core-nucleated accretion mechanism in the outer regions of protoplanetary disks.
2. Hot-Jupiters arrive at their final orbits via type II migration.
3. At distances of ≤ 0.1 AU, giant planets cease migrating due to the presence of an inner disk cavity, and at greater distances, because of fortuitous disk dispersal.

1.3 Are terrestrial planets present in hot-Jupiter systems?

1.3.1 Central issues and questions

Although it is not yet possible to detect terrestrial exoplanets accompanying main sequence stars, the question of whether Earth-like planets can form and endure in hot Jupiter systems is of considerable interest. The issue is of importance for three reasons.

Astronomical. Future space-based observatories, such as the 'Kepler' transit detector (Gillon *et al.*, 2005) and the proposed 'Darwin' infrared interferometer (Kaltenegger and Fridlund, 2005), may provide a definitive answer to this question within the next decade or two. Theory-based predictions therefore will be of use as input to target selection for such future programmes to detect Earth-mass exoplanets and as a test of the validity of our understanding of planet formation.

Astrophysical. The architecture of hot-Jupiter systems is profoundly different to that of the solar system and hence poses a significant challenge to conventional terrestrial planet formation theory where planetary growth is envisaged as occurring in a setting that is undisturbed by large scale giant planet migration.

Astrobiological. Planetary systems containing a hot-Jupiter appear to be relatively abundant. Given that they occur around $\sim 1\%$ of F/G/K class stars, and $\sim 10\%$ of stars are of this type, and the Milky Way contains $\sim 10^{11}$ stars, then there exist $\sim 10^{8}$ such systems in the galaxy. The prevalence of habitable planets within such 'extreme solar systems' is therefore of clear relevance to the question of how common life is in the universe at large.

In the standard theory of planet formation, terrestrial planets are thought to be a natural by-product of star formation (Safronov, 1969) and are expected to grow in a number of stages (for a recent review see Nagasawa *et al.*, 2007).

1. *Grain growth.* The process begins when dust particles entrained within the gas of a young protoplanetary nebula stick together and coagulate into grains which settle gravitationally to the midplane of the system to form a thin and concentrated layer of solid material.

2. *Planetesimal growth.* Grains within this layer accumulate further via gravitational instability (Goldreich and Ward, 1973) or binary collisions (Weidenschilling and Cuzzi, 1993) into a swarm of trillions of kilometer-sized planetesimals.

3. *Runway growth.* The largest bodies, with the strongest gravitational focussing, accrete rapidly and preferentially from the swarm, the dynamics of which are well damped via gas drag and mutual collisions (e.g. Wetherill and Stewart, 1993; Lissauer and Stevenson, 1993). Planetary embryos of roughly lunar mass arise.

4. *Oligarchic growth.* When embryos become massive enough to significantly excite the orbits of surrounding planetesimals, gravitational focussing becomes less effective. Runaway growth then gives way to a lengthier phase of oligarchic growth where similar-sized protoplanets emerge from the swarm, accreting at similar rates, in well spaced orbits which remain near-circular due to dynamical friction from the surrounding sea of planetesimals (Kokubo and Ida, 1998).

5. *Chaotic growth.* When the mass remaining in planetesimals declines to the extent that their their damping effect on protoplanet orbits becomes insufficient

to prevent orbit crossing, oligarchic growth ends. The final planets emerge, positioned in stable non-crossing orbits, after a final phase of chaotic growth involving the clearing of residual debris and the removal of excess protoplanets via mutual accretion in 'giant impacts' (e.g. Agnor *et al.*, 1999), or ejection from the system.

The duration of these growth stages increases progressively by roughly an order of magnitude, as well as lengthening in general with distance from the central star due to longer dynamical times. Estimates of these timescales in the solar system context at $\sim$ 1 AU are illustrated in the left hand column of Fig. 1.3. Runaway growth is underway between $\sim 10^4 - 10^5$ yr after the origin of the protoplanetary disk, advancing to oligarchic growth between $\sim 10^5 - 10^6$ yr (Kokubo and Ida, 2000). Final terrestrial planet assembly via giant impacts is largely complete at an age of $\sim 10^7 - 10^8$ yr, as suggested from the evidence of ^{182}Hf – ^{182}W chronometry (Kleine *et al.*, 2002), and the results of formation models (e.g. Chambers, 2001; O'Brien *et al.*, 2006). Since the nebular gas disperses between $\sim 10^6 - 10^7$ yr (Haisch *et al.*, 2001), the final chaotic growth phase takes place in a predominantly gas-free environment.

Prediction of the presence of terrestrial planets in exoplanetary systems is complicated by the fact that the orbits of the most massive planets, and their previous dynamical evolution, constrain both the formation and long-term survival of smaller bodies and so models that explain the formation of the solar system terrestrial planets may only be of partial relevance. Moreover, the presence of a hot-Jupiter implies that it must have traversed the region where rocky planets are expected to form, including through the system's habitable zone (HZ) where planets with an Earth-like climate are possible (Kasting *et al.*, 1993). This must have happened early on (see the right hand column of Fig. 1.3), whilst the nebular gas was still present and before the completion of terrestrial planet growth. As a minimum, we might sensibly conjecture that such a potentially disruptive event would have significant consequences for the growth and survival of inner system planets. However, it has become customary to assume that interior planetary formation is prevented completely by the passage of the giant planet, and that the entire swept zone is cleared of material, rendering hot-Jupiter systems barren. This assumption is one of those at the heart of two well-known astrobiological hypotheses, the Rare Earth Hypothesis (Ward and Brownlee, 2000) and the Galactic Habitable Zone (Lineweaver, 2001; Lineweaver *et al.*, 2004), that draw on current knowledge and opinion in an attempt to place constraints on the occurrence of life elsewhere in the galaxy. The Rare Earth Hypothesis proposes that, whilst microbial life might originate and thrive in a variety of extraterrestrial settings, complex multicellular life requires such a restricted set of environmental

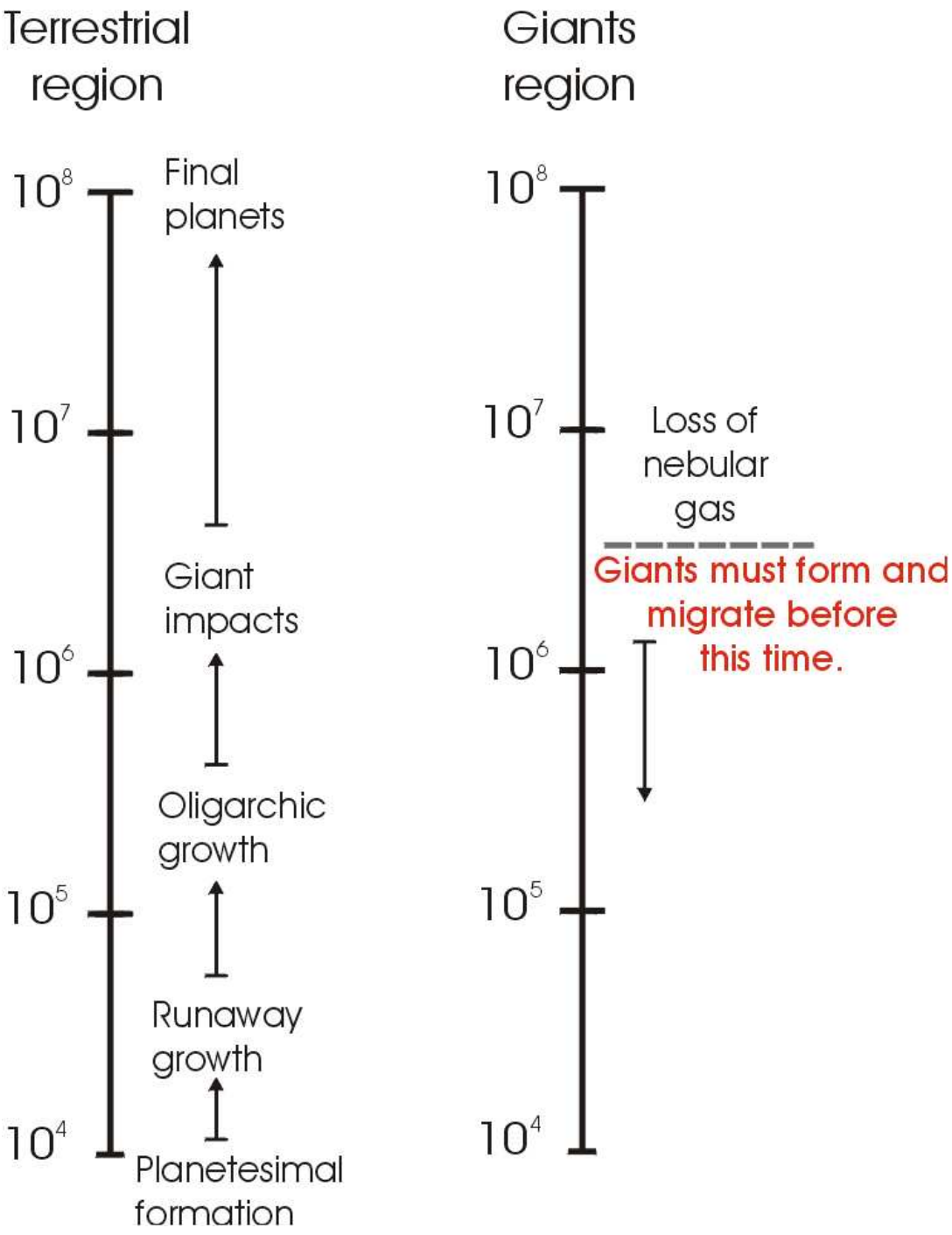

Figure 1.3: Comparison of the relevant simultaneous events in the terrestrial and giant planet formation regions. The vertical axes are timescales, measured in years.

conditions it is likely to be very rare or non-existent elsewhere in the universe. From its point of view, any significant deviation in planetary parameters away from those exemplified by the Earth's ideal reduces or negates prospects for complex life. Similarly, any deviation in planetary system architecture from that exemplified by the solar system will impair the habitability of any Earth-like planets formed there. Star systems containing hot-Jupiters therefore are an obvious target for pruning from the list of potentially habitable locations. The concept of the Galactic Habitable Zone also assumes hot-Jupiter systems to be hostile to biology. This assumption, in concert with the observation that hot-Jupiter host stars are typically more metal-rich than the Sun (Santos *et al.*, 2003; Fischer and Valenti, 2005), is then used to propose that the metal-rich inner regions of the entire galaxy are devoid of Earth-like planets.

How realistic is the conjecture that hot-Jupiter systems inevitably lack terrestrial planets? If the planet-forming material of the interior disk traversed by the giant is removed, how does this happen and where does it go? Is all this matter accreted by the central star or the giant, or does some fraction survive in sufficient quantity for renewed planetary growth after the giant has migrated to its final position? If the solids disk does survive, should we actually expect the presence of terrestrial planets in these systems? Should hot-Jupiter systems be a high or low priority on the target list for future observational programmes to detect Earth-like exoplanets?

Investigation of these unanswered questions is the purpose of this thesis and I conclude this introduction with a brief discussion of the relevance of recent discoveries of low-mass short period planets, followed by a review of previous works that have clarified peripheral issues and an account of the approach taken here to provide a more advanced and detailed understanding of the problem.

1.3.2 Hot-Neptunes and hot-Earths

The increasing sensitivity achieved with the radial velocity technique in the past few years has permitted the detection of some short-period planets with masses as low as $\sim 5 - 20\ \mathrm{M}_{\oplus}$. Whether the bulk composition of these planets, the so called 'hot-Neptunes' or 'hot-Earths', is predominantly rocky or icy is unknown, but is regarded as an important clue to establishing their origin (Irion, 2005). A rocky composition could point to a terrestrial-type accretion from inner system material, whereas an icy composition, such as that proposed for the transiting hot-Neptune GJ 436b (Gillon *et al.*, 2007), might indicate an ice giant-type origin at a remote location and subsequent type I migration to their present location.

Since the focus here is on the effect of large-scale giant planet migration on the

formation of inner system planets, the only exoplanetary systems with observed low-mass planets that are relevant to this discussion are those which also contain giant planets. Four such combination systems are known around the stars Gl 876 (Rivera *et al.*, 2005), 55 Cancri (McArthur *et al.*, 2004), μ Arae (Santos *et al.*, 2004), and Gl 777A (Vogt *et al.*, 2005) (see Fig. 1.4) . In each case, the hot-Neptune or hot-Earth is the innermost object in a non-resonant orbit circumscribed by one or more giant planets at larger distances. This arrangement raises the obvious question of whether hot-Earth formation in such a context is influenced by or perhaps dependent on giant planet migration, or occurs essentially independently. This issue is examined later in this thesis.

Two of the systems, Gl 876 and 55 Cnc, are most relevant to this investigation as their innermost giants orbit close to $\sim$ 0.1 AU, but they are untypical of hot-Jupiter systems in general as additional giant planets are present at greater distances. Conventional terrestrial planet formation will have been preempted due to their habitable zones being occupied by much larger bodies. This is not the case however in most hot-Jupiter systems where the giant planet appears to be the sole large object within ~ 5 AU of the central star.

1.3.3 Precursory studies relevant to this thesis

Dynamical habitability

The question of whether terrestrial planets can form in the habitable zone of a given exoplanetary system only becomes relevant to observational astronomy and astrobiology if planetary orbits there can remain stable over the long term. A number of studies have looked at this issue of dynamical habitability by using numerical integration to calculate the orbital evolution of fictitious terrestrial planets inserted into the habitable zones of exoplanetary systems simulated on a computer (e.g. Jones *et al.*, 2001).

The most useful to our discussion here are those that have addressed the entire set of systems known at the time, including those containing close-orbiting giant planets. There have been two distinct approaches: 1) short-term (1 Myr) integrations looking at the survival statistics in all the known systems of a large number of massless test particles scattered within the HZ (Menou and Tabachnik, 2003); and 2) long-term (1000 Myr) integrations of Earth-mass planets in the habitable zones of a limited, but representative, set of systems and evaluation of the habitability of other systems by extrapolation from this data set (Jones *et al.*, 2005). Although these studies differ in the detail of some of their assumptions - such as the width and age of the HZ, the

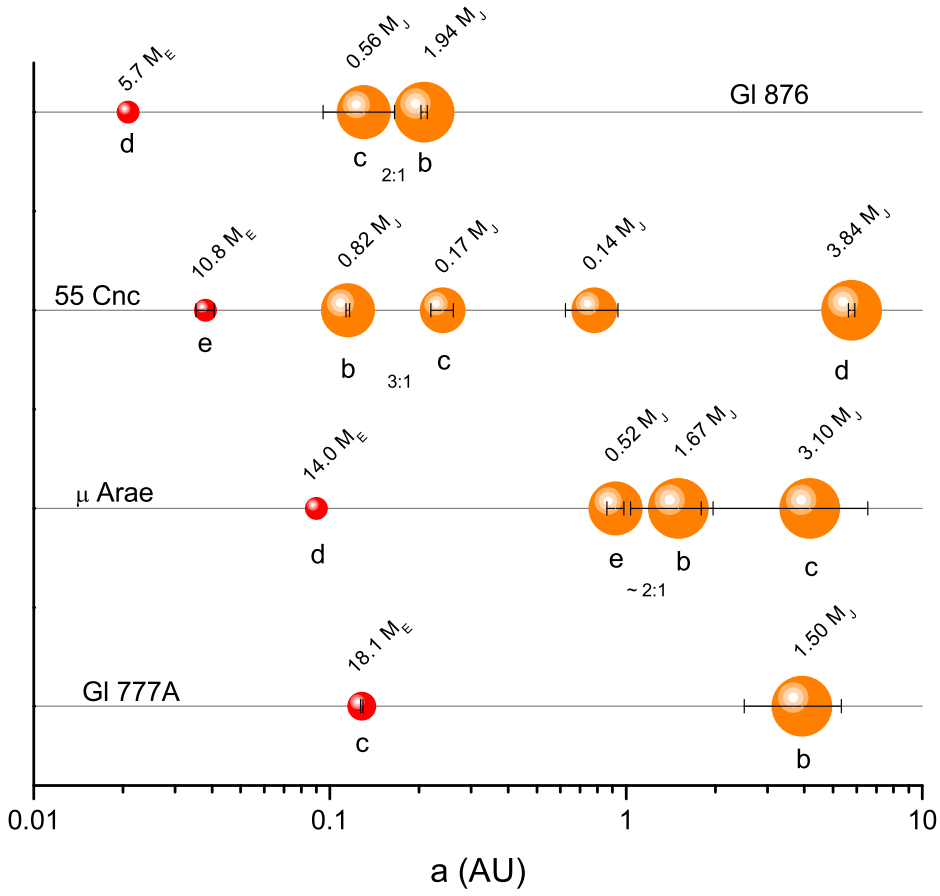

Figure 1.4: The four known exoplanetary systems containing both hot-Neptunes or hot-Earths and giant planets. Projected masses of the giants (coloured orange) are labelled in units of $\mathrm{M_J}$ and lesser objects (coloured red) in units of $\mathrm{M_\oplus}$. Orbital excursions due to eccentricities are indicated by the horizonal bars. Possible mean motion resonances between two planets are indicated by the n:1 label.

simulated mass of the giant, and their criteria as to what constitutes a habitable orbit - their conclusions are comparable. Both approaches conclude that $\sim 50\%$ of exoplanetary systems are unlikely to contain a habitable planet because the dominant giant planet in these systems orbits too close to or even through the HZ. The other $\sim 50\%$ of systems permit some degree of survival. Menou and Tabachnik (2003) estimate that the habitable zones of $\sim 25\%$ of exoplanetary systems are as dynamically stable as the solar system with the other $\sim 25\%$ exhibiting stable orbits in more restricted regions of the HZ. Jones *et al.* (2005), who include a stellar evolution model and an evolving habitable zone in their calculations, conclude that $\sim 49\%$ of exoplanetary systems could have had an Earth-mass planet confined to some or all of the HZ for at least the past 1000 Myr up to the present day.

An important detail to be gained from this work is that the habitable zones of hot-Jupiter systems, and other exoplanetary systems with close-orbiting giants at < 0.4 AU, exhibit good dynamical stability throughout their full width. The proximity of these giant planets to the central star and their low eccentricities precludes significant disturbance of planetary orbits in the $\sim$ 1 AU region. If habitable planets exist in these systems, then their orbits should stay put for billions of years. As Jones *et al.* (2005) have pointed out, this finding emphasizes the need to answer the unsolved question of whether habitable planets can actually form in hot-Jupiter systems, for if we accept the Rare Earth assumption that giant planet migration permanently clears the traversed zone of smaller planets, then their estimated fraction of exoplanetary systems that might host a habitable planet falls from $\sim 49\%$ to $\sim 7\%$. The effect of eliminating hot-Jupiter systems from the habitable planet equation is so drastic because most of the exoplanetary systems we know of which have dynamically stable habitable zones contain a close-orbiting giant planet.

Planet formation in hot-Jupiter systems: preliminary studies

The first paper to pay attention to some of the issues involved in terrestrial planet formation in hot-Jupiter systems was that of Armitage (2003). However, this work did not address any of the questions involving the actual effect of giant planet migration on an interior planet-forming disk. Instead it assumed the disk was destroyed and used a time-dependent model of a protoplanetary disk to calculate the subsequent evolution of both gas and dust in order to ascertain whether the evacuated interior could be replenished with sufficient solid matter from the outer disk to provide for a second generation of planetesimals and renewed planet formation. His conclusions were that, for reasonable disk parameters and lifetimes, replenishment is inefficient such that planetesimal surface densities would be reduced by 1 – 2 orders of magnitude

at 1 AU following giant planet migration. For sufficient time to elapse for good replenishment to occur, Armitage found that the migration episode must occur at a very early stage – within the first $\sim 0.1 - 1.0$ Myr of a disk where the gas component lasts for ~ 8 Myr. Since it appears improbable that gas giant planet core formation, envelope growth, and migration could all be squeezed into the first $\sim 1 - 10\%$ of the gas disk lifetime, he concluded that no substantial terrestrial planets will be found in hot-Jupiter systems in orbits interior to the original formation position of the giant planet.

A completely different approach to the problem was taken by Mandell and Sigurdsson (2003) who consided a late migration scenario and used N-body simulations to model the migration of a Jupiter-mass planet through a fully formed terrestrial planet system. Specifically, they took the example of the present day solar system and considered what would happen if Jupiter migrated inward to 0.1 AU over three different timescales of 0.5, 1.0 and 2.0 Myr. The typical pattern of events observed included: 1) capture of planetary orbits into sweeping resonances with the inward migrating giant, resulting in orbital shrinkage and excitation; 2) close encounters between the planets resulting in collisions or mutual scattering; and 3) slingshot encounters with the giant as it passed through the inner system, leading to ejection, collision with the central star, or scattering into eccentric but bound exterior orbits. Overall $\sim 25\%$ of the planets survived in a wide variety of orbits exterior to the giant, the survival probability being highest for the shortest migration times. Some of these orbits, they speculated, might subsequently become circularized as a result of dynamical friction with outer system planetesimals or interaction with a remnant gas disk (e.g Agnor and Ward, 2002; Kominami and Ida, 2002). Their conclusion therefore was that inward migration of a giant planet does not always remove pre-formed terrestrial planets and that, given an initial arrangement of bodies similar to that of the solar system, between $\sim 1 - 4\%$ of systems in which migration occurred could still possess a planet in the habitable zone.

Formation of terrestrial planets in the presence of a hot-Jupiter has been modelled by Raymond *et al.* (2005b). They did not model the preceding migration of the giant planet and the disk material it passes through was assumed to be lost. Thus, in order to provide the material for terrestrial planet formation, they proposed that the migration episode happens rapidly and early on, giving enough time for an exterior planetesimal disk to regenerate in the manner described by Armitage (2003). Their simulations therefore began with the hot-Jupiter placed in its final close orbit and they proceeded to model the later stages of terrestrial planet accretion from an exterior protoplanet disk using N-body methods. Their conclusion was that the presence of a hot-Jupiter

does little to interfere with terrestrial planet formation outside of an annulus that is within a factor of three in period to the giant (about a factor of two in semi-major axis). Planet formation in the habitable zone, and water delivery to these planets which they also modelled, was not adversely affected, spurring the authors to suggest that stars with hot-Jupiters might actually be good places to search for habitable planets.

The conclusions of these three papers are divergent in that they bracket the widest possible range of outcome, from the occurrence of terrestrial planets in hot-Jupiter systems being highly unlikely, through possible but rare, to commonplace. This confusion originates from the fact that all three models were different, adopted uncertain initial conditions, and were not modeling the same aspect of the problem. The central question of what happens to the original protoplanetary disk traversed by the giant was not addressed and both Armitage (2003) and Raymond *et al.* (2005b) assumed a total loss of planetary building blocks from the swept zone. Whilst Armitage (2003) then determined from this that future terrestrial planet formation is improbable, Raymond *et al.* (2005b) proposed the opposite by adopting an early migration scenario that gave time for a terrestrial planet forming disk to regenerate. The work of Mandell and Sigurdsson (2003) showing that planet-sized bodies can survive a giant planet migration episode suggested that the assumption of total inner disk loss is unrealistic and that some significant surviving remnant should be taken into account. However, the timing implicit in their scenario of a giant migrating through a mature terrestrial planetary system may be problematic, as giant planet migration is constrained to occur within the $\sim 1 - 10$ Myr lifetime of the gas disk whereas the terminal chaotic growth phase of terrestrial planet formation is thought to last ~ 100 Myr (Chambers, 2001). The accretion of an inner planetary system is therefore likely to be incomplete at the time of any migration epoch with its population consisting of a large number of protoplanets and planetesimals, rather than four full-sized planets.

The time at which giant planet migration occurs is therefore of critical importance in the study of this problem as it entangles initially isolated sequences of events inside and beyond the nebula snowline. Irrespective of whether giant planets form via core accretion or disk instability, type II migration through the inner system must occur before the loss of the nebular gas at the latest, at which time the material of the inner disk is expected to be relatively immature and still at a stage of oligarchic, or early chaotic, growth (see Fig. 1.3). Far from it being clear that all this inner disk material is lost, hypotheses or models that assume this may be oversimplifying the problem, affecting any conclusions they make. Modeling giant planet migration *simultaneously* with terrestrial planet accretion is a clear pre-requisite for a realistic appraisal of this problem.

1.4 This thesis

The key questions this thesis aims to answer are whether inner-system terrestrial planets are likely to be commonplace or rare in hot-Jupiter systems, and what the implications of this answer might be for astronomy and astrobiology. These goals are achieved by breaking down the problem into the following objectives.

1. Construction of a model of an inner-system protoplanetary disk and a migrating giant planet that is realistic in the light of current theory, with appropriate initial and boundary conditions, and practical to simulate on modern computers. The full version of this model computes:

   - Gas dynamics: including viscous evolution of the gas; its interaction with an embedded giant planet; gas accretion onto the central star; and photoevaporation.
   - Solid body dynamics of a population divided into four classes, a central star, a number of protoplanets, planetesimals, and a giant planet. Modelled physics includes mutual gravitational forces; dissipative forces, including gas drag, dynamical friction, collisional damping, and type I and II migration torques; and two-body accretion.
   - Chemical evolution of the solid component: including an algorithm that tracks the radial mixing of volatile-rich material from beyond the nebular snowline and the proportion of this incorporated into the final planets.

2. Use of this model to simulate the process of terrestrial planet formation in the presence of giant planet migration: i.e. *simultaneously* with the migration of a hot-Jupiter to its final orbital radius.

3. Study of the details of this process (i.e. what actually happens to the inner disk during the traverse of a giant planet, contrasted with what has been assumed to happen) and analysis of the properties of any residual surviving material.

4. Extended simulation, beyond the end-point of the migration epoch and the loss of the nebular gas, to model subsequent planet formation from residual material in the presence of the hot-Jupiter in its final orbit.

5. Characterization and prediction of the type of inner-system planets that might be found in hot-Jupiter systems, including objects such as hot-Earths and hot-Neptunes orbiting interior to the giant planet and systems of terrestrial planets in external orbits.

6. Discussion of the relevance of the results for future observational programmes to detect terrestrial exoplanets and their implications for astrobiology.

This thesis challenges the previous widespread view that hot-Jupiter systems lack terrestrial, and potentially habitable, planets: far from being devoid of other planetary bodies within their warmer regions, it asserts that they may be worthwhile targets for future investigation. Results of this research programme have been previously published in the following papers: Fogg and Nelson (2005, 2006, 2007a,b, 2008).

Chapter 2

Model foundations: method and initial conditions

2.1 Declaration of approach

The procedure adopted in this thesis to address the question of terrestrial planet formation in hot-Jupiter systems is to model planetary growth in an inner-system protoplanetary disk using N-body methods, augmented with additional computation of the evolution of the nebular gas and its influence on the dynamics of solid bodies. The basic physical picture is of planet formation about a single, solar mass, star, in a similar manner to that envisaged for the solar system, but with the additional complication of large-scale giant planet migration. The scope of the model does not encompass the formation of a giant planet in its initial orbit: instead a $0.5\ \mathrm{M_J}$ giant[1] is assumed to form at 5.0 AU and is allowed to pass through the inner system via type II migration and come to rest in its final orbit. The time at which the giant planet is assumed to form and migrate is varied in order to study its effect on disks of different maturity and to bracket the likely epoch of giant planet formation in nature. In some cases, where extensive disk material has survived the migration episode, the simulations are extended to beyond the time of nebular gas dispersal to model subsequent terrestrial planet accretion and dynamics.

The set of four models presented in this work are the outcome of a process of refinement involving the progressive addition of more complex algorithms to simulate the behaviour of the gaseous fraction of the protoplanetary disk and the disk-planet interactions that drive migration. The sequence of publications resulting from this development (in particular Fogg and Nelson, 2005, 2007a,b, hereafter referred to as Models I, II, & III) is reflected in the later Chapters of this thesis (see Table 2.1). This Chapter details the central processes and methods common to all versions of the model; its initial conditions and setup; and gives examples of the simulated evolution of the inner disk before the appearance of the giant planet.

2.2 Gravitational and gas drag forces

Four classes of object are recognized in the simulations presented here: 1) the central star; 2) a giant planet; 3) protoplanets (i.e. planetary embryos of $\sim$ lunar-mass or above); and 4) planetesimals (i.e. much smaller $\sim$ km-sized bodies). The Newtonian gravitational dynamics of these objects and planetary growth is modelled with the symplectic N-body simulation package *Mercury 6* (Chambers and Migliorini, 1997; Chambers, 1999). Symplectic integration methods, when applied to celestial mechanics, operate by splitting the Hamiltonian of an N-body system into several parts,

[1] A typical mass for a hot-Jupiter (see Fig. 1.2).

Table 2.1: The four gas disk/disk-planet interaction models

Model Number	Chapter	Gas Dynamics and Disk Planet Interactions
I	3	Constant gas density Prescribed type II migration Prescribed hot-Jupiter stranding at 0.1 AU
II	4	Viscously evolving gas disk Self-consistent type II migration Prescribed hot-Jupiter stranding at 0.1 AU
III	5	As Model II but with prescribed type I migration affecting protoplanets
IV	6	As Models II and III but with photoevaporating gas disk and self-consistent 'warm-Jupiter' stranding between 0.1 – 1.7 AU

one representing the unperturbed Keplerian motion of a particular body about a central star, and the others representing perturbations from other bodies. The Keplerian part can be integrated analytically in the absence of the others, provided the perturbation terms remain small. This method confers the major advantage of being an order of magnitude faster to compute than traditional methods of numerical integration, without suffering an accumulation of energy errors (Wisdom and Holman, 1991; Saha and Tremaine, 1992; Yoshida, 1993). However the fixed time-step required by symplectic integrators limits their ability to accurately compute close encounters and collisions. This problem is overcome in the *Mercury* package by running it in 'hybrid-symplectic' mode, which detects close encounters and integrates them numerically, using a smaller adaptive step-size, with the Burlisch-Stoer method (Press *et al.*, 1992). Physical collisions are resolved when the minimum interpolated separation of a pair of encountering bodies is less than their combined radii and is assumed to be inelastic, resulting in a single merged body, conserving mass and linear momentum (Chambers, 1999). Since kinetic energy is not conserved in inelastic collisions, the merger process inherently simulates *collisional damping* where the resulting body tends to an orbit that is tighter and more circular than that of its progenitors. The Mercury 6 package therefore is well suited to studying the problem of planetary growth, combining the speed of symplectic algorithms with the capacity to resolve a simplified accretion process (e.g. Chambers and Wetherill, 1998; Chambers, 2001; Chambers and Wetherill, 2001; Raymond *et al.*, 2005a).

The *Mercury* code has been extensively modified as part of this project to include a dynamically evolving gas disk and the forces arising from disk-planet interactions (covered in later Chapters: see Table 2.1) and the effect of gas drag on planetesi-

mals. Since it is proposed that hot-Jupiter migration occurs when the inner system solid material is in its oligarchic or chaotic growth stages (see Fig. 1.3) the initial ingredients required to model this region are a series of small protoplanets embedded within a swarm of planetesimals. However, due to the huge number of particles involved, the realization of a realistic planetesimal disk, with every body treated as fully interacting, is well beyond the current state of the art.

This problem can be rendered tractable by adopting the so-called $N + N'$-body approach which models all the protoplanets as N individual bodies, but which resolves the planetesimal swarm as a disk of N' 'super-planetesimals' – particles with masses a tenth that of the initial masses of protoplanets which act as statistical tracers of a much larger number of real planetesimals. The central star, the giant planet (when it is introduced) and the protoplanets can accrete and merge inelastically with all the other bodies in the simulation and feel all the modelled gravitational forces; whereas the super-planetesimals are non self-interacting – i.e. they can only accrete onto larger objects and feel gravitational forces from the central star, protoplanets, and giant planet, but no mutual gravitational attraction. This prevents their relatively high masses from unrealistically auto-exciting their eccentricities and inclinations to excessively high values. Super-planetesimals however, although over-massive, are modelled to behave dynamically as real planetesimals of realistic mass and size which are small enough to be subject to gas drag. A drag force is therefore imposed, calculated from their motion relative to the nebular gas which is equivalent in its dynamical action to the gas drag that would be experienced by a single 10 km radius planetesimal. The issue of the mass of super-planetesimals was addressed by Thommes *et al.* (2003) who found in tests of their model of oligarchic growth that protoplanets undergo realistic *dynamical friction* – a cumulative effect of numerous close encounters which tends to circularize the orbit of a large body at the expense of exciting the orbits of small bodies – if super-planetesimal masses are $\lesssim 0.1$ times the initial protoplanet masses.

Gravitational dynamics

The total number of particles in each simulation is $N + N'$: the giant and protoplanets are labelled from 1 to N, followed by the super-planetesimals labelled from $N + 1$ to $N + N'$. With the coordinate origin is based on the central star, the acceleration experienced by each of the super-planetesimals, where $i = N + 1$ to $N + N'$ is given

by:

$$\begin{aligned}\frac{d^2\boldsymbol{r}_i}{dt^2} = &- \frac{GM_*\boldsymbol{r}_i}{|\boldsymbol{r}_i|^3} - \sum_{j=1}^{N}\frac{Gm_j\boldsymbol{r}_{ij}}{|\boldsymbol{r}_{ij}|^3} - \sum_{j=1}^{N}\frac{Gm_j\boldsymbol{r}_j}{|\boldsymbol{r}_j|^3} \\ &- \sum_{k=N+1}^{N+N'}\frac{Gm_k\boldsymbol{r}_k}{|\boldsymbol{r}_k|^3} + \boldsymbol{a}_{\rm drag},\end{aligned} \tag{2.1}$$

where M_* is the stellar mass, m and $\boldsymbol{r}$ are particle masses and position vectors and $\boldsymbol{r}_{ij} = \boldsymbol{r}_i - \boldsymbol{r}_j$. The first term on the right hand side represents the acceleration from the central star, the second term the accelerations from the protoplanet and giant planet, the third and fourth terms are the indirect terms arising from the acceleration of the coordinate system, and $\boldsymbol{a}_{\rm drag}$ is the acceleration due to gas drag.

The acceleration experienced by the protoplanets and gas giant planet, where $i = 1$ to N, is given by:

$$\begin{aligned}\frac{d^2\boldsymbol{r}_i}{dt^2} = &- \frac{GM_*\boldsymbol{r}_i}{|\boldsymbol{r}_i|^3} - \sum_{j=1}^{N}\frac{Gm_j\boldsymbol{r}_{ij}}{|\boldsymbol{r}_{ij}|^3}(1-\delta_{ij}) - \sum_{k=N+1}^{N+N'}\frac{Gm_k\boldsymbol{r}_{ik}}{|\boldsymbol{r}_{ik}|^3} \\ &- \sum_{j=1}^{N}\frac{Gm_j\boldsymbol{r}_j}{|\boldsymbol{r}_j|^3} - \sum_{k=N+1}^{N+N'}\frac{Gm_k\boldsymbol{r}_k}{|\boldsymbol{r}_k|^3} + \boldsymbol{a}_{\rm TypeII} + \boldsymbol{a}_{\rm TypeI}.\end{aligned} \tag{2.2}$$

The first term again represents the acceleration due to the central star, the second and third terms respectively represent the accelerations due to the protoplanets/giant planet and super-planetesimals and δ_{ij} is the Kronecker delta function. The fourth and fifth terms are indirect terms, and $\boldsymbol{a}_{\rm TypeII}$ is the acceleration driving type II migration of the gas giant planet (when present, see Chapters 3 & 4), and $\boldsymbol{a}_{\rm TypeI}$ is the acceleration driving type I migration, which when it is assumed to operate, affects protoplanets only (see Chapter 5).

Gas drag

Planetesimals are small enough to experience a drag force from moving through the nebula gas (Adachi *et al.*, 1976; Rafikov, 2004). This acceleration, which acts both to cause an inward radial drift and a damping of eccentricities and inclinations, takes the form:

$$\boldsymbol{a}_{\rm drag} = -\frac{1}{2m_{\rm pl}}C_{\rm D}\pi r_{\rm pl}^2\rho_{\rm g}|\boldsymbol{u}|\boldsymbol{u}\ , \tag{2.3}$$

where $m_{\rm pl}$ and $r_{\rm pl}$ are the physical mass and radius of a single planetesimal respectively, $C_{\rm D}$ is the drag coefficient (taken here to be $C_{\rm D} = 1$), $\rho_{\rm g}$ is the volume density

of the gas, and $\boldsymbol{u} = \boldsymbol{v}_{\rm p} - \boldsymbol{v}_{\rm g}$ is the velocity of the planetesimal with respect to the gas. The gas is assumed to move in a circular orbit which, due to pressure support, revolves at slightly less than Keplerian speed. The relation is:

$$\boldsymbol{v}_{\rm g} = (1 - 2\eta)^{\frac{1}{2}}\, \boldsymbol{v}_{\rm K} \,, \tag{2.4}$$

where $\boldsymbol{v}_{\rm K}$ is the local Keplerian velocity and $\eta = 0.0019(r/1{\rm AU})^{1/2}$, where r is the radial distance from the central star and given the nebula scale height h introduced later in Eq. 2.10 (Adachi *et al.*, 1976).

2.3 The inner protoplanetary disk

All the models presented here assume the presence of a $M_* = 1\ {\rm M}_\odot$ central star and consider the solid contents of the inner protoplanetary disk between initial boundaries of 0.4 - 4.0 AU. The initial structure of this protoplanetary disk annulus is assumed to be compatible with the so-called 'Minimum Mass Solar Nebula Model' (MMSN) (Hayashi, 1981; Hayashi *et al.*, 1985) which is commonly used as an initial condition in planet formation studies. This model, which originates from early studies of the formation of the solar system, reconstructs the initial solar nebula by augmenting the masses of the planets with sufficient gas to restore them to solar composition, and then smooths out this mass into a distribution to which a power law can be fitted (Weidenschilling, 1977). Hayashi (1981) derived the following expressions to describe his transparent, equilibrium, disk model of a MMSN.

The radial temperature profile of the nebula is:

$$T_{\rm neb} = 280 \left(\frac{r}{1\ {\rm AU}} \right)^{-\frac{1}{2}}\ {\rm K} \,, \tag{2.5}$$

where r is the radial distance from the central star.

The initial surface density of solids is:

$$\Sigma_{\rm s}(r) = f_{\rm neb} f_{\rm ice} \Sigma_1 \left(\frac{r}{1{\rm AU}} \right)^{-1.5} \,, \tag{2.6}$$

where $f_{\rm neb}$ is a nebular mass scaling factor, $\Sigma_1 = 7$ g cm^{-2}, and the ice condensation coefficient $f_{\rm ice} = 1$ for $a < 2.7$ AU and $f_{\rm ice} = 4.2$ for $a \geq 2.7$ AU, the distance chosen for the nebula 'snowline', beyond which $T_{\rm neb} < 170$ K and the solids mass fraction of the disk is enhanced due to the condensation of ices. All cases presented here adopt $f_{\rm neb} = 3$ and hence are assuming a nebula that is more massive than the

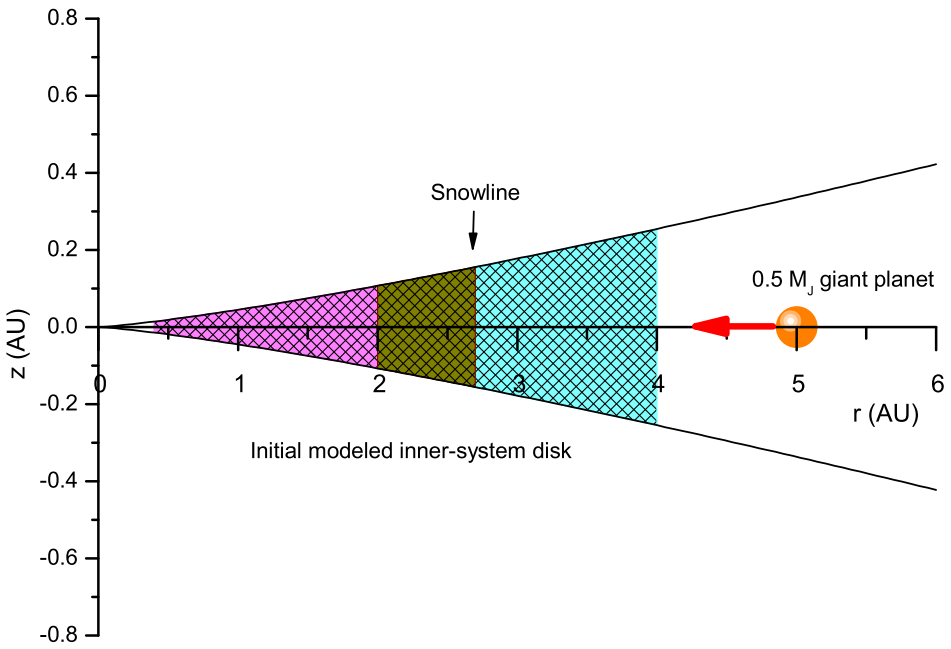

Figure 2.1: Cross section of the initial MMSN inner disk annulus, which takes the shape of a flared exocone, and is modelled here between 0.4 - 4.0 AU. The snowline is at 2.7 AU, beyond which ice condensation enhances the mass of solid material by the factor $f_{ice} = 4.2$. Thus, solid condensates in the inner region are composed of dry or hydrated 'rock' (coloured magenta and brown respectively); whereas those in the outer region (coloured cyan) are composed of a solar-composition mixture of 'rock' plus 'ice'. The insertion point of the giant planet at a future epoch is also shown.

bare minimum thought to be required to form the solar system. However, in the context of the core-accretion model of giant planet formation, a significant additional mass of solids seems to be required in order to form a core quickly enough to initiate gas accretion before the loss of the gaseous component of the nebula (Lissauer, 1987; Pollack *et al.*, 1996; Thommes *et al.*, 2003). Moreover, since hot-Jupiters are usually found around stars more metal-rich than the Sun, a greater solids content might reasonably be expected within their protoplanetary nebulae.

The initial surface density of gas is:

$$\Sigma_{\rm g}(r) = f_{\rm neb} f_{\rm gas} \Sigma_1 \left(\frac{r}{1{\rm AU}} \right)^{-1.5} , \tag{2.7}$$

where $f_{\rm gas}$ is the gas to dust ratio which is taken to be $f_{\rm gas} = 240$.

The initial volume density of gas is:

$$\rho_{\rm g}(r) = f_{\rm neb}\rho_1 \left(\frac{r}{1{\rm AU}}\right)^{-\frac{11}{4}} \exp\left[-z^2/h^2\right] \ , \tag{2.8}$$

where $\rho_1 = 2.0 \times 10^{-9}(f_{\rm gas}/240)(\Sigma_1/10)$ g cm^{-3}, $f_{\rm gas}$ is the gas to dust ratio, z is the height from the midplane of the nebula and h is the disk scale height given by Eq. 2.10.

The sound speed of a solar composition gas in cgs units is:

$$c_{\rm s} = \left(\frac{kT_{\rm neb}}{\mu m_{\rm H}}\right)^{\frac{1}{2}} = 9.9 \times 10^4 \left(\frac{T_{\rm neb}}{280 \ {\rm K}}\right)^{\frac{1}{2}} \left(\frac{2.34}{\mu}\right)^{\frac{1}{2}} \ , \tag{2.9}$$

where k is the Boltzmann constant, $m_{\rm H}$ is the mass of a hydrogen atom, and μ is the mean molecular weight of the gas. Usually, it is assumed that $\mu = 2.34$, the mean molecular weight of a gas composed mostly of H_2 and He, and this practice is followed here, cancelling the final term in Eq. 2.9.

The gas scale height $h = \sqrt{2}c_{\rm s}/\Omega$, where Ω is the local nebular angular velocity, which gives:

$$h = \left(\frac{2kT_{\rm neb}}{\mu m_{\rm H}}\frac{r^3}{{\rm G}M_*}\right)^{\frac{1}{2}} = 0.047 \left(\frac{r}{1 \ {\rm AU}}\right)^{\frac{5}{4}} {\rm AU} \ . \tag{2.10}$$

This combination of equations and parameters combines to give the physical picture of the initial inner disk annulus illustrated in Fig. 2.1 which shows a sagittal cross section of the disk, with the modelled region interior and exterior to the snowline coloured in magenta or brown and cyan respectively. Since the mass of the solid content of the region is defined by:

$$M_{\rm solid} = \int_{0.4 \ AU}^{4.0 \ AU} 2\pi r \Sigma_{\rm s}(r) {\rm d}r, \tag{2.11}$$

the total mass of protoplanets and planetesimals initially contained within the region is $M_{\rm solid} = 24.8 \ {\rm M}_\oplus$.

Given the above model of the inner protoplanetary disk, the action of gas drag imposes the following timescales on planetesimal dynamics. The timescale of inward radial drift is approximately:

$$t_{\rm r} \approx \frac{v_{\rm K}}{a_{\rm drag}} = \frac{8 r_{\rm pl}\rho_{\rm pl}}{3C_{\rm D}\eta^2 v_{\rm K}\rho_{\rm g}} \tag{2.12}$$

$$\approx 10^7 \left(f_{\rm neb} C_{\rm D}\right)^{-1} \left(\frac{r_{\rm pl}}{10 \text{ km}}\right) \left(\frac{\rho_{\rm pl}}{2 \text{ g cm}^3}\right) \left(\frac{M_*}{\text{M}_\odot}\right)^{-\frac{1}{2}} \left(\frac{r}{\text{AU}}\right)^{\frac{9}{4}} \text{ years},$$

where $\rho_{\rm pl}$ is the planetesimal density and assuming circular orbits with an orbital eccentricity of $e = 0 \Rightarrow u \approx \eta v_{\rm K}$.

The timescale for the damping of planetesimal orbital eccentricity e is approximately:

$$t_{\rm e} \approx \frac{u}{a_{\rm drag}} = \frac{8 r_{\rm pl} \rho_{\rm pl}}{3 C_{\rm D} e v_{\rm K} \rho_{\rm g}}, \tag{2.13}$$

$$\approx 10^3 \left(f_{\rm neb} C_{\rm D}\right)^{-1} \left(\frac{r_{\rm pl}}{10 \text{ km}}\right) \left(\frac{\rho_{\rm pl}}{2 \text{ g cm}^3}\right) \left(\frac{M_*}{\text{M}_\odot}\right)^{-\frac{1}{2}} \left(\frac{r}{\text{AU}}\right)^{3} \text{ years},$$

where it is assumed that $u \approx e v_{\rm K}$ and $e \approx h/r$.

The expected gas drag timescales in the disk's outer regions (where the bulk of the mass lies) are therefore $t_{\rm r} \gtrsim 10^7$ years and $t_{\rm e} \gtrsim 10^3$ years. Hence, since the gas is expected to decline in density from its initial condition and to be gone in $\sim 10^6$ years (see Fig. 1.3), gas drag is expected to cause a relatively minor orbital decay of $r_{\rm pl} = 10$ km planetesimals, but will have a much more significant influence on damping their eccentricities.

2.4 Generation of initial $N + N'$-body components

It is not possible now, or in the foreseeable future to use N-body methods to simulate accretion all the way from the initial grain growth stage to that of a final planetary system. The practical employment of N-body methods requires that the number of bodies involved in a computation is not so large that it involves excessive CPU-time. Hence, N-body simulations are used to simulate the middle or late stages of planetary formation in restricted regions, requiring assumptions to be made concerning boundary conditions and the previous evolution of the protoplanetary disk. *Thus, the earliest stages of planetesimal formation and runaway growth are not considered here and the $t = 0$ start date for the simulations is set at 0.5 Myr after the start of star formation*. By this time, it is assumed that there is no more in-fall of gas onto the protoplanetary disk and the solids component of the inner disk has reached its oligarchic growth stage (Kokubo and Ida, 1998). Simulations of planetesimal accretion by Kokubo and Ida (2000) have shown that it takes only ~ 0.5 Myr to generate $\sim 0.01 - 0.03$ $\text{M}_\oplus$ planetary embryos from a planetesimal disk at ~ 1 AU: producing a configuration where a succession of protoplanets, each being a few percent of

an Earth-mass, emerge from the planetesimal swarm in near-circular orbits and with roughly equidistant spacing in units of mutual Hill radii.

According the to oligarchic growth picture therefore, the distance between protoplanets can be expressed as:

$$\Delta r \approx b\, r_{\mathrm{H1,2}}, \tag{2.14}$$

where b is the spacing factor, and $r_{\mathrm{H1,2}}$ is the mutual Hill radius: the radial distance from each of a pair of nearby planets where their gravity dominates over that of the central star.

For equal mass planets, the mutual Hill radius is defined as:

$$r_{\mathrm{H1,2}} = \left(\frac{2m_p}{3M_*}\right)^{\frac{1}{3}} \frac{a_1 + a_2}{2} = \tilde{h}\frac{a_1 + a_2}{2}, \tag{2.15}$$

where m_p is the planetary mass, a_1 and a_2 are the semi-major axes of the two planets, and $\tilde{h} = (2m_p/3M_*)^{1/3}$ is the reduced mutual Hill radius.

Kokubo and Ida (2000) found that during oligarchic growth, the protoplanet spacing factor was typically $b \approx 5-10$. Assuming equal mass protoplanets, and some average value of b, the semi-major axes of a series of protoplanets would therefore be roughly distributed as:

$$a_i \approx a_1 \left(\frac{2 + b\tilde{h}}{2 - b\tilde{h}}\right)^{i-1}, \tag{2.16}$$

where a_1 is the semi-major axis of the of the innermost protoplanet and a_i is that of the i^{th} protoplanet in the series.

If the outermost semi-major axis a_N of an oligarchic series of N protoplanets is known, then Eq. 2.16 can be solved to give:

$$N \approx \frac{\log(a_N/a_1)}{\log\left(\frac{2+b\tilde{h}}{2-b\tilde{h}}\right)} + 1, \tag{2.17}$$

where N should be rounded to the nearest integer.

In order to generate the solid body initial input for the simulations presented here, it is necessary to discretize the continuous mass distribution given in Eq. 2.6 into

a number of objects with the mass total given by Eq. 2.11. There are a number of ways this has been done in past studies, including breaking up the solids disk into: a) equal masses (e.g. Beauge and Aarseth, 1990; Alexander and Agnor, 1998; Chambers, 2001; Chambers and Wetherill, 2001); b) a bimodal distribution of large and small equal mass bodies (e.g. Chambers, 2001; Thommes *et al.*, 2003; O'Brien *et al.*, 2006); c) 'isolation masses', generated by assuming that protoplanets consume all material in their feeding zones, typically producing an increasing mass of objects with distance from the central star (e.g. Chambers and Wetherill, 1998; Raymond *et al.*, 2005a); and d) importing a solid body mass spectrum from statistical simulations or semi-analytic models of earlier disk evolution (Agnor *et al.*, 1999; McNeil *et al.*, 2005). In practice, since such models integrate planetary accretion and chaotic dynamics over millions of years of simulated time, the characteristics of any initial setup are rapidly lost. Comparison of the results of the above-cited papers, which all succeed in producing reasonable analogues of the inner solar system, suggests that the method chosen to generate the initial solid body population has only a minor influence over the properties of the final planetary system.

Since the models presented here conform with an initial oligarchic growth picture, requiring the modeling of both protoplanets and planetesimals, and the modelled disk passes through the nebular snowline, a separate bimodal initial mass distribution is chosen for both parts of the disk. Initial protoplanet masses of $m_{\rm proto} = 0.025\ {\rm M}_\oplus$ and $m_{\rm proto} = 0.1\ {\rm M}_\oplus$ are therefore chosen to represent bodies interior and exterior to the snowline respectively. For both disk partitions, the number N of protoplanets was calculated from Eq. 2.17, assuming a spacing factor of $b = 8$. Semi-major axes for this number of protoplanets are then generated randomly with probabilities weighted in order to reproduce the $\Sigma_{\rm s} \propto r^{-1.5}$ disk surface density profile given in Eq. 2.6. Eccentricities and inclinations are randomized from a Rayleigh distribution with RMS values of 0.01 and 0.005 respectively. Additional orbital elements required are randomized uniformly from within their range. The total mass of protoplanets is then subtracted from the total mass of the disk partition and the mass that remains is divided into N' super-planetesimals with a mass ($m_{\rm s-pl}$) one tenth that of the protoplanets in their zone. The orbital elements of the super-planetesimals are then generated in the same manner. Note that the super-planetesimal mass $m_{\rm s-pl}$ is distinct from the physical planetesimal mass $m_{\rm pl}$ which is used solely for the purpose of calculating gas drag (see Eq. 2.3). Protoplanetary radii are calculated by assuming a bulk density of $3\ {\rm g\ cm^{-3}}$ (uncompressed rock) for objects with initial semi-major axes of $a < r_{\rm snow}$ and $2\ {\rm g\ cm^{-3}}$ (rock-ice mix) for objects at $a \geq r_{\rm snow}$. The giant planet's radius is calculated with an assumed density of $1\ {\rm g\ cm^{-3}}$. For the purpose

Table 2.2: Initial disk set-up

	Rocky Zone 0.4–2.7 AU	Icy Zone 2.7–4.0 AU	Total 0.4–4.0 AU
$M_{\rm solid}$	$9.99\ \mathrm{M}_\oplus$	$14.8\ \mathrm{M}_\oplus$	$24.8\ \mathrm{M}_\oplus$
$m_{\rm proto}$	$0.025\ \mathrm{M}_\oplus$	$0.1\ \mathrm{M}_\oplus$	
N	66	9	75
$m_{\rm s-pl}$	$0.0025\ \mathrm{M}_\oplus$	$0.01\ \mathrm{M}_\oplus$	
N'	3336	1392	4278
$f_{\rm proto}$	0.17	0.06	0.1

of determining collisions and computing the strength of gas drag (Eq. 2.3) the super-planetesimal radius is taken to be equal to the radius of a single, physically realistic, planetesimal, with this fixed at $r_{\rm pl} = 10$ km; $m_{\rm pl}$ is calculated from $r_{\rm pl}$ with a density $\rho_{\rm pl}$ that is the same as that of the local protoplanets.

Data for this initial disk model are shown in Table 2.2. The overall values are $N = 75$ and $N' = 4278$ and the mass fraction of the whole disk contained in protoplanets $f_{\rm proto} \approx 0.1$. The parameter $f_{\rm proto}$ is used here as a rough measure of the evolution of the disk and we take $f_{\rm proto} = 0.5$, the point where the total mass in protoplanets exceeds that in planetesimals, to denote the transition between oligarchic and giant impact growth regimes (Goldreich *et al.*, 2004).

2.5 Preparatory maturation of the inner disk

All models are initiated at a system age (the approximate time elapsed since the origin of the protostar and protoplanetary disk) of 0.5 Myr: the simulation time coordinate is therefore set to $t = 0$ at this point. This epoch is sufficiently advanced for accretion in the inner disk to be in its oligarchic growth phase, but is comparatively early from the standpoint of the core-accretion hypothesis of giant planet formation. The giant planet therefore does not appear on the scene straight away and the simulation is run for varied durations before the giant planet is assumed to have formed and is introduced at 5 AU. This approach has the following advantages: a) it allows the inner disk to mature via accretion and hence to relax into a configuration of active growth that removes any artificiality inherent in its initial setup; b) it provides the basis for a range of early to late hot-Jupiter migration scenarios, bracketing the possible times of giant planet formation; and c) it permits the examination of the effect of inner disk maturity (e.g. oligarchic vs. chaotic growth; high vs. low gas density) on its response to the traverse of the giant planet.

This maturation process is carried out by running the simulation, in the absence

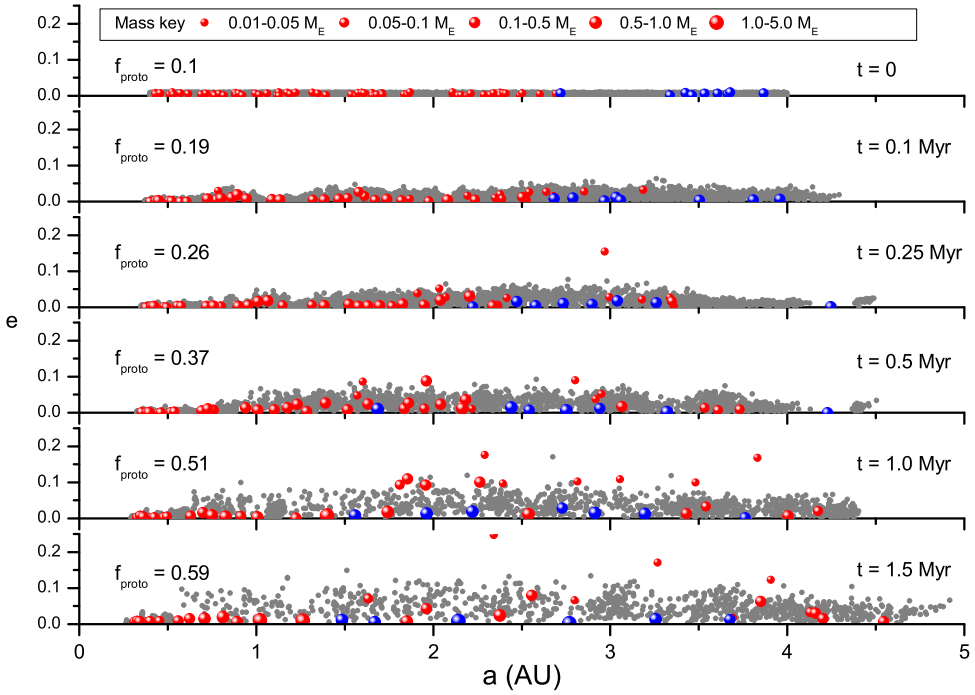

Figure 2.2: Inner disk maturation prepared for the Model II. Eccentricities are plotted against semi-major axis. Red and blue symbols show protoplanets originating interior and exterior to the snowline respectively; grey symbols are super-planetesimals. The top panel shows the initial condition and the lower panels show the subsequent evolution to the five scenario starting points.

of the giant planet, up to $t = 1.5$ Myr, storing the data at $t = 0.1$, 0.25, 0.5, 1.0 and 1.5 Myr in order to provide the basis for five scenarios of migration through progressively evolved inner system material[2]. Since the inner edge of the initial solids disk is at 0.4 AU, and the symplectic integrator within *Mercury 6* requires a time-step of $\lesssim$ one tenth of an orbital period to maintain accuracy, these preparatory runs adopt a symplectic time-step of $\tau_{\rm nbody} = 8$ days; an initial inner edge to the simulation domain is also set at $r_* = 0.1$ AU. (Note that r_* does not necessarily denote the physical radius of the central star, but it is the distance interior to which particles are removed from the simulation and their masses added to the central star.) In all cases presented in this thesis, the maturation process handles gravitational and gas drag forces in an identical manner, but since different versions of the model adopt different algorithms handling gas and migration dynamics (see Table 2.1), a separate set of preparatory runs is performed on each occasion.

[2]There is one exception to this timing scheme in Model I where maturation is run to $t = 3.0$ Myr.

During the evolution of all of these maturation run sets, dynamical spreading can cause some material to drift inward of 0.36 AU where the adequacy of the 8 day time-step is suspect. The quantity of this material is very small, except in models where dissipative forces from the disk are strong. In these cases however (e.g. Sect. 5.2), precursory testing of the model showed that strong dissipation also prevents any significant divergence of dynamical behaviour as a function of step size within the annulus bounded by 0.36 AU and r_*.

An example of a set of preparatory runs (those performed in advance of Model II, where the gas density declines with time due to viscous accretion onto the central star[3]) is shown in Fig. 2.2. Eccentricities of objects are plotted against their semi-major axes, with red and blue symbols representing protoplanets originating interior and exterior to the snowline respectively, and grey symbols representing super-planetesimals. The masses of protoplanets in units of $\mathrm{M}_\oplus$ are approximately indicated by the size of the symbol in comparison with the key at the top of the diagram. The top panel displays the initial setup (also detailed in Table 2.2) and the lower panels show the matured inner disk configuration at the succession of ages required for the migration scenario starting points. The mass fraction of the whole disk contained in protoplanets f_{proto} at each epoch is also given.

Many typical features of terrestrial planetary growth in a dynamically-cold environment show in Fig. 2.2. Protoplanets increase in mass and reduce in number as they accrete from the planetesimal field and undergo mergers. By $t = 1$ Myr, a few protoplanets of $\sim \mathrm{M}_\oplus$ have emerged and $f_{\mathrm{proto}} > 0.5$, meaning that in some parts of the disk at least, oligarchic growth has switched to chaotic growth. An increasing excitation of the remaining planetesimal and low-mass protoplanet population is also noticeable as the simulation progresses due to stronger dynamical stirring by the more massive protoplanets and reduced gas drag due to the decline in gas density. Dynamical friction exerted by this population however is still sufficient at $t = 1.5$ Myr to maintain the heavier protoplanets in circular orbits.

Once the scenario starting points have been prepared for each model, migration simulations are commenced by inserting a 0.5 M_J giant planet at 5 AU and then running the code further to allow the future hot-Jupiter to drift inward via type II migration. In Models I – III, the migration is halted by prescription at 0.1 AU due to the presence of an assumed inner disk cavity, whereas in Model IV, the giant planet self-consistently comes to rest between 0.1 – 1.7 AU due to the negation of migration forces because of dispersal of the gas disk. In all cases, in order to better model processes when the giant migrates down to small radial distances, the simulation inner

[3]See Table 2.1 and later description in Sect. 4.1 and Fig. 4.3

edge is contracted down to a realistic T-Tauri star radius: $r_* = 0.014$ AU $\cong 3\ R_\odot$ (Bertout, 1989). The initial time-step chosen for the symplectic integrator is determined from the position of the inner edge of the evolved solids disk and is typically $\tau_{\rm nbody} = 1 - 6$ days. However, it becomes necessary to reduce this substantially at late times as material is driven into closer orbits. Hence each scenario is divided into a number of sequential sub-runs with $\tau_{\rm nbody}$ being adjusted at each re-start so as to keep the time-step close to one tenth the orbital period of the innermost object.

Chapter 3

Model I: steady-state gas disk and prescribed type II migration

3.1 Migration through a steady state gas disk: a fast initial test of project merit

Given the commonplace assumption that hot-Jupiter systems should lack terrestrial planets (see Sect. 1.3), the merit of a research programme devoted to the modeling of terrestrial planet formation in hot-Jupiter systems demands an efficient initial assessment. Thus, the first model variant presented in this thesis (Model I) is the simplest and fastest to compute. Its results were the first description published in the literature of planetary growth *contemporaneously* with giant planet migration (Fogg and Nelson, 2005), and strongly suggested that the subject was deserving of further study with enhanced detail and realism.

Model I neglects the evolution of the gas component of the protoplanetary disk and assumes that the density of the gas and its power law profile remains fixed according to Eqs. 2.7 & 2.8. However, as the nebula is taken to be somewhat evolved by $t = 0$, considerable gas could already have been lost so the total mass of gas is reduced by a factor of 2/3. The relevant parameters in Eqs. 2.7 & 2.8 are therefore set to $f_{\rm neb} = 3$ and $f_{\rm gas} = 160$. The aspect ratio of the disk is taken to be $h/r = 0.05$ AU[1].

Inner system solids disks are generated and matured to create the starting points for five migration scenarios as described in Chapter 2, with the exception that the maturation process is carried on to $t = 3.0$ Myr. Under these circumstances, the inner disks evolve as illustrated in Fig. 3.1, with Table 3.1 giving numerical data of their remaining masses, $M_{\rm solid}$; the mass of the largest protoplanet, $m_{\rm max}$; the numbers of remaining protoplanets and super-planetesimals, N & N'; and the protoplanetary mass fraction, $f_{\rm proto}$.

It can be seen that protoplanetary growth is robust with $m_{\rm max}$ increasing and particle numbers decreasing with time. At late times, some protoplanets have grown to $\sim \mathrm{M}_\oplus$ and the style of accretion has switched from oligarchic to chaotic growth ($f_{\rm proto} > 0.5$) with an increased frequency of protoplanet mergers via giant impact. The $24.8\ \mathrm{M}_\oplus$ total of the original solids disk lost beyond the maturation phase inner boundary ($r_* = 0.1$ AU) is modest, except in the case of Scenario V. This occurs because the steady state gas disk exerts a constant and strong gas drag, which is sufficient by 3.0 Myr to cause significant orbital decay and loss of interior planetesimals, and the loss of some interior protoplanets as well which are coupled to the net planetesimal motion via dynamical friction.

[1]This fixed aspect ratio does not match that given in Eq. 2.10 and is a remnant of the earliest stages of model development. All the later models in this thesis use the MMSN flared scale height given by Eq. 2.10. The difference between the two relations does not have a major impact on model behaviour.

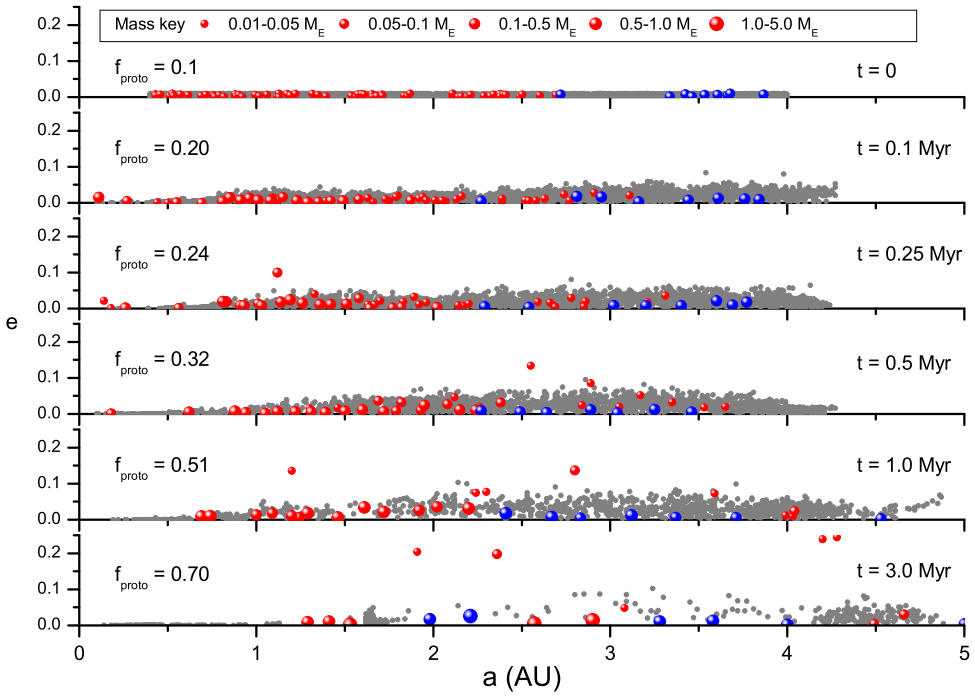

Figure 3.1: Inner disk maturation prepared for Model I. Eccentricities are plotted against semi-major axis. Red and blue symbols show protoplanets originating interior and exterior to the snowline respectively; grey symbols are super-planetesimals. The top panel shows the initial condition and the panels below show the subsequent evolution to the five scenario starting points.

Table 3.1: Overall solids disk data for Model I: after 0.1–3.0 Myr of evolution

Time t (Myr)	0.1	0.25	0.5	1.0	3.0
Scenario ID	I	II	III	IV	V
$M_{\rm solid}$ ($M_\oplus$)	24.4	23.7	22.9	20.6	14.6
$m_{\rm max}$ ($M_\oplus$)	0.22	0.33	0.52	0.91	1.28
N	56	51	40	29	19
N'	3863	3312	2660	1341	499
$f_{\rm proto}$	0.20	0.24	0.32	0.51	0.70

In order to simulate type II migration of a giant planet, Model I adopts a simple prescription by assuming that the migration rate is controlled by the local viscous disk evolution timescale. According to the alpha viscosity accretion disk model (Shakura and Sunyaev, 1973), the viscosity ν is parameterized as:

$$\nu = \alpha h^2 \Omega, \tag{3.1}$$

where α is the alpha parameter which is used to scale the viscosity, h is the disk scale height, and Ω is the disk's angular velocity which at the location of the giant planet is:

$$\Omega = \sqrt{\frac{\mathrm{G}M_*}{a^3}}, \tag{3.2}$$

where a is the semi-major axis.

Type II migration occurs when the giant planet has opened a gap in the surrounding gas disk. Two conditions have been identified that must be satisfied for this to happen (Lin and Papaloizou, 1993; Bryden *et al.*, 1999). The first is that the planet's gravity is strong enough to dissipate the density waves it excites in the disk locally through shock formation (a condition that the disk's response is non-linear). A rough estimate for this requirement is that the planet's Hill sphere radius exceeds the disk scale height:

$$a \left(\frac{m_\mathrm{p}}{3M_*} \right)^{\frac{1}{3}} > h. \tag{3.3}$$

For a planet of $m_\mathrm{p} = 0.5\ \mathrm{M_J}$, at $a = 5$ AU, with $h/a = 0.05$, Eq. 3.3 gives $0.27 > 0.25$, so the first condition is satisfied.

The second condition allows the disk gap to be maintained and requires that the tidal torques exerted by the planet on the disk exceed its intrinsic viscous torques. This can be expressed as:

$$\frac{m_\mathrm{p}}{M_*} > \frac{40\nu}{\Omega a^2}. \tag{3.4}$$

Taking the parameter values given above, Eq. 3.4 gives $m_\mathrm{p} > 2 \times 10^{-4} M_* \approx 0.2\ \mathrm{M_J}$, so the second condition is satisfied also. A 0.5 $\mathrm{M_J}$ planet is thus expected to undergo type II migration.

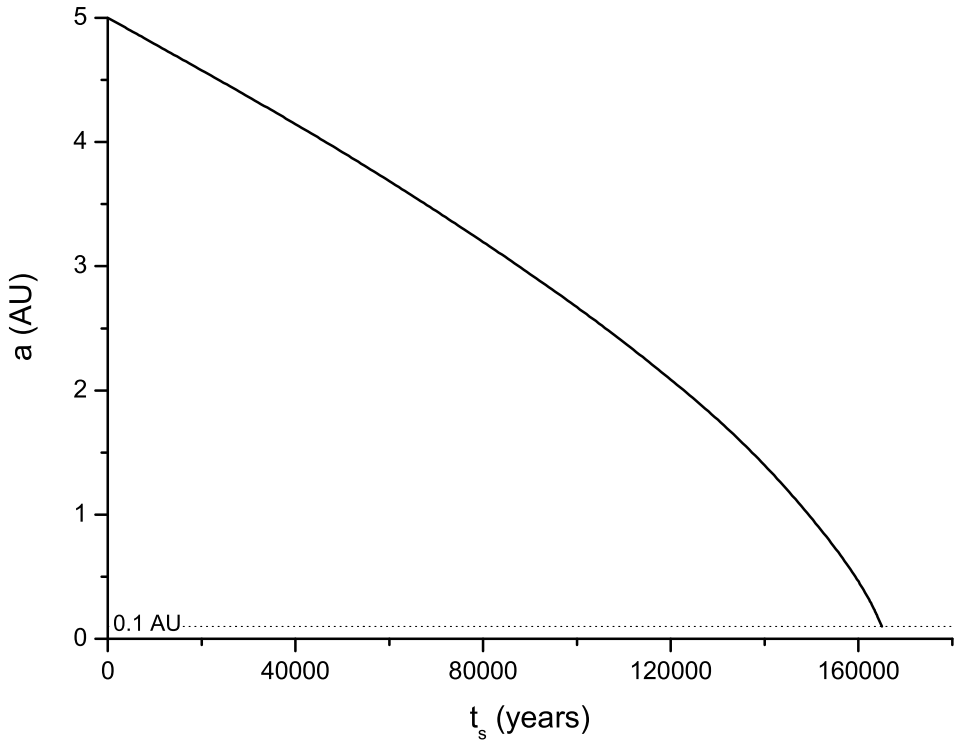

Figure 3.2: Migration of the giant planet in Model I. Semi-major axis a is plotted against $t_{\rm s}$: time measured from the starting point of each scenario.

The local viscous evolution timescale of an alpha-model disk is:

$$\tau_\nu \sim \frac{2r^2}{3\nu} = \frac{2}{3}\left(\frac{r}{h}\right)^2 (\alpha\Omega)^{-1}, \tag{3.5}$$

where r is radial distance from the central star and the alpha parameter is taken to be $\alpha = 2 \times 10^{-3}$ throughout this thesis. Since the giant planet is assumed to be migrating in step with the viscous evolution of the disk, the type II migration timescale $\tau_{\rm mig} \equiv \tau_\nu$, with $a \equiv r$. At $r = 5$ AU, $\tau_{\rm mig} \approx 0.237$ Myr, but since $\tau_{\rm mig} \propto a^{1.5}$, $\dot{a} \propto a^{-0.5}$ and inward migration speeds up as it proceeds (see Fig. 3.2). Time measured from the start of migration is referred to with the variable $t_{\rm s}$, where $t_{\rm s} = 0$ at the scenario start time t given in Table 3.1.

Since the modelled giant planet is of relatively low mass, the type II migration process is also assumed to exert strong eccentricity and inclination damping (e.g. Papaloizou *et al.*, 2001), which is taken here to operate over a timescale $= \tau_{\rm mig}/50$: a factor that is in rough agreement with the findings of Snellgrove *et al.* (2001) and Lee and Peale

(2002) who used a convergent type II migration model to explain the resonant orbital configuration of the giant planets in the GJ 876 system. The acceleration $\boldsymbol{a}_{\rm TypeII}$ (see Eq. 2.2) is therefore implemented as:

$$\boldsymbol{a}_{\rm TypeII} = -\frac{\boldsymbol{v}}{2\tau_{\rm mig}} - 25\left[\frac{2(\boldsymbol{v}\cdot\boldsymbol{r})\boldsymbol{r}}{r^2\tau_{\rm mig}} + \frac{2(\boldsymbol{v}\cdot\boldsymbol{k})\boldsymbol{k}}{\tau_{\rm mig}}\right], \tag{3.6}$$

where $\boldsymbol{v}$ is the giant planet's velocity vector, $\boldsymbol{r}$ is its position vector, and $\boldsymbol{k}$ is a unit vector in the vertical direction. Note that the factor of 2 appearing in the the first term on the right hand side arises because the migration time is half the angular momentum removal time.

With the above prescription in place, and with the five progressively matured inner disks shown in Fig. 3.1 generated as scenario starting points, a giant planet of mass $0.5\ {\rm M_J}$ is placed into each simulation at 5 AU and allowed to migrate inward with $\tau_{\rm mig}(5\ {\rm AU}) \approx 237\,000$ years (see Eq. 3.5). The giant migrates down to 0.1 AU in $t_{\rm s} \gtrsim 160\,000$ years (Fig. 3.2). The exact migration time depends slightly on the amount of solids disk mass remaining interior to its orbit with which the giant planet interacts gravitationally; but because of the assumption of an unvarying gas disk, this variation is minor and in all scenarios of Model I the migration behaviour of the giant is essentially that shown in Fig. 3.2[2]. All simulations therefore are run for $170\,000$ years, with the type II migration algorithm being switched off once the giant reached 0.1 AU. As described in Chapter 2, in order to better model processes when the giant migrates down to small radial distances, collision with the central star is computed by setting the simulation inner boundary to $r_* = 0.014\ {\rm AU} \cong 3\ {\rm R_\odot}$, the approximate radius of a T-Tauri star (Bertout, 1989). The initial time-step chosen for the symplectic integrator is set at a tenth of the orbital period of the innermost object; but as dynamical spreading and the effects of migration and drag drives some material into closer orbits, the time-step is reduced as the simulation progresses, by splitting it into a series of 20 000 year sub-runs with the time-step adjusted at each re-start. This considerably increases the run times of these simulations, especially at late times when the time-step is typically reduced to $\tau_{\rm nbody} < 1$ day, requiring about a month of processor time for completion.

When comparing the results of the models presented in this thesis, it is important to note that Model I is the most strongly dissipative. This can be appreciated in a qualitative way by considering the contents of Table 3.2, which indicates the presence in each model of five dissipative processes: gas drag; type II migration; type I migration; dynamical friction; and collisional damping. It indicates that, because of

[2]This is not the case in the later models presented in this thesis, which include an evolving gas disk, hence producing a unique migration curve for each scenario

Table 3.2: Qualitative indication of dissipative forces present in the models, with emphasis on Model I

Dissipative forces	Models				
	I	II	III	IV	After gas loss
Gas drag	↔	↓	↓	⇊	×
Type II migration	↔	↓	↓	⇊	×
Type I migration	×	×	↓	⇊ or ×	×
Dynamical friction	↓	⇊	⇊	⇊	⇊
Collisional damping	↔	↔	↔	↔	↔

Key:
↔ : no change with time
↓ : reduces with time
⇊ : stronger reduction due to late start or combination effect
× : not present

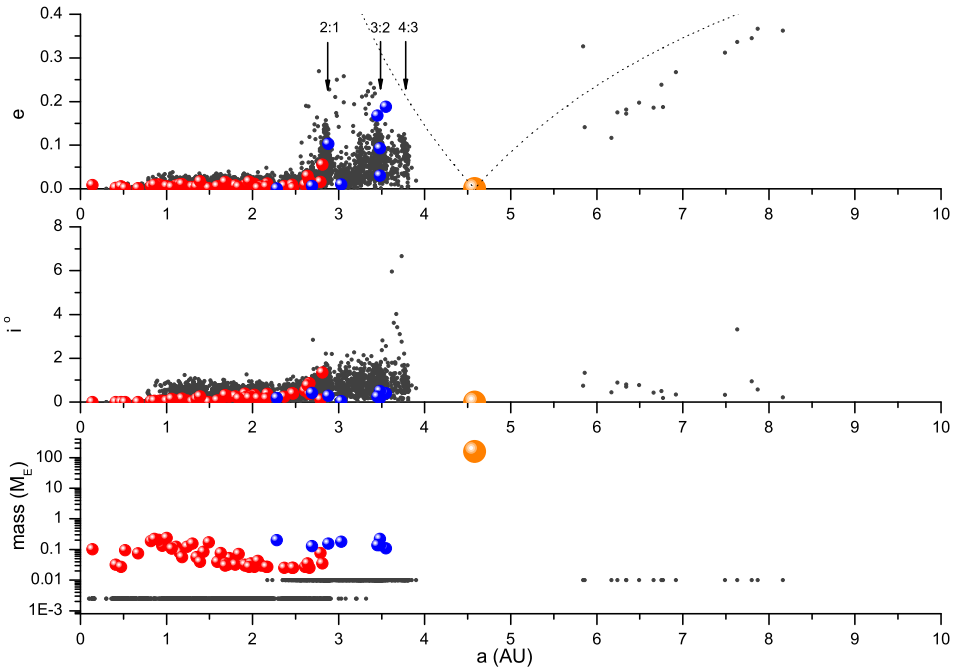

Figure 3.3: Scenario I at $t_s = 20\,000$ years, showing the mass, inclination and eccentricity of objects. Small dark dots represent super-planetesimals; red and blue symbols are rocky and icy protoplanets respectively; and the large orange symbol is the giant. Objects located within the dotted lines in the upper panel have orbits that intersect the orbit of the giant. The location of the 2:1, 3:2 and 4:3 resonances with the giant planet are indicated.

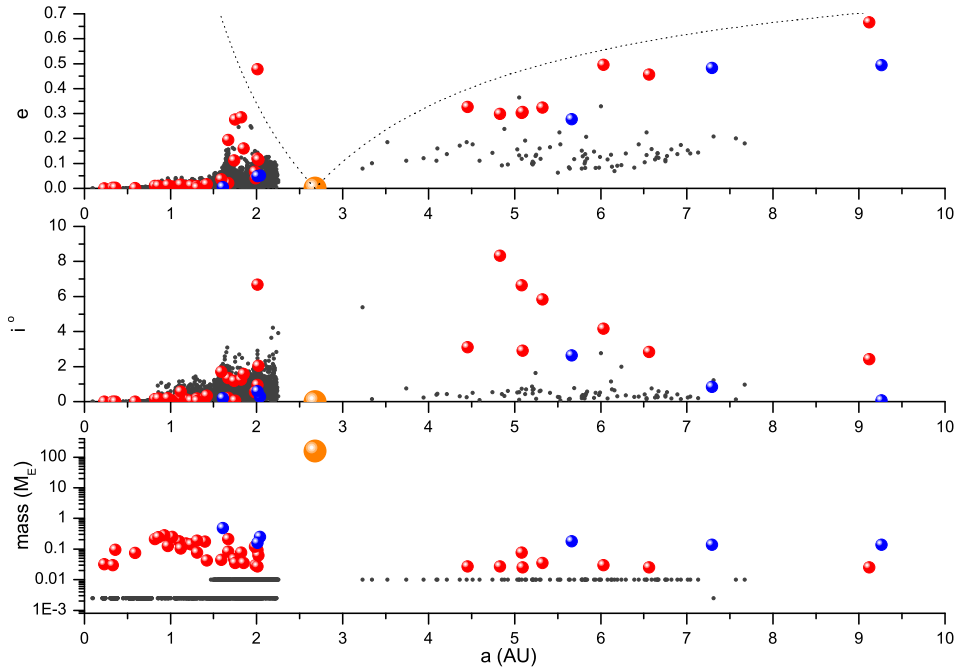

Figure 3.4: Scenario I at $t_s = 100\,000$ years. The giant has now moved inward to 2.68 AU and has scattered a significant amount of mass into exterior orbits.

Model I's steady state gas disk, gas drag and type II migration operate at a constant strength in both early and late migration scenarios; only dynamical friction falls with time as the planetesimal swarm thins out due to accretion onto protoplanets.

3.2 Results of Model I

3.2.1 Typical features of a run

The character of the planetary systems formed from these runs is found to vary systematically with the age of the inner disk. However, all scenarios also exhibit a number of behavioural features in common. These are discussed first by describing one of the scenarios in detail.

Five snapshots of the evolution of Scenario I are illustrated in Figs. 3.3 – 3.7 showing the mass, inclination and eccentricity of objects vs. semi-major axis. The original provenance of the protoplanets (interior or exterior to the snowline) is denoted by the shading of its symbol as described in the caption to Fig. 3.3. In the case of a merger between rocky and icy protoplanets, this shading is determined by that of the most

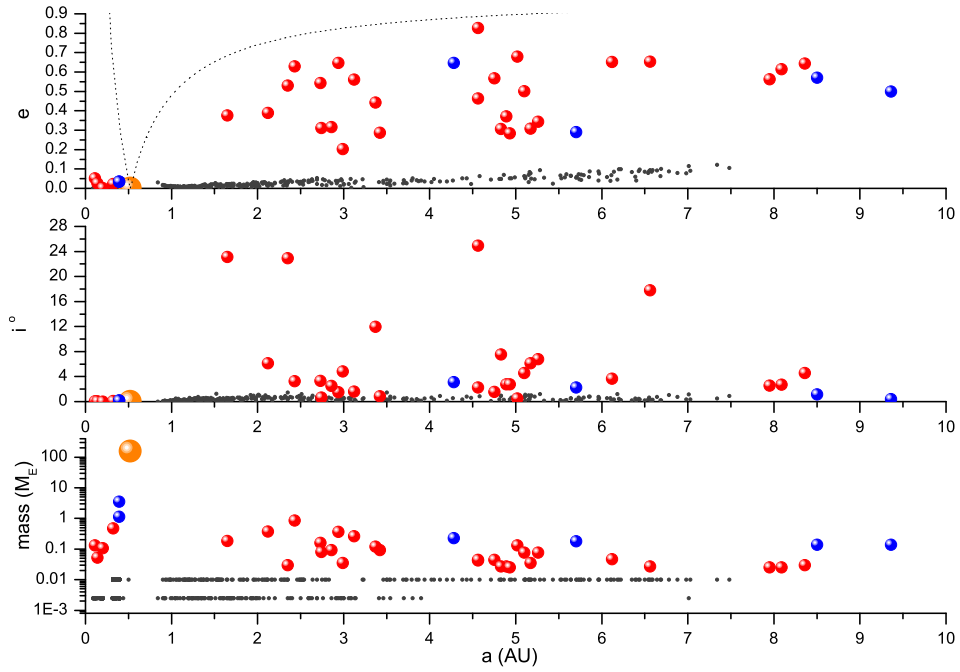

Figure 3.5: Scenario I at $t_s = 160\,000$ years. The giant has now moved inward to 0.52 AU. The scattered exterior disk has grown, but a substantial amount of mass in planetesimals and six rapidly accreting protoplanets remain interior to the giant. The outer three of these six are in first order resonances with the giant.

massive of the pair.

A juncture early in the simulation is illustrated in Fig. 3.3, 20 000 years after the start of migration when the giant has moved inward to 4.58 AU. Several prominent features have developed and the outer edge of the disk has been pushed inward by the giant planet through a combination of two processes. 1) A shepherding mechanism acting on planetesimals damped by gas drag, which operates when gravitational perturbations by the approaching giant planet force an increase of the eccentricity of a planetesimal, raising its velocity with respect to the gas, and hence increasing the opposing tendency of gas drag to circularize the orbit (see Eq. 2.3). The net effect is that orbital energy is dissipated and planetesimals are driven inward ahead of the migrating giant planet (Tanaka and Ida, 1999). 2) Trapping of objects at sweeping mean-motion resonances, which pushes the outer disk edge inward at the 4:3 resonance and causes the capture of a substantial population of planetesimals and some protoplanets at 3:2 and 2:1, increasing their concentration at these locations and exciting their orbits. The overall effect is a compaction and excitation of the outermost

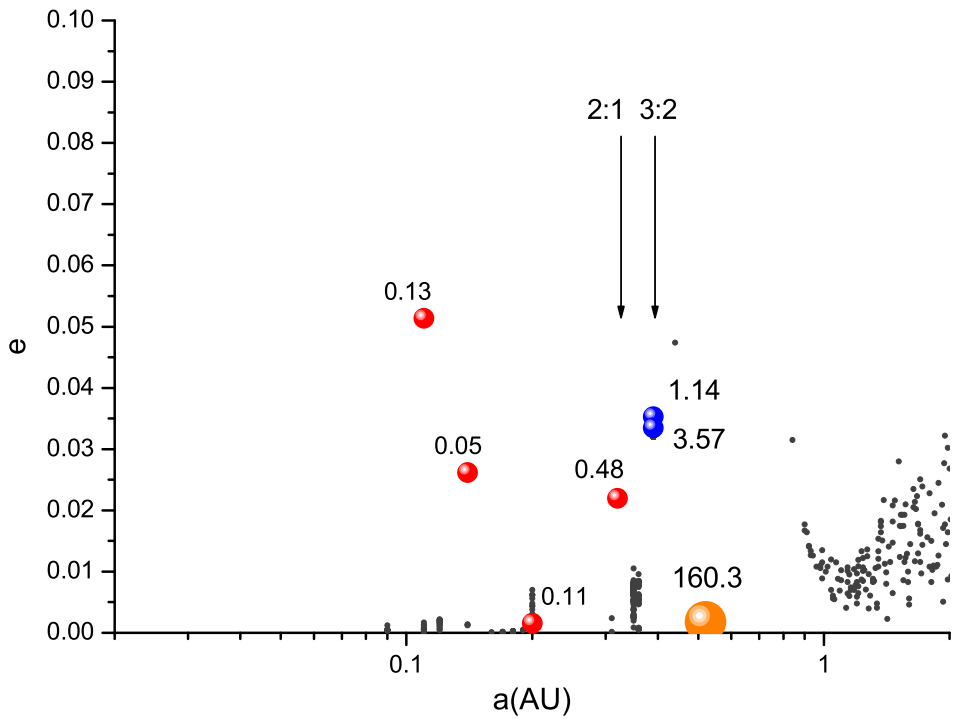

Figure 3.6: Detail of the interior regions of Scenario I at $t_s = 160\,000$ years, showing e vs a for objects ≤ 2 AU. Planetary masses are indicated in units of $M_\oplus$. A total of $\sim 15\ M_\oplus$ of material has been pushed inward by the giant, $\sim$ two thirds of it remaining in super-planetesimals, many of which do not show individually in this diagram as they are over-plotted in the vicinity of the 3:2 and 2:1 resonances.

annulus of the disk between the 4:3 and 2:1 resonances. Interior to this zone, the presence of the approaching giant has had little influence.

The state of play some time later at $t_s = 100\,000$ years is shown in Fig. 3.4. The giant has now moved inward to 2.68 AU, continuing to push the outer edge of the disk ahead of it at the 4:3 resonance. An increased amount of mass has been entrained in the region between 4:3 and 2:1, and resonant pumping and mutual scattering has raised the eccentricities of some protoplanets to high values. This has allowed some objects to cross the gap between the disk and giant whereupon a close slingshot encounter causes expulsion into an exterior orbit. A sparsely populated and excited exterior disk is now in the process of formation, composed predominantly of the more weakly damped protoplanet material. An example of the scattering process taking place can be seen in the top panel of Fig. 3.4, where one protoplanet with $e \approx 0.5$ is in an orbit that crosses that of the giant planet.

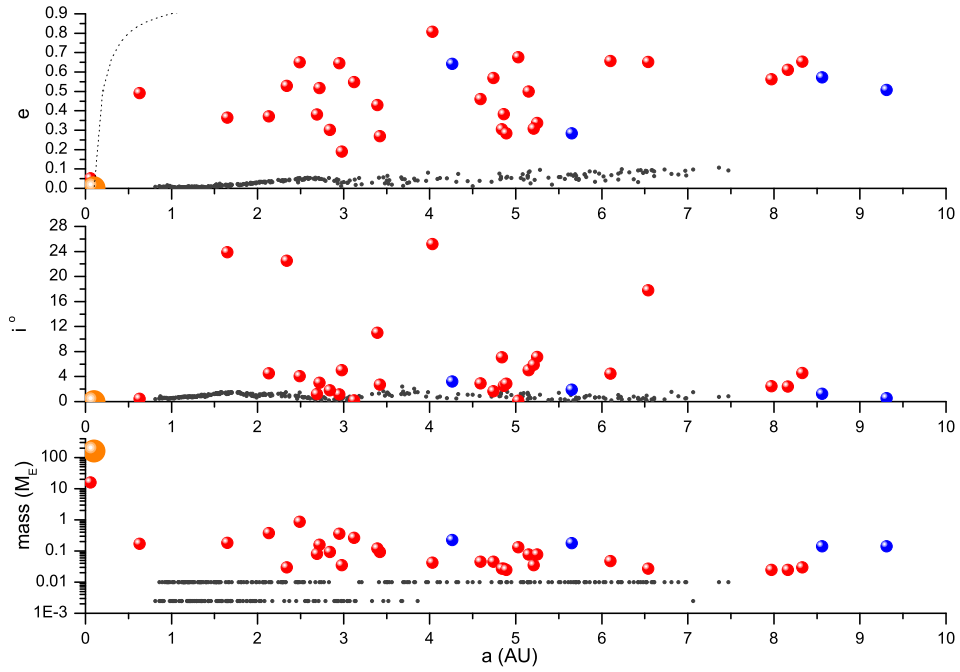

Figure 3.7: Scenario I at $t_{\rm s} = 170\,000$ years. The giant has now stopped at 0.1 AU. All interior mass has accreted into a single $15.65\ {\rm M}_{\oplus}$ object after an intense episode of runaway accretion and giant impacts.

At $t_{\rm s} = 160\,000$ years the giant has moved inward to 0.52 AU as shown in Fig. 3.5. The most prominent feature now appears to be the scattered exterior disk made up of numerous protoplanets with large a and e and a diffuse population of planetesimals with a $\Sigma_{\rm s}$ of only a few percent of the original disk. This however still represents the minority of solids mass. Two thirds of the disk mass remains interior to the giant in the form of remaining planetesimals and six protoplanets. A blow-up of the interior regions of the system at this juncture is shown in Fig. 3.6. A total of $\sim 15\ {\rm M}_{\oplus}$ of solid material has been compacted interior to the giant, most of which lies between 0.32–0.39 AU. Two massive protoplanets of 3.57 and 1.14 $\rm M_{\oplus}$ are captured at the 3:2 resonance with the giant and a smaller 0.48 $\rm M_{\oplus}$ protoplanet is found at the 2:1 resonance. The majority of the mass however remains in super-planetesimals entrained at these resonances (and mostly over-plotted in the figure) and in a ring of shepherded matter between them. Protoplanetary eccentricities therefore remain low, even at resonances, due to strong dynamical friction. In addition, accretion rates onto these objects have now become so high that collisional damping is also acting to control the growth of their eccentricities.

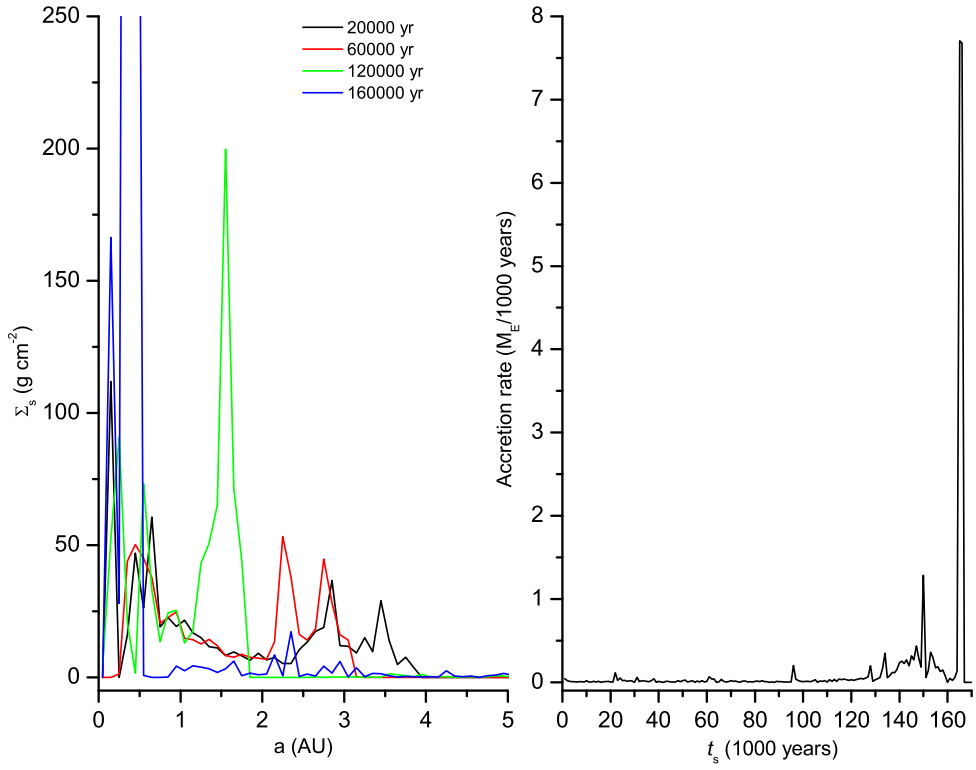

Figure 3.8: Surface density evolution (left hand panel) and accretion rates (right hand panel) for Scenario I. Growing surface density peaks at the 2:1 and 3:2 resonances sweep through the inner system ahead of the giant. Accretion rates increase after $t_{\rm s} \approx 120\,000$ years and the final intense accretion spike represents clear up of remaining material shepherded within 0.1 AU.

The final snapshot of Scenario I at $t_{\rm s} = 170\,000$ years is shown in Fig. 3.7. The giant has stopped its migration at 0.1 AU and, whilst the character of the exterior disk is unchanged, evolution has proceeded rapidly to $f_{\rm proto} = 1$ within the compacted interior material. No planetesimals remain, having either been swept up by protoplanets or accreted by the central star. An intense episode of runaway accretion and giant impacts has ended in the assembly of a single $15.65\ {\rm M}_{\oplus}$ planet out of resonance with the giant at 0.055 AU. As can be seen in Fig. 1.4, this arrangement of close orbiting giant and an inner Neptune-mass planet has a striking similarity to the two innermost planets in the 55 Cancri system (McArthur *et al.*, 2004).

To reinforce the above interpretation of processes at work in Scenario I, the surface density evolution of the disk and its accretion rate are shown in Fig. 3.8. The left hand panel shows the disk surface density profile (obtained by summing all protoplanets and super-planetesimals in 0.1 AU width bins) at 20 000, 60 000, 120 000 and

160 000 years after the start of migration; the right hand panel plots the amount of mass accreted onto protoplanets only (including giant impacts) every 1 000 years for the duration of the run. In the $\Sigma_{\rm s}$ plot, two surface density enhancements are clearly visible as spikes at the 3:2 and 2:1 resonances and are seen to grow whilst moving inward. At 120 000 years, these have merged into one: the outer half of the original disk having by now been squeezed into a dense ring. By 160 000 years, most of this mass is now confined within 0.5 AU and $\Sigma_{\rm s}$ here has risen to $\sim\ 10^3\ {\rm g\ cm^{-2}}$ (an increase by a factor of $\gtrsim 10$ over the previous, undisturbed, disk surface density) which is off the vertical scale in the figure. The effect of this disk compaction process is seen clearly in the accretion rate plot. Mass accretion rises significantly after 120 000 years due to both the resultant high values of $\Sigma_{\rm s}$ and the fact that much of this mass now resides in a zone where dynamical times are shorter. Growth interior to the giant ends in a short-lived and dramatic phase of runaway planetesimal accumulation and giant impacts within the material pushed into the small volume inside 0.1 AU from the central star.

This acceleration of growth within the compacted region can be readily understood by considering the 'particle in a box' approximation of planetary growth, which adopts the simple picture of a protoplanet accreting as it sweeps through a swarm of smaller particles (Safronov, 1969). The growth rate of the protoplanet can be expressed as:

$$\frac{{\rm d}m_{\rm p}}{{\rm d}t} \approx n m_{\rm pl} v_{\rm rel} \pi r_{\rm p}^2 \left(1 + \frac{v_{\rm esc}^2}{v_{\rm rel}^2}\right), \tag{3.7}$$

where $m_{\rm p}$, $r_{\rm p}$ and $v_{\rm esc}$ are the mass, radius, and escape velocity of the protoplanet; and n, $m_{\rm pl}$ and $v_{\rm rel}$ are the number density, characteristic mass, and the velocity dispersion of the planetesimal population respectively. The quantity in brackets at the right hand side of the equation is the factor by which gravitational focussing enlarges the accretion cross section of the protoplanet. If negligible gravitational focussing is assumed ($v_{\rm esc} \approx v_{\rm rel}$); and $n m_{\rm pl} \sim \Sigma_{\rm s}/(2h_{\rm s})$, where $\Sigma_{\rm s}$ and $h_{\rm s}$ are the surface density and scale height of the swarm; and $v_{\rm rel} \sim h_{\rm s}\Omega$, where Ω is the angular velocity (Eq, 3.2) then:

$$\frac{{\rm d}m_{\rm p}}{{\rm d}t} \approx \Sigma_{\rm s} \Omega \pi r_{\rm p}^2. \tag{3.8}$$

In this case, the relative growth rate of the protoplanet is:

$$\frac{1}{m_{\rm p}} \frac{{\rm d}m_{\rm p}}{{\rm d}t} \propto \Sigma_{\rm s} \Omega m_{\rm p}^{-\frac{1}{3}}, \tag{3.9}$$

where the negative index of $m_{\rm p}$ is indicative of oligarchic growth (Kokubo and Ida, 1998). Since the original surface density of solids is $\Sigma_{\rm s} \propto r^{-1.5}$ (Eq. 2.6), the semi-major axis dependence of the growth rate would be roughly $\dot{m}_{\rm p} \propto a^{-3}$, leading one to expect growth rates $\sim$ 100 – 1 000 times faster in the compacted portion of the disk within 0.5 AU than those within the original disk as a whole. In reality it is at least an order of magnitude faster than this as the compaction process concentrates planetary building blocks within an ever shrinking annulus, boosting $\Sigma_{\rm s}$ substantially higher than its original value (see the left panel in Fig. 3.8).

Since dynamical friction is strong in Scenario I, due to an abundance of well-damped super-planetesimals, and because of the appearance of protoplanets of $> {\rm M}_{\oplus}$ in the compacted disk at late times (see Fig. 3.6), gravitational focussing is particularly effective ($v_{\rm esc} \gg v_{\rm rel}$) and Eq. 3.7 becomes:

$$\frac{{\rm d}m_{\rm p}}{{\rm d}t} \approx \frac{\pi m_{\rm p} r_{\rm p} \Sigma_{\rm s}}{e^2} \left(\frac{\rm G}{M_* a} \right)^{\frac{1}{2}}, \tag{3.10}$$

where $v_{\rm esc} = \sqrt{2{\rm G}m_{\rm p}/r_{\rm p}}$ and $v_{\rm rel} \sim ea\Omega$.

In this situation, the relative growth rate of the protoplanet becomes:

$$\frac{1}{m_{\rm p}} \frac{{\rm d}m_{\rm p}}{{\rm d}t} \propto \Sigma_{\rm s} \Omega^{\frac{1}{3}} m_{\rm p}^{\frac{1}{3}}. \tag{3.11}$$

Now, including the original $\Sigma_{\rm s} \propto r^{-1.5}$ as before, the semi-major axis dependence of the growth rate is shallower at roughly $\dot{m}_{\rm p} \propto a^{-2}$; however, the positive index of $m_{\rm p}$ is indicative of *runaway* growth, resulting in rapid and preferential accretion onto the largest bodies – exactly as observed during the final 10 000 years of Scenario I, when all of the remaining mass of the compacted inner disk shown in Fig. 3.6 ends up accreting into a single hot-Neptune type planet.

The behavioural features seen to a greater or lesser extent in all the runs summarize as follows.

1. *Shepherding of planetesimals.* As planetesimal random velocities are continuously damped by gas drag, their tendency is to be pushed inward, ahead of the giant. Shepherding of protoplanets also results as a weaker secondary effect as they are, to a varying extent, coupled to the planetesimal disk by dynamical friction.

2. *Resonant capture.* First order resonances with the giant gather an increasing amount of mass as they sweep inward. This, in addition to the shepherding effect eventually results in the compacting of some of the disk mass into a zone close to the central star.

3. *Acceleration of planetary growth interior to the giant.* Accretion speeds up within the compacted interior disk. This is particularly rapid within the disk remnant squeezed inside 0.1 AU, where the final evolutionary phases of accretion are rushed through in mere thousands rather than millions of years. Typically, 1–3 massive close orbiting planets are the end result. Where there is one survivor, its mass and configuration can be reminiscent of the 'hot-Neptune' or 'hot-Earth' type of planet identified recently.

4. *Creation of a scattered exterior disk.* Pumping of eccentricities at resonances and by mutual perturbations permit some disk material to undergo a close encounter with the giant where it is scattered into an external orbit. Protoplanets, being less strongly damped, are more likely to have this happen than planetesimals. The result is a dynamically excited and widely dispersed external disk of material.

3.2.2 Dependence on the maturity of the inner disk

The purpose of running five scenarios through a progressively more mature inner disk is to explore the issue of whether the timing of migration has any systematic effect on the results. This is possible because when a disk evolves and small objects accumulate onto larger ones, dynamical friction becomes less effective overall, influencing both the shepherding and scattering behaviours previously described. The characteristics of the five systems at the end point of each scenario are illustrated in Fig.3.9: it can be seen that scattered disks form in all cases and the configuration of the hot-Neptunes and hot-Earths accreted from shepherded material is made clearer by plotting semi-major axis a on a log scale.

In all the simulations there were five possible fates awaiting all the modelled disk particles: 1) survival in a body orbiting interior to the giant; 2) survival in a body orbiting exterior to the giant; 3) accretion by the central star; 4) accretion by the giant; and 5) ejection from the system. These data are shown in Table 3.3 which lists the fate of the disk mass at the end of the simulations: the total surviving solids and the five end points being shown as a percentage of the total initial solids. It is noticeable from Table 3.3 that systematic trends in the fractionation of solids between some of

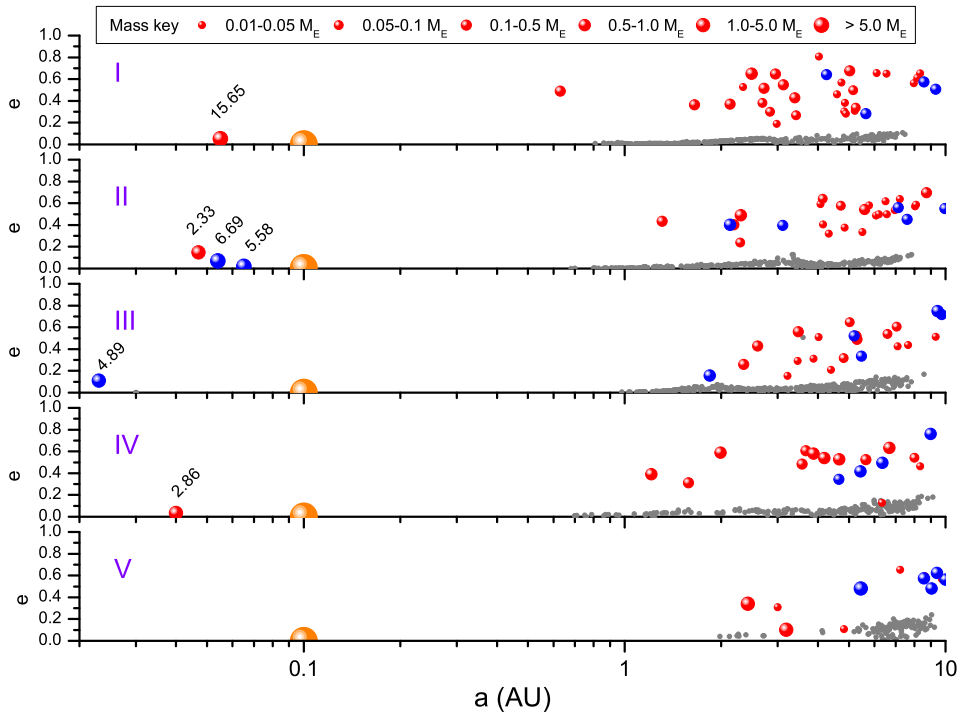

Figure 3.9: End points of all five scenarios at 170 000 years after the start of giant planet migration. Semi-major axis a is plotted on a log scale vs. eccentricity e. The masses of the planets accreted interior to the giant planet at 0.1 AU are labelled in units of $\mathrm{M}_{\oplus}$.

Table 3.3: Fate of the disk mass at the scenario end points

Scenario	I	II	III	IV	V
Total Initial Solids ($\mathrm{M}_{\oplus}$)	24.39	23.68	22.89	20.61	14.59
Total Surviving Solids ($\mathrm{M}_{\oplus}$)	22.06 (90%)	21.04 (89%)	12.05 (53%)	14.75 (70%)	9.91 (68%)
Interior Surviving Solids ($\mathrm{M}_{\oplus}$)	15.65 (64%)	14.60 (62%)	4.96 (22%)	2.86 (14%)	0.00 (0%)
N, f_{proto}	1, 1	3, 1	1, 0.99	1, 1	0, 0
Exterior Surviving Solids ($\mathrm{M}_{\oplus}$)	6.41 (26%)	6.44 (27%)	7.09 (31%)	11.59 (56%)	9.91 (68%)
N, f_{proto}	32, 0.66	32, 0.63	25, 0.65	23, 0.93	16, 0.89
Accreted by Star ($\mathrm{M}_{\oplus}$)	1.05 (4%)	0.74 (3%)	9.60 (42%)	5.81 (28%)	3.03 (21%)
Accreted by Giant ($\mathrm{M}_{\oplus}$)	1.19 (5%)	1.88 (8%)	1.24 (5%)	0.34 (2%)	1.65 (11%)
Ejected ($\mathrm{M}_{\oplus}$)	0.00 (0%)	0.025 (0.1%)	0.00 (0%)	0.025 (0.1%)	0.00 (0%)

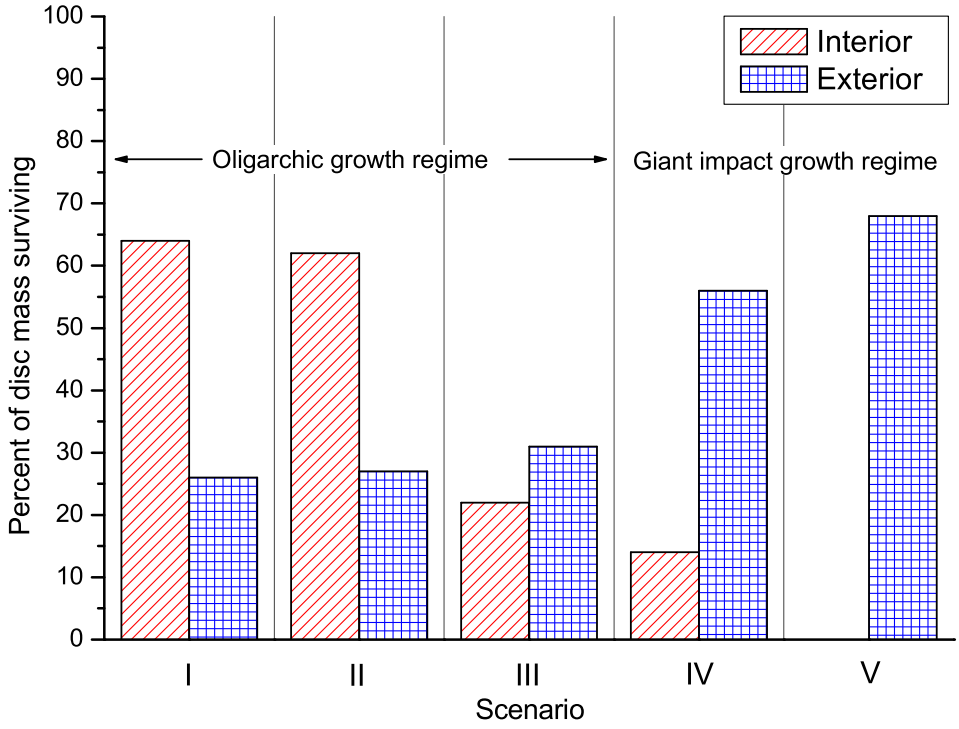

Figure 3.10: Interior and exterior surviving solids as a percentage of initial disk mass at the scenario end points.

these end points do appear.

The most obvious trends are that the percentage of the original disk mass that ends up surviving interior to the giant falls with disk maturity whereas that expelled into exterior orbits rises with disk maturity (see Fig.3.10). The protoplanet mass fraction $f_{\rm proto} = 1$ for the inner material is indicative of its rapid evolution, whereas the values of $f_{\rm proto} \approx 0.6$ – 0.9 for the outer material are as much influenced by the preferential tendency for protoplanets to be widely scattered as it is by their previous growth. The implication is that scattering is noticeably more effective in older, less dissipative disks. Giant planet migration through a protoplanet/planetesimal disk rapidly advances its evolution (as measured by $f_{\rm proto}$), both by speeding up accretion and by fractionating objects according to the magnitude of their damping, but solids disks in an oligarchic stage of growth have more of a tendency to be pushed ahead of the giant and disks undergoing giant impact type growth tend to result in a greater amount of mass transfer into external orbits.

The fraction of this scattered mass that is ejected from the system is tiny: the reason being that ejection can only occur when $v_{\rm esc} \gtrsim \sqrt{2}\Omega a$, at distances greater than

$a \gtrsim r_{\rm p} M_*/m_{\rm p}$, which is $a \gtrsim 0.85$ AU in this model. Further out than this, ejections typically happen only after a succession of encounters with the giant planet which can recur when an externally scattered object returns to its periastron. However, in these simulations this incremental ejection process is usually interrupted by the giant planet migrating out of range, or by the raising of a scattered object's periastron due to gravitational interactions with other bodies in the scattered disk.

The amount of mass accreted by the giant is also minor in all cases but the picture is complicated by the statistics of mass accreted by the central star. In the last three scenarios, this is significant. However, the high values in Scenarios III & IV result mainly from the impact of a single massive protoplanet during the final energetic phase of accretion within 0.1 AU. The loss of mass to the star in Scenario V resulted from the orbital decay of a substantial annulus of super-planetesimals in the absence of any remaining interior protoplanet which could accrete them. The stochastic fate of large individual bodies at late times can therefore overwrite and partially obscure systematic trends in the data. In Scenario III, for example, if a single close encounter near the end of the simulation had resulted in a giant impact rather than a scattering into the star, a single interior planet of (~ 12.5 $\mathrm{M}_\oplus$) would have formed instead – another hot Neptune analogue.

There are, however, many examples of hot Jupiters that have migrated further inward than 0.1 AU. Orbits at $\sim$ 0.05 AU are common and some objects have been found as close as $\sim$ 0.02 AU. It is less likely that interior planets would survive in such systems. If it is assumed that all remaining interior mass is accreted by the star (which is not always true, as demonstrated in Sect. 3.2.3) then the total surviving mass reduces to the exterior surviving mass which, as illustrated in Fig.3.10, shows a clear trend with disk maturity. The later the migration episode the more disk mass will remain: from $\sim 30\%$ for the earliest scenario to $\sim 70\%$ for the latest. None of the simulations support the conjecture of a near-complete loss of solids from the swept zone.

3.2.3 The interior planets

In all scenarios, barring the latest, giant planet migration is found to stimulate accretion within the portion of the disk shepherded inward. By the end of the simulations, this mass had accumulated into one or more massive planets within 0.1 AU. Details of these planets and the giant, including their simulation ID[3], mass, a, e, and the pres-

[3] A label composed of a three letter prefix followed by a number that is used by the code to refer to individual particles. Those with prefixes of OLI or ICE refer to protoplanets originating interior or exterior to the snowline respectively.

Table 3.4: Interior surviving planets at scenario end points compared with three currently known systems containing 'hot Neptunes' and circumscribing giant planets. Data include the closest giant planet and were updated from the Extrasolar Planets Encyclopedia (http://exoplanet.eu) on 2/2/08.

Scenario	ID	Mass ($M_\oplus$)	a (AU)	e	Resonances
I	OLI8	15.65	0.055	0.052	None
	GIA1	160.3	0.100	0.003	
II	OLI9	2.33	0.047	0.148	5:4 with ICE9, 5:3 with ICE1
	ICE9	6.69	0.054	0.071	4:3 with ICE1
	ICE1	5.58	0.065	0.022	
	GIA1	160.9	0.100	0.005	
III	ICE1	4.89	0.023	0.110	None
	GIA1	160.3	0.100	0.001	
IV	OLI28	2.86	0.036	0.035	None
	GIA1	159.8	0.100	0.002	
55 Cancri	e	$10.8 \sin i$	0.038	0.07	None
	b	$262.2 \sin i$	0.115	0.014	
μ Arae	d	$13.4 \sin i$	0.09	0.0	None
	e	$165.5 \sin i$	0.921	0.066	
GJ 876	d	$5.89 \sin i$	0.021	0.0	None
	c	$177.9 \sin i$	0.13	0.27	

ence of resonances are given in Table 3.4, and their configuration can be appreciated visually from Fig.3.9.

A single interior planet is the most common result of Model I, but in one case there are three survivors. Their masses range between $\sim 2 - 16\ M_\oplus$ with semi-major axes between $\sim$ 0.02 – 0.07 AU. None of them remain in resonance with the giant even though some of their precursor bodies would have been originally been pushed inward at first order resonances (see Fig. 3.6). These resonances were broken during the final accretion phase within 0.1 AU. In Scenario II however, the three planets that remain are all in resonant relation with each other. The inner planet is in the 5:4 resonance with the middle planet and the 5:3 resonance with the outer planet. The middle planet is in the 4:3 resonance with the outer planet, giving a 5:4:3 commensurability overall. It is possible that such a relationship could act to stabilize the orbits of these planets, but they are closely spaced, the orbits of OLI9 and ICE9 cross, and the giant acts to perturb the system, so accretion here is likely to be incomplete. Running the inner system of Scenario II for an additional 1.0 Myr results in a prompt giant impact between the inner pair (ICE9 & OLI9, see Table 3.4), followed by a longer phase of interaction of the two 9.02 and 5.58 $M_\oplus$ survivors. Their orbits gradually became more elliptical, especially that of the lighter outer planet (ICE1). Seven close encoun-

ters follow, causing an outward scattering and a further excitation of the outer planet's eccentricity. Just before the end of the extended run, ICE1 encounters the giant for the first time and 18 close encounters later they collide. Thus, the final outcome for Scenario II is a single remaining inner planet, separated from the giant by 12.9 mutual Hill radii with a mass of 9.02 $\mathrm{M}_{\oplus}$, a = 0.0465 AU, e = 0.132.

Generation of these massive interior planets by these simulations is particularly interesting as three examples of short period ($a < 0.1$ AU) Neptune or super-Earth mass objects, in orbits circumscribed by that of a giant planet, have been recently discovered in the systems 55 Cancri (McArthur *et al.*, 2004), μ Arae (Santos *et al.*, 2004) and GJ 876 (Rivera *et al.*, 2005). Data for the interior planet and the closest giant in these systems are contrasted with those generated here in Table 3.4 and configurations can be related visually by comparing Fig. 1.4 with Fig. 3.9. In all of these natural systems the inner Neptune-mass planet is accompanied by more than one outer giant and, in the cases of 55 Cancri and GJ 876, the innermost giant is placed close to where our simulated giant ends its migration. The results of the simulations do have a particular resemblance to reality in these two cases. The best matches are given by Scenario I, where the mass and orbital radius of the interior planet are similar to the $m \sin i$ and a of 55 Cnc e, and Scenario III where the resemblance is closer to the configuration of GJ 876 d & c. One might speculate therefore that, rather than hot Neptune type planets forming far out in the disk and migrating inward to their present location, they might, as illustrated here, form at these locations from disk material shepherded and compacted by a migrating giant.

Against this proposition is the fact that hot-Neptunes and hot-Earths are also found in systems apparently unaccompanied by an exterior giant (e.g. Butler *et al.*, 2004; Udry *et al.*, 2007). However, the primaries of these systems are often red dwarf stars which might affect the comparison. Giant planets appear to be rare in red dwarf systems and it may be that they do not form efficiently from the lower mass protoplanetary disks expected around low mass stars (Laughlin *et al.*, 2004). Hot-Neptunes may therefore be the largest planets in many red dwarf systems, rather than secondary objects, and perhaps formed at larger radii before an inward type I migration stranded them in close orbits. However, not all red dwarf stars lack giant planets. In the one known case where giants are present (GJ 876) and past migration may have played a role in their current configuration (e.g. Snellgrove *et al.*, 2001), an interior hot-Earth appears to be present. The hot-Neptune in the μ Arae system is accompanied by giant planets, but the nearest one is situated much further out (at 0.91 AU) than the final location of the giant in the simulations. Model I does not evaluate the outcome of

stopping the giant migration at ~ 0.5 – 1.5 AU[4], but at the point in the runs where the giant passes through 1.5 AU (at $t_{\rm s} \approx 140\,000$ years) about 60% of the original mass of the disk is compacted within ~ 1 AU. This is enough mass to assemble a $\gtrsim 13\ {\rm M}_\oplus$ hot-Neptune over a longer period.

Another reason for the apparent rarity of hot-Neptune type objects could be that many hot-Jupiter systems are more compact than 0.1 AU; a typical example being 51 Pegasi b: $m \sin i \approx 0.5\ {\rm M_J}$, $a \approx 0.05$ AU (Mayor and Queloz, 1995). For a planet shepherded well within this distance, the significant eccentricity excitation by the giant companion may cause it to impact the star.

To examine this possibility, Scenarios I–IV are run for an extra 400 years, allowing the giant in each case to migrate further in to stop at 0.05 AU, with orbital elements stored at a high time-resolution in order to compute resonant angles. Given the $p+q:p$ mean motion resonance (where p and q are integers and q is the order of the resonance), the nominal resonance location of the inner body is:

$$a = \left(\frac{p}{p+q}\right)^{\frac{2}{3}} a' \,, \tag{3.12}$$

where a' is the semi-major axis of the outer body.

The resonant argument is:

$$\theta = (p+q)\lambda' - p\lambda - q\varpi, \tag{3.13}$$

where λ is the mean longitude, ϖ is the longitude of periastron, and primed quantities are those belonging to the outer object (Murray and Dermott, 1999).

The resonant angles are:

$$\phi = (p+q)\lambda' - p\lambda - i\varpi - j\varpi' \,, \tag{3.14}$$

where $\{i, j \in \mathbb{N} \mid i + j = q\}$. Thus, in the case of the 2:1 resonance, there are two resonant angles: $\phi_1 = 2\lambda' - \lambda - \varpi'$ and $\phi_2 = 2\lambda' - \lambda - \varpi$. When two objects are mutually captured into a 2:1 resonance, these angles librate through a restricted range, rather than circulating through 360°.

In Scenarios I & II all the interior planets are driven into the central star. The mechanism at work is illustrated for the case of Scenario I in Fig.3.11 where the semi major axis, periastron and apastron distances, for both the giant and terrestrial planet,

[4]This is done in the context of a fortuitous disk dispersal scenario with Model IV – see Chapter 6.

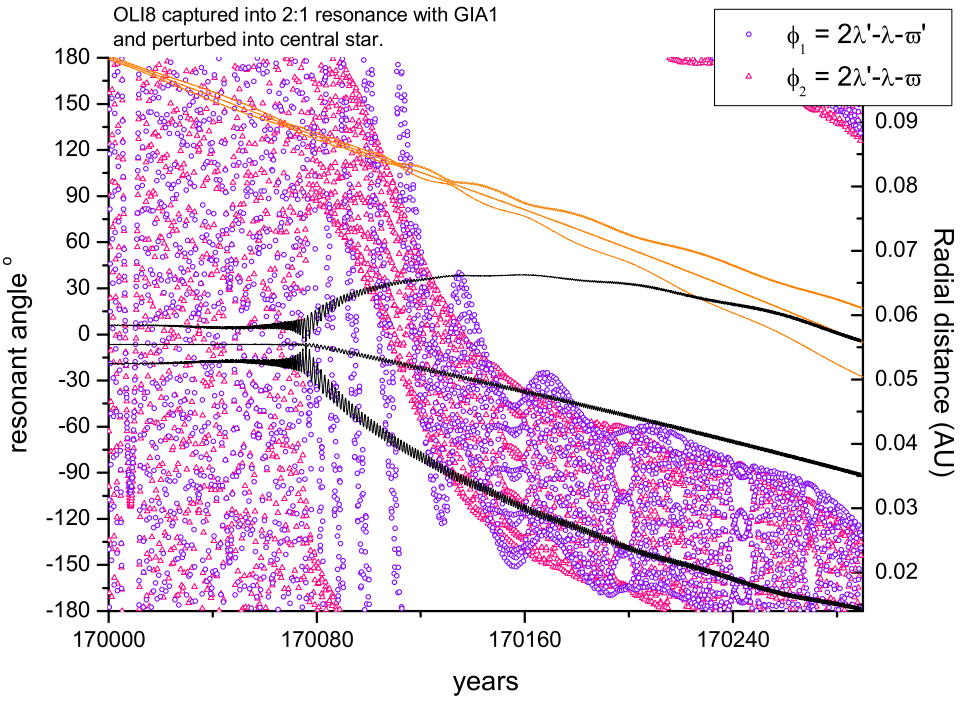

Figure 3.11: Scenario I: collision of the inner planet with the central star as the giant moves inward to 0.05 AU. Resonant angles for the 2:1 resonance are read on the left hand axis. The semi major axis, periastron and apastron for both the giant and the inner planet are plotted as orange and black lines respectively, and are read on the right hand axis.

and the resonant angles for the 2:1 resonance, are all plotted against time. The orbit of the interior planet is initially undisturbed, but when the giant has moved inward to 0.087 AU the planet is captured into the 2:1 resonance as can be seen from the libration of the resonant angles. From this point the planet is pushed in ahead of the giant at the 2:1 resonance, its eccentricity increasing progressively. By the time the planet has reached $a \approx 0.035$ AU, its eccentricity has increased to $e \approx 0.6$ and impact with the star occurs when its periastron falls to 0.014 AU. The events in Scenario II are similar: the migrating giant in this case causes the three interior planets present to accrete each other, capturing the single 14.6 $\mathrm{M}_{\oplus}$ survivor into the 2:1 resonance. From here, evolution proceeds as in Fig.3.11, the planet eventually hitting the star through having been forced into a tighter, more elongated, orbit.

In Scenarios III & IV, both the interior planets survive this additional migration by the giant. This is because their initial orbits are closer to the star (see Table 3.4) so the planet only becomes captured at the 2:1 resonance much later, or not at all.

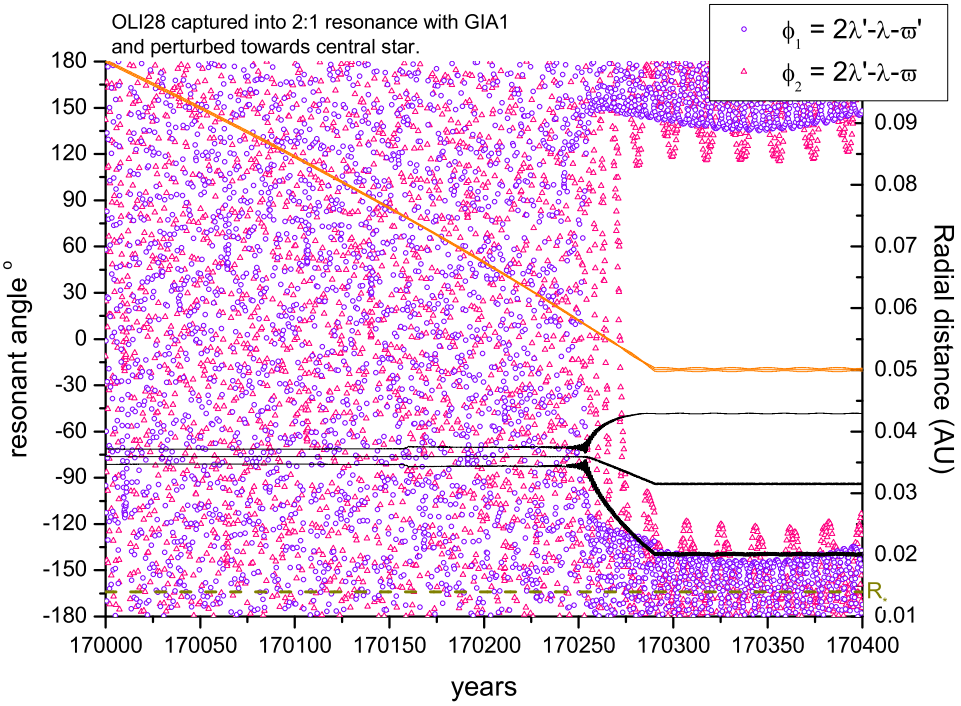

Figure 3.12: Scenario IV: survival of the inner planet as the giant moves inward to 0.05 AU. The semi major axis, periastron and apastron for both the giant and the inner planet are plotted as orange and black lines respectively and are read on the right hand axis.

The interior planet in Scenario III remains stable as the 2:1 resonance does not reach its location and sweeping higher order resonances have no apparent effect. Survival of such a planet for the long term is therefore probable, since orbital decay due to tidal interaction with the star is expected to be very slow (see below). In Scenario IV, the interior planet is captured into the 2:1 resonance late: at the point where the giant reaches 0.057 AU. Its orbit is compressed and elongated to $a = 0.032$ AU and $e = 0.35$ but the progressive increase in eccentricity ceases when the giant finishes migrating and impact with the star is avoided (see Fig.3.12).

The effect of tidal interactions with a slowly rotating star will cause the lower mass planet obtained in Scenarios III and IV to migrate inward slowly. For a circular orbit, once the planet's spin becomes synchronized – which happens quickly, tidal dissipation occurs within the star only, with turbulent convection in the stellar envelope being responsible for dissipating the tidally induced motions. The estimated

orbital evolution time in this case is given by (Terquem *et al.*, 1998):

$$t_{\rm orb} \approx 2.8 \times 10^{-4} \left(\frac{\rm M_\odot}{m_{\rm p}}\right) \left(\frac{P}{1\ {\rm day}}\right)^{\frac{13}{3}}\ {\rm Gyr}. \tag{3.15}$$

where P is the orbital period and $m_{\rm p}$ is the mass of the planet.

For a 15 $\rm M_\oplus$ planet with an orbital period of 1.5 days this gives a orbital decay time of ~ 36 Gyr – i.e. comfortably longer than the age of the universe. For a planet on an eccentric orbit, tidal dissipation within the planet becomes important due to more effective dissipation within the solid body (e.g. Goldreich and Soter, 1966). The raising and dissipation of tides within the planet leads to eccentricity damping, and the low moment of inertia of the planet ensures that it maintains near-synchronous rotation. This also means that effective removal of orbital angular momentum can only be achieved through tidal dissipation in the star. It is expected therefore that a planetary system consisting of an exterior gas giant planet and an interior rocky planet, orbiting in close proximity to a solar type star, will evolve such that the rocky planet orbit decays on a time scale on the order of that given by Eq. (3.15). The inner planet will have an eccentricity determined by a balance between tidal dissipation originating in the planet itself and eccentricity excitation caused by the exterior giant. In general, the long term effects of this will be to make the orbits of both the inner terrestrial and outer giant planet more circular. This will be enhanced by the tidal interaction between the gas giant and the central star which will also tend to circularize its orbit (e.g. Rasio *et al.*, 1996), though this effect is not particularly relevant here as the giant planet is assumed to maintain a near-circular orbit through tidal interaction with the gas disk.

For the specific case of Scenario IV, where the inner planet is in 2:1 resonance with the gas giant, tidal dissipation will cause the rocky planet orbit to circularize at a smaller semi major axis, probably removing the inner planet from the 2:1 resonance in the process. Time scales estimated from Eq. (3.15) indicate that the rocky planet formed in Scenario III will spiral into its host star in ~ 54 Gyr, and that formed in Scenario IV in $\lesssim 700$ Gyr, again durations that are both comfortably longer than the age of the universe.

If the disk shepherding and compaction scenario advanced here has some validity, then it suggests the formation of hot-Neptunes or hot-Earths as a by-product of giant planet migration. However, if the giant comes to rest too close to the star ($\lesssim 0.05$ AU) then the effects of mean motion resonances may cause interior planets to hit the star. The best prospect therefore of detecting close orbiting terrestrial type planets of $\gtrsim \rm M_\oplus$ might be in systems with a circumscribing giant at $a \sim 0.05$ – 1.5 AU.

Table 3.5: External surviving protoplanets at the scenario end points.

Scenario	N	$\bar{m}_{\rm proto}$ ($M_\oplus$)	$m_{\rm max}$ ($M_\oplus$)	$\bar{a}$ (AU)	$a_{\rm min}$ (AU)	$a_{\rm max}$ (AU)	$\bar{e}$	$e_{\rm min}$	$e_{\rm max}$	$\bar{i}^\circ$	$i^\circ_{\rm max}$
I	32	0.13	0.86	4.59	0.63	9.31	0.48	0.19	0.81	5.65	25.18
II	32	0.13	0.86	7.04	1.31	28.24	0.53	0.24	0.86	3.64	9.35
III	25	0.19	0.67	5.81	1.84	13.07	0.47	0.16	0.87	4.33	14.90
IV	23	0.42	0.99	8.18	1.21	33.5	0.53	0.13	0.89	2.71	11.54
V	16	0.55	1.34	10.26	2.42	40.97	0.52	0.10	0.96	4.62	11.33

3.2.4 The exterior scattered disk.

As the giant migrates through the inner disk it scatters ~ 30 – 70% of the disk mass into external orbits (see Figs. 3.10 and Table 3.3). In each case, a diffuse and dynamically excited external disk is generated, composed predominantly of protoplanet material ($f_{\rm proto} \approx 0.7 - 0.9$): individual protoplanets having a wide range of mass and orbital parameters. Data for the external protoplanets are presented in Table 3.5, giving their number, mean and maximum masses and orbital inclinations, and their mean, minimum and maximum semi major axes and eccentricities. It can be seen from the data that the number of external protoplanets reduced and their masses increased with disk maturity. Similarly, there is a tendency for protoplanets from a more mature disk to be more widely scattered. The former trend is primarily due to previous accretion, whereas the latter is a result of the decreased dynamical friction operating at later times.

The ejecta that comprised the scattered disk are spread over a much wider volume than their original location at < 4 AU. Planetesimal orbits are damped quite rapidly by gas drag to form a thin ($\sim 1 - 2\ M_\oplus$) external disk with a surface density $\lesssim$ a few percent of the pre-existing $\Sigma_{\rm s}$. Protoplanets are often in highly eccentric orbits, passing well beyond the confines of the original disk but with their periastra still located close to the location of their scattering within 4 AU. Mean orbital inclinations are comparable to the solar system planets, but with a larger number of outliers as high as $i \approx 25^\circ$ (see Fig. 3.7). Thus, by selectively pushing planetesimals inward and widely scattering its external ejecta, the migrating giant partially evacuates a cavity within its swept zone.

Further accretion in this disk will therefore be characterized by low $\Sigma_{\rm s}$ and high random velocities, reducing both the mass available and the effect of gravitational focussing. In some collisions, impact velocities could be high enough to cause disruption of the protoplanets rather than accretion and a reversal of growth (Agnor and Asphaug, 2004). Long evolution times are implied for the mass contained in the scat-

Table 3.6: Total mass and number of protoplanets orbiting within, or crossing, the habitable zone (0.84 – 1.67 AU) at the scenario end points.

Scenario	In	Crossing	Total
I	0.18 $M_\oplus$	2.13 $M_\oplus$	2.31 $M_\oplus$
	N = 1	N = 8	N = 9
II	0.18 $M_\oplus$	1.79 $M_\oplus$	1.97 $M_\oplus$
	N = 1	N = 5	N = 6
III		1.28 $M_\oplus$	1.28 $M_\oplus$
		N = 4	N = 4
IV	1.17 $M_\oplus$	2.00 $M_\oplus$	3.17 $M_\oplus$
	N = 2	N = 3	N = 5
V		1.34 $M_\oplus$	1.34 $M_\oplus$
		N = 1	N = 1

tered disk to rearrange itself into a smaller number of planets in stable orbits. This final configuration cannot be predicted from the juvenile stage illustrated in Fig. 3.7.

No original matter more distant than the giant's starting position is modelled here. Objects in the external scattered disk traverse more widely than this and so could interact with matter in the outer disk beyond ~ 6 AU. A fresh supply of planetesimals would be encountered which could act to circularize and contract protoplanet orbits via dynamical friction (Thommes *et al.*, 2002). Alternatively, encounters with other giant planets remaining in the outer system could have a role to play in clearing material via ejection. The long term end product of the mass scattered by the migrating giant therefore depends partially on the nature of the outer disk: what other planets have formed there and its remaining population of small bodies. In a hot Jupiter system where no other gas giants have formed, one might speculate over the resulting planetary configuration at ~ 1 Gyr: a hot Neptune, or hot-Earth at ~ 0.05 AU, the giant at ~ 0.1 AU, then from ~ 0.5 AU a succession of Mars to Earth-mass planets, some still in eccentric or inclined orbits, extending as far out as ~ 5 AU. Beyond this, the content of the original outer disk would determine what is to be found.

The ejection of low mass planets to large ($\sim$30 AU) semi-major axes may have some influence on the observed morphology of the system in its debris disk phase. Observational features in systems such as Fomalhaut and ϵ Eridani (Wyatt and Dent, 2002; Quillen and Thorndike, 2002) have been explained by resonant trapping of planetesimals (Wyatt and Dent, 2002) or dust grains in mean motion resonances with a planet. It is possible that the dust trapping proposed by Quillen and Thorndike (2002) will also occur for lower mass planets (they considered $m_\mathrm{p} \approx 30\ M_\oplus$), but is likely to occur for resonances that lie closer to the planet than the 3:2 resonance that

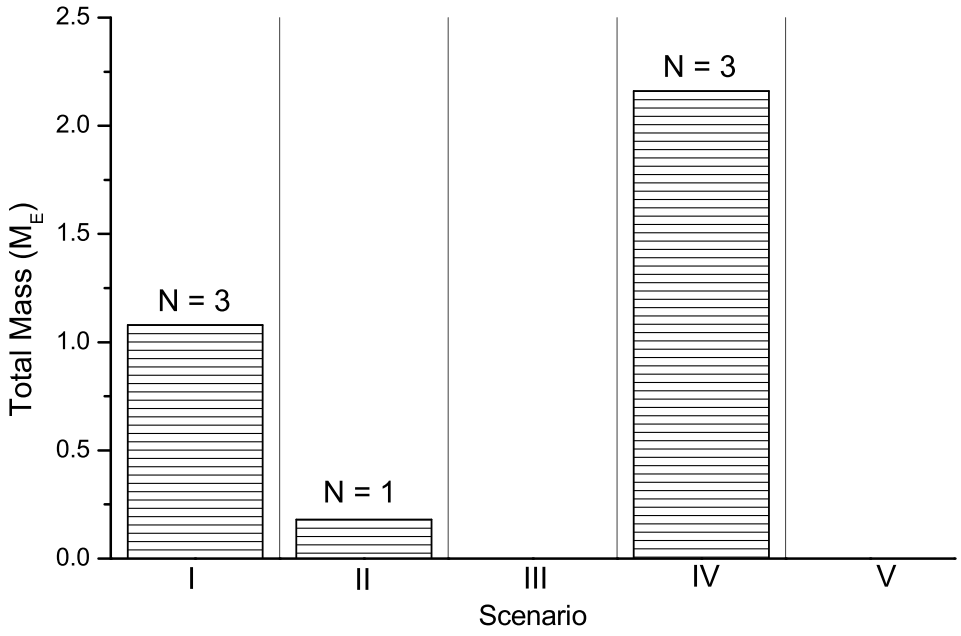

Figure 3.13: Number and total mass of protoplanets predicted in the habitable zone assuming orbital re-circularization with conservation of angular momentum.

was dominant in their study.

What of the probability of one of these surviving planets residing in the system's habitable zone? Habitable zones are dynamically stable in hot Jupiter systems (Menou and Tabachnik, 2003; Jones *et al.*, 2005) so a planet forming there would have a stable orbit if sufficiently well-spaced from neighbors. Model I cannot provide any numerical estimate that might address this question: the simulations have not been run for long enough and, in any case, ignore the strong potential influence of an outer disk. However, protoplanets are found within, or with their orbits passing though, the habitable zone (taken to be 0.84 – 1.67 AU; Kasting *et al.*, 1993) at the end of each run (see Table 3.6). Thus, some mass is available for forming a completed planet in the right place, especially in view of the fact that damping of the protoplanet's orbits from interaction with outer disk material, collisional damping during ensuing accretion, destructive collisions, and gas drag on remaining planetesimals and debris could act to return some material into closer orbits. Assuming eventual re-circularization of orbits with conservation of angular momentum, the data in Table 3.6 convert to those illustrated in Fig. 3.13 which shows, for each scenario, the number of protoplanets and their total mass predicted in the habitable zone. Protoplanets occupy the habitable zone in three out of the five cases and, in two scenarios, more than an Earth-

mass of material is present. Thus, since there is dynamical room available within the habitable zone of a hot Jupiter system, it is perhaps more likely than not that long term evolution of the scattered external disk could result in a terrestrial planet being located there.

3.3 A research programme validated: potential model improvements

The results of Model I contradict the previous view that giant planet migration should clear their inner systems of planet-forming material (see Sect. 1.3), and clearly indicate that a more detailed research programme devoted to the modeling of terrestrial planet formation in hot-Jupiter systems is worthwhile. Inevitably a number of assumptions have been used in constructing Model I, with the consequence that potentially important physical processes have been omitted. These are listed and discussed in Fogg and Nelson (2005) and those incorporated as improvements into this research programme (see Table 2.1) include:

1. *Gap formation & cavity clearing*. A giant planet is expected to form an annular gap in the gas disk centered around its orbit. As a Jupiter mass planet migrates inward, hydrodynamic simulations indicate that the inner disk becomes depleted of gas, forming a low density cavity there (e.g. Nelson *et al.*, 2000). This arises in part because the viscous time scale in the inner disk is shorter than the migration time (see Eq. 3.5). The depletion is probably enhanced artificially by the use of an outflow boundary condition at the disk inner edge, which for computational reasons is located at a radius much larger than the expected surface of the central star. At this time it is not known accurately to what degree the inner disk is depleted, although the use of a 0.5 $\mathrm{M_J}$ planet will lead to significantly less gas depletion than obtained in hydrodynamic simulations performed using more massive planets. Model I assumes an undepleted disk, and the effects of including a disk which viscously evolves and accretes onto the central star are examined in Chapter 4. The expected effect of depleting the gas disk interior to the giant planet will be to reduce the gas drag experienced by the planetesimals. Reducing the dissipation level is likely to lead to greater scattering of bodies into the outer disk by the giant planet, which may reduce the efficiency of planet formation in the inner disk.

2. *Type I migration*. The effects of type I migration, which operates for non–

gap forming sub–Jovian planets (Ward, 1997), are neglected in Model I. This process may become important for bodies more massive than ~ 1 $M_\oplus$, causing inward migration and strong eccentricity damping. For the disk parameters assumed in Model I, type I migration proceeds faster than the gas giant migration for bodies more massive than ~ 5 $M_\oplus$. Such bodies usually form during a rapid burst of accretion as the planet approaches the star, so their formation and subsequent evolution will depend on the gas density in the inner disk, which at present is unknown, as discussed in point 1 above. Type I disk-planet interactions are also thought to include significant eccentricity damping on a timescale $\sim$100 times shorter than the migration timescale (Papaloizou and Larwood, 2000), an effect that could exert additional dissipation on the protoplanets and hence increase their probability of being shepherded by the giant. Type I damping would also effect the evolution of the scattered external disc and would be an additional influence acting to return some planet-forming material into closer orbits. Its integrated effect however would depend on how much of the nebula's gas remains and how much longer it lasts for. Eccentricity damping from a thin residual gas disk could act to circularize the orbits of any final planetary configuration (Agnor and Ward, 2002; Kominami and Ida, 2002), whereas if ample gas persists and type I migration is also in force, a pileup of mass could also occur exterior to the giant as migrating protoplanets are entrained in its exterior mean-motion resonances (Thommes, 2005). It is possible therefore that a modest degree of type I eccentricity damping could promote, rather than hinder, the accretion of a planetary system external to the orbit of the giant planet. These issues are examined in Chapter 5 by including a prescription for type I migration in the model.

3. *Gas disk removal*. Implicit within Model I is a mechanism for preventing the gas giant planet from migrating all the way into the central star. While the presence of a magnetospheric cavity has been cited as a possible stopping mechanism for hot-Jupiters (e.g. Lin *et al.*, 1996), planets are found to exist with a range of semi major axes for which this mechanism cannot be invoked. A more plausible reason for migration halting is the removal of the gas disk during migration (Trilling *et al.*, 1998). The removal of the outer gas disk would remove a source of dissipation for the scattered protoplanets and planetesimals and the effects of dispersing the gas disk via photoevaporation are examined in Chapter 6.

3.4 Model I: conclusions

There are three preliminary conclusions that arise from the results of Model I (Fogg and Nelson, 2005) and which are reappraised through the more detailed models that comprise the remainder of this thesis.

1. Migration of a giant planet through an inner disk partitions the mass of that disk into internal and external remnants. The fraction of disk mass in either remnant is dependent on the level of dissipation and is thus sensitive to the maturity of the disk material at the time of the migration episode. Late migration favors the escape of more material into external orbits. The survival of an inner remnant is also sensitive to the final position of the giant at the end of migration, this becoming increasingly unlikely in hot Jupiter systems with $a \lesssim 0.05$ AU. The concept that giant planet migration would eliminate all the mass in its swept zone is not supported.

2. Hot Neptunes and hot-Earths are a possible by-product of type II migration, being formed from an inner system disk compacted by a migrating giant. Future searches of hot Jupiter systems for radial velocity signals close to the current detection limit might uncover more examples of these planets.

3. It is possible that a number of terrestrial planets orbiting exterior to the giant, including within the system's habitable zone, might eventually accumulate from the external disk remnant. Thus, the early evolution and the final architecture of Hot Jupiter systems does necessarily eliminate their possibility of hosting Earth-like planets.

Chapter 4

Model II: viscous gas disk and self-consistent type II migration

4.1 An improved nebula model

Model I assumed a steady state gas disk model with a constant surface density profile $\propto r^{-1.5}$. The migration rate of the giant was prescribed from a calculation of the local viscous evolution timescale. More realistically, the quantity of nebular gas should decline due to viscous evolution and accretion onto the central star, progressively depleting the inner disk. The gas density should also decrease in the vicinity of the giant due to the generation and dissipation of density waves at Lindblad resonance positions, clearing an annular gap in a zone where the planetary tidal torques dominate the intrinsic viscous torques of the disk. A consistent calculation of the type II migration rate should involve the back-reaction to these tidal torques.

In Model II, the realism with which gas dynamics is simulated is substantially improved (Fogg and Nelson, 2007a). A 1-D evolving viscous gas disk model is linked to the N-body code that: 1) allows the gas to deplete over time via viscous accretion onto the central star; 2) allows an annular gap to form in the vicinity of the giant planet; 3) includes the creation of a partial inner cavity due to dissipation of propagating spiral waves excited by the giant planet; and 4) self-consistently drives the giant inward. Compared to the unevolving gas disk assumed previously, this new model reduces the strength of dissipation present in all scenarios, especially in regions close to the central star and the giant. The strength of gas drag and type II migration forces fall over time due to the declining density of the gas, and dynamical friction falls both due to the accretion of smaller objects (as before) and the fact that their remaining population is progressively less well damped by the attenuating gas (see Table 4.1).

To account for these processes the gas disk is modelled by solving numerically the disk viscous diffusion equation (Pringle, 1981), with modifications included to account for the tidal influence of an embedded giant planet. Such a method has been used previously in studies that attempt to explain the statistical distribution of exoplanetary orbits through type II migration and disk dispersal (Trilling *et al.*, 1998; Armitage *et al.*, 2002; Alibert *et al.*, 2005). The simplest technique for including the effect of the planet is the impulse approximation of Lin and Papaloizou (1986), where wave dissipation is assumed to occur close to the planet. A more sophisticated treatment of the problem is the WKB approximation[1] (Takeuchi *et al.*, 1996) which involves summing the torque contributions from a series of Lindblad resonances in the disk. The former technique was adopted in the studies cited above as it requires considerably less computation and generates comparable results. This approach is

[1] A method for approximating the solution to a differential equation developed by the physicists Wentzel, Kramers and Brillouin in 1926.

Table 4.1: Qualitative indication of dissipative forces present in the models, with emphasis on Model II

Dissipative forces	Models				
	I	II	III	IV	After gas loss
Gas drag	$\leftrightarrow$	$\downarrow$	$\downarrow$	$\downarrow\downarrow$	$\times$
Type II migration	$\leftrightarrow$	$\downarrow$	$\downarrow$	$\downarrow\downarrow$	$\times$
Type I migration	$\times$	$\times$	$\downarrow$	$\downarrow\downarrow$ or $\times$	$\times$
Dynamical friction	$\downarrow$	$\downarrow\downarrow$	$\downarrow\downarrow$	$\downarrow\downarrow$	$\downarrow\downarrow$
Collisional damping	$\leftrightarrow$	$\leftrightarrow$	$\leftrightarrow$	$\leftrightarrow$	$\leftrightarrow$

Key:
$\leftrightarrow$: no change with time
$\downarrow$: reduces with time
$\downarrow\downarrow$: stronger reduction due to late start or combination effect
$\times$: not present

followed here, but in order to include the effect of non-local dissipation of waves that travel far into the disk we also include the WKB approximation torques due to the waves launched at the two innermost and outermost Lindblad resonances.

As before, a MMSN-type protoplanetary disk around a $M_* = 1\ \mathrm{M}_\odot$ star is assumed, as described in Chapter 2, Sect. 2.3, with the initial surface density of solids $\Sigma_\mathrm{s}(r)$ given by Eq. 2.6, the initial surface density of gas $\Sigma_\mathrm{g}(r)$ given by Eq. 2.7, the sound speed c_s given by Eq. 2.9, and the gas scale height h given by Eq. 2.10. Since the kinematic viscosity in an alpha-disk model is $\nu = \alpha h^2 \Omega$, where Ω is the local Keplerian angular velocity, the turbulent shear viscosity function of the disk in cgs units is taken to be:

$$\nu(r) = 9.84 \times 10^{16} \alpha \left(\frac{r}{1\ \mathrm{AU}} \right) \ . \tag{4.1}$$

Since all the models presented here assume a disk alpha viscosity of $\alpha = 2 \times 10^{-3}$, the viscous evolution time of the disk gas at 5 AU is $\tau_\nu(5\ \mathrm{AU}) \approx 120\,000$ years (see Eq. 3.5). This is roughly the time expected for the giant planet to complete its migration in the absence of a significant depletion of the nebular gas.

The diffusion equation for $\Sigma_\mathrm{g}(r)$ is solved in the form:

$$\frac{\partial \Sigma_\mathrm{g}}{\partial t} = \frac{1}{r} \frac{\partial}{\partial r} \left[3 r^{\frac{1}{2}} \frac{\partial}{\partial r} \left(\nu \Sigma_\mathrm{g} r^{\frac{1}{2}} \right) - \frac{2 \Lambda \Sigma_\mathrm{g} r^{\frac{3}{2}}}{(G M_*)^{\frac{1}{2}}} - \frac{T r^{\frac{1}{2}}}{3\pi (G M_*)^{\frac{1}{2}}} \right] \ , \tag{4.2}$$

where the first term in square brackets describes the diffusion of gas under the action of internal viscous torques (Pringle, 1981); the second term describes the impulse

approximation of the local tidal interaction of the planet with the disk, with Λ being the specific torque exerted by the planet (Lin and Papaloizou, 1986); and the third term, which derives from the WKB approximation (Takeuchi *et al.*, 1996), is included to account for more distant angular momentum transfer via the damping of waves launched from the innermost and outermost two Lindblad resonances, with T being a summation of the torque densities exerted by these waves. Because their launch sites stand off a substantial distance from the planet, these waves are expected to be linear and not damped locally in the disk. Their angular momentum content is therefore deposited in the disk through viscous damping as they propagate.

The exchange of angular momentum between the planet and disk leads to a radial migration of the planet at a rate:

$$\frac{\mathrm{d}a}{\mathrm{d}t} = -\left(\frac{a}{GM_*}\right)^{\frac{1}{2}} \frac{1}{m_\mathrm{p}} \left[4\pi \int_{r_\mathrm{in}}^{r_\mathrm{out}} r\Lambda\Sigma_\mathrm{g}\mathrm{d}r + 2\int_{r_\mathrm{in}}^{r_\mathrm{out}} T\mathrm{d}r\right] , \tag{4.3}$$

where m_p is the mass of the planet, a is its semi-major axis and r_in and r_out are the inner and outer boundaries of the disk respectively.

The rate of specific angular momentum transfer to the disk in the impulse approximation is given by Lin and Papaloizou (1986) as:

$$\Lambda = \mathrm{sign}\,(r-a)\ q^2\ \frac{GM_*}{2r}\left(\frac{r}{|\Delta_\mathrm{p}|}\right)^4 , \tag{4.4}$$

where $q = m_\mathrm{p}/M_*$, and $\Delta_\mathrm{p} = \max(h, |r-a|)$. In order to prevent a discontinuous change of sign of Λ at a, an ad hoc approximation is adopted in which $\mathrm{sign}\,(r-a)$ is replaced with $(r-a)/h$ when $|r-a| \leq h$.

The total torque density exerted on the disk in the WKB approximation via the damping of waves excited by the planet is (Takeuchi *et al.*, 1996):

$$T(r) = \sum_m T_m(r) , \tag{4.5}$$

where m is the mode number of the mth order Lindblad resonance at:

$$r_\mathrm{L} = \left(1 \mp \frac{1}{m}\right)^{\frac{2}{3}} a , \tag{4.6}$$

where use of the minus sign gives the radial distances of the inner resonances r_IL and the plus sign those of the outer resonances r_OL. Since only the innermost and outermost two Lindblad resonances are accounted for here, $m = 2, 3$ for the resonance

positions interior and $m = 1, 2$ for those exterior to the planet.

The torque density is calculated from the radial gradient of the angular momentum flux $F_m(r)$:

$$T_m(r) = -\frac{\mathrm{d}F_m(r)}{\mathrm{d}r} \,, \tag{4.7}$$

which is given in Takeuchi *et al.* (1996) as:

$$F_m(r) = F_{m0} \exp\left[-\int_{r_\mathrm{L}}^{r} \left\{ \zeta + \left(\frac{4}{3} + \frac{\kappa^2}{m^2(\Omega - \Omega_\mathrm{p})^2} \right) \nu \right\} \times \frac{m(\Omega_\mathrm{p} - \Omega)}{c_\mathrm{s}^2} k \mathrm{d}\widetilde{r} \right] \,, \tag{4.8}$$

where $F_m(r) = 0$ for $r_\mathrm{IL} < r < r_\mathrm{OL}$, ζ is the bulk viscosity (set here to zero), $\kappa = \Omega$ for a Keplerian disk, Ω_p is the angular velocity of the planet (Eq.3.2) and $k(r)$ is the radial wavenumber:

$$k(r) = \left[\frac{m^2(\Omega - \Omega_\mathrm{p})^2 - \kappa^2}{c_\mathrm{s}^2} \right]^{\frac{1}{2}} \,. \tag{4.9}$$

Takeuchi *et al.* (1996) give this approximation for the angular momentum flux originating at a given $m\mathrm{th}$ order resonance:

$$F_{m0} = \frac{4}{3} m^2 f_\mathrm{c} \Sigma_\mathrm{g}(r_\mathrm{L}) \left(\frac{G m_\mathrm{p}}{a \Omega_\mathrm{p}} \right)^2 \times \left[2\mathrm{K}_0\left(\frac{2}{3}\right) + \mathrm{K}_1\left(\frac{2}{3}\right) - \frac{\pi}{2} \delta_{m,1}(2 \pm 1) \right]^2 \,, \tag{4.10}$$

where K_0 and K_1 are modified Bessel functions, $\delta_{m,1}$ is the Kronecker delta function, and the upper component of the $\pm$ is used for the inner and the lower component for the outer resonances respectively.

The parameter f_c is a torque cutoff function (Artymowicz, 1993) given by:

$$f_\mathrm{c} = \frac{1}{H(1 + 4\xi^2)} \left[\frac{2H\mathrm{K}_0(2H/3) + \mathrm{K}_1(2H/3)}{2\mathrm{K}_0(2/3) + \mathrm{K}_1(2/3)} \right]^2 \,, \tag{4.11}$$

where $H = (1 + \xi^2)^{1/2}$ and $\xi = m(c_\mathrm{s}/a\Omega_\mathrm{p})$.

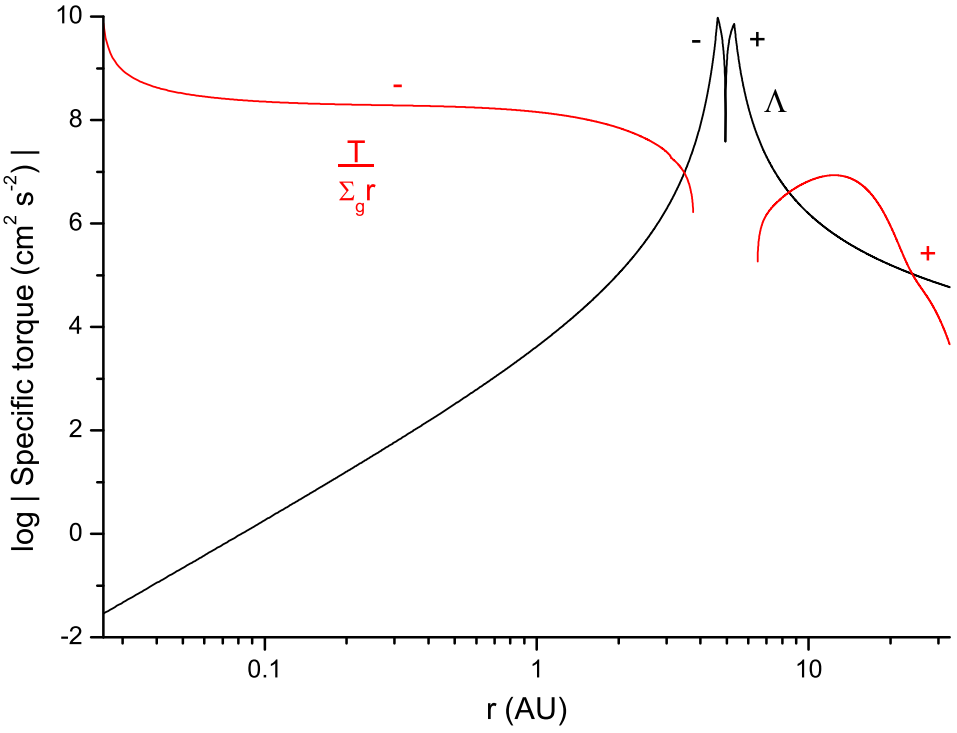

Figure 4.1: Specific torques, plotted as log of the absolute value, generated by the impulse approximation (black) and truncated WKB algorithms (red) with the giant planet at 5 AU. The signs of the torques are labelled.

Results for these two torque calculations, with the 0.5 $\mathrm{M_J}$ giant planet at 5 AU, are shown in Fig. 4.1, plotted as the logarithm of the absolute values of Λ and $T/(\Sigma_g r)$ versus r. Specific torques are negative and positive, interior and exterior to the planet respectively, as it pushes gas away from its vicinity. The strongest torques are generated by the impulse approximation algorithm and occur close to the planet (representing the overall effect of damping of waves of high mode numbers) and are responsible for clearing a gap in the gas and driving type II migration. Those generated by the truncated WKB algorithm dominate in the disk interior and accelerate the loss of gas onto the central star.

The evolution of the nebular gas is computed by solving Eq. 4.2 with an explicit finite-difference technique on a grid with a cell width $\Delta r \propto \sqrt{r}$. The resulting type II migration forces on the giant planet are computed from Eq. 4.3 by deriving an instantaneous time scale, $\tau_{\mathrm{mig}} = a/\dot{a}$, and inserting this into Eq. 3.6. Strong eccentricity damping for the giant planet is assumed, with the damping time scale being 1/50th of the radial migration timescale, as adopted in Model I.

The gas disk adopted here extends from an inner radius $r_{\rm in} = 0.025$ AU to an outer radius of $r_{\rm out} = 33$ AU with an initial gas profile given by Eqs. 2.7 & 2.8. Since a $3 \times$ MMSN disk is considered, $f_{\rm neb} = 3$, $f_{\rm gas} = 240$, and the initial disk mass is $M_{\rm gas} = 0.0398\ {\rm M}_\odot \approx 42\ {\rm M}_{\rm J}$. Note that this initial disk mass is greater than the $2 \times$ MMSN of gas assumed in Model I; however since that amount was kept fixed, the gas present in the simulations presented here falls below this level after $t \approx 140\,000$ years. The boundary conditions for the computation are $\Sigma_{\rm g}(r_{\rm in}) = 0$, representing gas accretion onto the central star and at $r_{\rm out}$ the radial velocity of the gas is set to zero.

To correctly couple the evolving gas disk algorithm with the N-body code, synchronization of their respective time-steps is necessary. In each simulation sub-run (see Sect. 2.5) the symplectic N-body time-step $\tau_{\rm nbody}$ is fixed whereas the gas disk time-step $\tau_{\rm gas}$ is adaptive and taken to be:

$$\tau_{\rm gas} = \min \left(\frac{w\ \Delta r(i)}{|v_r(i)|} \right) \ , \tag{4.12}$$

where i is the grid cell label and w is a coefficient of order unity that is tuned to ensure computational stability. Including all the torques given above, the gas radial velocity is:

$$v_r = 2\sqrt{\frac{r}{GM_*}} \left(\Lambda + \frac{T}{\Sigma_{\rm g} r} \right) - \frac{3}{\Sigma_{\rm g} r^{1/2}} \frac{\partial}{\partial r} \left[\nu \Sigma_{\rm g} r^{1/2} \right] \ . \tag{4.13}$$

Thus, if $\tau_{\rm gas} \geqslant \tau_{\rm nbody}$ then $\tau_{\rm gas} = \tau_{\rm nbody}$; if $\tau_{\rm gas} < \tau_{\rm nbody}$ then the gas disk is evolved for ${\rm INT}(\tau_{\rm nbody}/\tau_{\rm gas})$ steps of duration $\tau_{\rm gas}$ plus an extra step of ${\rm MOD}(\tau_{\rm nbody}/\tau_{\rm gas})$.

4.2 Radial mixing of solid material.

At early times, the solid component of a young protoplanetary nebula will exhibit a radial pattern of chemical composition, controlled by the temperature-dependent condensation sequence of a variety of metals, rock minerals and ices. As the planetary system grows and evolves, phenomena such as dynamical spreading, gas drag induced orbital decay and resonant interactions can cause a radial mixing of material. According to one school of thought (e.g. Morbidelli *et al.*, 2000) the original matter that condensed in the Earth's orbit is thought to have been dry (for an alternative opinion see Drake and Righter, 2002) and the origin of the Earth's water, and its D/H ratio, can be explained if $\sim 10\%$ of the planet's mass is composed of carbonaceous

chondrite-type material, originating from between 2.5 – 4 AU, and $\sim 10\%$ of the water gained thereby is retained at the end of accretion. N-body simulations of terrestrial planet formation from disks that extend out close to the orbit of Jupiter are supportive of this idea and all demonstrate substantial mixing of water rich material into the inner disk (e.g. Morbidelli *et al.*, 2000; Chambers, 2001; Raymond *et al.*, 2004, 2005b, 2007).

In Fogg and Nelson (2005) (Model I: see Chapter 3) it was noted that one consequence of the inward migration of a giant planet is the shepherding of planetesimals that are damped by gas drag (Tanaka and Ida, 1999), and the trapping of bodies at first order mean motion resonances. Hence the outer, more volatile-rich, regions of the protoplanetary disk are actively mixed into its inner regions. However, the composition of planetesimals and protoplanets, and their accretion products, were not logged in the simulations.

This is amended in Model II (Fogg and Nelson, 2007a) by labeling all particles with a composition based on its original position in the disk, and summing the composition of protoplanets as they grow. In a similar manner to most other studies, a crude three-phase initial radial composition is assumed with rocky material originating at < 2 AU, material characteristic of chondritic meteorites between 2 – 2.7 AU, and trans-snowline material at > 2.7 AU. For convenience, these phases are referred to as "dry", "damp" and "wet" respectively but, in contrast to the studies cited above, an actual water mass fraction is not assigned to them. Instead the results are used to make more generalized observations and predictions.

4.3 Running Model II

The initial conditions of Model II, and the preparatory runs to mature the inner solids disk, are handled exactly as described in Chapter 2. The three differences from Model I are: 1) replacement of a steady state gas disk with a viscously evolving one; 2) commencement at $t = 0$ with a full complement of gas (i.e. $f_{\rm gas} = 240$); and 3) Scenario V is only matured to $t = 1.5$ Myr, as not far beyond this there remains too little gas left in the nebula to provide for the gas giant's envelope.

Thus, from $t = 0$, the model is run for 0.1, 0.25, 0.5, 1.0 and 1.5 Myr in the absence of the giant, with $\tau_{\rm nbody} = 8$ days and a simulation inner edge of $r_* = 0.1$ AU. The evolution of the nebular mass over this time span and the particular nebular mass at each of these five epochs are shown in Fig. 4.2. The gas surface density profiles resulting at these times are shown in Fig. 4.3. It is apparent that gas drains onto the central star very rapidly at first, as the density gradient relaxes to a shallower profile.

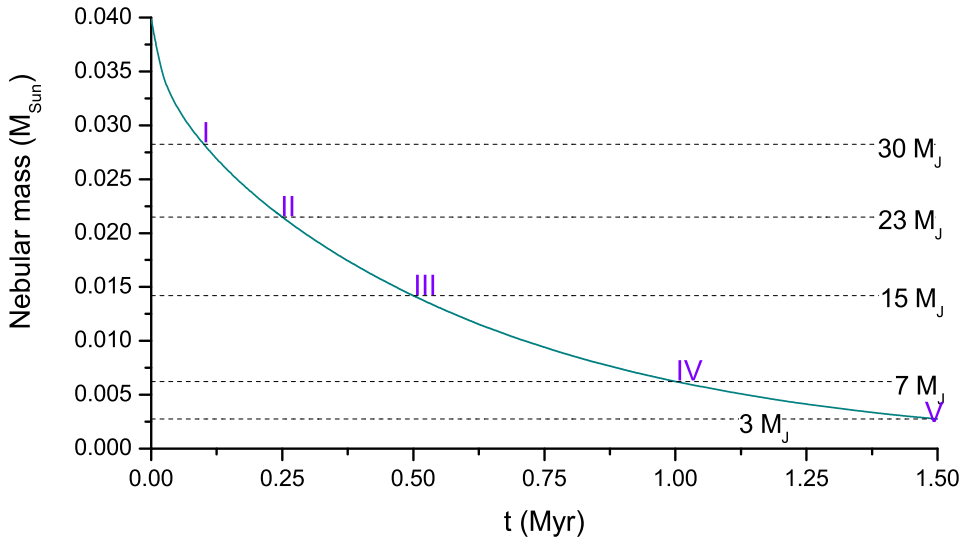

Figure 4.2: Evolution of the mass of the gas disk in Model II. The mass of gas (in Jupiter masses) remaining at the launch point for each of the five migration scenarios is indicated.

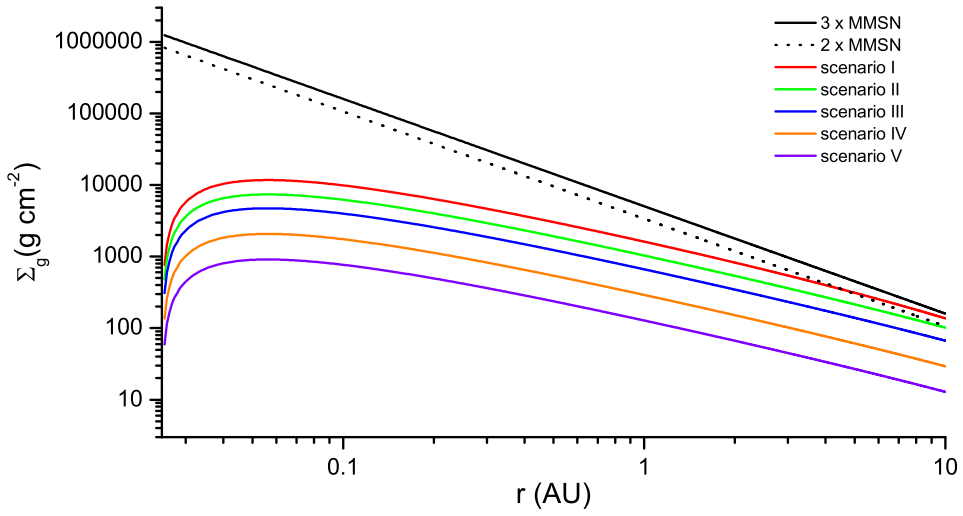

Figure 4.3: Evolution of the gas surface density within the inner 10 AU of the disk. The upper solid line is the $r^{-1.5}$ $\Sigma_{\rm g}$-profile for a $3 \times$ MMSN disk. The lower coloured curves, in descending order, are the profiles at 0.1, 0.25, 0.5, 1.0 and 1.5 Myr respectively. The dashed line is the fixed $\Sigma_{\rm g}$-profile assumed in Model I.

Table 4.2: Overall solids disk data for Model II: after 0.1–1.5 Myr of evolution

Time (Myr)	0.1	0.25	0.5	1.0	1.5
Scenario ID	I	II	III	IV	V
$M_{\rm solid}$ ($M_\oplus$)	24.8	24.8	24.8	24.8	24.8
$m_{\rm max}$ ($M_\oplus$)	0.29	0.37	0.63	1.40	2.13
N	50	47	44	38	34
N'	4031	3665	3036	2342	1964
$f_{\rm proto}$	0.19	0.26	0.37	0.51	0.59

Compared to the unevolved profile, order of magnitude reductions in gas density occur within the disk's inner regions. Data for the evolved solid components are given in Table 4.2 and include the values of $m_{\rm max}$, the mass of the largest protoplanet to have evolved in each case. The advance of planetary growth with time is indicated by the progressive increase of $m_{\rm max}$ and $f_{\rm proto}$ and the reduction in particle numbers as super-planetesimals are accreted and protoplanets merge. When compared to the equivalent data from Model I, no planetesimals are lost beyond the inner edge of the simulation because of much lower gas densities near the central star.

The five type II migration scenarios prepared for Model II are constructed from the five evolved nebulae indicated in Fig. 4.2 and summarized in Table 4.2. The state of their solids components are illustrated in the example of the disk maturation process given in Chapter 2 – see Fig. 2.2. Scenarios I – III take place whilst the solids disk remains in its oligarchic growth phase ($f_{\rm proto} < 0.5$) whereas Scenarios IV – V have just entered the final giant impact stage of growth ($f_{\rm proto} > 0.5$). A giant planet of mass $0.5\ M_{\rm J}$ is placed into each simulation at 5.0 AU after removing $0.4\ M_{\rm J}$ of gas from between 3 – 7 AU. The giant then proceeds to clear out a tidally generated annular gap in the disk and migrates inward according to the orbital evolution equations described in Sect. 4.1. Since $h/r \propto r^{1/4}$ (as given by Eq. 2.10), $\tau_{\rm mig} \equiv \tau_\nu \propto a$, so $\dot{a} \sim$ constant and the runs are halted once the giant reaches 0.1 AU (see Fig. 4.4). For Scenarios I – III, this takes $t_{\rm s} \approx 110\,000 - 120\,000$ years, close to the prediction of the viscous evolution time τ_ν given by Eq. 3.5. The process takes longer to complete in the cases of Scenarios IV – V ($t_{\rm s} \approx 150\,000$ and $220\,000$ years respectively) because by the time of the appearance of the giant planet the gas disk is substantially depleted and is less effective at driving migration. The migration time in such lightweight disks is longer than the local viscous evolution time as it is based on the time required for a mass of gas roughly equal to the mass of the giant to accrete through the disk and accumulate outside the planetary orbit (Syer and Clarke, 1995; Ivanov *et al.*, 1999). As before, the simulation inner edge is contracted down to a realistic T-Tauri star radius: $r_* = 0.014$ AU $\cong 3\ R_\odot$ after the appearance of the giant in order to

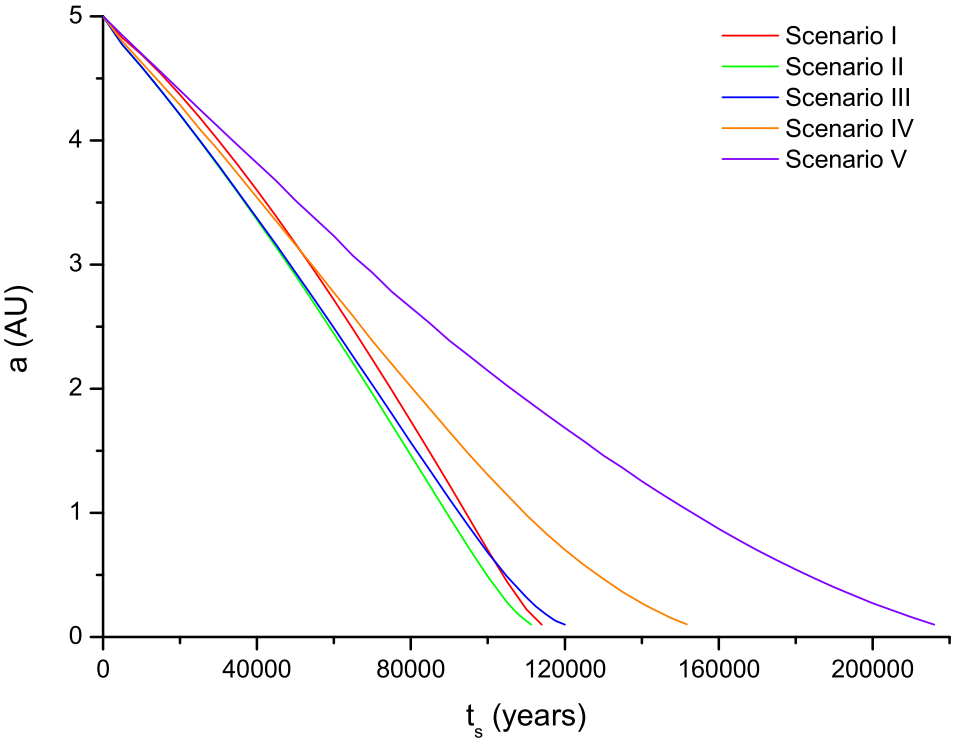

Figure 4.4: Semi-major axis evolution of the giant planet in each scenario normalized to the launch time (the top row in Table 4.2)

better model processes at small radial distances. The initial time-step chosen for the symplectic integrator was $\tau_{\rm nbody} = 6$ days, but it was necessary to reduce this at late times as material is driven into closer orbits. Hence each scenario was divided into a number of sequential sub-runs with $\tau_{\rm nbody}$ being adjusted at each re-start so as to keep the time-step close to one tenth the orbital period of the innermost object. Since planetesimals in this new model suffer less orbital decay due to gas drag, it is possible to conduct these runs with a higher value of $\tau_{\rm nbody}$ than in Model I. However, this advantage is negated, especially at late times, due to the computational load of the gas disk algorithm and the fact that its adaptive time-step $\tau_{\rm gas}$ (Eq. 4.12) falls steeply as the giant planet moves within 1 AU. From $t = 0$, the scenarios presented here each required 4 – 8 weeks of 2.8 GHz CPU-time for completion, over double that required for Model I.

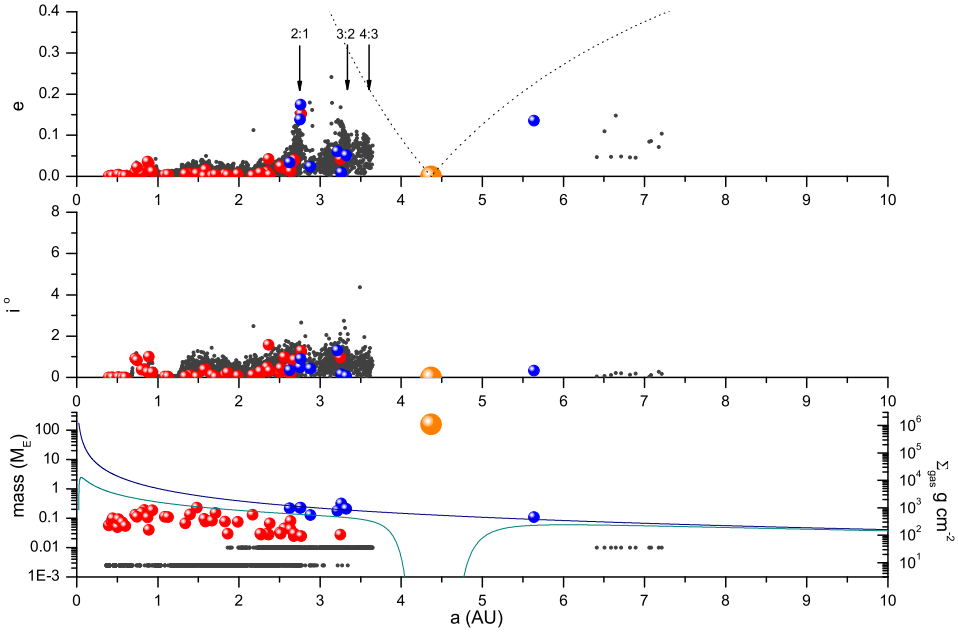

Figure 4.5: Scenario I at $t_s = 20\,000$ years, showing the mass, inclination and eccentricity of objects. Small black dots represent super-planetesimals; red symbols are rocky protoplanets; blue symbols are icy protoplanets and the large orange symbol is the giant. Objects plotted between the dotted lines in the upper panel have orbits that intersect the orbit of the giant. The location of the 2:1, 3:2 and 4:3 resonances with the giant are indicated. Gas surface density is read on the right hand axis of the lower panel, the upper curve being the unevolved profile at $t = 0$ and the lower curve being the current profile.

4.4 Results of Model II

4.4.1 Typical features of a run

The results of all scenarios showed a number of behavioural features in common. As in Model I, these are illustrated first by describing the results of Scenario I in detail. The issues of how the results differ between scenarios (dependence on disk maturity) and how the results differ from those of Model I are then examined.

The typical effects of a migrating giant planet on an inner solids disk observed in Model I were as follows: 1) shepherding of planetesimals; 2) capture of objects at first order mean motion resonances; 3) acceleration of accretion interior to the giant with possible hot-Neptune or hot-Earth formation; and 4) generation of a scattered exterior disk. To a greater or lesser extent, these features are also observed in Model II.

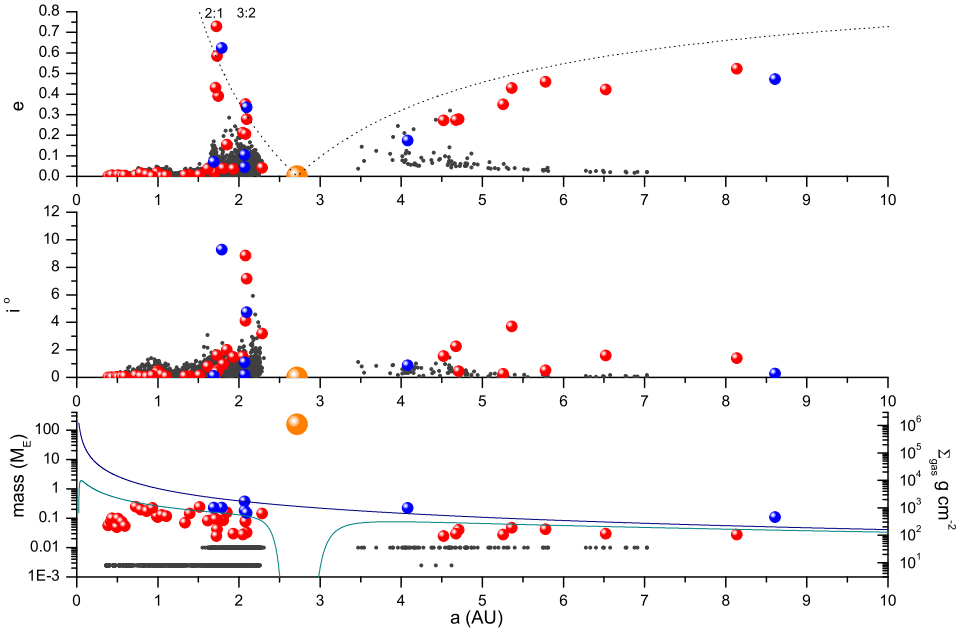

Figure 4.6: Scenario I at $t_s = 60\,000$ years. The giant has now moved inward to 2.72 AU. Increasing excitation of the orbits of protoplanets captured at resonances is apparent, as is the build-up of matter scattered into external orbits.

Four snapshots of the evolution of Scenario I are illustrated in Figs. 4.5–4.8, showing the mass, inclination and eccentricity of objects, and the gas surface density vs. semi-major axis. The original provenance of the protoplanets (interior or exterior to the snowline) is denoted by the shading of its symbol as described in the caption to Fig. 4.5. In the case of a merger between rocky and icy protoplanets, this shading is determined by that of the most massive of the pair.

An early stage in the evolution of Scenario I, 20 000 years after the introduction of the giant planet, is shown in Fig. 4.5. The giant has opened a ~ 0.75 AU gap in the gas and has migrated inward to 4.37 AU, shepherding the outer disk edge at the 4:3 resonance, now at 3.61 AU. Capture of objects at the 3:2 and 2:1 resonances, at 3.33 and 2.75 AU respectively, is apparent from eccentricity spikes visible in the upper panel and a clustering of protoplanets in the lower panel. Even at this early phase, before the giant has entered the original confines of the interior disk, one protoplanet and a handful of super-planetesimals have been scattered into external orbits.

The system midway through the run, 60 000 years after the introduction of the giant planet, is shown in Fig. 4.6. The giant has now migrated to 2.72 AU, putting the positions of the 3:2 and 2:1 resonances at 2.07 and 1.71 AU respectively. Strong

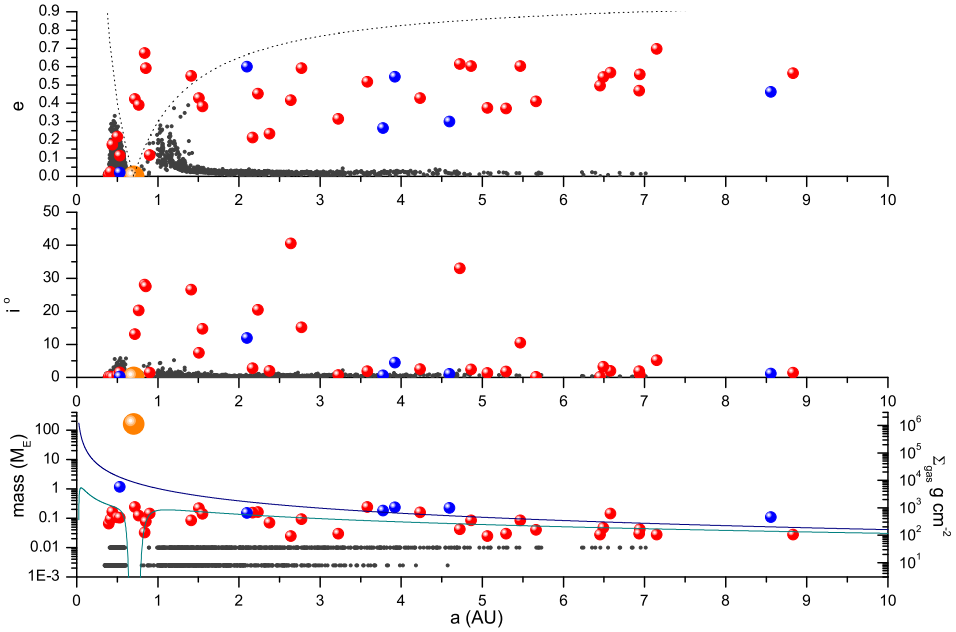

Figure 4.7: Scenario I at $t_s = 100\,000$ years. The giant has now moved inward to 0.70 AU. Five protoplanets are currently crossing the orbit of the giant. The scattered disk has grown and a $> 1\ M_\oplus$ planet is accreting within the compacted interior disk.

excitation of protoplanetary orbits is now apparent at these locations, as is the build-up of scattered material in external orbits. The primary mechanism of this expulsion is evident from the behaviour of material captured at resonances. Continuous resonant pumping results in orbits becoming eccentric enough to eventually intersect the orbit of the giant planet. A series of close encounters with the giant then follows, eventually resulting in a final encounter where the object is accreted or expelled into a non-intersecting exterior orbit.

An advanced stage of Scenario I, 100 000 years after the introduction of the giant planet is shown in Fig. 4.7. The giant planet is now at 0.70 AU and the 3:2 and 2:1 resonances are at 0.54 and 0.44 AU respectively. A substantial scattered external disk has now formed and sufficient gas remains in this early scenario to rapidly damp the orbits of scattered planetesimals. An impression of the scattering process in action is given by the five protoplanets currently crossing the giant's orbit. The interior disk is compacted to high surface densities, but now that strong first order resonances with the giant are influential throughout its width, and gas densities have fallen by a factor of > 10, there is a noticeable dynamical stirring of its entire remaining population. Nevertheless, accretion has speeded up in this shepherded zone with the growth of

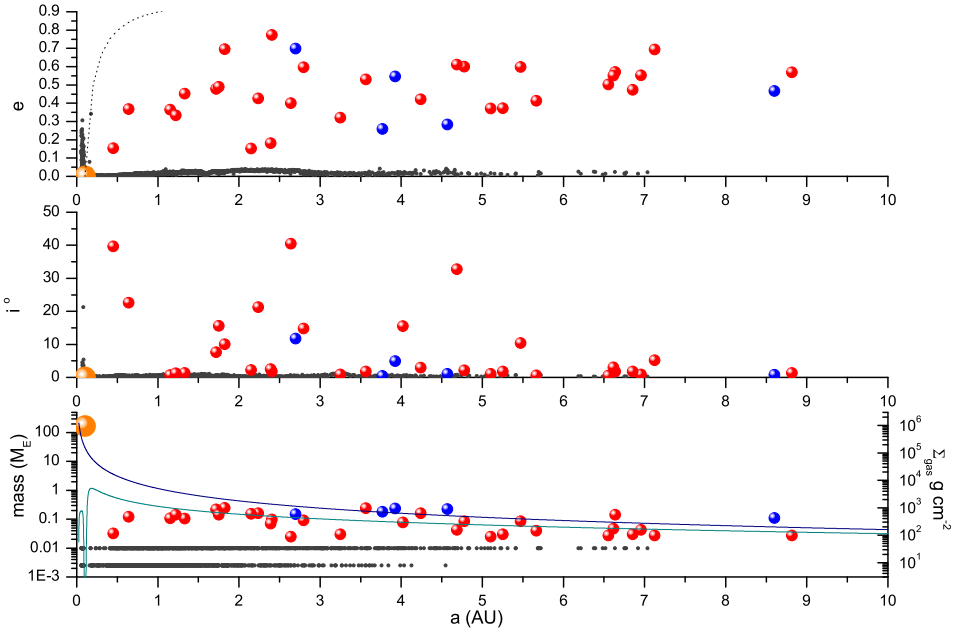

Figure 4.8: Scenario I at $t_s = 114\,000$ years. The giant planet has migrated to 0.1 AU. Most interior mass has been lost after the most massive interior protoplanet impacts the giant. 63% of the original solids disk mass now resides in exterior orbits.

one protoplanet of 1.17 $M_\oplus$ at 0.53 AU outrunning that of its neighbors.

Scenario I is terminated at $t_s = 114\,000$ years when the giant planet arrives at 0.1 AU and the system is illustrated at this point in Fig. 4.8. Two thirds of the original solids disk mass has survived the migration episode – the great majority of this residing in the scattered exterior disk. Most of the remainder has been accreted by the giant planet. Just $\sim 4\%$ of the original disk mass remains interior to the giant and none of this is in the form of large bodies. The rapidly accreting interior protoplanet seen in Fig. 4.7 continued its inward progress close to the 3:2 resonance position with its orbit being well-damped by strong collisional damping and dynamical friction from planetesimals and smaller protoplanets (see Fig. 4.12 in Sect. 4.4.4). However, ~ 2000 years before its demise, the protoplanet drifted outward and became captured at the 4:3 resonance. At this location, both accretion and dynamical friction were reduced allowing the protoplanet's orbit to become progressively more eccentric. At 109 220 years the protoplanet, now weighing in at 2.41 $M_\oplus$, collided with and was accreted by the giant. The five other less massive interior planets visible in Fig. 4.7 grew very little, remaining between $\sim 0.03 - 0.2$ $M_\oplus$, and in due course one of them impacted the giant and four were scattered.

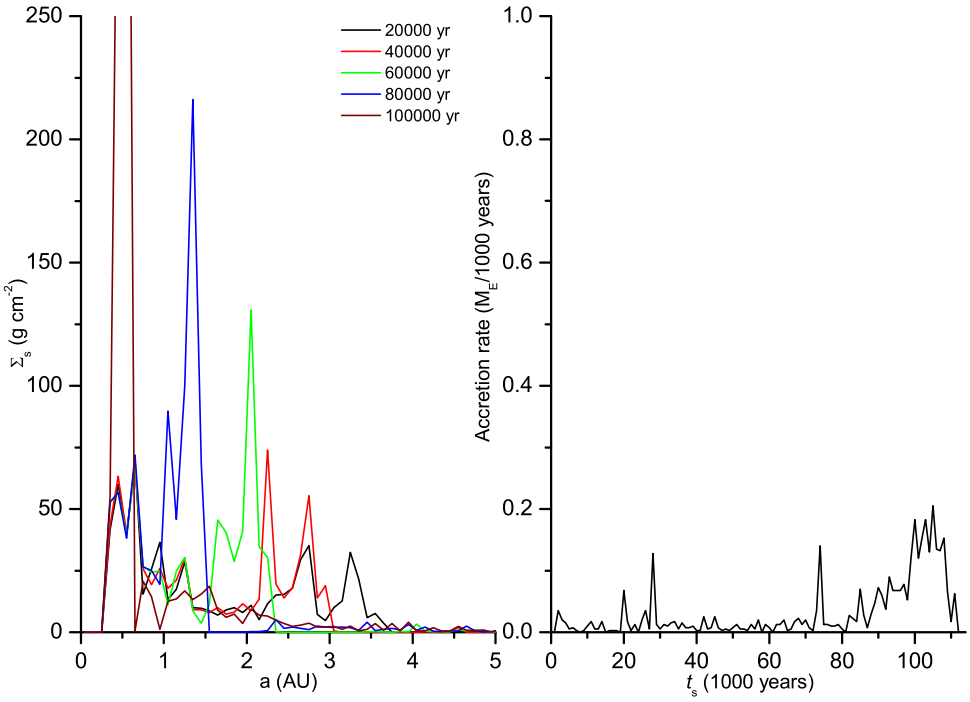

Figure 4.9: Surface density evolution (left hand panel) and accretion rates (right hand panel) for Scenario I. Growing surface density peaks at the 2:1 and 3:2 resonances sweep through the inner system ahead of the giant. Accretion rates increase after $\sim 80\,000$ years within the compacted portion of the disk.

To emphasize the above description of Scenario I, the surface density evolution of the disk and its accretion rate are shown in Fig. 4.9. The left hand panel shows the disk surface density profile (obtained by summing all protoplanets and super-planetesimals in 0.1 AU width bins) at $t_{\rm s} = 20\,000$, 40 000, 60 000, 80 000 and 100 000 years; the right hand panel plots the amount of mass accreted onto protoplanets only (including protoplanet mergers) every 1 000 years for the duration of the run. In the $\Sigma_{\rm s}$ plot, two surface density enhancements are clearly visible as spikes at the 3:2 and 2:1 resonances and are seen to grow whilst moving inward. At $t_{\rm s} = 80\,000$ years, these have almost merged into one: the shepherded portion of the original disk having by now been squeezed into a dense ring. By 100 000 years, most of this mass is now confined within 0.6 AU and $\Sigma_{\rm s}$ here has risen to $\sim$ 500 g cm^{-2} which is off the vertical scale in the figure. This amounts to an increase by a factor of ~ 10 over the previous, undisturbed, disk surface density, but is only about half the increase seen in the equivalent Scenario presented in Model I.

The effect of this disk compaction process is visible in the accretion rate plot.

Mass accretion rises significantly after 80 000 years due to both the high values of $\Sigma_{\rm s}$ and the fact that much of this mass now resides in a zone where dynamical times are shorter. However, the large, terminal, accretion rate spike described in Model I is not reproduced here (compare Fig. 4.9 with Fig.3.8). This is because close to the end of that previous simulation a 15.65 $\rm M_{\oplus}$ hot-Neptune was assembled in a dramatic phase of runaway accretion interior to 0.1 AU (see Fig.3.7). In the case presented here the compacted interior disk is only half as dense and is much less well damped (note the large difference between the upper and lower gas density curves in Fig. 4.8) and, whilst a protoplanet does grow to 2.41 $\rm M_{\oplus}$ in this region, as described above, it does not survive and is accreted by the giant planet. The formation and fate of interior planets is described in more detail in Sect. 4.4.4.

4.4.2 Dependence on the maturity of the inner disk

The reason for running five scenarios through a progressively more mature inner disk is to see if the timing of migration has any systematic effect on the results. This is possible as the partitioning of the solids disk between inner and outer remnants is influenced by the level of damping that particles are subject to, which declines with age. In Model I, where $\Sigma_g(r)$ is fixed, this occurs as a side effect of accretion: as planetesimals are accreted by protoplanets ($f_{\rm proto}$ increases), fewer small particles remain that are subject to gas drag and which can exert dynamical friction. In Model II, since the gas disk evolves via viscous accretion onto the central star, the strength of gas drag on susceptible particles also declines with time and is particularly marked close to the central star and giant planet.

The characteristics of the five systems at the end point of each scenario are illustrated in Fig. 4.10 and can be compared with the results of Model I by referring to Fig. 3.9. Data describing the fate of the solids disk mass at the end of each scenario are shown in Table 4.3. Disk mass that is lost is either accreted by the central star, ejected from the system, or accreted by the giant planet; that which survives is partitioned between bodies orbiting interior or exterior to the final orbit of the giant planet at 0.1 AU.

For the reasons discussed in Sect 3.2.2, a negligible quantity of mass was ejected in all scenarios. However, in contrast to Model I, negligible mass was also lost to the central star and a significant fraction of the disk mass (14 – 33%) was accreted by the giant, especially towards the end of the migration. At these late times, planetesimals are shepherded into the partially evacuated inner regions of the gas disk where gas drag is less effective at damping orbital perturbations from the giant and

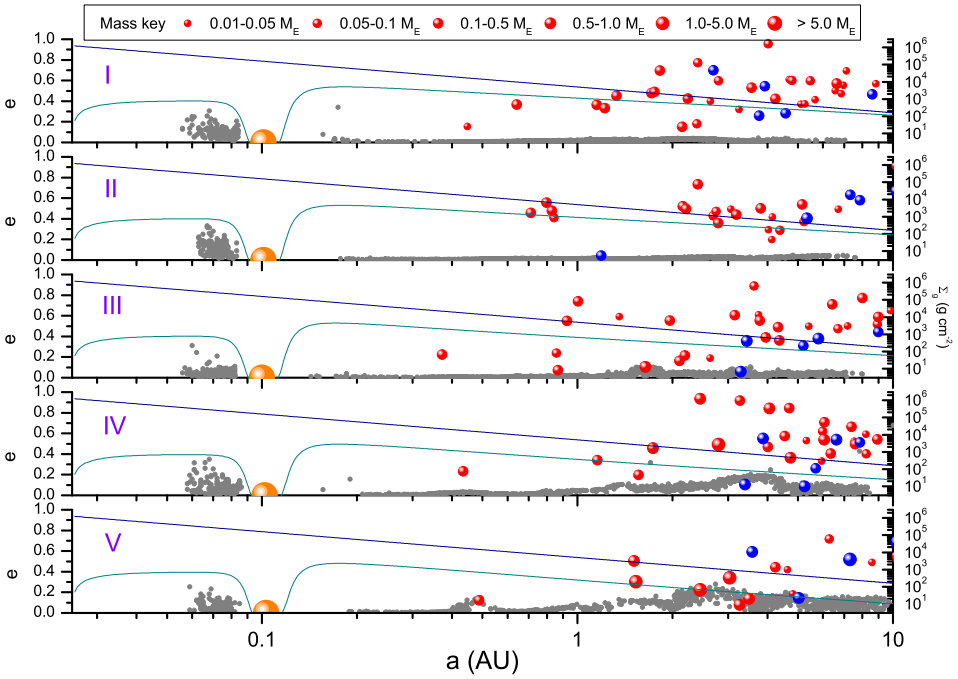

Figure 4.10: End points of all five scenarios at the point where the giant planet stops at 0.1 AU. Semi-major axis a is plotted on a log scale vs. eccentricity e. Gas surface density in $\mathrm{g\ cm^{-2}}$ is read off the right hand axes, the upper curve being the unevolved profile at $t = 0$ and the lower curve being the current profile.

Table 4.3: Fate of the disk mass at the scenario end points.

Scenario	I	II	III	IV	V
Total Initial Solids ($\mathrm{M_\oplus}$)	24.81	24.81	24.81	24.81	24.81
Total Surviving Solids ($\mathrm{M_\oplus}$)	16.60 (67%)	16.69 (67%)	17.40 (70%)	21.23 (86%)	20.22 (81%)
Interior Surviving Solids ($\mathrm{M_\oplus}$)	0.88 (4%)	0.65 (2%)	1.00 (4%)	0.84 (3%)	0.31 (1%)
N, f_{proto}	0, 0	0, 0	0, 0	0, 0	0, 0
Exterior Surviving Solids ($\mathrm{M_\oplus}$)	15.72 (63%)	16.04 (65%)	16.40 (66%)	20.39 (82%)	19.90 (80%)
N, f_{proto}	39, 0.27	29, 0.28	33, 0.42	31, 0.63	23, 0.66
Accreted by Star ($\mathrm{M_\oplus}$)	0.01 (0.04%)	0.01 (0.04%)	0.11 (0.4%)	0.0 (0%)	0.0 (0%)
Accreted by Giant ($\mathrm{M_\oplus}$)	8.20 (33%)	7.85 (32%)	6.77 (27%)	3.41 (14%)	4.59 (19%)
Ejected ($\mathrm{M_\oplus}$)	0.00 (0%)	0.26 (1%)	0.51 (2%)	0.17 (1%)	0.0 (0%)

growing protoplanets. Once a planetesimal strays into the annular gap in the gas containing the giant, gas drag vanishes and accretion or scattering by the giant follows. This increased excitation of the shepherded planetesimal population, and the thinning down of their number, renders them less effective at damping protoplanetary orbits via dynamical friction and collisions. Hence, at late times the orbits of the remaining interior protoplanets also tend to destabilize, with one of the same two fates in store. A trend can be seen in Table 4.3 for the giant planet to accrete less material with disk maturity. This occurs because as the disk ages the gas density and the solids mass fraction in small bodies both decline, resulting in less dynamical dissipation of both planetesimals and protoplanets. Less matter is shepherded and more is scattered in such mature disks so there is less of an interior remnant for the giant to accrete from at late times.

In all scenarios, a large majority of the disk solids are found to survive the migration episode – over two thirds of the original inventory. Table 4.3 shows only a weak trend with disk maturity in the partitioning of surviving mass between interior and exterior remnants. Just a few percent of the mass remains interior to the giant in all cases. When the giant planet migrates through a disk undergoing oligarchic growth ($f_{\rm proto} < 0.5$; Scenarios I – III) $\sim 65\%$ of the original disk mass survives by being scattered into the exterior disk and most of the remainder is accreted by the giant at late times. This exterior fraction increases for less dissipative disks undergoing giant impact-style growth ($f_{\rm proto} > 0.5$; Scenarios IV – V) to $> 80\%$.

4.4.3 Dependence on an evolving gas disk.

The salient dynamical behaviours of solids disk particles such as shepherding, resonant capture, scattering by the giant planet and eventual partition into interior and exterior remnants are observed generally in the results of Model II and those of Model I. However, the introduction of an evolving gas disk causes the relative predominance of these outcomes to differ. This is because both the principal sources of dissipation, dynamical friction and gas drag, fall with time, whereas in Model I only the former declines. There are five systematic differences between the results of Model I and those presented in this Chapter.

1. Much less mass is lost to the central star.

2. Much more mass is accreted by the giant planet.

3. Disk partitioning between inner and outer remnants is much less sensitive to disk maturity.

4. The protoplanet mass fraction ($f_{\rm proto}$) in the exterior scattered disk is lower.

5. Interior hot-Neptune-type planets grow to smaller masses and do not survive.

The reasons for the first two items are the large reductions in gas density close to the central star and in the vicinity of the giant planet. Planetesimals do not have time to spiral into the central star and feel little eccentricity damping when close to the giant because of the low gas drag in these regions. The reasons for the last three items stem from the fact that the system is less dissipative so scattering behaviour predominates over shepherding at all epochs. Interior remnants are consistently much smaller than outer remnants which always include $> 60\%$ of the original solids disk mass. The increased tendency for planetesimals to scatter means that there is less of a fractionation of planetesimals from protoplanets between interior and exterior remnants. More planetesimals are expelled into the exterior disk and hence its overall mass fraction contained in protoplanets ($f_{\rm proto}$) is lower.

These tendencies are illustrated in Fig. 4.11 where the percent of the original solids disk mass surviving at the end of the simulations presented here are compared with the simulation results from Model I. Interior and exterior remnants are plotted as dashed and solid lines respectively; red lines are the results of Model I and blue lines are those of Model II. It can be seen that partitioning varies strongly with disk maturity in the case of a steady-state gas model and weakly, if at all, when the nebula gas is allowed to viscously evolve. Since gas drag does not decline in the former case, the shepherding of planetesimals is more influential and more mass remains in the interior remnant in early scenarios, which is mostly contained in surviving hot-Neptune-type planets. Late scenarios from Model I behave more similarly to the ones presented here as a greater fraction of the solids disk mass is contained within protoplanets, which do not feel the gas, and their source of dissipation, dynamical friction, is weaker due to a decline in super-planetesimal numbers. [2]

The increased tendency in the present model for planetesimals to scatter into the exterior disk can also be appreciated from Fig. 4.11 by comparing, for the two models, the ratio of the protoplanet mass fraction in the final exterior disk to that of the original disk, $f_{\rm proto}({\rm final})/f_{\rm proto}({\rm initial})$. If the scattering process does not discriminate between protoplanets and planetesimals, and there is no further accretion after scattering, this ratio would remain at $f_{\rm proto}({\rm final})/f_{\rm proto}({\rm initial}) = 1$. Subsequent accretion will raise this ratio, but not by much over the timescale considered, especially as accretion rates are reduced in the exterior disk due to its dy-

[2]Note that Scenario V is less comparable to its counterpart in Model I as it is initiated at a different time, 1.5 Myr earlier.

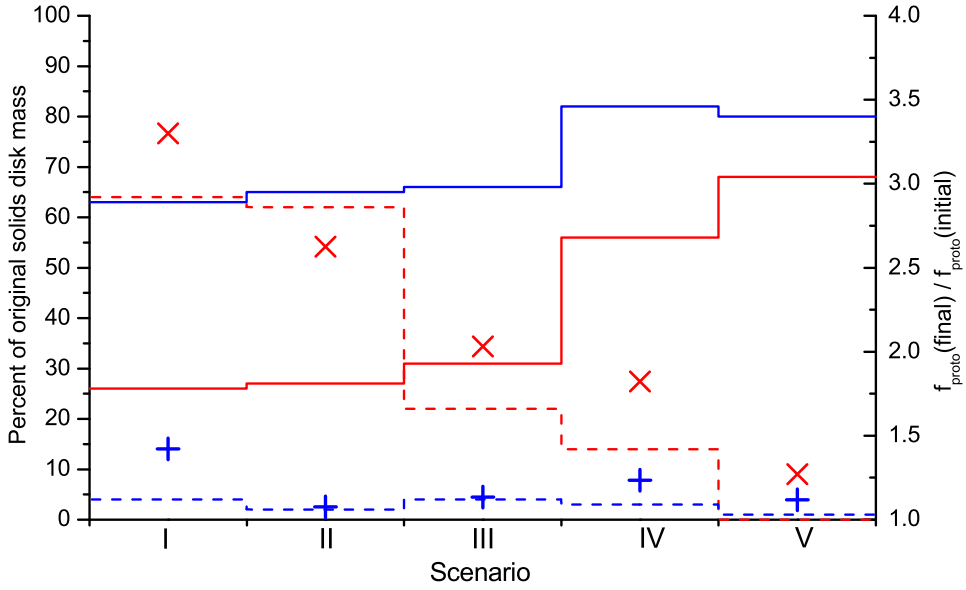

Figure 4.11: Comparison of the results of Model I (red lines and $\times$ symbols) and the results of Model II (blue lines and $+$ symbols). Dashed lines and solid lines are the percentage of original disk mass found in the interior and exterior remnants respectively. The ratios of the protoplanet mass fraction in the final exterior disk to that of the original disk, $f_{\rm proto}({\rm final})\ /f_{\rm proto}({\rm initial})$, are indicated by the $\times$ and $+$ symbols and are read off the right hand y-axis.

namically excited state. Reading from the right hand y-axis, Fig. 4.11 shows that $f_{\rm proto}({\rm final})/f_{\rm proto}({\rm initial}) < 1.5$ for all of Model II results whereas much higher values are obtained from Model I. Protoplanets are preferentially scattered into the exterior disk when there is strong and unvarying gas drag, whereas fractionation is much less marked when gas drag declines over time and falls to near zero in the vicinity of the giant planet.

4.4.4 Formation and survival of hot–Neptunes

A striking feature of the results of Model I was the growth and survival, interior to the final orbit of the giant, of hot-Neptune and hot-Earth type planets ranging between $\sim 2-16\ {\rm M}_\oplus$. *No such planets are found to survive in Model II*. Accelerated accretion in the shepherded disk is observed with some protoplanets growing to $\sim 1-3\ {\rm M}_\oplus$ (see Figs. 4.7 and 4.9), but in each scenario their eventual fate was to impact the giant planet just before the end of the simulation. After formation, these planets become locked in a mean motion resonance (3:2 or 4:3) with the giant, and subsequent

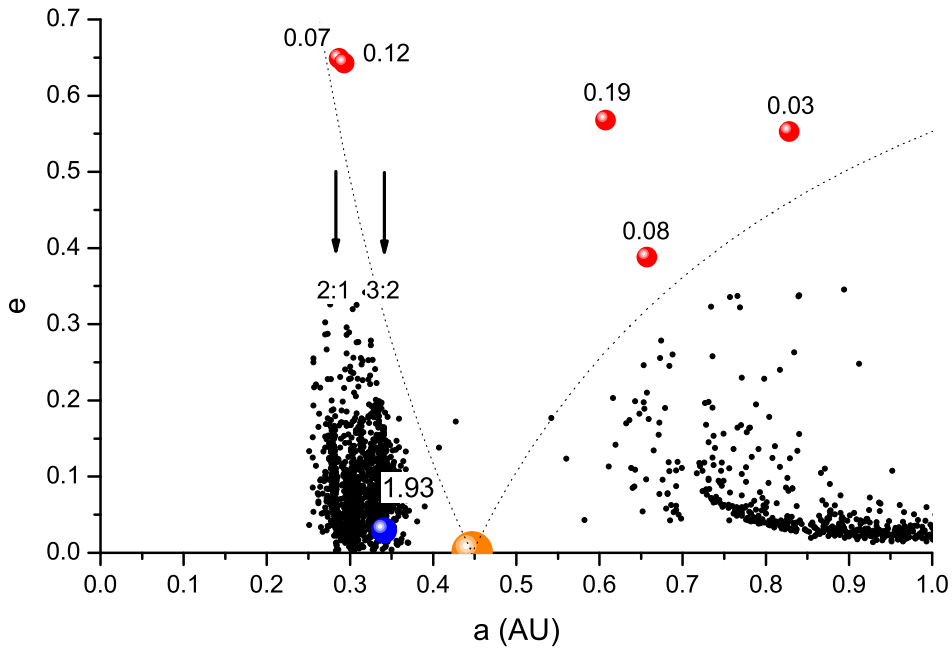

Figure 4.12: Blow-up of the inner 1 AU of Scenario I, showing eccentricity vs semi-major axis at $t_s = 105\,000$ years. Protoplanetary masses are indicated in $M_\oplus$ and the locations of the 2:1 and 3:2 resonances are shown with arrows. The giant planet is at 0.48 AU and the hot-Earth candidate is a $1.93\ M_\oplus$ planet at 0.34 AU with $e \approx 0.03$. Five lower mass protoplanets are in the process of being scattered into the exterior disk. (Compare with Fig. 4.7 which shows the situation 5 000 years earlier.) As described in Sect. 4.4.1, the hot-Earth candidate is eventually accreted by the giant planet $\sim 4\,000$ years later once it has migrated further inward to ~ 0.26 AU.

eccentricity pumping during migration leads to collision and merger with the giant shortly before migration halts. However, had giant planet migration halted earlier, at ~ 0.25 – 0.5 AU instead of 0.1 AU, Model II would still predict the existence of hot–Earths (e.g. see Fig. 4.12).

In order to examine further the sensitivity of hot-Earth formation and survival to the quantity of gas remaining interior to the giant planet, supplementary calculations have been performed, very similar to those presented in this Chapter, in which the effect of dissipating spiral waves travelling into the disk is switched off (i.e. $T(r) = 0$ in Eq. 4.2). This term helps create a partial inner cavity in the gas disk as the planet migrates inward and removing its influence results in a more dense and dissipative disk interior. These modified calculations produce interior planets ranging in mass ~ 2 – 4 $M_\oplus$ during giant planet migration. A variety of final outcomes are noted: 1)

some of them are accreted by the giant planet; 2) others are scattered externally into stable orbits at $a \sim 0.4$ AU; and 3) a few remain in interior orbits, typically close to 0.076 AU (the 3:2 resonance). These results, taken alongside the five scenarios of Model II and those from Model I show a distinct trend: a strongly dissipating gas disk interior to the giant planet leads to the formation of fairly massive, hot–Neptune–like planets which survive; a gas disk of lower density leads to the formation of lower mass interior planets that often do not survive.

It is worth noting at this point that Model II neglects some potentially important sources of dissipation due to general uncertainty about how planetary formation can proceed in their presence, such as type I migration (Ward, 1997; Tanaka *et al.*, 2002; Tanaka and Ward, 2004) and the circularization of orbits due to stellar tides. Associated with the former is strong eccentricity and inclination damping of low mass planets which may facilitate the survival of inner planets. This possibility is investigated in Model III, presented in Chapter 5. Tidal damping of orbits however is unlikely to have a significant effect on the results because all shepherded protoplanets are scattered or accreted by the giant at $a \gtrsim 0.1$ AU. Whilst tidal circularization times at these radii are uncertain, due to the uncertainty of Q, they probably range from $\sim 10^8 - 10^{10}$ yr (Goldreich and Soter, 1966), orders of magnitude greater than the millennia it takes for hot-Jupiters to traverse the final 0.5 AU of their migration.

4.4.5 The exterior scattered disk.

The exterior solids disks generated by the giant planet migration are dynamically excited and spread over a greater radial extent than the original disk. However, in the Model I scenarios only $\sim 1 - 2$ $\mathrm{M}_\oplus$ of planetesimals are scattered into the exterior disk, whereas in Model II this quantity rises to $\sim 8 - 11$ $\mathrm{M}_\oplus$. In addition, planetesimals are not scattered as widely as protoplanets and their excited orbits damp rapidly when remote from the influence of the giant planet. Whilst the decline in gas drag with time lessens this trend in later scenarios, in all cases the inner regions of scattered disks generated by Model II remain well populated.

There is a greater similarity between the models in the outcome of scattering of the protoplanetary population and Model II data for the external protoplanets are shown in Table 4.4, giving their number, mean and maximum masses and orbital inclinations, and their mean, minimum and maximum semi major axes and eccentricities. As expected, protoplanetary numbers fall and masses rise with disk maturity, an effect largely due to prior accretion before the appearance of the giant planet. Allowing for stochastic events, such as giant impacts and strong scatterings, these data are

Table 4.4: Data describing the external surviving protoplanets at the end of giant planet migration.

Scenario	N	$\bar{m}_{\rm proto}$ ($M_\oplus$)	$m_{\rm max}$ ($M_\oplus$)	$\bar{a}$ (AU)	$a_{\rm min}$ (AU)	$a_{\rm max}$ (AU)	$\bar{e}$	$e_{\rm min}$	$e_{\rm max}$	$\bar{i}^\circ$	$i^\circ_{\rm max}$
I	39	0.11	0.25	5.43	0.45	37.92	0.51	0.15	0.99	8.85	40.45
II	29	0.16	0.74	4.99	0.71	15.25	0.49	0.045	0.91	8.59	35.45
III	33	0.21	0.64	4.68	0.37	12.22	0.46	0.059	0.89	8.32	43.97
IV	31	0.41	2.35	5.16	0.43	8.92	0.50	0.086	0.94	5.81	41.93
V	23	0.57	2.19	6.88	0.49	18.18	0.45	0.079	0.83	3.53	16.24

much the same in Model I (compare Table 3.5), as are the mean semi-major axes and eccentricities ($\bar{a} \approx 5$ AU, $\bar{e} \approx 0.5$). However the minimum values of the semi-major axes and eccentricities ($a_{\rm min}$ and $e_{\rm min}$) are lower than in Model I. This is because late-shepherded protoplanets tend to scatter rather than assembling into hot-Neptunes and their resultant orbits damp more rapidly as many more planetesimals are available to exert dynamical friction.

4.5 Post–migration terrestrial planet formation

What do the results of the five scenarios presented here have to say about the probability of forming terrestrial planets in the scattered disks ? Considering the Scenarios I – V overall, if the factor of long–term importance is the mass distribution, rather than initial dynamics, then such planets should form and await discovery in hot–Jupiter systems. This point is made in Fig. 4.13 where the total solids mass with semi-major axes between 0.75 – 1.75 AU, before and after giant planet migration, is plotted for each scenario. A clear trend is visible for less matter to be found in this region with increasing disk maturity as it is more widely scattered. Mass dispersal in late scenarios, however, is partially offset by the pre-existing inward evolution of material in more mature disks which enhances the mass present in inner regions. It is also offset by the fact that fairly massive protoplanets are scattered into the external disk in late Scenarios (IV and V – see table 4.4), so that terrestrial planet formation in the scattered disk has already received a significant boost from accretion prior to and during migration. In all cases, more than $2\ M_\oplus$ of planet forming material remains in the 'maximum greenhouse' habitable zone ($\sim$ 0.84 – 1.67 AU; Kasting *et al.*, 1993) of the system after the passage of the giant planet.

Extending the runs for the additional $\sim$ 100 Myr it would take to form a completed external planetary system is impractical. The principal difficulty is the presence of the hot–Jupiter at 0.1 AU which limits the time-step size to an excessively

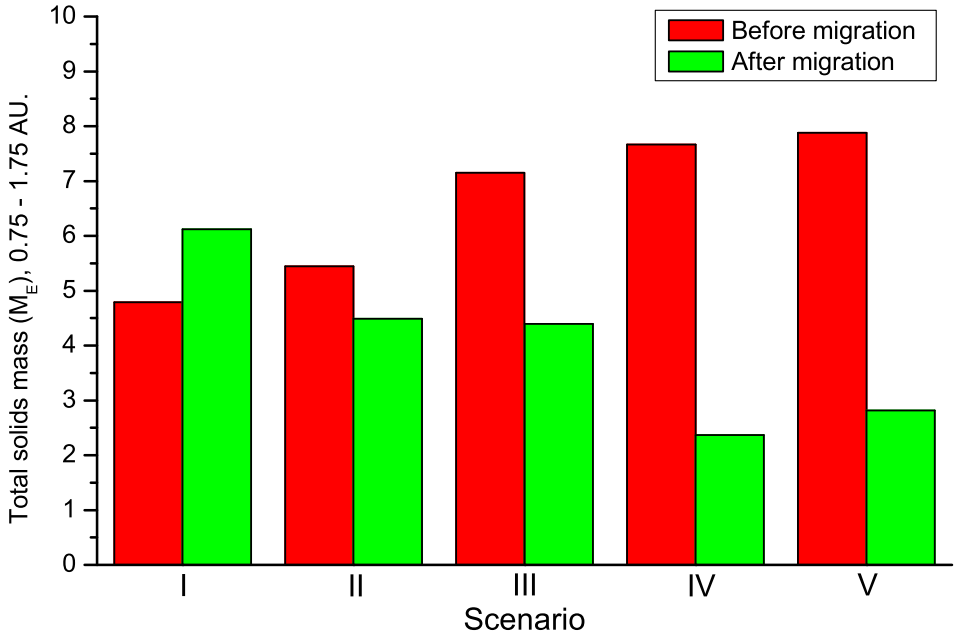

Figure 4.13: The total solids mass between 0.75 – 1.75 AU, before and after the giant planet migration, plotted for each scenario.

low value. Modeling of planetary growth in Scenario V however has been extended for an additional 30 Myr to demonstrate that (apparently stable) terrestrial planets *do* form in the habitable zone of this system.

All super planetesimals interior to the giant planet are removed (they are of little consequence as they are non-self interacting and are not accompanied by a proto-planet that can accrete them); and since the gas density is low when migration of the giant planet halts in Scenario V, rapid removal of the remnant gas is assumed *via* photoevaporation and the system is evolved in the absence of gas with an N-body time-step of $\tau_{\rm nbody} = 1$ day.

Fig. 4.14 shows the region between 0 – 4 AU for the scattered disk of Scenario V at the point when the giant planet reaches 0.1 AU (top panel). Protoplanets of substantial size have been scattered into the external disk, eight of them having semi-major axes within 4 AU, along with a significant population of planetesimals, which are generally in less excited orbits due to the drag of the residual gas. The result after a further 30 Myr of gas-free accretion is shown in the bottom panel.

Dynamical friction is sufficient to have caused a general damping of protoplanetary orbits at the expense of excitation of the planetesimals, the majority of which

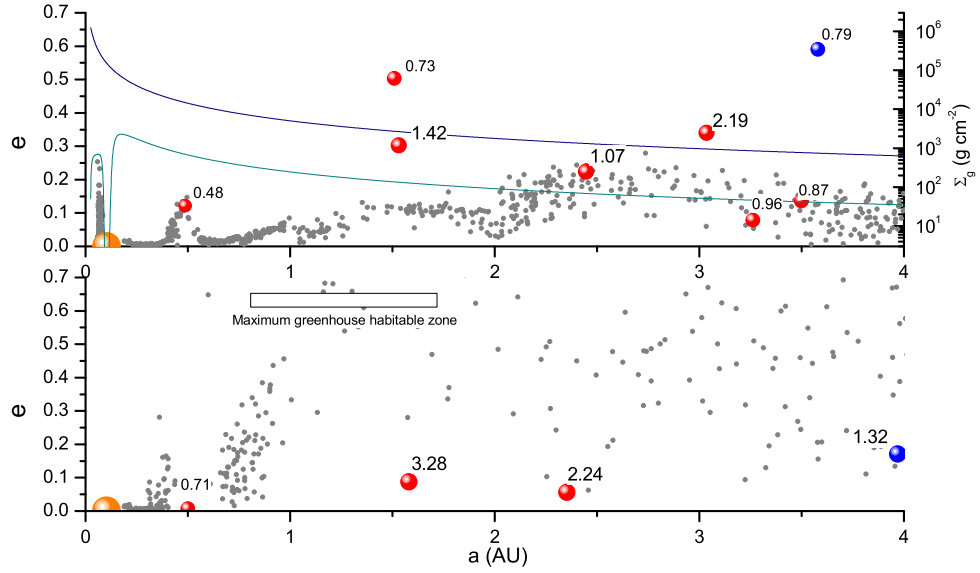

Figure 4.14: Eccentricity versus semi-major axis for bodies within 4 AU at the end of Scenario V (top panel) and after a further 30 Myr of gas-free accretion (bottom panel). Protoplanets are red or blue symbols and are labelled with their mass in $\mathrm{M}_\oplus$. Super-planetesimals are grey dots and the orange symbol at 0.1 AU is the hot-Jupiter in its post-migration orbit. Gas density at the end of Scenario V is shown as the lower curve in the top panel (read off the right-hand axis), the upper curve being the unevolved profile at $t = 0$.

have been cleared from the plotted region due to accretion, outward scattering, and ejection. The system's largest terrestrial planet, a 3.28 $\mathrm{M}_\oplus$ body sited within the 'maximum greenhouse' habitable zone with $a = 1.58$ AU, $e = 0.09$, results from two giant impacts within the first 3 Myr of the extended run between the original 1.42, 1.07 and 0.73 $\mathrm{M}_\oplus$ protoplanets, along with some subsequent sweep-up of planetesimals. The original 2.19 $\mathrm{M}_\oplus$ protoplanet grows via planetesimal accretion only to 2.24 $\mathrm{M}_\oplus$, but moves inward to $a = 2.35$ AU after a phase of strong dynamical interactions which result in the scattering of the two 0.96 and 0.87 $\mathrm{M}_\oplus$ protoplanets out to ~ 6 – 7 AU. The 0.79 $\mathrm{M}_\oplus$ protoplanet shown in blue in the upper panel of the figure does not survive and undergoes a giant impact with a larger body at ~ 4.9 AU, whereas the 1.32 $\mathrm{M}_\oplus$ planet at ~ 4 AU in the bottom panel is an interloper, having undergone a net scattering inwards from ~ 7 AU. The protoplanet that grows most effectively at the expense of smaller bodies is the innermost protoplanet at ~ 0.5 AU, which is embedded within a well-populated and initially well-damped annulus of planetesimals from which there are rich pickings.

The emergence of a stable terrestrial planetary system from such a configuration shown in the lower panel of Fig. 4.14 seems highly probable, and this result provides a clear prediction that terrestrial planets will be found in the habitable zones of hot–Jupiter systems (see also Raymond *et al.*, 2006; Mandell *et al.*, 2007).

What will be the physical nature of such planets? The issue of disk and protoplanet composition after migration is discussed in Sect. 4.6. Here it is noted that the 3.28 and 2.24 $M_\oplus$ planets observed in Fig. 4.14 are composed of $\sim 32\%$ and 45% of material originating from beyond the snowline, respectively. Assuming that trans–snowline planetesimals and protoplanets contain 75% water, a naive prediction is that these planets will contain between 20 – 30 % water by mass. The current water inventory of the Earth is estimated to be ~ 0.1 % by mass. Evidently terrestrial planets forming in the habitable zones of hot–Jupiter systems are likely to host deep global oceans – essentially being 'water-worlds' (Kuchner, 2003; L*é*ger *et al.*, 2004), even if significant loss of volatiles occurs during high–impact accretion.

This prediction about water content, however, depends on the giant planet forming out beyond the inner edge of the snowline, rather than at its inner edge. The closer to the inner edge the giant forms, the smaller the amount of volatile-rich material that will be shepherded inward, and the lower the degree of volatile enrichment experienced by terrestrial planets forming after migration of the giant.

4.6 Migration-driven compositional mixing.

A result found in all Scenarios I–V is homogenization of the solids disk composition. This mixing occurs as the giant planet drives material inward from the outer part of the disk whilst generating the external disk via random scattering. An example is given in Fig. 4.15 which shows, for Scenario I, the composition of the solids disk before migration (top panel) and that of the surviving external disk after migration (bottom panel). In each case the total mass of solid material is plotted in 0.5 AU width bins with the histograms labelled "dry", "damp" and "wet" representing rocky material originating at < 2 AU, material characteristic of chondritic meteorites between 2 – 2.7 AU, and trans-snowline material at > 2.7 AU, respectively. It is evident that a large amount of material from beyond the snowline is shepherded into the inner regions before being left behind. Compositional mixing is similar in other scenarios, although a little less smooth in Scenarios IV & V which have had more time to accrete substantial protoplanets from local material before the appearance of the giant planet.

In contrast to other studies of water delivery to terrestrial planets (e.g. Morbidelli *et al.*, 2000; Chambers, 2001; Raymond *et al.*, 2004, 2005a,b, 2006, 2007), an actual

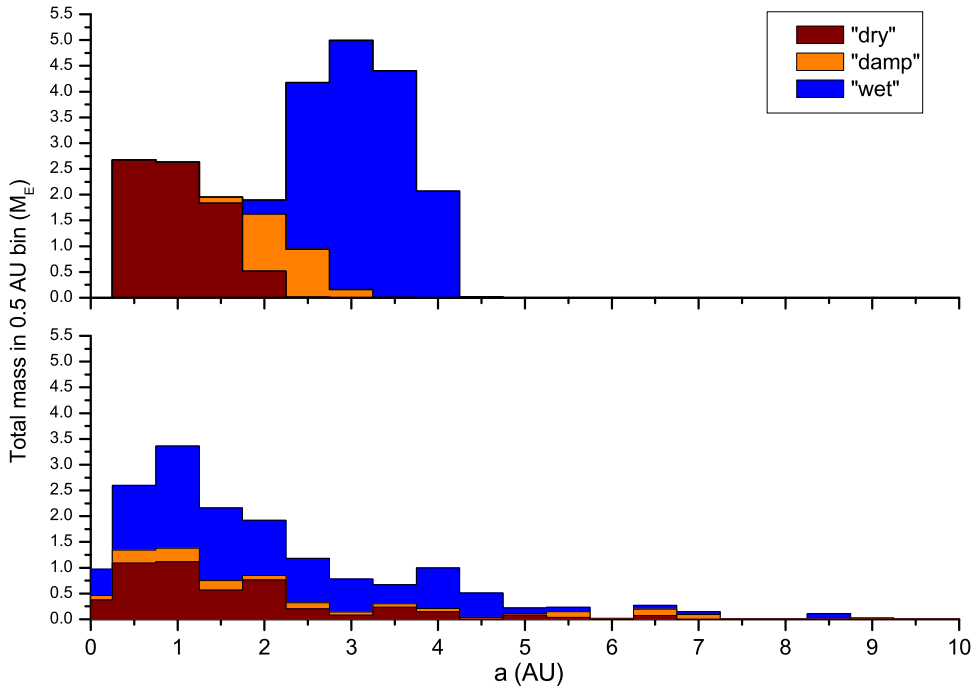

Figure 4.15: Composition of the original solids disk in Scenario I (top panel) compared with the composition of the scattered disk generated through giant planet migration (bottom panel). The key is explained in the text.

water mass fraction to is not assigned to the compositional phases. This is because the simulations do not extend to the completion of planetary accretion and the assumed MMSN-type original solids surface density profile, which includes a large step-increase at 2.7 AU (see Eq. 2.6), is different from those adopted in the above-cited papers making a detailed comparison difficult. The typical finding is that at the end point for early-migration scenarios (I – III) originally dry protoplanets that have found their way into the scattered disk contain 0 – 25% of trans-snowline material, but are surrounded by a large quantity of volatile-rich planetesimals from which to accrete further. In later scenarios (IV – V), where the surviving protoplanets are more mature, this range increases to 5 – 70%, and whilst there is less remaining mass in small bodies to sweep up in these systems, the accretion of volatile-rich material is not yet complete.

In general one can predict that the final terrestrial planets that form in hot-Jupiter systems are likely to be much more volatile-rich than the Earth, those in the habitable zone ending up with $> 10\%$ of their material originating from beyond the snowline. Accretion in the external disk, however, may pass through an early high velocity phase

before completion with some protoplanets potentially losing much of their volatile inventory during giant impacts (Genda and Abe, 2005; Asphaug *et al.*, 2006; Canup and Pierazzo, 2006). Since water-rich planetesimals are abundant throughout our external disks, however, protoplanets that have lost their original volatile endowment in a catastrophic event should be able to re-acquire some water before planetary accretion is complete. Dry terrestrial planets appear improbable in hot-Jupiter systems whereas Earth-like worlds and planets with deep global oceans (Raymond *et al.*, 2006; Fogg and Nelson, 2007a; Mandell *et al.*, 2007) may well be commonplace.

4.7 Model II: conclusions

In common with Model I, the results of Model II indicate that the outcome of giant planet migration through an inner system disk is a combination of shepherding of the original solids ahead of the giant, and random scattering of the majority of this compacted material into orbits external to the giant. The net effect is not a disappearance of planetary building blocks from the inner system, but rather a stirring and mixing of material originally formed at different radial distances.

Now that more realistic gas dynamics are included, generating partial cavity formation close to the central star, gap formation in the vicinity of the giant planet's orbit, consistent type II migration rates, and a decline in the overall mass of gas present with time, the following qualitative differences are found between the results of Model II and Model I:

1. Scattering is favored over shepherding irrespective of the maturity of the inner solids disk at the epoch of giant planet migration. This occurs because of the rapid loss of gas from the disk interior to the giant, and in the vicinity of the giant planet's orbit, which reduces the damping of planetesimal trajectories. The efficiency of shepherding and dynamical friction is therefore reduced, increasing the probability that a given body will come close enough to the giant to be scattered into an external orbit. In all our scenarios $\gtrsim 60\%$ of the original solids disk material survives in a regenerated external disk.

2. The principal mass loss mechanism is accretion by the giant planet, rather than the central star. This is because gas densities close to the central star are reduced by 2 – 3 orders of magnitude, suppressing the gas-drag-induced orbital decay of planetesimals and allowing the giant planet to catch up with and sweep through even the innermost solids disk material. Most accretion by the giant occurs at

late times when scattering by the giant becomes less effective due to the system being contained deep within the star's gravitational potential well.

3. Hot-Neptune and/or hot-Earth survival is not favored in Model II because of the enhanced tendency of the giant planet to scatter material outward and to accrete material at late times during the migration. Accelerated protoplanetary accretion within the compacted shepherded portion of the disk is observed, with objects growing to several $\mathrm{M}_{\oplus}$, but their orbits typically destabilize at late times due to capture in eccentricity–pumping mean motion resonances, resulting in eventual collision with the giant planet. However, due to the sensitivity of the results to levels of dissipation close to the central star at late times, and the potential influence of type I migration and eccentricity damping that is neglected, it is premature to rule out the possibility that hot–Neptunes or hot–Earths can form and survive interior to Jovian planets during their migration to become hot–Jupiters. This issue is investigated in detail in the next Chapter.

4. Whilst terrestrial planet formation in hot-Jupiter systems was predicted from the results of Model I, the external disks generated by Model II appear to be even more benign places for this to occur. These disks contain a greater mass of material, are less dispersed, and are composed of a higher fraction of small bodies capable of exerting dynamical friction and hence damping the excited orbits of scattered protoplanets. The formation of terrestrial planets of masses in the range $1 \lesssim m_{\rm p} \lesssim 3\ \mathrm{M}_{\oplus}$ occurred in or near the habitable zone during a simulation continued after the giant stopped migrating. The radial mixing of volatile–rich material from beyond the snowline means that terrestrial planets forming in the habitable zones of hot–Jupiter systems are likely to be "water–worlds", hosting deep, global oceans.

Chapter 5

Model III: type I migration affecting protoplanets

5.1 Including type I migration

The most striking difference between the outcomes of Models I & II is the presence of hot-Neptunes or hot-Earths, orbiting interior to the hot-Jupiter, as an outcome of the former model, and their complete absence as an outcome of the latter. Since Model II is the more realistic, as it includes a time-dependent gas disk, its results cast doubt on the disk compaction hypothesis for the origin of hot-Neptunes and hot-Earths articulated previously (Fogg and Nelson, 2005, and Sect 3.2.3), whilst making the point that the survival of these planets appears to be sensitive to how well damped are the contents of the shepherded disk fraction late on during the migration episode.

One potentially important dissipative process neglected in Model II is type I migration which operates on sub-gap opening bodies of $\sim 0.1 - 30$ $\mathrm{M}_{\oplus}$ (e.g. Ward, 1997; Papaloizou and Larwood, 2000; Tanaka *et al.*, 2002; Tanaka and Ward, 2004). Type I migration is generated by the asymmetric torques exerted on a protoplanet from the wakes it creates in the gas disk and is expected to impart an inward radial drift and strong eccentricity and inclination damping that increases in effectiveness linearly with protoplanetary mass. The realism of type I migration has long been problematic as theoretically predicted spiral-in times can be short enough to threaten protoplanetary survival, leading many modelers of planet formation to ignore the process entirely, or to include it with greatly reduced efficiency (e.g. Alibert *et al.*, 2005; Ida and Lin, 2008). It is possible that type I migration does not operate as rapidly as predicted: one proposal being that stochastic torques from density fluctuations in a turbulent disk could superimpose a random walk in semi-major axis over the smooth inward drift predicted by theory (Nelson and Papaloizou, 2004; Nelson, 2005). However, it is becoming apparent that even near-nominal rates of type I migration are not necessarily fatal to planet formation and survival. Work by McNeil *et al.* (2005) has shown that it is possible to grow a terrestrial planetary system in a simulation including type I migration forces by enhancing the original quantity of solid material present whilst including a rapidly dissipating gas disk. The model of Daisaka *et al.* (2006) succeeds in retaining sufficient material in the terrestrial region by invoking a shorter gas depletion timescale in the inner system than the observational value (based on infrared observations at $a \sim 100$ AU), or if the initial gas to dust ratio is smaller than the conventional minimum mass solar nebula (MMSN) model.

The problem with preventing the more massive giant planet cores from being lost to the central star is of greater severity, but recent work by Thommes and Murray (2006) suggests that this may be possible late in the lifetime of the gas disk when accretion and migration timescales become comparable. Proposed system properties

Table 5.1: Qualitative indication of dissipative forces present in the models, with emphasis on Model III

Dissipative forces	Models				
	I	II	III	IV	After gas loss
Gas drag	$\leftrightarrow$	$\downarrow$	$\downarrow$	$\downarrow\downarrow$	$\times$
Type II migration	$\leftrightarrow$	$\downarrow$	$\downarrow$	$\downarrow\downarrow$	$\times$
Type I migration	$\times$	$\times$	$\downarrow$	$\downarrow\downarrow$ or $\times$	$\times$
Dynamical friction	$\downarrow$	$\downarrow\downarrow$	$\downarrow\downarrow$	$\downarrow\downarrow$	$\downarrow\downarrow$
Collisional damping	$\leftrightarrow$	$\leftrightarrow$	$\leftrightarrow$	$\leftrightarrow$	$\leftrightarrow$

Key:
$\leftrightarrow$: no change with time
$\downarrow$: reduces with time
$\downarrow\downarrow$: stronger reduction due to late start or combination effect
$\times$: not present

that might widen such a window for core survival include small planetesimal sizes, low midplane gas disk viscosities and enhanced collision cross sections due to core atmospheres (Chambers, 2006b; Thommes *et al.*, 2007). Other proposed solutions to the core survival problem include a slowing or reversal of type I migration in dense non-isothermal disks due to changes in gas density in locations trailing and leading a protoplanet (Paardekooper and Mellema, 2006); and a trapping of migrating protoplanets at a steep gas density transition, such as that envisaged to occur at a boundary between turbulent (ionized) and 'dead' (non-ionized) zones of the disk (Masset *et al.*, 2006; Morbidelli *et al.*, 2008).

The possible realism of strong type I migration forces is of obvious and perhaps critical relevance to models of giant planet migration through an inner system solids disk. Even if the issue of pre-existing type I migration of the giant planet's core is neglected and the assumption of the fully formed giant planet undergoing type II migration is retained, type I migration forces would still be expected to operate on the protoplanetary components of the inner system disk, introducing another source of damping additional to dynamical friction. Extra dissipation would be expected to affect the partitioning of inner system material by enhancing the shepherded fraction at the expense of the scattered fraction, potentially restoring surviving hot-Earths as an outcome, or possibly even invalidating previous results showing sufficient solid material surviving the passage of the giant to permit the formation of terrestrial planets. This issue is investigated here by re-running one early and two late scenarios from Model II, using Model III which is augmented with a prescription for type I migration (Fogg and Nelson, 2007b, see Table 5.1).

Type I migration forces are included in Model III, and applied to protoplanets

only, by implementing the approach of Cresswell and Nelson (2006) who adopted the migration time prescription of Tanaka *et al.* (2002) and eccentricity damping time prescription of Tanaka and Ward (2004) and modified them with factors derived by Papaloizou and Larwood (2000) to describe evolution in the case of large eccentricity.

Their formula for the type I migration time is:

$$t_{\rm m} = \frac{2}{2.7 + 1.1\beta} \left(\frac{M_*}{m_{\rm p}}\right) \left(\frac{M_*}{\Sigma_{\rm g} a^2}\right) \left(\frac{h}{r}\right)^2 \left(\frac{1 + \left(\frac{e\ r}{1.3h}\right)^5}{1 - \left(\frac{e\ r}{1.1h}\right)^4}\right) \Omega^{-1}, \tag{5.1}$$

where M_* is the mass of the central star, $\Sigma_{\rm g}$ is the gas surface density in the vicinity of the planet, h is the gas scale height, and $m_{\rm p}, a, r, e$ and Ω are the planet's mass, semi-major axis, distance from the star, orbital eccentricity and orbital frequency respectively. The factor β in the first term is the gas disk surface density profile index ($\Sigma_{\rm g} \propto r^{-\beta}$), which is taken to be fixed at its initial value of $\beta = 1.5$, even though β falls in value during the evolution of the inner disk as gas drains onto the star. In practise, this simplification makes only a $\sim 15\%$ difference to t_m at later times and avoids the need for additional, time-consuming, measurement of β at every protoplanetary location each gas disk time step. Important behavioural features to note from Eq. 5.1 are that type I migration speeds up with an increase in planetary mass and slows down with a decrease in gas density or increased eccentricity. When $e > 1.1\ h/r$, inward migration halts as t_m becomes negative and only resumes when eccentricity is damped to lower values.

The control of $\Sigma_{\rm g}(r,t)$ by the viscous disk algorithm (described previously in Sect. 4.1) causes $t_{\rm m}(r,t)$ to behave in an interesting way. Since the migration time $t_{\rm m} \propto \Sigma_{\rm g}^{-1} a^{-2} (h/r)^2 \Omega^{-1}$ and $\Sigma_{\rm g} \propto r^{-\beta}$, and $h/r \propto a^{1/4}$ (Eq. 2.10), then $t_{\rm m} \propto a^{\beta}$ and $\dot{a} \propto a^{1-\beta}$. At early times and in the outer disk, $\beta \simeq 1.5$ and $\dot{a} \propto a^{-1/2}$, so migration is faster for interior objects of a given mass. However, the viscous draining of gas onto the central star rapidly results in much of the nebula declining to a shallower profile index of $\beta \simeq 1$, falling further to $\beta \simeq 0.75$ interior to 1 AU (see Fig. 4.3 in Sect. 4.3); in this situation $\dot{a} \propto a^{1/4}$, so relative migration rates are slower for interior objects.

Cresswell and Nelson's formula for eccentricity damping time is:

$$t_{\rm e} = \frac{Q_{\rm e}}{0.78} \left(\frac{M_*}{m_{\rm p}}\right) \left(\frac{M_*}{\Sigma_{\rm g} a^2}\right) \left(\frac{h}{r}\right)^4 \left(1 + \frac{1}{4}\left(e\frac{r}{h}\right)^3\right) \Omega^{-1}, \tag{5.2}$$

where $Q_{\rm e} = 0.1$ was chosen as a normalization factor to get $t_{\rm e}$ into good agreement with values measured from hydrodynamic simulations. It is additionally assumed that

the timescale for inclination damping is the same as that for eccentricity damping, i.e. $t_{\rm i} = t_{\rm e}$. As with the behaviour for inward migration, eccentricity damping is also stronger with increasing planetary mass and weaker with decreasing gas density or higher eccentricity.

Given $t_{\rm m}$ and $t_{\rm e}$, type I migration forces are then applied via the following accelerations to each protoplanet:

$$\boldsymbol{a}_{\rm m} = -\frac{\boldsymbol{v}}{t_{\rm m}}, \tag{5.3}$$

$$\boldsymbol{a}_{\rm d} = -2\frac{(\boldsymbol{v}\cdot\boldsymbol{r})\boldsymbol{r}}{r^2 t_{\rm e}} - 2\frac{(\boldsymbol{v}\cdot\boldsymbol{k})\boldsymbol{k}}{t_{\rm i}}, \tag{5.4}$$

where $\boldsymbol{v}$ is the protoplanet's velocity vector, $\boldsymbol{k}$ is a unit vector in the vertical direction, and $\boldsymbol{a}_{\rm typeI} = \boldsymbol{a}_{\rm m} + \boldsymbol{a}_{\rm d}$ (see Eq.2.2).

5.2 Running Model III

The initial conditions and setup of the solids component of the Model III nebula are identical to those described in Chapter 2. The initial state and parameters of its gas component are the same as those for Model II, described in Chapter 4, and hence the nebular mass and gas surface density continues to decline with time as illustrated in Figs. 4.2 & 4.3 respectively. Runs to mature the inner disk before the introduction of the giant planet are carried out as before, with the exception that this time only three scenarios are generated: one "early" and two "late" scenarios, ageing the system for 0.1, 1.0 and 1.5 Myr. These are the equivalent of Scenarios I, IV and V from Model II and to facilitate comparison with previous results this nomenclature is retained.

Numerical data for the evolved disks, including the remaining mass of gas ($M_{\rm gas}$) and solid material ($M_{\rm solid}$), the maximum protoplanetary mass ($m_{\rm max}$), the number of surviving particles (N & N'), and the protoplanet mass fraction ($f_{\rm proto}$) are given in Table 5.2. Large reductions in gas are indicated, especially in the inner regions of the system (see also Fig. 4.3). Particle numbers fall and $m_{\rm max}$ and $f_{\rm proto}$ rise with time as expected and by the time of the latest scenario at $t = 1.5$ Myr, some solid material has been lost within 0.1 AU. It might be thought that this loss (just $\sim 5\%$ of the solids inventory) is considerably less than would be expected given the inclusion of type I migration forces, however at early times the protoplanetary masses are too small to be greatly effected by inward type I drift and by the time they have grown an order of magnitude to $\sim {\rm M}_{\oplus}$, inward drift remains slow as the gas density in the inner system has fallen by an even larger factor.

Table 5.2: Overall solids disk data for Model III: after 0.1–1.5 Myr of evolution

Time (Myr)	0.1	1.0	1.5
Scenario ID	I	IV	V
$M_{\rm gas}$ (M_J)	30	7	3
$M_{\rm solid}$ ($M_\oplus$)	24.8	24.8	23.5
$m_{\rm max}$ ($M_\oplus$)	0.55	1.07	1.83
N	51	24	16
N'	4087	2171	1585
$f_{\rm proto}$	0.20	0.47	0.51

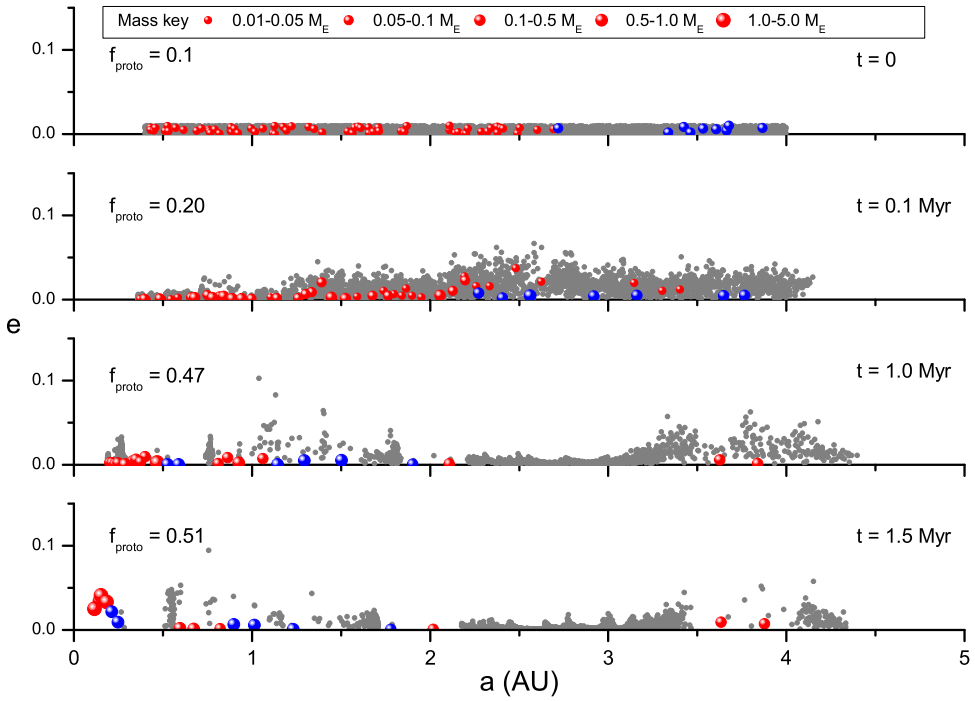

Figure 5.1: Inner disk maturation prepared for Model III. Eccentricities are plotted against semi-major axis. Red and blue symbols show protoplanets originating interior and exterior to the snowline respectively; grey symbols are super-planetesimals. The top panel shows the initial condition and the lower panels show the subsequent evolution to the three scenario starting points.

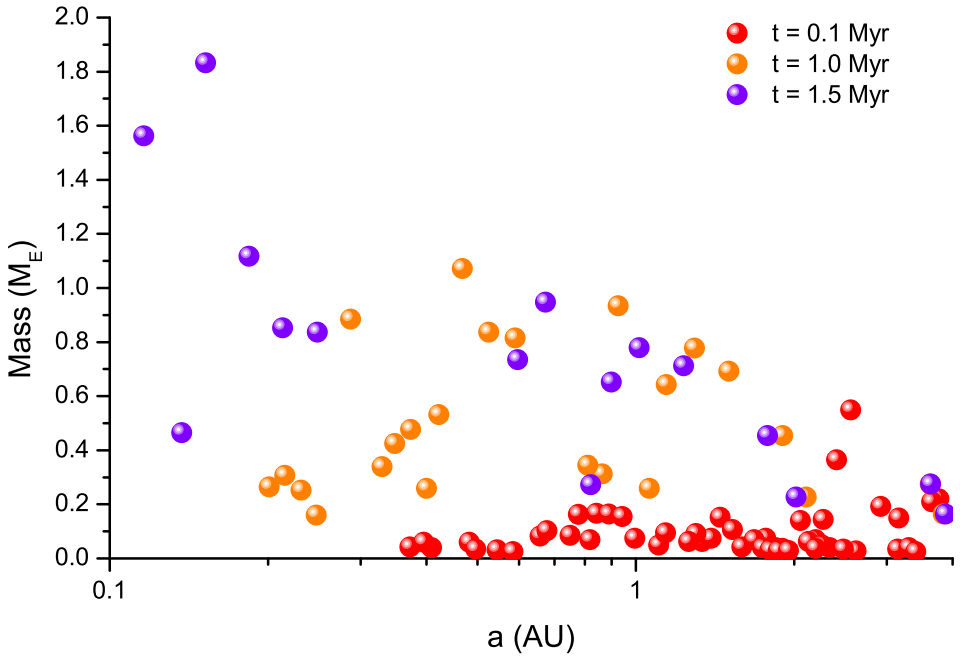

Figure 5.2: Protoplanetary masses vs. semi-major axis obtained after evolution to the starting points of Scenarios I, IV and V. Substantial inward drift is visible at late times due to type I migration.

The matured solids disks at the starting point of each scenario are illustrated in Fig. 5.1. The state of the solid components of the disk at the starting point of Scenario I shows little difference to its equivalent case with no type I migration operating (compare Fig. 2.2); however by the time the system is aged to the starting point of Scenarios IV & V, substantial inward movement of the protoplanetary population has happened, depleting the outer disk and crowding the inner regions with protoplanets. This is illustrated by plotting protoplanetary masses against semi-major axis on a log scale in Fig. 5.2. Once protoplanets become sufficiently massive for type I migration and eccentricity damping to become influential, they tend to migrate inward in stacked, resonantly locked, groups – the 'resonant convoys' originally described by McNeil *et al.* (2005). This is especially the case here as the inward migration rate declines with decreasing distance from the star (as explained above) with the result that protoplanets converge and are readily captured into close, first order, mean motion resonances. An example of this behaviour can be seen in the case of the 1.5 Myr maturation run in Fig. 5.2 where the first six protoplanets, starting from the innermost, are locked in 5:4, 7:6, 4:3, 5:4 and 5:4 resonances respectively.

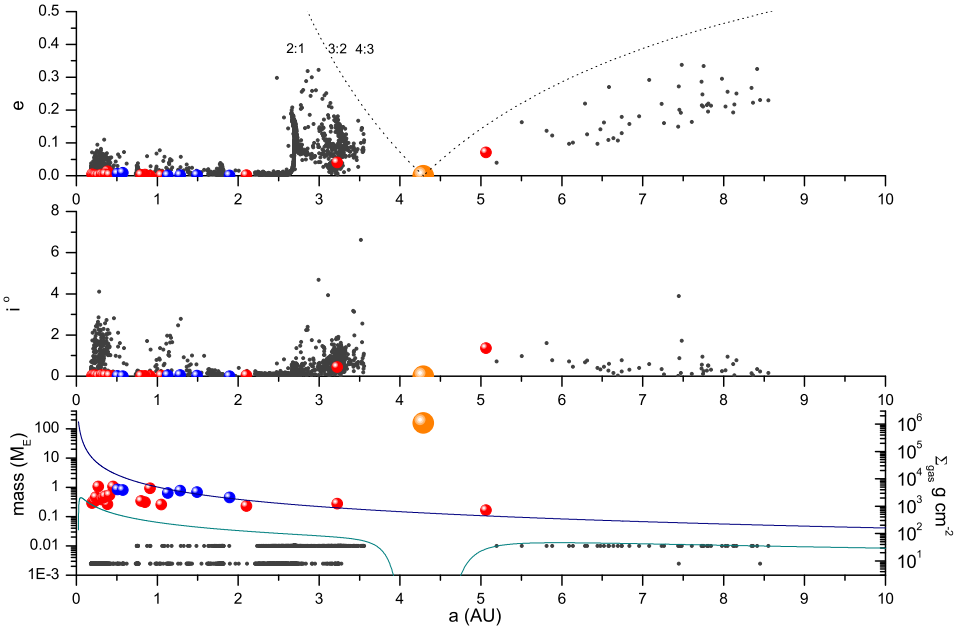

Figure 5.3: Scenario IV at $t_s = 20\,000$ years. For a definition of symbols and colours see the caption to fig. 4.5

The adequacy of an 8 day time-step for the late maturation runs is questionable as significant material has moved inside 0.4 AU at $t > 1$ Myr. However, protoplanetary growth in the inner part of the model disk occurs rapidly and mostly at distances of > 0.4 AU and tests conducted to examine this issue showed that disk forces prevent strongly divergent behaviour as a function of step size. The mass distribution of the matured disks interior to 0.4 AU is therefore not significantly affected by the choice of step size and, once the giant planet is inserted at the start of each scenario, orbital evolution is resolved with a shorter time-step of one tenth the orbital period of the innermost object. As well as type I migration generating edge effects at the inner edge of our solids disk, it is likely that it would drive in other objects into the simulation region from beyond 4 AU over this time but this possibility is not included here.

Thus, the three aged disks summarized in Table 5.2 and shown in Fig 5.1 are used as the basis for the type II giant planet/type I protoplanet migration scenarios that are the subject of Model III. As previously, a giant planet of 0.5 $\mathrm{M_J}$ is inserted at 5 AU after removing 0.4 $\mathrm{M_J}$ of gas from the disk between 3–7 AU and the inner boundary of the simulation is reset to 0.014 AU. The giant planet then proceeds to clear an annular gap in the gas and migrates inward in step with its viscous evolution in a close parallel to the behaviour of the giant planet in Model II, illustrated in Fig 4.4.

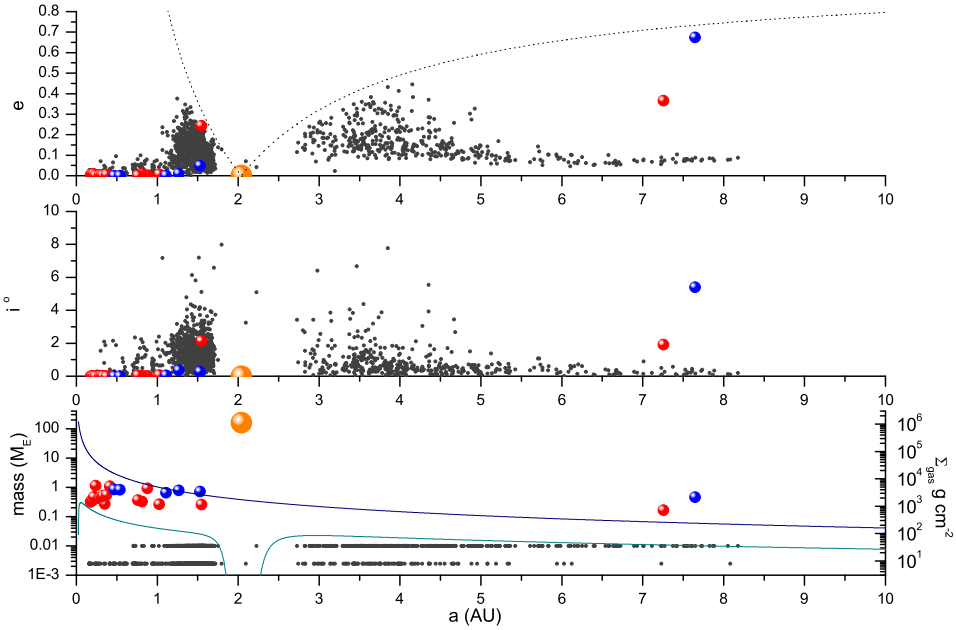

Figure 5.4: Scenario IV at $t_s = 80\,000$ years. The giant has now moved inward to 2.04 AU and is beginning to enter the inner zone that has become packed with protoplanets due to previous type I migration.

The simulations are halted when the giant reaches hot-Jupiter territory at 0.1 AU: in Scenario I, this takes $t_s \approx 114\,000$ years, but in Scenarios IV and V the process takes longer ($t_s \approx 152\,500$ and $220\,000$ years respectively) because at their late times of starting most of the gas has been lost and the remainder is less effective at driving migration. The symplectic time-step for these runs is set to one tenth the orbital period of the innermost object which is achieved by dividing each simulation into a set of sequential sub-runs with the time-step adjusted appropriately at each re-start. At late times in each scenario when material had drifted interior to 0.1 AU, this entails working with time-steps of less than one day. This, and the additional overhead of computing type I migration forces for each protoplanet, led to overall run times of several months as a consequence.

5.3 Results of Model III

5.3.1 An account of Scenario IV

The behaviour of one of the runs is described in detail first followed by a discussion of the effect of adding type I migration to the model by contrasting the results of the three scenarios presented here with their counterparts in Model II.

Scenario IV is one of the "late" scenarios, taking place 1 Myr after the model start time at a system age of $\sim$ 1.5 Myr. By this point, and after removing the gas required for the giant planet's envelope, the amount of gas remaining in the disk has fallen to just 16% of its initial value with the result that the giant takes 152 000 years to migrate inward to 0.1 AU, longer than would be predicted from the viscous evolution time. Four snapshots of the evolution of Scenario IV are illustrated in Figs. 5.3 – 5.6 showing the mass, inclination and eccentricity of objects, and the gas surface density vs. semi-major axis. The original provenance of the protoplanets (interior or exterior to the snowline) is denoted by the shading of its symbol as described in the caption to Fig. 4.5. In the case of a merger between rocky and icy protoplanets, this shading is determined by that of the most massive of the pair.

An early stage in the run at 20 000 years after the introduction of the giant planet is shown in Fig. 5.3. The giant has moved in to 4.29 AU and has caused significant excitation of the outer solids disk material at first order resonances. Noticeable also is that the outer disk beyond $\sim$ 2 AU has been largely cleared of protoplanets due to previous type I migration. Only two low mass protoplanets remain in this region, one of them having recently become caught at the interior 3:2 resonance with the giant planet and the other having already been scattered into an external orbit.

An intermediate stage in Scenario IV at $t_{\rm s} = 80\,000$ years is shown in Fig. 5.4 where the giant planet has migrated inward to 2.04 AU and is at the point of entering the zone that is crowded with protoplanets at $a < 2$ AU. Most of the planetesimals originating in the outer disk have now been shepherded interior to 2 AU, greatly increasing the surface density of solids caught between the 2:1 and 4:3 resonances. Two protoplanets have been captured at the 3:2 resonance and are in the process of having their orbits excited to an eccentricity where they will cross the giant planet's orbit and become vulnerable to scattering or accretion. Type I eccentricity damping is therefore not always strong enough to counteract the resonant pumping exerted by the giant planet as is shown by the additional 0.46 $\mathrm{M}_{\oplus}$ protoplanet that has been expelled into the growing scattered disk. One reason for this is that t_e increases with the cube of eccentricity (Eq. 5.2) greatly reducing the resistance of type I eccentricity damping to strong perturbations. It is also evident by this stage that the giant planet is

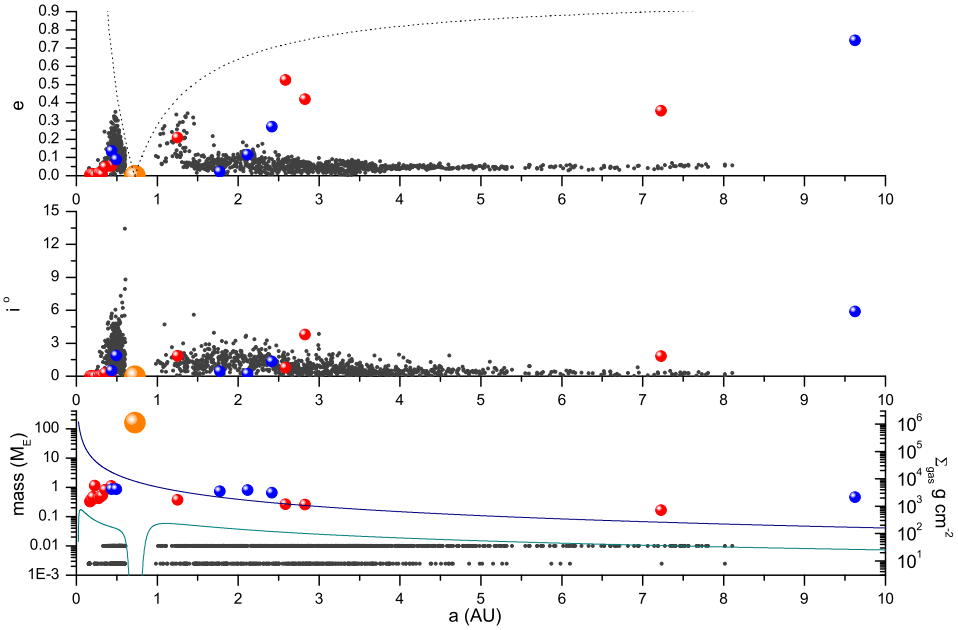

Figure 5.5: Scenario IV at $t_{\rm s} = 120\,000$ years. The giant has now moved inward to 0.72 AU. Six more protoplanets and a substantial number of planetesimals have been scattered into the external disk.

easily capable of catching up and overtaking the protoplanets which have only moved inward slightly in the meantime. For example, the type I migration time given by Eq. 5.1 for a 0.5 $\mathrm{M}_{\oplus}$ protoplanet at 2 AU, with $e = 0$, $h/r = 0.056$ and $\Sigma_{\rm g} = 150$ g cm^{-2} (a twelve-fold reduction in gas surface density at this location from that at $t = 0$) is $t_{\rm m} \approx 6$ Myr, comfortably larger than the type II migration time of the giant.

Fig. 5.5 shows the system 120 000 years after the introduction of the giant planet which has now reached 0.72 AU. An external disk is building up. Eight more protoplanets have had close encounters with the giant planet, resulting in two of them being accreted and six undergoing external scattering. The orbits of the most massive and least eccentric of these bodies are seen to be damping fast, as would be expected from the influence of Eq. 5.2. Some of this damping might also be due to dynamical friction as a substantial number of super-planetesimals have also been scattered into the same vicinity. Most of the solids mass however remains in the shepherded disk fraction, interior to the giant planet. Gas drag and type I damping forces in this region however are now two orders of magnitude weaker than a nominal $3 \times$ MMSN model as gas accretion onto the central star has reduced $\Sigma_{\rm g}$ here by a factor of ~ 25

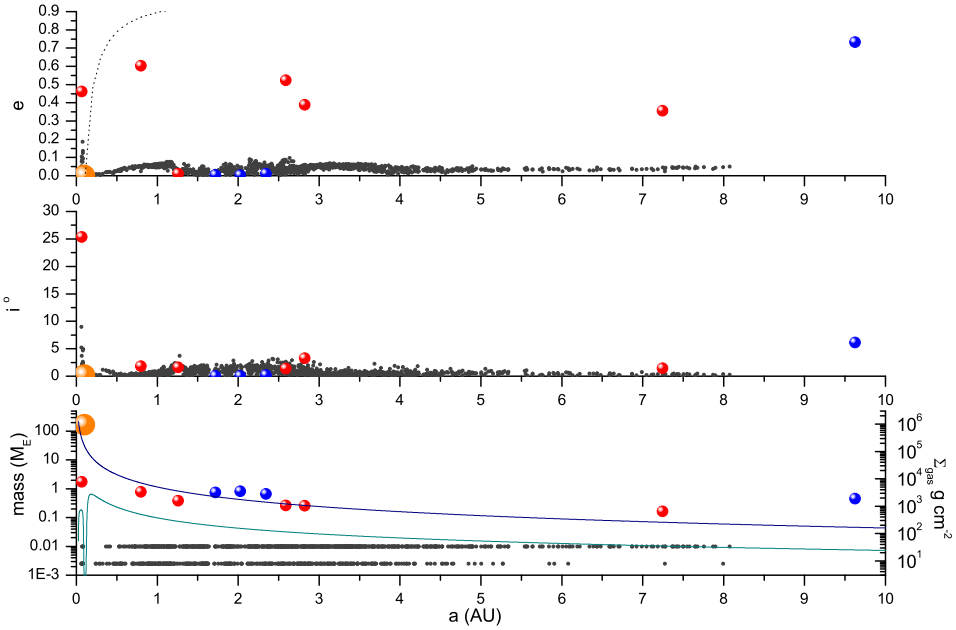

Figure 5.6: The end point of Scenario IV at $t_{\rm s} = 152\,500$ years. The giant is at 0.1 AU. About half of the original solids disk mass survives in external orbits and seven protoplanets are found between 0.7 – 3 AU. A hot-Earth remains interior to the giant planet in an eccentric and inclined orbit.

since $t = 0$ and dissipation of spiral waves generated by the approaching giant have recently reduced $\Sigma_{\rm g}$ by an additional factor of ~ 4.

Scenario IV ends at 152 500 years after the introduction of the giant planet when it reaches 0.1 AU and the system configuration at this point is shown in Fig. 5.6. The final 0.6 AU of the giant's migration has had a destructive effect on the densely packed inner system material. Of the twelve protoplanets remaining interior to the giant at the point shown in Fig. 5.5, there are only two remaining: a $0.79\ {\rm M}_\oplus$ planet scattered to 0.8 AU, and a $1.77\ {\rm M}_\oplus$ hot-Earth candidate at 0.062 AU, close to the 2:1 resonance, with an eccentric, inclined orbit ($e = 0.46, i = 25.3°$). The other ten, which were poorly damped due to low gas densities, and compacted into an ever shrinking volume, underwent a series of violent mutual impacts followed by eventual accretion by the giant planet. A close encounter with the last of these hot-Earths to hit the giant was responsible for the high inclination of the orbit of the one survivor which, at $i = 25.3°$, is too low for the Kozai mechanism (Kozai, 1962) to play a role in subsequent orbital evolution. Despite these losses however, about half the mass of the original solids disk survives in the scattered external disk and most of

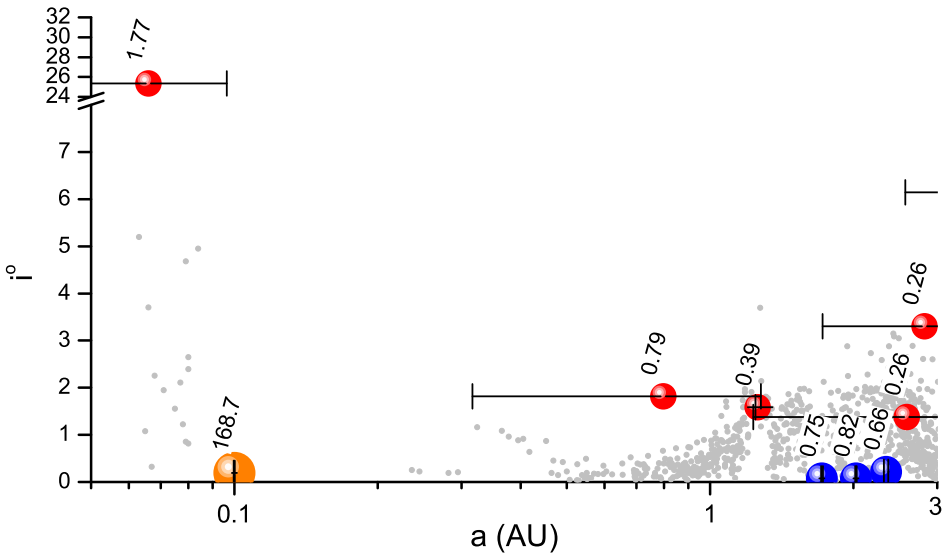

Figure 5.7: Scenario IV interior to 3 AU at the point where the giant planet reaches 0.1 AU. Inclination is plotted vs semi-major axis. Super planetesimals are the grey dots and protoplanets the open circles. Planets also have marked their masses in $\mathrm{M}_{\oplus}$ and their radial excursions due to orbital eccentricity.

this at radial distances $0.7 < r < 3$ AU (see the magnified illustration in Fig. 5.7). Seven substantial protoplanets ranging in mass from $0.26 - 0.82$ $\mathrm{M}_{\oplus}$ now occupy this region along with a large quantity of yet to be accreted planetesimals. Type I eccentricity damping has already circularized the orbits of four of the protoplanets which might be expected to undergo some degree of renewed inward type I migration before complete gas dispersal followed by a final phase of planetesimal clear-up and giant impacts. Allowing for this, the configuration shown in Fig. 5.7 suggests a good chance that the final planetary arrangement here could include a planet in the system's habitable zone and this issue is returned to in Sect. 5.4.

5.3.2 Comparison with simulations not including type I migration.

Data showing the fate of the solids disk mass at the end of the three Model III scenarios that include type I migration are given in Table 5.3 in the columns headed with a $\rightarrow$ symbol and are compared against their counterparts from Model II (Fogg and Nelson, 2007a) in the columns headed with a $\nrightarrow$ symbol. Each column gives the total mass of solid material in the disk at the start of giant planet migration; the mass and

Table 5.3: Fate of the disk mass at the end of each run: results for scenarios without ($\nrightarrow$) and with ($\rightarrow$) type I migration.

Scenario	I$\nrightarrow$	I$\rightarrow$	IV$\nrightarrow$	IV$\rightarrow$	V$\nrightarrow$	V$\rightarrow$
Total Initial Solids ($M_\oplus$)	24.81	24.81	24.81	24.81	24.81	23.47
Total Surviving Solids ($M_\oplus$)	16.60 (67%)	18.70 (75%)	21.23 (86%)	15.13 (61%)	20.22 (81%)	18.23 (78%)
Interior Surviving Solids ($M_\oplus$)	0.88 (4%)	3.44 (14%)	0.84 (3%)	1.84 (7%)	0.31 (1%)	6.23 (27%)
N, $f_{\rm proto}$	0, 0	1, 0.9	0, 0	1, 0.96	0, 0	1, 1
Exterior Surviving Solids ($M_\oplus$)	15.72 (63%)	15.27 (62%)	20.39 (82%)	13.29 (54%)	19.90 (80%)	12.00 (51%)
N, $f_{\rm proto}$	39, 0.27	34, 0.22	31, 0.63	9, 0.34	23, 0.66	7, 0.24
Accreted by Star ($M_\oplus$)	0.01 (0.04%)	0.0 (0%)	0.0 (0%)	0.0 (0%)	0.0 (0%)	0.01 (0.04%)
Accreted by Giant ($M_\oplus$)	8.20 (33%)	6.01 (24%)	3.41 (14%)	9.68 (39%)	4.59 (19%)	5.23 (22%)
Ejected ($M_\oplus$)	0.00 (0%)	0.1 (0.4%)	0.17 (1%)	0.0 (0%)	0.0 (0%)	0.0 (0%)

the percentage of the initial disk surviving at the end of the migration; and the mass surviving interior and exterior to the giant planet's final orbit at 0.1 AU, including the number of remaining protoplanets and the protoplanetary mass fraction in each respective partition. The bottom three rows give the data for the mass loss channels which are accretion by the central star, accretion by the giant planet and ejection into a hyperbolic orbit. The characteristics of the three systems at the end point of each scenario are illustrated in Fig.5.8 and can be compared with the results of Model I by referring to Fig 3.9 and those of Model II by referring to Fig. 4.10.

These data show that a large fraction of the disk mass survives the passage of the giant planet in each case: inclusion of type I migration at the nominal rate does not result in the inner system being cleared of planet-forming material. In the two versions of Scenario I slightly more mass remains with type I migration operating than without. However, this is largely due to the presence of a $3.42\ M_\oplus$ hot-Earth inside 0.1 AU captured in the 3:2 resonance with the giant planet with an eccentricity of 0.29. Generally the data for Scenarios I$\nrightarrow$ and I$\rightarrow$ are similar, suggesting that type I migration only has a small influence on the outcome of giant planet migration through a young inner system disk where protoplanetary masses remain small. In the more mature Scenarios IV & V less solids mass survives when type I migration is included, but this loss is not severe: 61% of the solids disk remains at the end of Scenario IV (see Figs. 5.6 & 5.7) and 78% remains at the end of Scenario V.

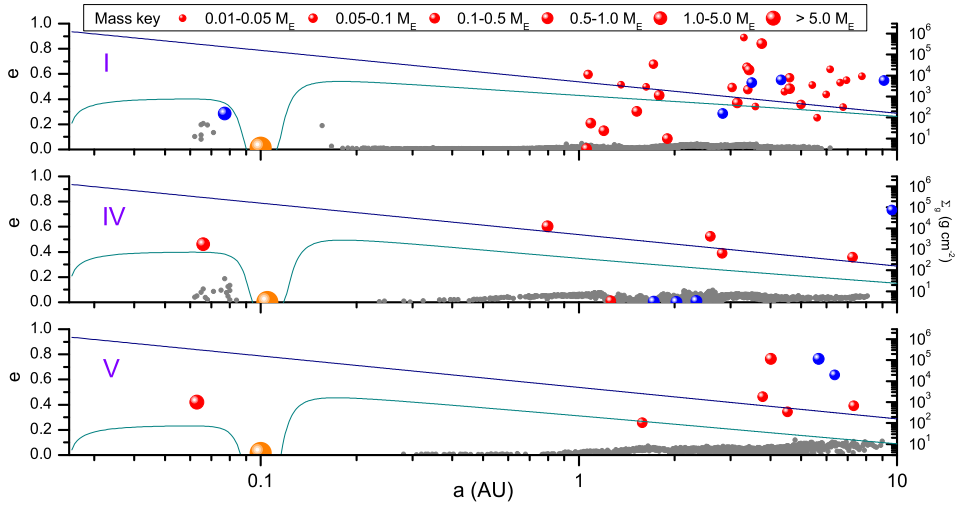

Figure 5.8: End points of all three scenarios at the point where the giant planet stops at 0.1 AU. Semi-major axis a is plotted on a log scale vs. eccentricity e. Gas surface density in $\mathrm{g\ cm^{-2}}$ is read off the right hand axes, the upper curve being the unevolved profile at $t = 0$ and the lower curve being the current profile.

Almost exclusively, the mass that is lost is accreted by the giant planet. The increase in efficiency of this loss channel results from the fact that, due to previous inward type I migration, protoplanetary encounters with the giant planet tend to occur at smaller orbital radii where the probability of accretion versus scattering is relatively enhanced. In Scenario V this additional mass loss is minor as much of the inner system material had by this late time accreted into substantial protoplanets which were able to migrate ahead of the giant inside 0.1 AU: a situation that can be seen developing in Fig. 5.2. These eventually co-accreted to form a $6.23\ \mathrm{M_\oplus}$ hot-Earth that was captured into the 2:1 resonance with the giant planet near the end of the simulation exciting its orbit to an eccentricity of 0.41. Future accretion of this body by the giant planet is a possibility and the issue of the long-term survival of the generated hot-Earth planets is examined in Sect. 5.5.

Across the board in Table 5.3, the consistent trends that emerge when type I migration is included are:

1. *Shepherding is modestly enhanced.* This can be seen from the larger percentage of the original solids disk mass that is found in the interior surviving solids fraction, which includes in each case a single hot-Earth type planet with an eccentric orbit captured at a first order resonance with the giant planet. Such objects were seen to form, but not to survive, in the analogous runs in Model II:

their typical fate being accretion by the giant planet. The hot-Earths generated here have narrowly escaped this fate themselves and their long-term survival would depend on the cessation of any further inward migration of the giant and the effectiveness of any continuing type I eccentricity damping exerted by the tenuous gas (reduced by over two orders of magnitude from a $\Sigma_{\rm g} \propto r^{-1.5}$ model) remaining in the planet's vicinity. The well-damped hot-Neptune or hot-Earth type planets generated in Model I (Fogg and Nelson, 2005), where a steady state gas disk with a fixed $\Sigma_{\rm g} \propto r^{-1.5}$ surface density profile is present, are not recovered. In this case, the persistently high gas densities caused more rapid orbital decay of planetesimals, strong dynamical friction and high rates of collisional damping which were sufficient to drag several protoplanets into low orbits where a rapid final phase of accretion was often sufficient to free the remaining body from resonant locking with the giant planet. Here, the evolving and decaying gas disk weakens both dynamical friction and type I eccentricity damping; whilst type I orbital decay facilitates inward movement of protoplanets, at late times it also brings about a separation of protoplanets from the bulk of planetesimals, further reducing the influence of dynamical friction on the innermost bodies. The overall dissipation in Model III therefore only results in a maximum of 27% of the original solids disk partitioned into the inner remnant.

2. *Scattering is modestly reduced and strongly selective.* Simulations that include type I migration produce less massive scattered disks, but not dramatically so. A stronger effect is that the likelihood of external scattering is now biassed in favor of planetesimals, generating immature exterior solids disks with fewer protoplanets. This can be seen in Fig. 5.9 where the black bars show the mass of the scattered disk resulting from runs of Model II and the grey bars show those resulting from Model III. The superimposed lozenge symbols show the disk protoplanet mass fraction ($f_{\rm proto}$) at the start of each scenario and the circle symbols give the value of $f_{\rm proto}$ at the end. In late scenarios the addition of type I migration to the model has resulted in the reduction of the mass of the outer disk remnant by $\sim 30\%$ which still leaves $\sim 50\%$ of the mass of the original ending up in the scattered disk. These disks however are less mature in the sense that they contain a greater fraction of small bodies. In Fogg and Nelson (2007a) it was noted that one effect of giant planet migration through a solids disk was to increase $f_{\rm proto}$ in the external remnant by selectively scattering protoplanets. Fig. 5.9 shows that in late scenarios, this trend is reversed

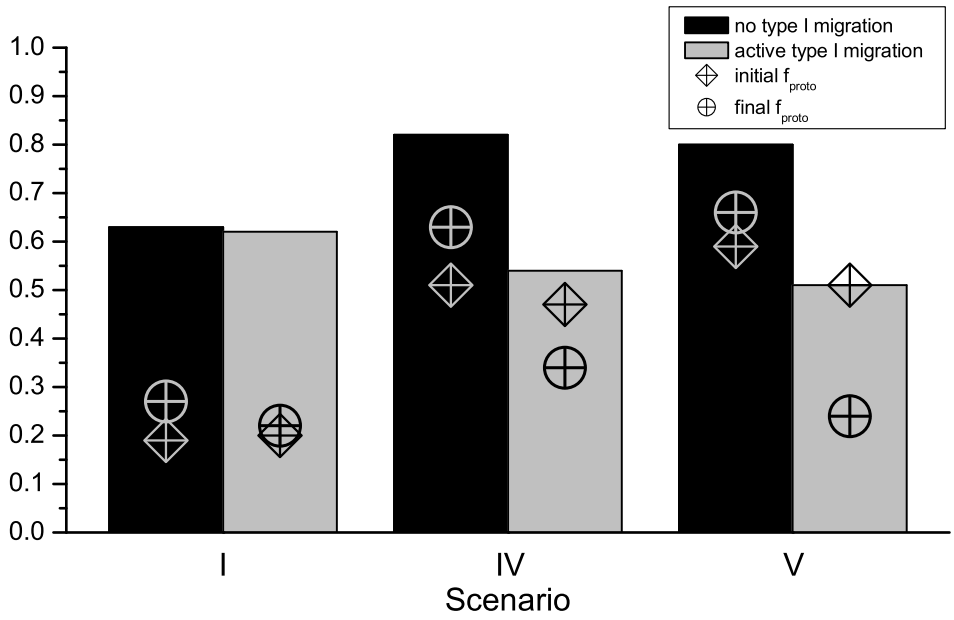

Figure 5.9: Mass fractions of scattered disks generated in the present work compared to those of analogous scenarios not including type I migration and before and after protoplanet mass fractions.

here as type I migration, especially at late times, causes protoplanets to be preferentially shepherded: encounters with the giant tend to occur closer in so that fewer of them escape into the external remnant allowing the scattered planetesimal population to dominate. The external disks generated by Model III however, though of reduced mass, should still be capable of supporting future planet formation. The protoplanets they contain can be of substantial mass and are typically emplaced at smaller semi-major axes and the more abundant planetesimal population and residual type I migration forces provide for stronger damping of protoplanets after scattering has occurred.

5.4 Post–migration terrestrial planet formation

To model the completion of planet formation in the scattered disks would require simulating a further $\gtrsim$ 100 Myr of accretion. Shorter range integrations however are still of considerable interest as type I migration forces only decline to zero when all the remaining local gas has gone. In this section, the evolution of Scenario IV is continued

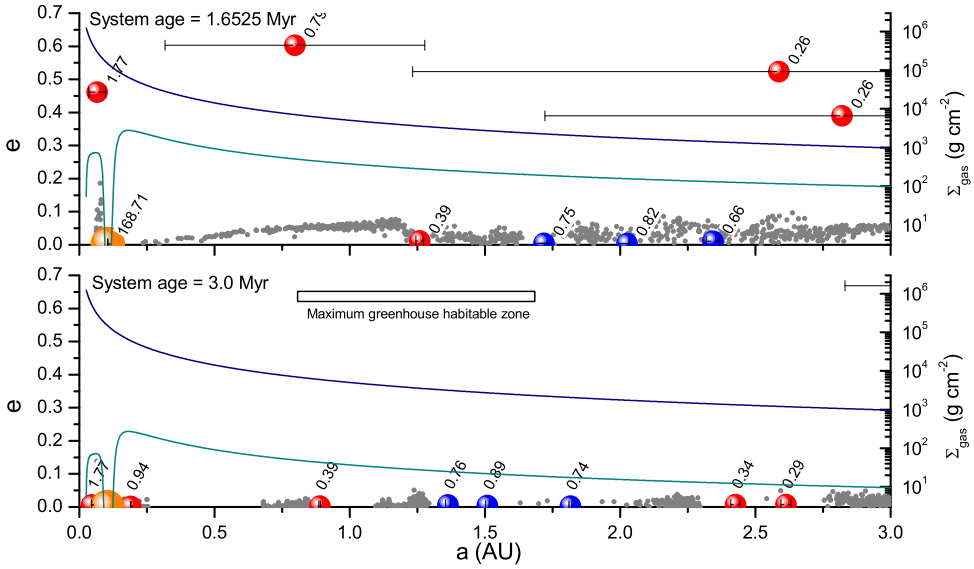

Figure 5.10: Details of the inner 3 AU at the end of Scenario IV (top panel) and 1.3475 Myr later at the point of gas dispersal. Eccentricity is plotted against semi-major axis with orbital excursions due to eccentricity illustrated with error bars. Planetary masses are labelled in units of $\mathrm{M}_{\oplus}$. Σ_{g} is read from the right hand axes: the upper curve being the profile at $t = 0$ (system age = 0.5 Myr) and the lower curve being the present profile. The extent of the maximum greenhouse habitable zone ($\sim$ 0.84 - 1.67 AU) is shown by the horizontal bar.

to a system age of 3 Myr, requiring an additional 1.3475 Myr of simulated run time, at which point it is assumed that all residual gas is rapidly lost to photoevaporation. Over this period the mass of the gas disk falls from $\sim 5.5\ \mathrm{M_J}$ to $\sim 0.55\ \mathrm{M_J}$. In order to evade the severe limitations of the viscous disk algorithm time-step, which adapts to a tiny value with the giant planet at ~ 0.1 AU, the type II migration forces effecting the hot-Jupiter are turned off and the viscous disk is replaced with an exponentially declining disk that maintains the previous surface density profile and declines with a mass e-folding time of 582 000 years (derived from a curve fit to Fig. 4.2). The system is evolved henceforth with a 2 day N-body time-step.

Details of the evolution of the inner 3 AU of the system during this terminal phase of gas depletion are shown in Fig. 5.10 where the top panel shows the state of play at the end of Scenario IV and the bottom panel shows it at 1.3475 Myr later at a system age of 3 Myr. During this period it can be seen that dynamical friction and residual type I migration forces rapidly damp and circularize the orbits of protoplanets. Gas drag is also sufficient to maintain the eccentricities of planetesimals at a low value.

The four well damped protoplanets between 1.25 – 2.5 AU in the upper panel of Fig. 5.10 grow by only a few percent from the surrounding planetesimal field and migrate inward an additional ~ 0.6 AU. There are two reasons for this slow growth rate: 1) type I eccentricity damping delays any transition to giant impact growth by circularizing protoplanetary orbits; and 2) type I migration combined with gas drag causes the shepherding of gaps in the planetesimal distribution, cutting down the supply of impactors and hence restricting continued oligarchic growth.

At the time of gas removal, shown in the bottom panel of Fig. 5.10, two more planets have moved into the maximum greenhouse habitable zone (Kasting *et al.*, 1993) giving a total of three planets sited between 0.84 – 1.67 AU. The migration of these four protoplanets shows some of the convoying behaviour described in McNeil *et al.* (2005): convergent migration can cause protoplanets to bunch together and lock into a stable arrangement of mean motion resonances whereupon the pattern then migrates inward at some average drift rate. In the bottom panel, the 0.76 $\mathrm{M}_{\oplus}$ planet and its 0.89 $\mathrm{M}_{\oplus}$ neighbour are caught at their 7:6 resonance and the outermost of this pair is close to the 4:3 resonance with its outer 0.74 $\mathrm{M}_{\oplus}$ neighbour. The innermost external protoplanet, having only recently been scattered, starts with $m_{\mathrm{proto}} \simeq 0.78\ \mathrm{M}_{\oplus}$, $a \simeq 0.8$ AU and $e \simeq 0.6$ but damps rapidly and migrates inward, growing to 0.94 $\mathrm{M}_{\oplus}$ as its orbit circularizes and eventually halting at $a = 0.19$ AU at a non-resonant 2:5 period ratio with the hot-Jupiter.

The model also tracks the volatile composition of protoplanets (see Sect. 4.2), recognizing three crude material provenances: material originating at $a < 2$ AU is assumed to be dry rock; from between $2\ \mathrm{AU} < a < 2.7\ \mathrm{AU}$ its water content is assumed to be similar to that of chondritic asteroids; and from beyond $a > 2.7$ AU it is assumed to be water-rich trans-snowline material. Previous models have demonstrated how a migrating giant planet drives volatile-rich material into its inner system, boosting the potential water content of any planets that form there (Raymond *et al.*, 2006; Fogg and Nelson, 2007a; Mandell *et al.*, 2007). This trend is accentuated when type I migration forces are included as volatile-rich protoplanets can now migrate directly inward. The compositions of the protoplanets in the extended Scenario IV, at a system age of 3 Myr, are shown in Fig. 5.11. All the bodies have a substantial endowment of outer solids disk material especially those at $a > 0.8$ AU. The largest three of these planets, the resonant trio situated between 1.3 – 1.9 AU, all originated from beyond the snowline at $a > 2.7$ AU and accreted copious volatile-rich material during their inward journey. Ocean worlds are a probable outcome of this kind of evolution (Kuchner and Lecar, 2002; L*é*ger *et al.*, 2004).

The Scenario IV system is evolved, in the absence of gas, for a further 27 Myr

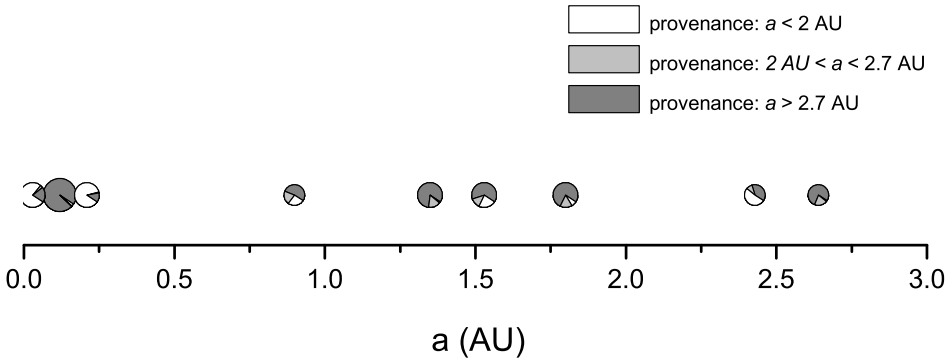

Figure 5.11: Material composition of protoplanets in the extended Scenario IV at the stage shown in the bottom panel of Fig. 5.10.

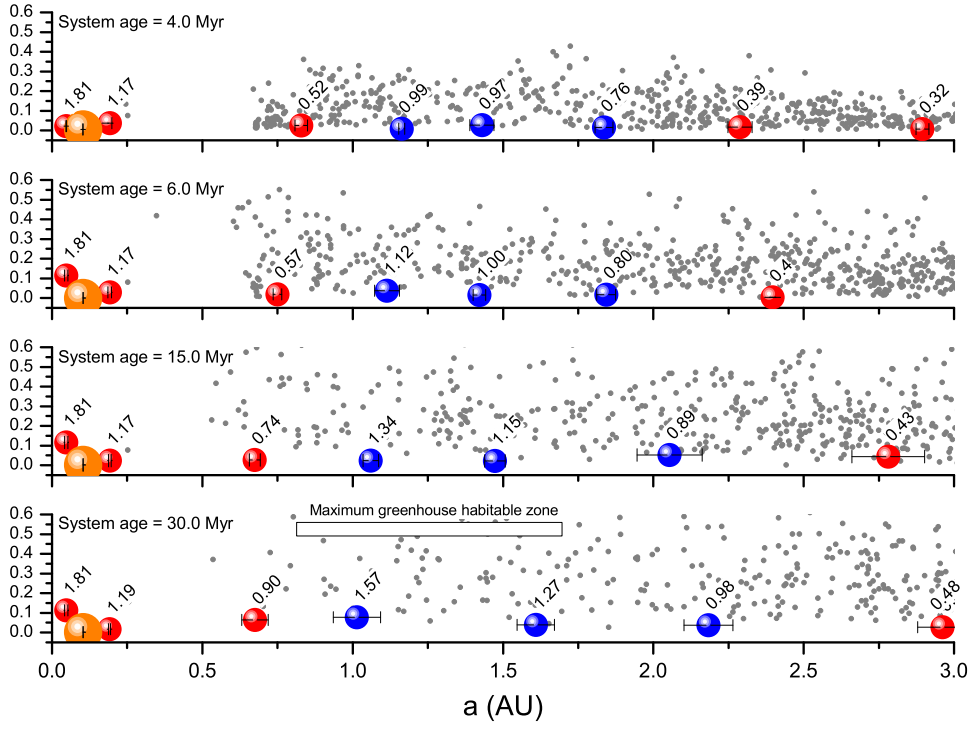

Figure 5.12: Details of the inner 3 AU of the Scenario IV system during gas-free accretion. From the top the panels show configurations at system ages of 4, 6, 15, & 30 Myr respectively.

to a system age of 30 Myr and four configurations over this period are shown in Fig. 5.12. The cessation of type I migration forces causes a shift to a more vigourous oligarchic style of growth (Kokubo and Ida, 1998). The resonant convoy showing in Fig. 5.10 breaks up and the entire protoplanet chain dynamically expands. The cessation of gas drag results in planetesimal orbits becoming much more excited in the process of exerting dynamical friction. Although this reduces protoplanetary accretion cross-sections, protoplanets no longer shepherd gaps in the solids disk and continuing growth is in progress.

The final state of the system shown in the bottom panel of Fig. 5.12 cannot be predicted in detail. Planetesimals will eventually be cleared by accretion, outward scattering, or ejection. Future mergers of protoplanets via giant impacts are less certain as they all lie in near-circular and well-spaced orbits: the closest being the two bodies at 0.68 and 1.01 AU which are nonetheless separated by ~ 30 mutual Hill radii. By chance, the bottom panel of Fig. 5.12 shows the 1.57 and 1.27 $\mathrm{M}_\oplus$ planets at the point of crossing their 2:1 mean motion resonance. Resonant capture does not occur for receding objects however, so this commensurability will probably not persist. Whilst the two planets have received an eccentricity excitation from the resonance crossing, a future strong interaction or impact between them is unlikely, as their orbits are separated by 32 $r_{\mathrm{H1,2}}$, well in excess of the 26 $r_{\mathrm{H1,2}}$ separation of the Earth and Venus. One can confidently expect therefore that the final configuration of the Scenario IV system will contain at least one, and probably two, Earth-mass planets in its habitable zone.

5.5 Hot-Earth survival

Having used a 2 day time-step, the additional simulation represented by Fig. 5.12 does not adequately resolve the orbital evolution of the hot-Earth planet at 0.062 AU. Single hot-Earths, captured at interior first order mean motion resonances resulted from all the scenarios of Model III, but their eccentric orbits with apastra close to the radial distance of the giant planet raise questions over long term survival. This issue is examined by running the orbits of the hot-Earth candidates for a further 10 000 years ($\sim 10^6$ orbits at 0.05 AU), with a half day time-step, in the absence of gas and including the giant planet and any remaining debris interior to 0.1 AU.

The orbital evolution resulting from these extended runs is shown in Fig. 5.13 and their final configuration is shown in Fig. 5.14. All the interior planets remain. The least convincing as a longer-term survivor is the 3.43 $\mathrm{M}_\oplus$ hot-Earth present in Scenario I: it accretes very little additional debris (which is accreted by the giant

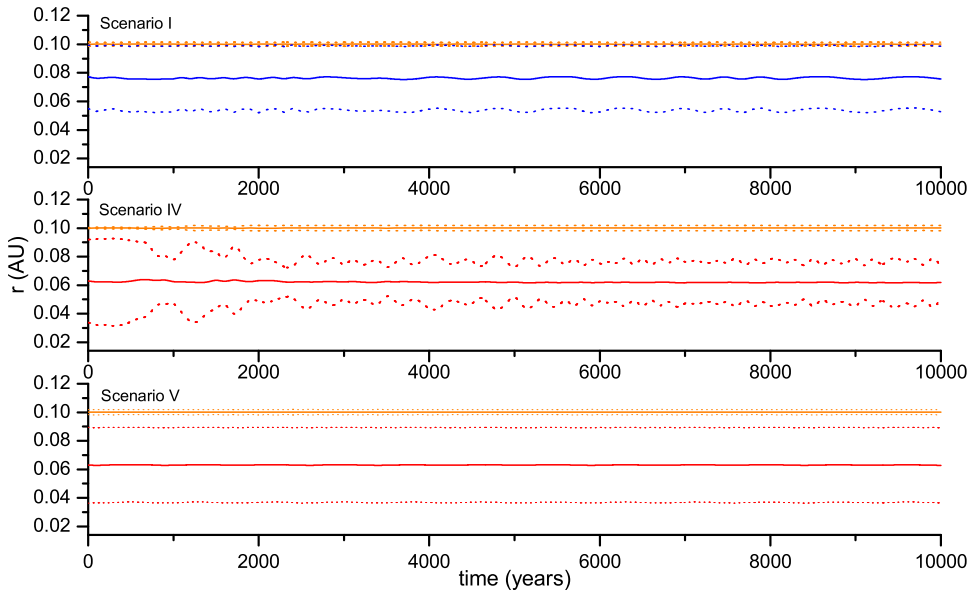

Figure 5.13: Further evolution of the orbits of the interior planets resulting from the three scenarios. Solid lines are semi-major axes, dotted lines are periastra and apastra. Orange represents the giant planet and red or blue represents the hot-Earths.

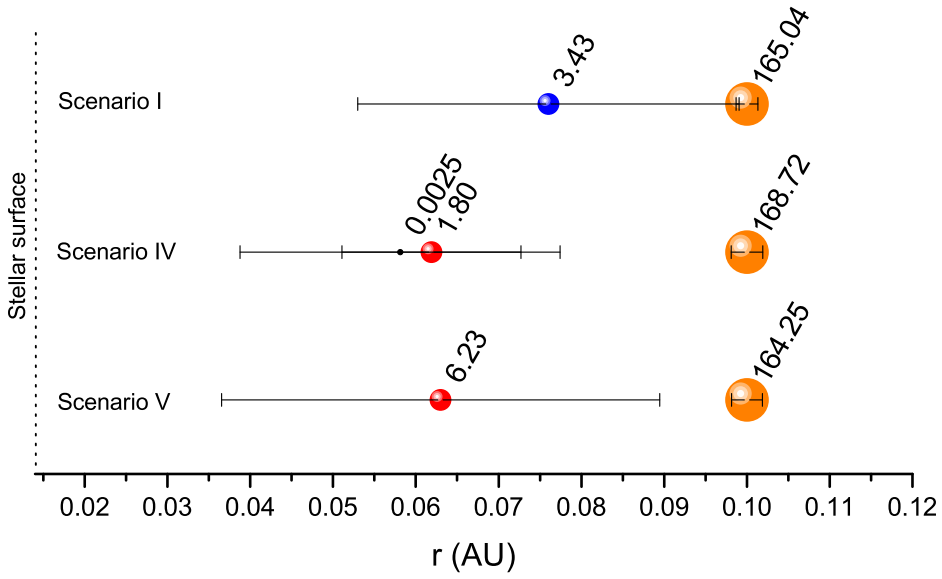

Figure 5.14: Hot-Earth – hot-Jupiter systems resulting from an additional 10 000 years of simulation. Error bars show the radial distance between periastron and apastron. Numeric labels give masses in $M_\oplus$.

instead) and continues to orbit at the 3:2 resonance with an eccentricity of $\simeq 0.3$, bringing it very close to crossing the giant's orbit at apastron. Close encounters have so far been avoided by the orbital phasing resulting from the resonance, but it is uncertain how long this state could persist. In the case of Scenario IV, a 1.77 $\mathrm{M}_{\oplus}$ hot-Earth starts at the 2:1 resonance in an excited orbit with $e = 0.46$ and $i = 25°$, but this planet succeeds in accreting an extra 0.03 $\mathrm{M}_{\oplus}$ of debris, cleaning up all of it but the one remaining super-planetesimal showing in Fig. 5.14, with the result that its eccentricity is damped to $e \simeq 0.2$ by the end of the run period. Its inclination is not damped and one accretion event increases it slightly to $i \simeq 30°$ but the hot-Earth and the hot-Jupiter are now well separated and long-term survival looks promising. In Scenario V there is no debris for the hot Earth to clean up and Fig. 5.13 shows that its orbit remains unchanged over 10 000 years. This 6.23 $\mathrm{M}_{\oplus}$ planet remains close to the 2:1 resonance in a very low inclination orbit with $e \simeq 0.41$ which at no point comes dangerously close to the orbit of the giant planet. This hot-Earth is also a possible long-term survivor, especially as stellar tidal forces would be expected to gradually circularize its orbit over much longer timescales.

5.6 Model III: conclusions

The previous models of a giant planet migrating through an inner system protoplanetary disk, presented in Chapters 3 & 4, have all predicted that the process generates a scattered external disk massive enough to support renewed planet formation (Fogg and Nelson, 2005, 2007a). None of these works included the possible action of type I migration forces exerted by the gas which would cause heavier bodies to drift progressively closer to the central star. Since this process would clearly act to counter scattering, its operation could invalidate previous conclusions concerning subsequent terrestrial planet formation. Having updated the model to include type I migration and having re-run three scenarios from Chapter 4, the clear conclusion is that the extra dissipation generated is still not sufficient to prevent the buildup of a scattered disk $\sim 50\%$ the mass of the original (Fogg and Nelson, 2007b). Although these scattered disks are of lower mass, they are generally less dispersed and better damped, supporting a more rapid renewal of planetary growth. As shown in the extended run, whilst the gas remains, residual type I forces can act on scattered protoplanets to draw them back into the ~ 1 AU region and the habitable zone (Fig 5.10). The model also generates planets of several Earth masses in potentially stable orbits interior to the final orbit of the giant planet (Fig 5.13) and is thus supportive of the proposals of Fogg and Nelson (2005) that hot-Earths and hot-Neptunes found interior to hot-Jupiters may

have originated from material shepherded inward by a migrating giant planet.

Chapter 6

Model IV: photoevaporating gas disk and the termination of migration

6.1 A self-consistent model of hot- or warm-Jupiter stranding

One simplification common to the previous models presented in this thesis is that the physical mechanism that actually halts giant planet migration is not simulated. Type II migration is artificially halted when the giant planet has reached a preset final semi-major axis of 0.1 AU and hence is not determined by the structure or evolution of the gas disk. This stranding mechanism is unknown and proposed explanations include the presence of a central magnetospheric cavity in the gas which could decouple an intruding giant planet from the disk (Lin *et al.*, 1996; Kuchner and Lecar, 2002; Masset *et al.*, 2006; Papaloizou, 2007); another is that of fortuitous gas disk dispersal where the eventual loss of the gas disk strands those migrating giant planets that still remain at arbitrary orbital radii (Trilling *et al.*, 1998; Armitage *et al.*, 2002; Armitage, 2007). Since the previous models stop migration close to the central star, whilst significant gas is still present, they appear most realistic in the context of a central gaseous cavity halting mechanism. The examples that come closest to implicitly assuming fortuitous gas disk dispersal as the halting mechanism are the late scenarios (IV & V) of Models II & III (Fogg and Nelson, 2007a,b, & Chapters 4 & 5) where gas densities have fallen to low levels and migration is decelerating (see Fig. 4.4).

Neither of these mechanisms however are fully consistent with the previous modeling as final hot-Jupiter orbits are still artificially imposed at 0.1 AU and are not computed self-consistently with the evolution of the gas. If the code were to be run further, one would expect the giant planet to come to rest somewhere between 0.02–0.1 AU but none of the physics of a magnetospheric cavity is modelled and time-step limitations that stem from the viscous disk algorithm make it impractical to simulate further type II migration interior to 0.1 AU. The only difference that stopping the hot-Jupiter closer to the star would make to the results is that more compact systems would be less likely to host interior hot-Earth or hot-Neptune type planets as further resonant shepherding of such objects inward of 0.1 AU runs the risk of driving them into the central star (Sect 3.2.3 & Fogg and Nelson, 2005).

In this Chapter, Model IV, the final and most complete version of the set of models presented in this thesis is detailed. The difference from its forebears stems from the specific assumption and simulation of *fortuitous disk dispersal* as the mechanism that strands giant planets. Post-migration orbits are no longer prescribed, but take place self-consistently when migration runs out of steam at the time of the disappearance of the nebular gas. Terrestrial planetary formation in this context is of interest because, for a hot-Jupiter to strand at ~ 0.1 AU, it must form and migrate late in the lifetime

Table 6.1: Qualitative indication of dissipative forces present in the models, with emphasis on Model IV

Dissipative forces	Models				
	I	II	III	IV	After gas loss
Gas drag	$\leftrightarrow$	$\downarrow$	$\downarrow$	$\Downarrow$	$\times$
Type II migration	$\leftrightarrow$	$\downarrow$	$\downarrow$	$\Downarrow$	$\times$
Type I migration	$\times$	$\times$	$\downarrow$	$\Downarrow$ or $\times$	$\times$
Dynamical friction	$\downarrow$	$\Downarrow$	$\Downarrow$	$\Downarrow$	$\Downarrow$
Collisional damping	$\leftrightarrow$	$\leftrightarrow$	$\leftrightarrow$	$\leftrightarrow$	$\leftrightarrow$

Key:
$\leftrightarrow$: no change with time
$\downarrow$: reduces with time
$\Downarrow$: stronger reduction due to late start or combination effect
$\times$: not present

of the gas disk, when gas densities – and the strength of dissipative forces – are lower (see Table 6.1) and accretion in the inner system is at a more advanced stage than previously considered. In addition, a succession of later scenarios than this results in a succession of shorter migrations and larger standing distances. This permits an extension of the scope of Model IV to model terrestrial planet growth in those 'warm-Jupiter' systems that may have originated as the result of a late, partial, inward migration.

One problem is that the viscous disk algorithm detailed in Sect. 4.1 is inadequate to simulate the final stages of gas loss. This is because gas is removed solely via accretion onto the central star, predicting an exponential decline in the gas quantity with the final traces of gas disappearing over a protracted period. Such behaviour is at odds with observations of disks around T Tauri stars which are observed to last for $\sim$ 1 – 10 Myr (Haisch *et al.*, 2001), but which disperse abruptly over a much shorter $\sim 10^5$ year timescale (Simon and Prato, 1995; Wolk and Walter, 1996). However, Clarke *et al.* (2001) have shown that the performance of such models can be made much more realistic by including a model of photoevaporation of the disk driven by the diffuse UV flux from the central star (Hollenbach *et al.*, 1994). Their results show that this process has little effect on the evolution and structure of the gas disk at early times, but comes to dominate at later times once the rate of gas loss onto the central star falls below the photoevaporation rate. At this point, the inner disk ceases to be resupplied from larger radii and rapidly drains onto the star. The formation of this inner cavity then permits direct UV illumination of the outer disk which disperses in turn in $\sim 10^5$ years (Alexander *et al.*, 2006).

For the purposes of Model IV it is only necessary to adopt a simple parameteriza-

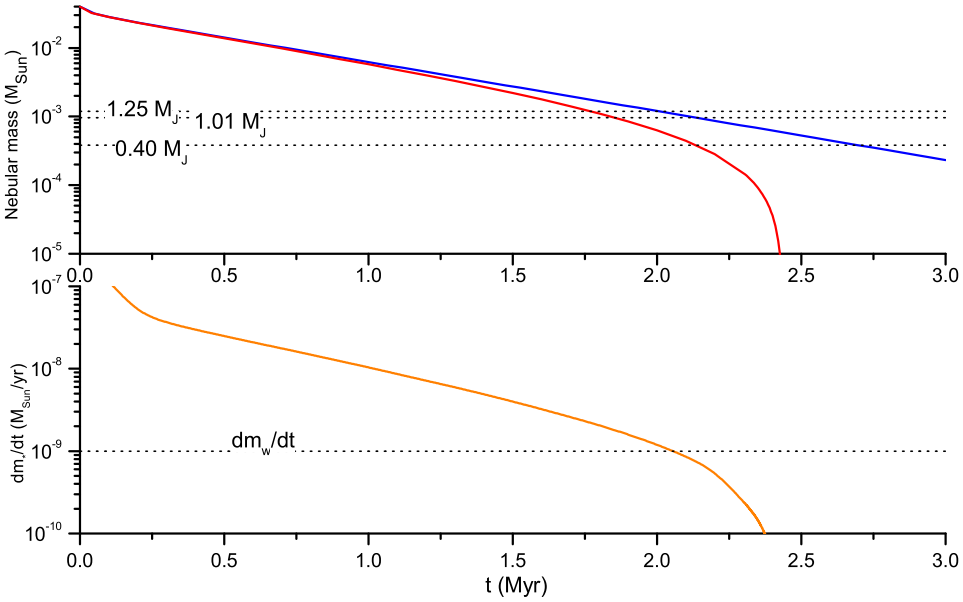

Figure 6.1: *Upper panel.* Mass of the nebular gas vs. time: the blue curve represents former models where mass loss occurs solely via viscous accretion onto the central star; the red curve represents Model IV which includes photoevaporation. *Lower panel.* Accretion rate onto the central star $\mathrm{d}m_*/\mathrm{d}t$. The dotted horizonal line represents the photoevaporation rate $\mathrm{d}m_\mathrm{w}/\mathrm{d}t = 10^{-9}\ \mathrm{M}_\odot\ \mathrm{yr}^{-1}$

tion of this type of photoevaporation model by subtracting an extra term representing a disk wind $\dot{\Sigma}_\mathrm{w}$ from the right hand side of the disk diffusion equation (Eq. 4.2):

$$\dot{\Sigma}_\mathrm{w} = K\left(\frac{r_\mathrm{g}}{r}\right)^{2.5};\ \ r_\mathrm{g} \leq r \leq r_\mathrm{out}, \tag{6.1}$$

where $\dot{\Sigma}_\mathrm{w}$ is the rate of change of gas surface density due to photoevaporation, r is radial distance, r_out is the disk radius, and r_g is the gravitational radius: the distance beyond which ionized gas can become unbound from the star. The constant of proportionality K depends directly on the disk's total photoevaporative mass loss rate $\dot{m}_\mathrm{w}$:

$$K = \dot{m}_\mathrm{w}\left(-2\pi r_\mathrm{g}^{2.5}\int_{r_\mathrm{g}}^{r_\mathrm{out}} r^{-1.5}dr\right)^{-1}. \tag{6.2}$$

To fit with the pre-existing viscous gas disk model, $r_\mathrm{out} = 33$ AU. The gravitational radius is assumed to be $r_\mathrm{g} = 5$ AU, and the mass loss rate $\dot{m}_\mathrm{w} = 10^{-9}\ \mathrm{M}_\odot\ \mathrm{yr}^{-1}$, which gives $K = 1.4685 \times 10^{-12}\mathrm{g\ cm^{-2}\ s^{-1}}$.

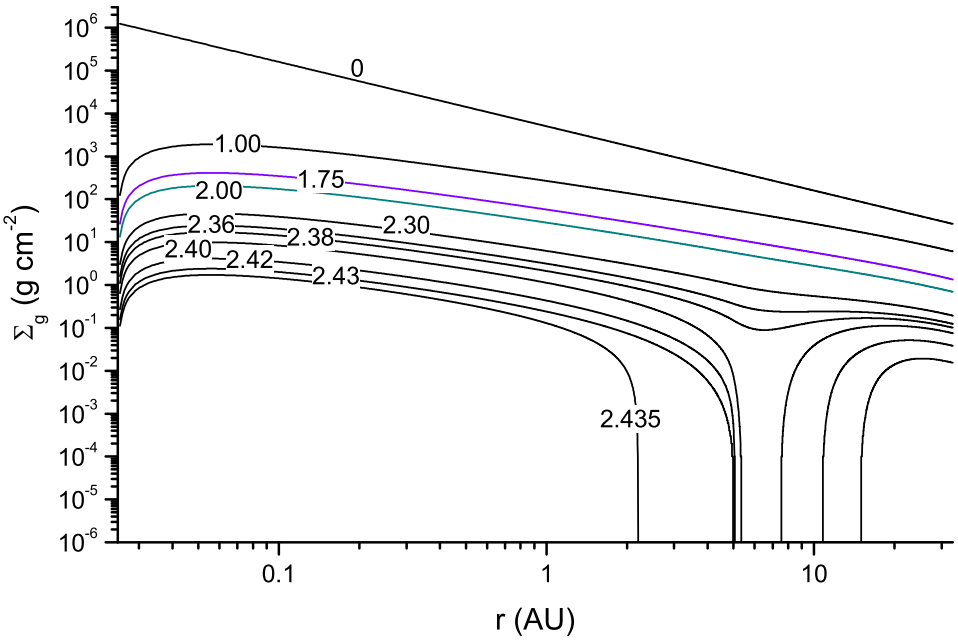

Figure 6.2: Model gas disk surface density evolution. The uppermost curve is the initial condition; successive curves are labelled with their age in t/Myr. Σ_g at the time of the stranding window, referred to in Sect. 6.2, lies within the two coloured curves.

In Models II & III an initial condition is assumed of a minimum mass solar nebula model (Hayashi, 1981), scaled up in mass by a factor of three (3×MMSN), extending between 0.025 – 33 AU from a solar mass protostar, with an initial surface density profile of $\Sigma_\mathrm{g} \propto r^{-1.5}$ and a total mass of 0.039 $\mathrm{M}_\odot$. Adopting an alpha viscosity of $\alpha = 2 \times 10^{-3}$, the finding is that, after a short lived $\sim 10^5$ year period where Σ_g close to the star relaxes to a shallower profile, the mass of the gas disk declines predictably with an e-folding time of 582 000 years. This behaviour is illustrated as the upper blue curve in the top panel of Fig. 6.1, which plots the nebular mass vs. time. The effect in Model IV of starting from the same initial conditions, but including photoevaporation at the rate given by Eq. 6.1, is shown as the red curve. It is evident that the two models only diverge slowly for the first ~ 2 Myr, but thereafter the mass of the photoevaporating disk drops steeply and vanishes in just a few $\times 10^5$ years. The lower panel of Fig. 6.1, which plots the accretion rate onto the star $\dot{m}_*(t)$, shows that this transition in behaviour occurs around the time when $\dot{m}_* \approx \dot{m}_\mathrm{w}$.

The evolution of the gas disk surface density $\Sigma_\mathrm{g}(r,t)$ is shown in Fig. 6.2, where the uppermost curve represents the initial $\Sigma_\mathrm{g} \propto r^{-1.5}$ profile and the lower curves

represent successively more evolved configurations. It can be seen that the evolution of the nebula speeds up after $t \sim 2$ Myr, with a gap at $r \approx r_{\rm g}$ starting to open up at $t \approx 2.38$ Myr, followed by an accelerated decline of the inner disk thereafter. This behaviour is qualitatively similar to that described by Clarke *et al.* (2001), with the exception that at late times the outer disk, which is truncated to a much smaller radius, is lost even more rapidly. This makes no difference to the mechanism for stranding giant planets as the divergence occurs when the nebular mass has already fallen below the level where it can drive migration. In test runs of Model IV it was found that if giant planets strand well inward of $r_{\rm g}$ they can act against the efficient draining of the last dregs of the inner disk onto the central star, slightly altering the picture given in Fig. 6.2. Again however, this effect is minor as it occurs at times when the gas is very thin and does not significantly delay the date of overall disk dispersal.

6.2 Running Model IV

The initial setup of Model IV, describing the protoplanetary disk at $t = 0$, is identical to that described previously for Models II & III, with the exception that a wider solids disk is considered with its outer edge extended from 4 to 5 AU.

The motivation for this increase in scale stems from observed differences in the matured solids disks depending on whether type I migration is excluded or not. In models without type I migration, the radial drift of protoplanets in the preparatory runs is due to dynamical stirring and a degree of coupling to the slow inward movement of planetesimals via dynamical friction. In these cases it was reasonable to assume that the giant planet formed at 5 AU and that any supply of extra material over our run times into the inner disk from beyond that distance would be insignificant. However the inclusion of type I migration makes the heaviest and most evolved objects more inwardly mobile. As shown in Fig. 5.2, the late matured disks are largely cleared of protoplanets outward of $\sim$2 AU, making one wonder if this region could have been repopulated in the interim by objects which migrated from beyond 4 AU. This seems plausible as the giant planet's core must also have migrated inward to some extent so that one can no longer propose consistently that it accreted its core at 5 AU. Modeling a time dependent addition of fresh material from beyond 4 AU is not attempted here as it requires some poorly constrained assumptions concerning the condition and evolution of the outer disk. An extra stock of material is added instead at the beginning by simply widening the initial solids disk to 0.4 – 5.0 AU, with some presupposition that the protogiant forms further out than 5 AU and migrates to this distance by the scenario starting point.

Table 6.2: Data describing initial solids disk set-up for Model IV

	Rocky Zone 0.4–2.7 AU	Icy Zone 2.7–5.0 AU	Total 0.4–5.0 AU
$M_{\rm solid}$	$9.99\ {\rm M}_\oplus$	$24.65\ {\rm M}_\oplus$	$34.64\ {\rm M}_\oplus$
$m_{\rm proto}$	$0.025\ {\rm M}_\oplus$	$0.1\ {\rm M}_\oplus$	
N	66	15	81
$m_{\rm s-pl}$	$0.0025\ {\rm M}_\oplus$	$0.01\ {\rm M}_\oplus$	
N'	3336	2315	5651
$f_{\rm proto}$	0.17	0.06	0.09

Relevant data for the initial components of the wider Model IV solids disk are shown in Table 6.2 which gives, for zones interior and exterior to the snowline, values for the total mass of solid material $M_{\rm solid}$, the number and mass of protoplanets N and $m_{\rm proto}$, and the number and mass of super-planetesimals N' and $m_{\rm s-pl}$. The parameter $f_{\rm proto}$, at the foot of Table 6.2, is the mass fraction of the solids disk contained in protoplanets which is used here as a rough measure of the evolution of the disk, taking $f_{\rm proto} = 0.5$ to denote the transition between oligarchic and chaotic, or 'giant impact', growth regimes. To compare these data with those for the previous initial solids adopted in this thesis, refer to Table 2.2.

The procedure to generate the scenarios for Model IV has to be different from its predecessors. The previous approach was to run the combined N-body and gas disk model, in the absence of a giant planet, from $t = 0$ to a set of durations distributed between 0.1 - 1.5 Myr, in order to mature the disk to different ages and to generate a set of migration scenarios. At the end of each of these maturation runs, a $0.5\ {\rm M_J}$ giant planet was introduced at 5 AU after removing $0.4\ {\rm M_J}$ of gas from a local disk annulus to provide for the giant planet's envelope. Re-starting the run at this point resulted in an inward type II migration of the giant planet which was allowed to continue until it reached the prescribed stranding radius of 0.1 AU. This approach is not appropriate here as the timing is tied to gas disk dispersal, and the requirement is therefore to mature the disk to between the boundaries of a temporal window within which the giant planet can both accrete sufficient gas for its envelope and strand at $\gtrsim 0.1$ AU. The lower limit of this window, the age where a $0.5\ {\rm M_J}$ giant planet introduced at 5 AU will naturally cease migrating and come to rest at ~ 0.1 AU, was located via experiments with Model IV and was found to be $t \approx 1.77$ Myr. By this time, the mass of the nebula has fallen to $M_{\rm gas} \approx 1.25\ {\rm M_J}$ which is shown as the upper dotted line in Fig. 6.1. The maximum possible upper age limit of the stranding window would be when $M_{\rm gas} = 0.4\ {\rm M_J}$, at $t \approx 2.13$ Myr (see the lower dotted line in Fig. 6.1), giving a window duration of $\sim 17\%$ of the simulated disk lifetime. However, this limit would

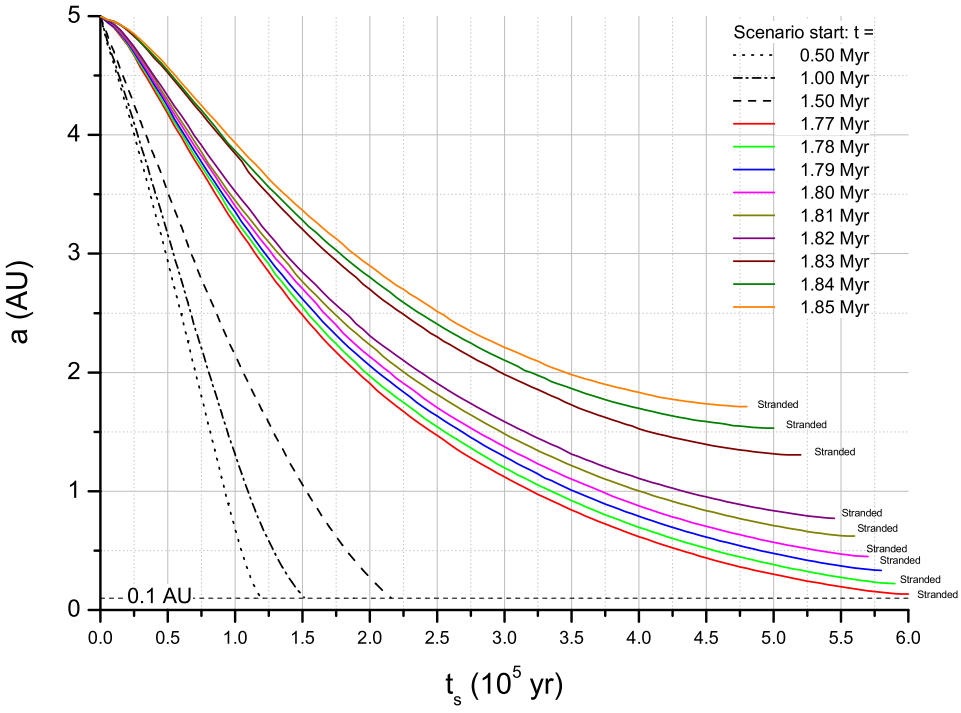

Figure 6.3: Migration and stranding of $0.5\ \mathrm{M_J}$ giant planets in Model IV and Models II–III. Giant planet semi major axis in AU is plotted against t_s in units of 10^5 yr. Coloured curves show the behaviour of giant planets stranding naturally due to gas disk photoevaporation in Model IV. Numeric labels are launch dates: the respective disk ages t/Myr at which the giant planet is introduced. Dashed curves show giant planet migrations in Scenarios III, IV, and V from Models II–III, where migration was artificially halted at 0.1 AU.

require the unrealistic condition of all the remaining nebular gas being accreted by the giant planet. Since the process of gas accretion onto the giant planet's core is not simulated, the upper age limit of the stranding window is arbitrarily restricted to $t = 1.85$ Myr (see the middle dotted line in Fig. 6.1) by which time the mass of the nebula has fallen to $M_{\rm gas} \approx 1.0\ {\rm M_J}$, reducing the window duration to $\sim 4\%$ of the simulated disk lifetime. Variation of the many free parameters in a model such as this would produce a variety of stranding behaviours in simulations. The model of Armitage *et al.* (2002), for example, predicts a stranding window of duration $\approx 20\%$ of the disk lifetime: a longer duration that can be attributed to their use of a more slowly evolving disk model and their simulation of the stranding of more massive giant planets that are better able to resist disk forces.

The behaviour of $0.5\ {\rm M_J}$ giant planets launched into the model disks, between the lower and upper age limits discussed above, is illustrated by the solid curves in Fig. 6.3 and shows that stranding takes place between 0.13 – 1.71 AU. Also illustrated by the dashed curves in Fig. 6.3 are the migration trajectories of the giant planets in Scenarios III, IV, and V of Model II (Fogg and Nelson, 2007a, & Chapter 4) where migration takes place in a younger disk and is artificially halted at 0.1 AU. The fastest of these (launched at $t = 0.5$ Myr) takes place at a time when the gas disk is still quite massive and completes its migration in the viscous evolution time of $\sim 120\,000$ years. Later scenarios entail longer migration times as the gas mass progressively declines and is less effective at driving migration. In order for giant planets to strand naturally, Model IV requires still later launch times, in a context where photoevaporation is starting to have a significant influence on the disk. Fig. 6.3 shows that migration speeds are considerably slower and decelerate steadily until migration ceases after $t_s = 600\,000$ years for the farthest travelling planet and 470 000 years for the planet that migrates the least. Migration in all these cases halts at $t \approx 2.4$ Myr.[1]

Thus, the Model IV scenarios are generated by running the model from its initial condition, without a giant planet present, to mature the protoplanetary disk to a minimum of $t = 1.77$ Myr and then in successive 10 000 year increments to $t = 1.85$ Myr. Given that the reality of strong type I migration is controversial, and to bracket the range of possibilities, two parallel sets of scenarios are generated: one with no type I migration forces (Run Set **A**) and the other with type I migration and eccentricity and inclination damping set at the maximum rate determined by Eqs. 5.1 & 5.2 (Run Set **B**). To accommodate this total of 18 simulations, a change

[1] Note that the gap between the $t = 1.82$ and 1.83 Myr curves is because of the substantial depletion of disk gas at these late times, dictating the removal of the quantity required for the giant planet's envelope from a wider annulus of the disk than previously.

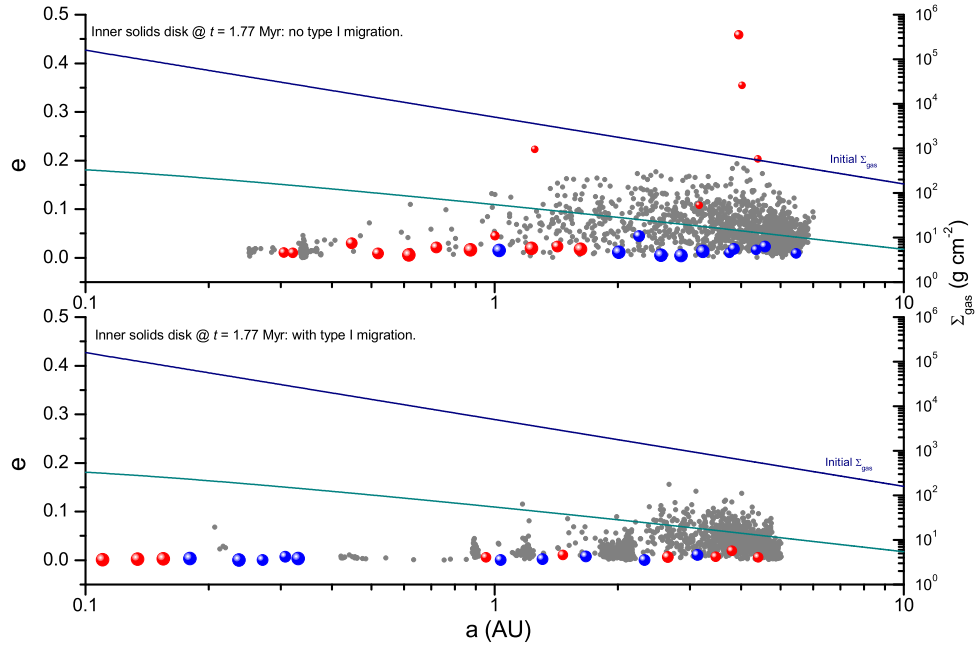

Figure 6.4: Eccentricity vs semi-major axis for matured solids disks at $t = 1.77$ Myr for no type I migration (top panel) and with type I migration (bottom panel). Grey dots are super-planetesimals; red and blue circles are protoplanets originating interior and exterior to the snowline respectively. Gas densities are read on the right hand axes: the upper lines of each pair show gas density at $t = 0$ and the lower lines are the current densities.

from the previous scenario ID system is also required. Thus, Roman numerals are substituted with Arabic numerals and labelling is generated by the following formula: $\text{Scenario ID} = 1 + (t/\text{Myr} - 1.77)/0.01$. This gives Scenarios 1, 2, .., 9 for $t = 1.77$, 1.78, .., 1.85 Myr. Run set **B** which includes type I migration is denoted by an I subscript: e.g Scenarios 1_{I}, 2_{I}, .., 9_{I}. During these maturation runs the simulation inner edge was set at 0.1 AU and any material passing interior to this boundary was eliminated and assumed to be consumed by the central star. The configurations of the matured solids disks at $t = 1.77$ Myr (Scenarios 1 & 1_{I}), the opening of the stranding window, are shown in Fig. 6.4; and Table 6.3 gives relevant data including values for the remaining total mass M_{solid}, the maximum protoplanetary mass m_{max}, the numbers of surviving protoplanets and super-planetesimals N & N', and the protoplanet to solids disk mass fraction f_{proto}. Since the scenarios of Model IV start much closer together in time than those of previous Models (0.01 Myr *vs.* 0.15 – 0.5 Myr), the state of the solids disks generated for Scenarios 2 – 9 does not change greatly from that of Scenario 1.

Table 6.3: Matured solids disk at the start of the stranding window

t (Myr)	1.77	1.77
Type I migration ?	no	yes
$M_{\rm solid}$	$33.52\ {\rm M}_\oplus$	$30.42\ {\rm M}_\oplus$
$m_{\rm max}$	$2.67\ {\rm M}_\oplus$	$1.62\ {\rm M}_\oplus$
N	27	19
N'	1854	1809
$f_{\rm proto}$	0.62	0.52

It can be seen, when comparing with the initial condition data in Table 6.2, that planetary growth has been strong, especially where no type I migration is operating. In this case (the upper panel in Fig. 6.4), mergers have reduced protoplanets to a third of their former number, $m_{\rm max}$ is high (there being a $2.67\ {\rm M}_\oplus$ planet present at 2.01 AU), and $f_{\rm proto}$ indicates that the accretion pattern of the disk has progressed way beyond oligarchic growth into the chaotic growth regime. Very little mass has been lost interior to 0.1 AU ($\sim 3\%$) via dynamical spreading and gas drag induced orbital decay of planetesimals. With type I migration, there is in play an additional preferential damping and inward migration of the most massive protoplanets (clearly visible in the lower panel in Fig. 6.4) resulting in the loss of $\sim 12\%$ of the disk mass beyond the simulation inner edge. This loss is mostly in the form of large bodies as can be inferred from the lower values of $m_{\rm max}$, N, and $f_{\rm proto}$. It might be thought that this loss is quite modest considering the inclusion of type I migration forces. However since type I migration is proportional to planetary mass, in a rapidly dispersing gas disk model inward drift is limited at early times by the small size of protoplanets, and at late times by low gas densities (see also McNeil *et al.*, 2005; Daisaka *et al.*, 2006); Fig. 6.4 shows that at $t = 1.77$ Myr, $\Sigma_{\rm g}$ interior to 1 AU has fallen by two orders of magnitude. The effect of Type I migration on the radial distribution of the solids disk mass is shown in Fig. 6.5 where the total solids mass for both models at $t = 1.77$ Myr is plotted in 0.5 AU width bins against radial distance. It can be seen that beyond ~ 2 AU the radial mass profile of the disks in the two models remains similar, but interior to 2 AU the more rapid pace of protoplanetary growth has resulted, in the type I migration case, in an inward displacement of mass caused mainly by a fractionation of the most massive bodies from the rest of the swarm which are now crowding the inner 0.5 AU of the system. It is shown in Fogg and Nelson (2007b, & Chapter 5) that hot-Earth type planets are more likely to accrete and survive when a giant planet migrates through such a solids disk, where previous type I migration has caused a radial contraction of the inner mass distribution.

The matured disks summarized above, aged in 10 000 year stages from $t =$

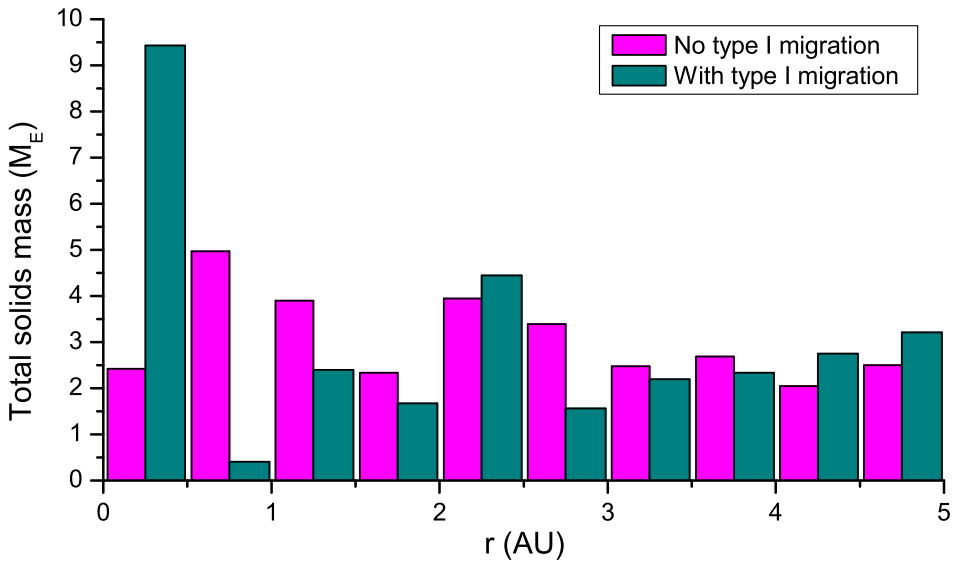

Figure 6.5: Total solids mass in 0.5 AU width bins at $t = 1.77$ Myr for maturation runs with no type I migration and with type I migration.

1.77 Myr, are used as the basis for the type II giant planet migration scenarios presented here. In each case, a giant planet of 0.5 $\mathrm{M_J}$ is inserted at 5 AU after removing 0.4 $\mathrm{M_J}$ of gas from the disk and the inner boundary of the simulation is reset to 0.014 AU $\cong 3\ \mathrm{R_\odot}$. The giant planet then proceeds to clear an annular gap in the gas and undergoes inward type II migration. The simulations are halted when the giant planet strands as a result of the near complete loss of the disk gas. In practise, since the viscous disk algorithm requires a finite amount of gas in each cell to remain stable, it is assumed that the giant halts inward migration when the migration rate falls below $-0.2\ \mathrm{cm\ s^{-1}} \cong -4.2 \times 10^{-7}\ \mathrm{AU\ yr^{-1}}$. By this time the total gas remaining in the entire modelled disk is $< 10^{-5}\ \mathrm{M_\odot}$ and any error in stranding radius caused by this procedure is only on the order of $\sim 10^{-3}$ AU. As before, the symplectic time-step for these scenario runs is set to one tenth the orbital period of the innermost object which was achieved by dividing each simulation into a set of sequential sub-runs with the time-step adjusted appropriately at each re-start. Since these new simulations involve a migration of roughly triple the simulated duration of previous models (see Fig. 6.3), and since small time steps are usually needed during the long drawn out 'end game' when the giant planet and the shepherded fraction of the solids disk are close to their final positions, these runs take a particularly long while to complete, requiring 4 – 6 months of CPU time each.

6.3 Results of Model IV

All Model IV scenarios, when run to the point at which the giant planet ceases migrating, exhibit a varying mix of the same shepherding and scattering effects on the solids disk shown by previous models. It is unnecessary therefore to repeat the previous procedure of giving a detailed account of the evolution of one representative case. The big difference is that the Model IV scenarios result in a more restricted type II migration, with the giant planet stranding between semi-major axes of $a_{\rm g} \approx 0.1$ – 1.7 AU, in a context where all the damping forces that are dependent on the disk gas are close to their minimum possible values.

The end points[2] of Scenarios 1 – 9, those *without* type I migration (Run Set **A**), are all illustrated in Fig. 6.6. Their counterparts, Scenarios $1_{\rm I}$ – $9_{\rm I}$, *with* type I migration operating (Run Set **B**), are illustrated in Fig. 6.7. Comparison of the figures shows the familiar partitioning of the solids disk into shepherded interior and scattered exterior fractions, systematically truncated by the extent of the traverse of the giant planet. Early scenarios (1 – 3 and $1_{\rm I}$ – $3_{\rm I}$) are the closest to previous models and result in relatively better populated exterior disks and sparser interior disks without type I migration in force, and the opposite tendency with type I migration. This is in accord with the previous findings of Models II & III respectively (see Figs. 4.10 & 5.8).

No surviving protoplanets are found in or close to the system's habitable zone ($\sim$ 0.84 – 1.67 AU) when the giant strands between $0.4 \lesssim a_{\rm g} \lesssim 1.2$ AU. When stranding occurs at $a_{\rm g} \lesssim 0.4$ AU, late scattered protoplanets can find themselves emplaced in the exterior disk at distances of $\lesssim 2$ AU and are hence candidates for evolving into future habitable planets. However, this eventuality appears less likely if type I migration is influential on the dynamics, as interior disk fractions evolve closer to the star, are better damped, and hence are less likely to lose their contents via late scattering. When stranding occurs at $a_{\rm g} \gtrsim 1.2$ AU, protoplanets are found to survive in the inner regions of the HZ at ~ 1 AU in both scenario sets. The reason that interior HZ planets are found much closer to the giant planet than those in external orbits is simply a reflection of the asymmetry between shepherding and scattering behaviours. Shepherding of the interior population occurs between the 2:1 and 4:3 resonances, causing material to accumulate via disk compaction between $a \approx 0.63 - 0.83\ a_{\rm g}$. In contrast, scattering typically results in the expulsion of a protoplanet into the exterior disk with an initial $e \gtrsim 0.5$ and periastron $\approx a_{\rm g}$ at the time of scattering; hence, after migration of the giant planet is complete, exterior HZ planets are usually found

[2]The phrase 'end point' here refers to the time at which type II migration of the giant planet ceases due to gas disk dispersal.

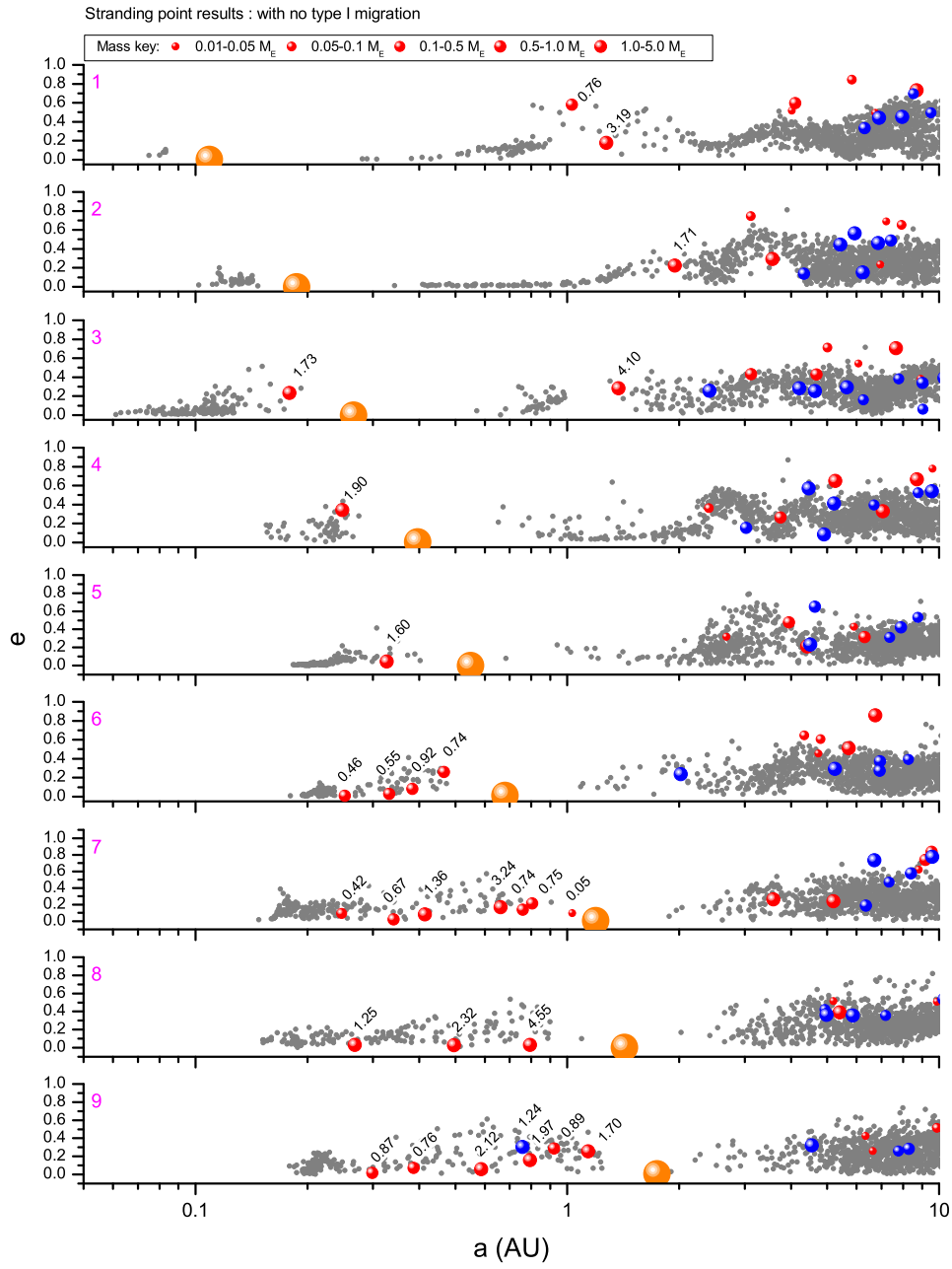

Figure 6.6: Run Set **A**. End points of all nine Model IV scenarios that *exclude* type I migration, at the time when the giant planet strands at its final semi-major axis. Eccentricity is plotted vs. semi-major axis with symbols colour coded as in previous examples and sized according to the mass key. Scenario ID is given at the top left of each panel. Protoplanets interior to the giant, or within 1 – 2 AU, are labelled with their mass in $M_{\oplus}$.

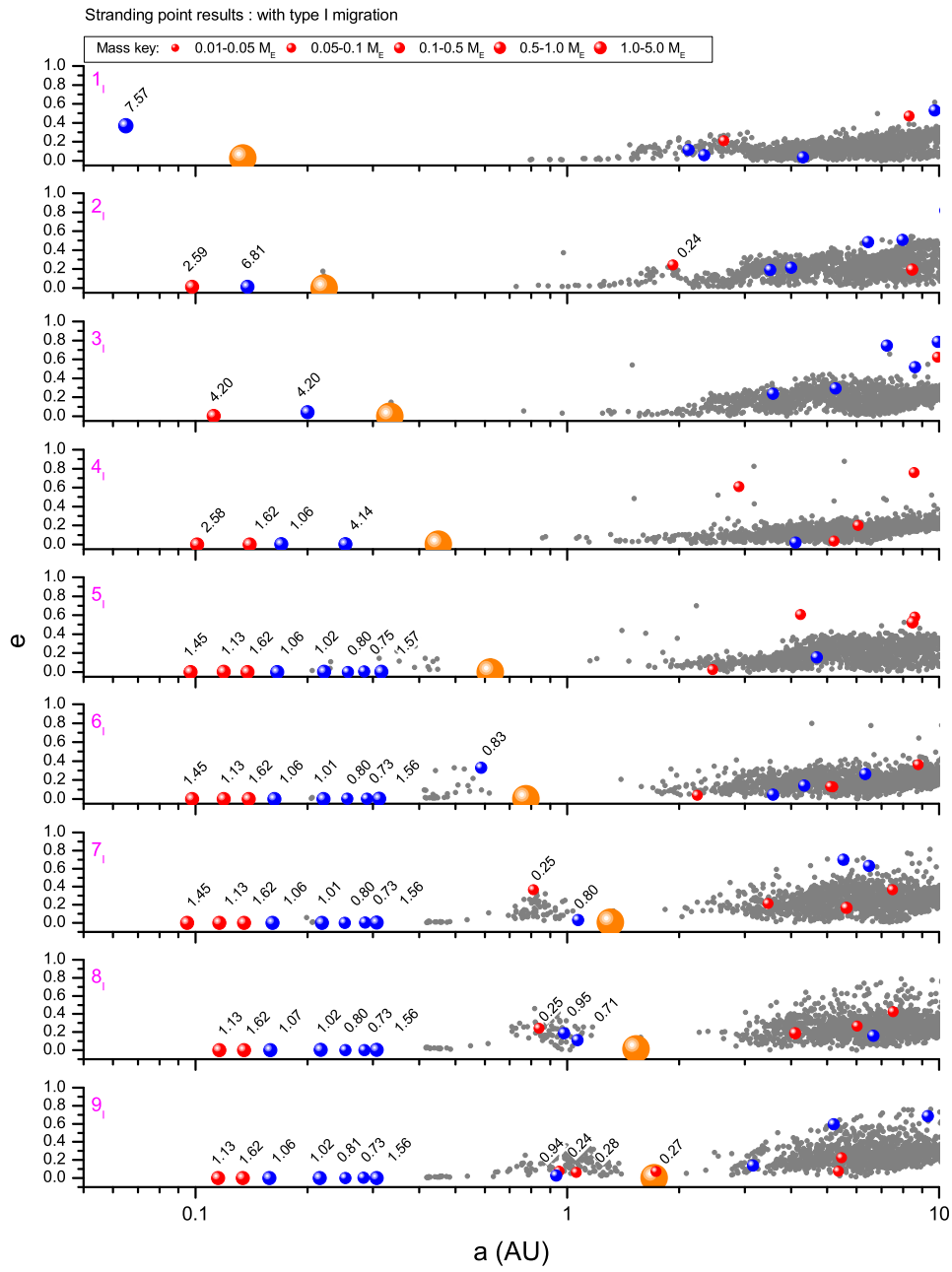

Figure 6.7: Run Set **B**. End points of all nine Model IV scenarios that *include* type I migration, at the time when the giant planet strands at its final semi-major axis. Details of the plot are explained in the caption to Fig. 6.6.

at $a > 2\ a_{\rm g}$. *Habitable planet candidates can therefore be expected if a migrating giant planet makes a limited excursion into the HZ. However, if it traverses the HZ, such candidates are only expected to be common if the giant continues its migration to a radial distance of less than half that of the inner edge of the HZ.* Whether the potential habitable planets visible in Figs. 6.6 & 6.7 can survive the long final phase of accretion that remains to be played out in their respective systems is examined in Sect. 6.4.

The interior disks that result after the giant planet's migration stalls show a considerable difference when the two figures are compared. When type I migration operates (Fig. 6.7), interior partitions tend to be more massive and have cleared almost all of their planetesimal population. Hence $f_{\rm proto} \approx 1$, but large numbers of protoplanets are also found, as type I eccentricity damping exerted by the residual gas acts to reduce the effects of mutual scattering, causing protoplanets to dynamically settle into stable resonant convoys with closely spaced, and near-circular, orbits. For example, the inner eight protoplanets at the end points of Scenarios $5_{\rm I} - 7_{\rm I}$, from the inside out, are locked into a 4:3, 5:4, 4:3, 3:2, 5:4, 7:6, 7:6 configuration of mean motion resonances. Oligarchic growth therefore ends in these interior systems when the planetesimal field is accreted, but giant impact growth is delayed, at least for as long as the disk gas persists. When no type I migration operates (Fig. 6.6), interior partitions are relatively depleted of mass and contain fewer protoplanets, in more excited orbits, alongside a surviving population of planetesimals ($f_{\rm proto} < 1$). In Scenarios 1 – 2, where the giant planet has experienced the lengthiest migration to $a_{\rm g} \lesssim 0.2$ AU, late scattering or accretion has removed all interior protoplanets (similar to the results of Model II). In Scenarios 3 – 5, just one relatively low mass hot-Earth remains at the end point. The inner disk fares better in late scenarios (7 – 9) when migration is limited to $a_{\rm g} \gtrsim 1$ AU. Numerous interior protoplanets remain in these cases, and since type I migration forces are absent, accretion via giant impacts is not suppressed and protoplanetary growth is more advanced. Since both run sets produce such different interior partitions, it is of considerable interest to determine if this affects their final architectures after the subsequent phase of gas-free accretion. This issue is followed up in Sect. 6.4.

Some features of the interior systems illustrated in Figs 6.6 & 6.7 are worthy of further comment.

Scenarios 3 – 5: Only one interior planet survives in these scenarios where the giant planet strands between $a_{\rm g} = 0.27$ – 0.55 AU, and only one of these is found at a first order resonance with the giant at the end point. This is the $1.90\ {\rm M}_\oplus$ planet in Scenario 4, which is captured at the 2:1 resonance. In the case of Scenario 3, the

interior planet is found closer to the giant planet, whilst in Scenario 5 the sweeping 2:1 resonance has not quite reached the surviving $1.60\ \mathrm{M}_\oplus$ planet.

Scenario 6: The giant planet has stranded at $a_\mathrm{g} = 0.68$ AU, leaving four surviving protoplanets in the interior partition. The outermost of these has an orbit with $e \approx 0.3$, close to a 7:4 period ratio with the giant planet, that crosses the orbit of its nearest neighbor. To an accuracy of $< 1\ \%$, period ratios between the protoplanets, from the outside in, are 4:3, 5:4, and 3:2 respectively, which are a feature reminiscent of the resonant convoys of protoplanets commonly observed in simulations where type I eccentricity damping is included. In this case, dynamical friction from surviving planetesimals exerts the damping, but its relative weakness produces an arrangement that is more dynamically excited and likely to be unstable as the outermost pair of protoplanets are in crossing orbits.

Scenario 8: This case stands out from its adjacent Scenarios 7 & 9, where the giant planet also strands at $a_\mathrm{g} > 1$ AU, because planetary growth in the interior partition appears to be much more advanced, resulting in three planets in well-spaced orbits. This is entirely due to chance giant impacts shortly before the scenario end point. It is shown in Sect. 6.4 that, if carried through into the gas-free phase, accretion within the interior partitions of Scenarios 7 & 9 rapidly catches up, with excess protoplanets being eliminated by co-accretion or impact onto the giant planet.

Scenario 1_I: The single interior planet resulting from this run is the best hot-Neptune/Earth analogue generated by Model IV. Its mass of $7.57\ \mathrm{M}_\oplus$ puts it within the observed range for such objects (see Fig. 1.4). However, in contrast with the results of Model III (Fig. 5.14), the planet is not found at the first order 3:2 or 2:1 resonances, but it is located further away from the giant planet, at the second order 3:1 resonance (see Fig. 6.8). Study of this system's evolution however reveals that this object was originally shepherded inward at the 2:1, but within the last 0.12 Myr of the run it scatters with and eventually accretes two other protoplanets interior to it, contracting the orbit of the merged body, whereupon it is fortuitously captured at the 3:1 resonance. This phenomenon of resonance capture through scattering has been recently described by Raymond *et al.* (2008). The arrangement of hot-Neptune and hot-Jupiter in Scenario 1_I is most similar to that observed between the two inner planets e and b in the 55 Cancri system (panel 2, Fig. 1.4), although the orbits of these two natural objects are separated by a wider $\sim$ 5:1 period ratio.

Scenario 2_I: Two interior planets survive in this case where the giant strands at $a_\mathrm{g} = 0.22$ AU. The outermost planet of this pair is in the 2:1 resonance with the giant planet.

Scenario 3_I: Two equal mass hot-Earths survive at the end point of this scenario

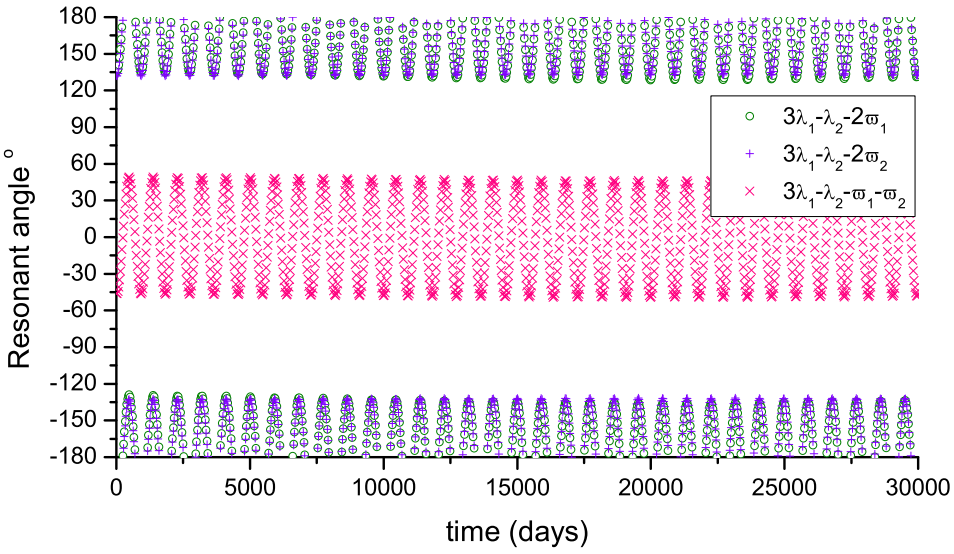

Figure 6.8: Resonant angles for the 3:1 mean motion resonance between the hot-Jupiter and the interior $7.57\ \mathrm{M}_{\oplus}$ hot-Neptune in Scenario 1_{I}. Capture in resonance is indicated by libration of the resonant angles.

($a_{\mathrm{g}} = 0.33$ AU), but neither of them are in resonant orbits. A resonant convoy of five interior planets becomes unstable in the last 40 000 yr of the simulation and is broken up by giant impacts.

Scenario 9_{I}: A noteworthy feature of the end point of this run is the presence of a $0.27\ \mathrm{M}_{\oplus}$ Trojan protoplanet, located in a stable co-orbital resonance with the giant planet. This object was captured into this 1:1 resonance shortly after the introduction of the giant and escorts the larger body inward during type II migration. Although the capture of the Trojan planet in this case may have been influenced by the abrupt introduction of the giant planet at the scenario start time, its presence at the end point is not necessarily unrealistic or unexpected. Dvorak *et al.* (2004) & Erdi and Sandor (2005) have shown that co-orbital motions can be stable for long time scales and 1:1 capture and co-migration, in a context where type I migration forces are active, has previously been observed in simulations by Cresswell and Nelson (2006, 2008).

Alternate visualizations of the data for the end points of Scenarios 1 – 9 and Scenarios $1_{\mathrm{I}} - 9_{\mathrm{I}}$ are presented in Figs. 6.9 & 6.10 respectively. These data are the equivalent of the 'fate of the disk mass' results of previous models set out in Tables 3.3, 4.3, & 5.3 and have to be recast into graphical format for Model IV since 18 scenarios are under consideration, rather than 5 or 6. The nine scenarios of each run set are indicated on the x-axis by their start time t and the cumulative percentage of

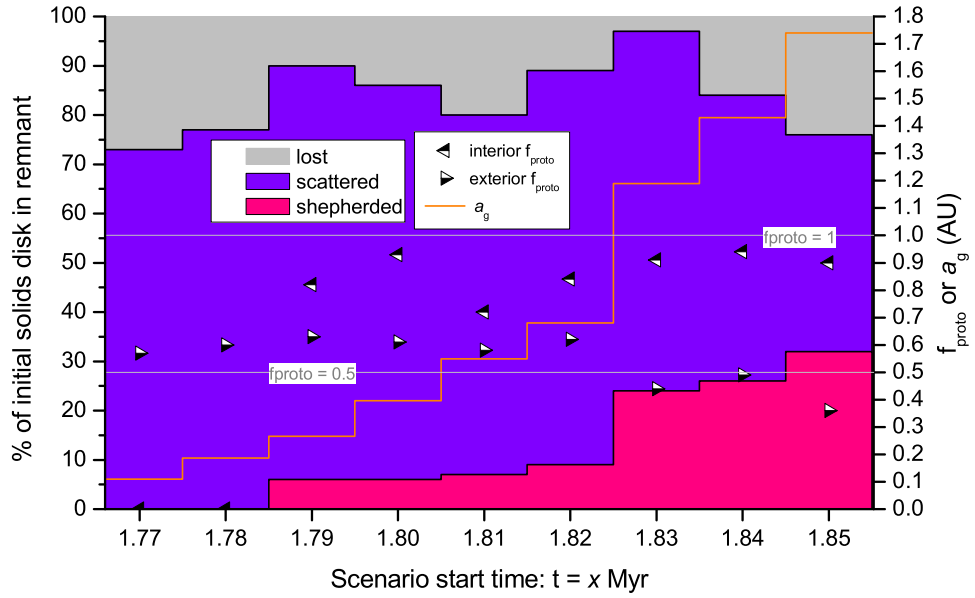

Figure 6.9: Run Set **A**. Fate of the disk mass at the end points of Scenarios 1 – 9 (*without* type I migration). Data include the % of initial solids disk in the shepherded or scattered remnant, or lost; $f_{\rm proto}$ of the inner or outer remnant; and $a_{\rm g}$. See the key and text for details.

the initial solids disk remaining is read off the left hand y-axis, with the red bars representing the fraction remaining in the shepherded remnant, the blue bars that in the scattered remnant, and the grey bars that which is lost – predominantly via accretion onto the giant planet. The right hand y-axis gives $f_{\rm proto}$ for the interior or exterior remnant (the symbols being given in the key), or the stranding position of the giant planet $a_{\rm g}$/AU which is shown by the orange line. Horizontal lines $f_{\rm proto} = 0.5$ and $f_{\rm proto} = 1$ are drawn for reference.

Both figures show that the great majority of the solids disk ($\sim 80 - 90$ %) survives giant planet migration, regardless of whether type I migration operates or not, and regardless of the stranding position of the giant planet. The bias toward scattering behaviour in the absence of type I migration shows well in Fig. 6.9 as, when $a_{\rm g} < 1$ AU, less than 10 % of the disk mass remains in the shepherded partition. The biassed scattering of protoplanets is indicated by the value of exterior $f_{\rm proto} > 0.5$. In contrast, in the presence of type I migration (Fig. 6.10), partitioning of the solids disk is largely insensitive to $a_{\rm g}$ with $\sim 30\%$ and $\sim 60\%$ of the mass remaining in the interior and exterior partitions respectively in all scenarios. The bias against the scattering of protoplanets is indicated by the value of exterior $f_{\rm proto} \approx 0.3$.

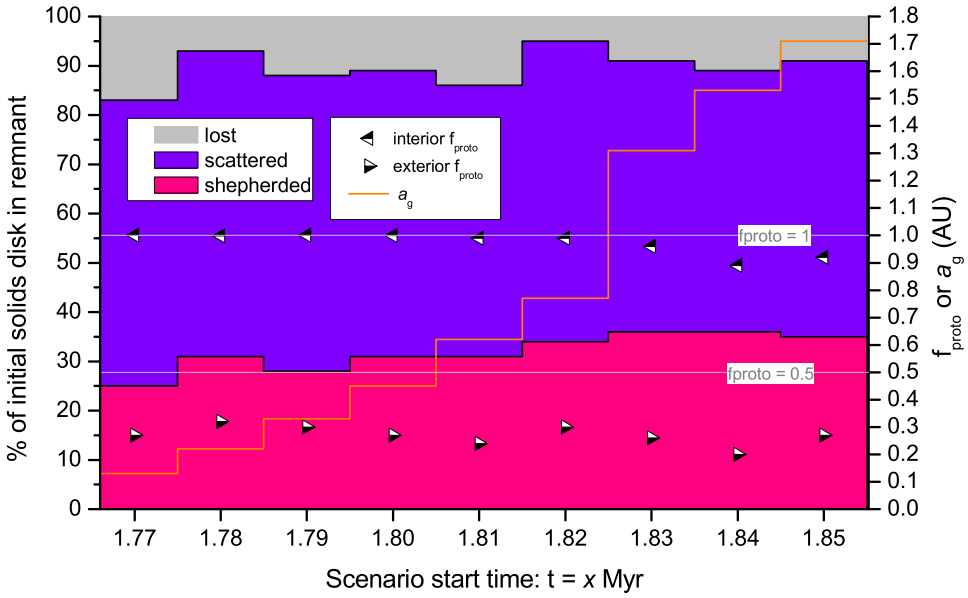

Figure 6.10: Run Set **B**. Fate of the disk mass at the end points of Scenarios $1_{\rm I} - 9_{\rm I}$ (*with* type I migration). Data include the % of initial solids disk in the shepherded or scattered remnant, or lost; $f_{\rm proto}$ of the inner or outer remnant; and $a_{\rm g}$. See the key and text for details.

One might reasonably speculate, given the details in Figs. 6.6 – 6.10, that the final systems of terrestrial planets that should emerge from these scenarios might be either internally or externally weighted (in terms of both planetary numbers and masses) depending on the strength of type I migration forces operating during gas-phase formation. If Model IV reflects reality, its results may help contribute to the debate over the reality of type I migration once observational techniques have advanced sufficiently to enable a more complete inventory of terrestrial planets in exoplanetary systems where type II giant planet migration is thought to have occurred.

6.4 Post–migration terrestrial planet formation

The results of Model IV, shown in Figs. 6.6 & 6.7, have taken the accretion process only to the point at which the giant planet strands due to the loss of the nebular gas. Planet formation in all exterior and most interior partitions of the original inner system disk is clearly incomplete and awaits a much lengthier phase of gas-free accumulation. Simulation of at least part of this gas-free accretion phase is of clear interest to see if the conclusions drawn from running the model to the end point of migra-

tion might stand up over the long-term. Would a more complete accretion reduce the observed differences between the two run sets? What will be the fate of the closely packed resonant convoys of protoplanets created by type I migration (Fig. 6.7)? Are habitable zones containing protoplanets at the end of the migration epoch still likely to contain planets over the long-term?

Thus, after switching off all residual forces exerted by the last traces of gas, simulation of all the scenarios of both Run Sets has been extended with the aim of running them to a system age of 30 Myr ($t = 29.5$ Myr). However, this is not practical in every case as the time-step is constrained by the orbits of the innermost objects. The method adopted here is to chose a time step equivalent to one tenth of a circular orbit with a semi-major axis equal to the periastron of the innermost large object. This strategy typically dictates a time-step of 2 – 4 days and serves well in all but two scenarios. These are Scenario 3 in which a 2 day time-step inadequately resolves the orbits of a planetesimal swarm interior to the hot-Earth at 0.18 AU, resulting in an unrealistic loss of these objects via accretion onto both the star and the hot-Earth; and Scenario $1_{\rm I}$ where a hot-Neptune at 0.065 AU dictates too small a time-step – a problem that is tackled by splitting the problem into sub runs – 1) the hot-Neptune and hot-Jupiter with a 0.3 day time-step, 2) the hot-Jupiter and external disk with a 2 day time-step, and then assembling both as a composite. Even so, eight months after beginning most of these extended runs it has not been possible before submission of this thesis to complete every simulation. All but one scenario in Run Set **A** has attained the goal of 30 Myr, but in Run Set **B**, where previous type I migration has typically resulted in protoplanets closer to the star at the point of gas loss, the results presented here vary in their ages from 15 – 30 Myr.

The results of these extended simulations are illustrated in Figs. 6.11 (Run Set **A**) & 6.12 (Run Set **B**) and should be compared with their migration end-point equivalents in Figs. 6.6 & 6.7 respectively. A number of general observations can be made.

1. *Accretion interior to the giant planet.* Solitary, or paired, hot-Neptunes or hot-Earths that are present at the end of the migration epoch (e.g. Scenarios 3 – 5 and Scenarios $1_{\rm I} - 3_{\rm I}$) are found to survive the extended gas-free accretion phase with little change in their orbital parameters. The crowded interior disk partitions that result in later scenarios where the giant comes to rest at greater distances from the central star undergo rapid evolution to a state of near completion, with giant impacts thinning down the number of protoplanets which mop up almost all residual planetesimal debris.

As discussed in Sect. 6.3, giant impact growth in Run Set **A** is already underway

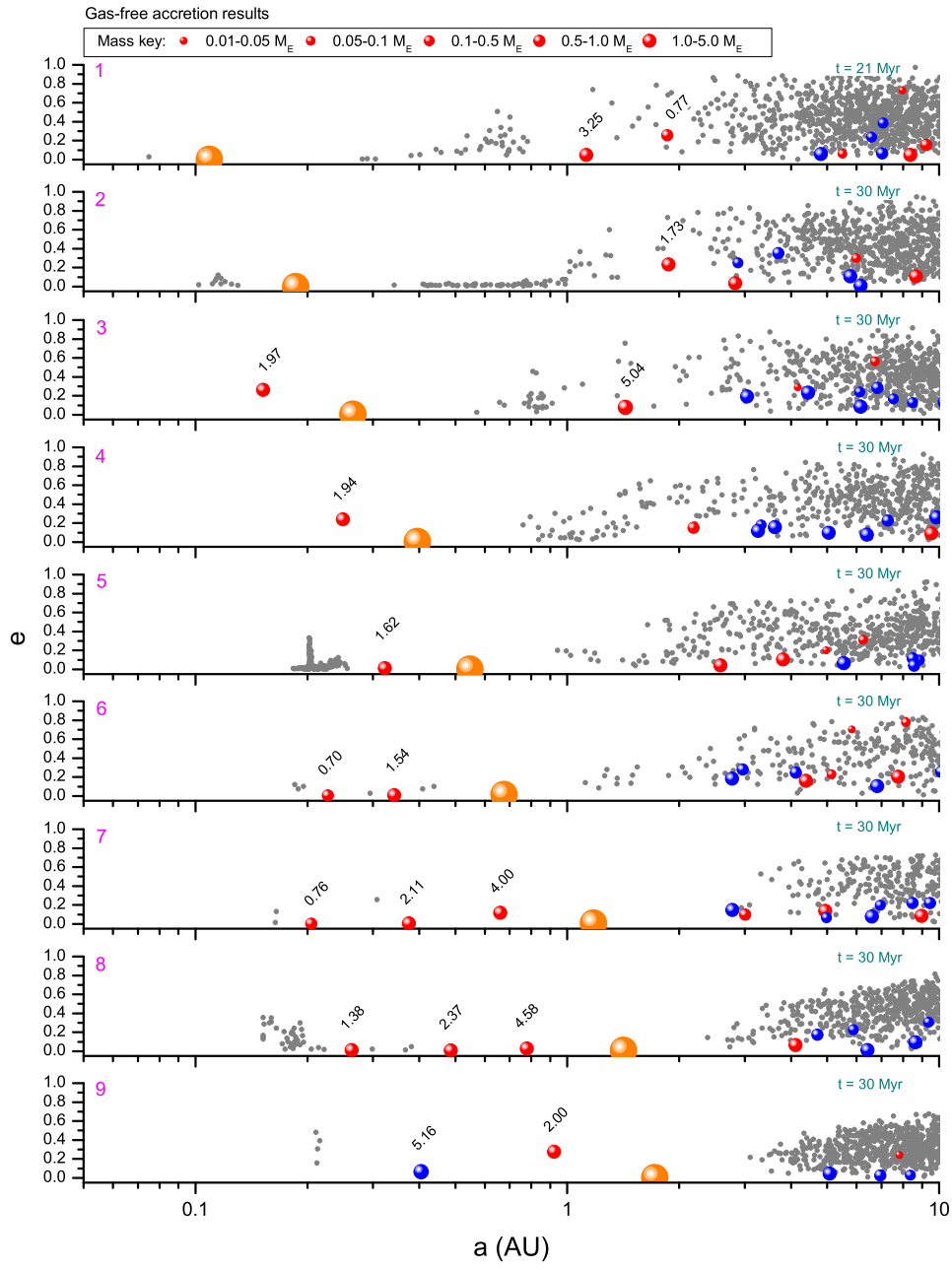

Figure 6.11: Run Set **A**. Gas-free accretion results of all nine Model IV scenarios that *exclude* previous type I migration. Eccentricity is plotted vs. semi-major axis with symbols colour coded as in previous examples and sized according to the mass key. Scenario ID is given at the top left of each panel. System age is given at the top right of each panel. Protoplanets interior to the giant, or within 1 – 2 AU, are labelled with their mass in $M_{\oplus}$.

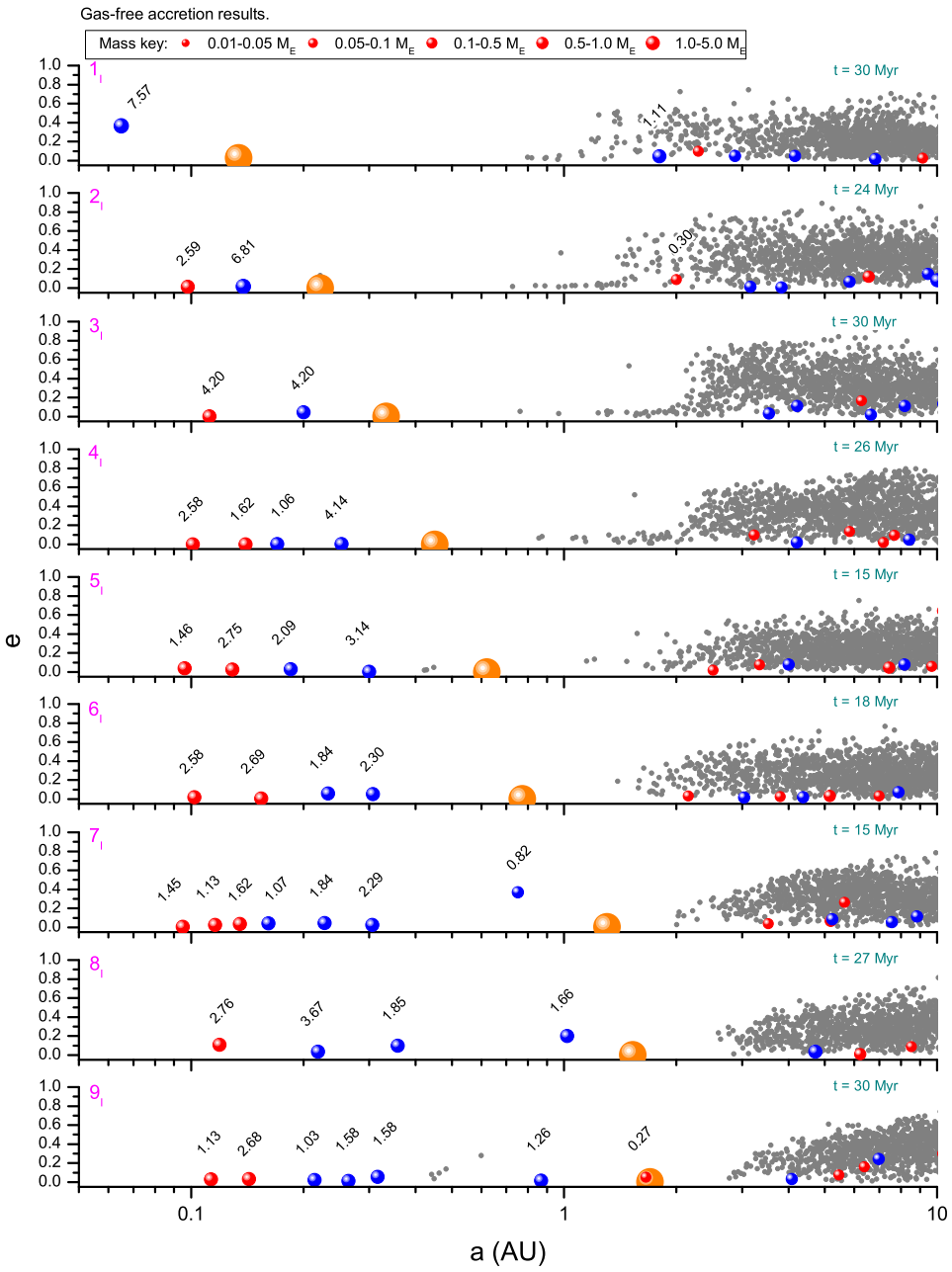

Figure 6.12: Run Set **B**. Gas-free accretion results of all nine Model IV scenarios that *include* previous type I migration. Scenario ID is given at the top left of each panel. System age is given at the top right of each panel. Protoplanets interior to the giant, or within 1 – 2 AU, are labelled with their mass in $M_{\oplus}$.

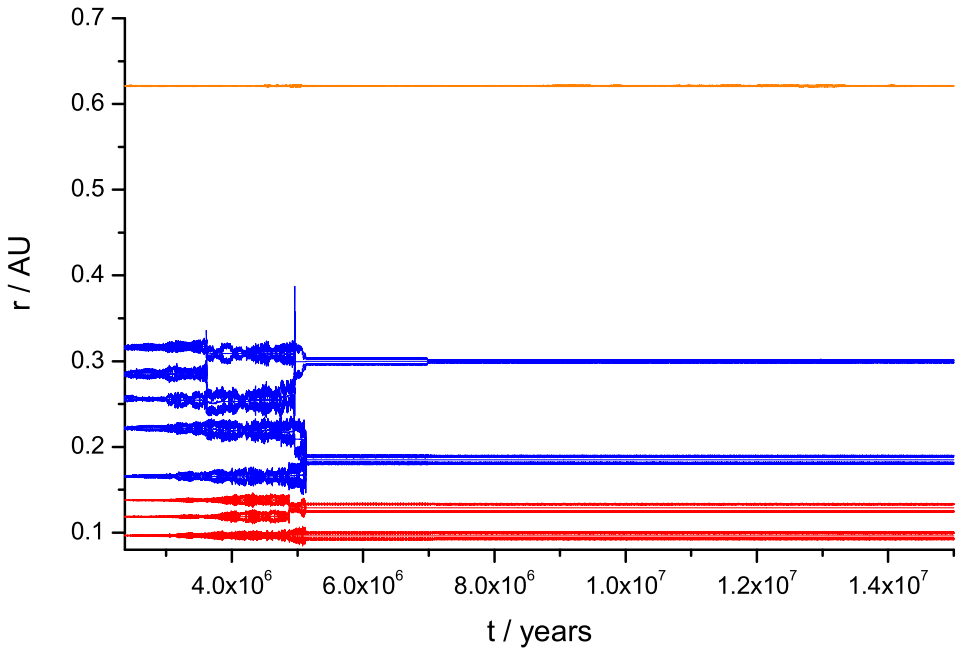

Figure 6.13: Destabilization of the resonant convoy in Scenario $5_{\rm I}$. Temporal evolution of the periastron, semi-major axis, and apastron for each object is shown, with the giant planet drawn in orange at the top of the graph. Protoplanets undergo a sequence of closest neighbour mergers, reducing their number from eight down to a stable quartet of hot-Earths.

before the end of the migration phase as the protoplanets within interior partitions are sufficiently dynamically excited to exhibit crossing orbits. This process completes rapidly after gas loss, with protoplanetary mergers reducing their numbers by $\sim 50\%$, resulting in apparently stable multiple interior systems of two or three hot-Earths separated by > 20 mutual Hill radii (note Scenarios 6 – 9, Fig. 6.11).

In Run Set **B**, type I migration forces have previously suppressed giant impact growth, causing protoplanets to stack into crowded resonant convoys (e.g. Scenarios $5_{\rm I} - 9_{\rm I}$, Fig. 6.7). After the gas is gone in these cases, all eccentricity damping ceases and the convoys start to destabilize within a few Myr, typically by protoplanets merging with their nearest neighbours, ultimately reducing their numbers by $\sim 50\%$. This occurs fastest in convoys that are the most compressed by the position of the giant planet (i.e. restricted within the narrowest annulus) and the process is clearly illustrated in the case of Scenario $5_{\rm I}$ in Fig. 6.13. Generally however, systems where strong type I migration has operated in the gas phase still retain more interior planets, although is it not certain that all giant impact growth is completed within the interior

partitions of the later scenarios illustrated in Fig. 6.12. Scenarios $7_{\rm I}$ & $9_{\rm I}$ have interior protoplanets still separated by as little as ~ 10 mutual Hill radii and some traces of the original resonant convoy structure remains, such as the 4:3, 5:4, 4:3 commensurability between the inner four planets of Scenario $7_{\rm I}$. Whatever the final outcome in these cases however, hot and warm-Earths, including multiple systems, are predicted as an outcome of type II migration induced disk compaction in all but the earliest scenarios of Run Set **A**.

2. *Accretion exterior to the giant planet.* Planetary growth in exterior partitions at $\gtrsim 2$ AU is ongoing and not yet complete. This is to be expected as dynamical times are longer, scattered material is spread over a larger volume, and does not have an opportunity to interact with disk solids originating beyond 5 AU which have not been modelled. However, it can be seen in Figs. 6.11 & 6.12 that dynamical friction exerted by the scattered planetesimal population has resulted in a degree of circularization of the orbits of scattered protoplanets, especially in the case of Run Set **B**, where dynamical friction is particularly strong due to the low exterior value of $f_{\rm proto}$ (see Fig. 6.10 and associated discussion).

3. *Planetary occupants of the habitable zone.* Three planets in each run set are found in their system's habitable zone ($\sim 0.84 - 1.67$ AU) after the extended gas-free runs. In Run Set **A**, these are 3.25, 5.04 & 2.00 $\rm M_{\oplus}$ planets in Scenarios 1, 3 & 9 respectively (Fig. 6.11); and in Run Set **B** a 1.66 $\rm M_{\oplus}$ planet in Scenario $8_{\rm I}$ and 1.26 & 0.27 $\rm M_{\oplus}$ planets in Scenario $9_{\rm I}$ (Fig. 6.12). This latter object is the Trojan planet captured into a 1:1 resonance with the giant early on in the migration phase (discussed in Sect. 6.3) and dragged inward to $a = 1.66$ AU, just inside the outer edge of the habitable zone. This exotic world remains in a continuously stable orbit up to a system age of 30 Myr, and has the potential for a prolonged existence (Dvorak *et al.*, 2004; Erdi and Sandor, 2005). The finding articulated in the previous Section that the giant planet must make either a limited excursion into the habitable zone, or a complete traversal down to $\lesssim 0.5 \times$ the radial distance of the inner edge of the HZ, for a habitable planet to be possible is reinforced by the results of the extended simulations. Potentially habitable planets are found in systems where the giant planet lies outside the region of $\sim 0.3 - 1.5$ AU.

4. *Volatile endowments.* In agreement with Models II & III, the habitable planets generated by Model IV are predicted to be richly endowed with volatiles driven inward from beyond the nebular snowline by the migrating giant planet. The composition of

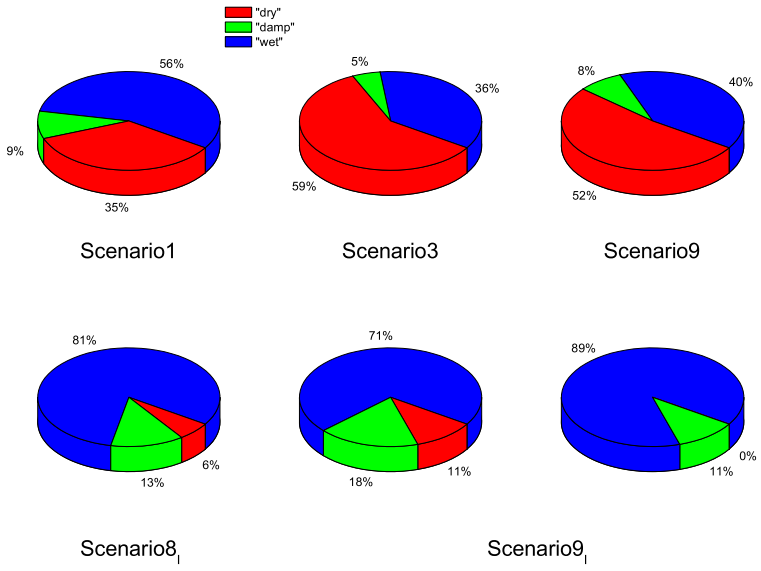

Figure 6.14: Material composition of habitable planet candidates in Model IV. Red indicates material of provenance $a < 2$ AU; green indicates material of provenance $2 \text{ AU} < a < 2.7 \text{ AU}$; and blue indicates trans-snowline material originating from $a > 2.7$ AU. The top row of charts are the results of Run Set **A** and the bottom charts the results of Run Set **B**.

the six habitable planet candidates, using the same crude three phases described in Sect. 4.2, are shown as pie charts in Fig. 6.14. Even with no previous type I migration operating (the top row in the figure), habitable planets have incorporated roughly a third to a half of their material from beyond the snowline. Where there has been pre-existing type I migration, more like three quarters of the planets' mass originates from beyond the snowline. Whether the habitable planets in question lie interior or exterior to the giant seems to make little difference to the composition. All such worlds are predicted to be richly endowed with water and gases.

6.5 Model IV: conclusions

All previous published models of terrestrial planet formation in the presence of type II giant planet migration have neglected the issue of what causes the giant planet to come to rest in its final orbit and have simply switched off migration forces at a pre-defined distance from the central star (Fogg and Nelson, 2005, 2006, 2007a,b, 2008; Raymond *et al.*, 2006; Mandell *et al.*, 2007). Model IV in this thesis is the first simulation of this

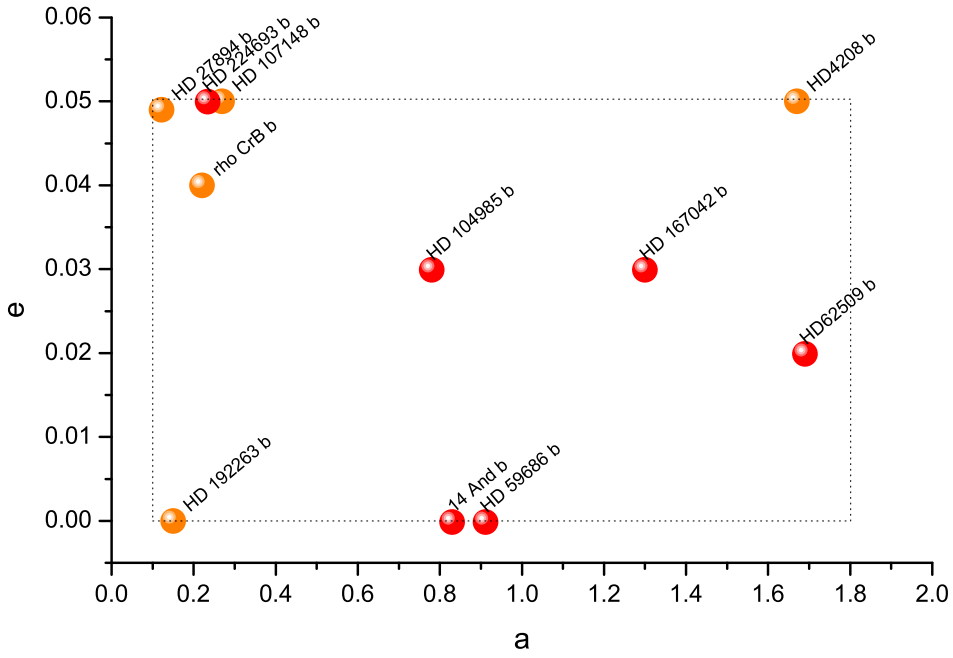

Figure 6.15: Data of low eccentricity exoplanets, plotted using data from the correlation diagrams tool at the Extrasolar Planets Encyclopedia: http://exoplanet.eu. Plotted objects correspond to the type of warm-Jupiters within the remit of Model IV: solitary giant planets orbiting single stars with $0.1\ \mathrm{AU} < a < 1.8\ \mathrm{AU}$, $e < 0.05$. Orange symbols represent exoplanets within main sequence star systems; red symbols represent exoplanets orbiting main sequence stars.

type to include a self-consistent scenario for the stranding of the giant planet, which comes to rest naturally at the point when the gaseous fraction of the protoplanetary disk is lost via a combination of accretion onto the central star and photoevaporation.

The results of the earliest Model IV scenarios – those which simulate hot-Jupiter emplacement at $a_{\mathrm{g}} \lesssim 0.2$ AU – are very similar to the late scenarios of Models II & III, where the evolution of the nebula is advanced and dissipative forces that stem from the presence of gas are relatively weak. Most of the inner system disk solids survive the traverse of the giant planet and most of this surviving matter is scattered into higher orbits where planet formation can resume. Water-rich habitable planets are possible within a habitable zone that is far removed from the final position of the giant planet. Where dissipative processes are enhanced by type I migration, one or two hot-Earths or hot-Neptunes are found to persist in orbits interior to the giant planet.

In ‘warm-Jupiter’ type scenarios, where $a_{\mathrm{g}} \gtrsim 0.2$ AU, the bulk of the disk solids

survive as before, but more complex systems of hot terrestrial planets interior to the giant are predicted, in larger numbers with increasing $a_{\rm g}$. If strong type I migration forces are a genuine influence on planet formation, relatively crowded systems of interior planets are predicted, although it has not been practical to check this forecast with Gyr-long integrations. Habitable planets in low eccentricity warm-Jupiter systems appear possible if the giant planet is outside the region of $\sim 0.3 - 1.5$ AU for a 1 $\mathrm{M}_{\odot}$ star. This finding should hold for stars with different luminosities with an appropriate scaling of radial distance.

However, warm-Jupiter type exoplanets with near-circular orbits, i.e. $e \lesssim 0.05$, are relatively uncommon (see Fig. 1.2) and e is typically observed to be considerably higher. Many of these exoplanets may have had an origin involving mutual giant planet scattering, perhaps combined with migration as discussed in Sect. 1.2.2, as opposed to the strongly damped pure type II migration mechanism adopted in Model IV. Nevertheless, low-e and solitary warm-Jupiters are known, which presumably could have originated in a similar manner to that simulated here. Fig. 6.15 uses the Extrasolar Planets Encyclopedia correlation tool to plot exoplanetary data between $a = 0.1 - 1.8$ AU vs. $e = 0 - 0.05$ which might be regarded as lying within the remit of Model IV. Solitary giant planets around single stars are labelled with their names. Four of these exoplanets, $\rho\,\mathrm{CrB\ b}$, HD 27894 b, HD 192263 b and HD 4208 b occur in systems where there is dynamical room for terrestrial planets in the habitable zone according to the stability calculations of Jones *et al.* (2005, 2006). Systems containing the exoplanets HD 224693 b (Jones *et al.*, 2006), HD 104985 and HD 59686 (Jones *et al.*, 2005) could also have hosted planets in their habitable zones in the past before their primaries left the main sequence. According to the results of Model IV, it appears feasible that habitable planets could have originated in these systems as well.

Chapter 7

Discussion and concluding remarks

> Events such as this can be calamitous for terrestrial planets. When a Jupiter spirals inward, the inner planets precede it and are pushed into the star.
>
> *Rare Earth: Why Complex Life is Uncommon in the Universe*, Ward and Brownlee (2000)

7.1 Salient findings of this thesis

The purpose of this thesis is to question whether the scenario exemplified by the quotation above is realistic and can be applied generally. Does large-scale giant planet migration during the early stages of planet formation inevitably prevent the growth and survival of terrestrial planets? Should hot-Jupiter systems therefore be assigned a low priority in the search for extraterrestrial life?

These questions are of interest not just from the perspectives of astrophysics and astrobiology, but give an insight into the culture of science also. In the absence of hard facts and concrete understanding, astrobiological hypotheses have to be erected on a set of assumptions that vary in their solidity. Hence, such 'educated guesses' can become flavored by the mood of the times and, once pruned of caveats in the media, can often be presented with a dubious air of certainty. It is perhaps not surprising in hindsight that the exuberance of the 1960's gave rise to a widespread optimism concerning the likely abundance of complex life in the universe and the possibility of interstellar communication (e.g. Cameron, 1963; Shklovskii and Sagan, 1966; Morrison *et al.*, 1977; Sagan, 1980). Fashions change however and tend to lurch between the extremes of their domain. Today, perhaps in sympathy with pervasive anxiety over environmental degradation and climate change, the trendiest astrobiological concept being pushed by the media (e.g. Stewart, 2008; Clark, 2008) is the Rare Earth Hypothesis of Ward and Brownlee (2000). This asserts that complex life is frail and demanding of a finely tuned environment, and that the existence of planets suitable for hosting it requires such a large number of coincidences to play out over geologic time that such worlds are likely exceptional and maybe, other than the Earth itself, non-existent. However, although 40 years have passed since the heyday of 'contact optimism', the validity of many assumptions drawn on in astrobiological arguments remains suspect, as do conclusions drawn from them.

The research presented in this thesis, and the papers it has generated (Fogg and Nelson, 2005, 2006, 2007a,b), represents the first attempt to model the effect of type II

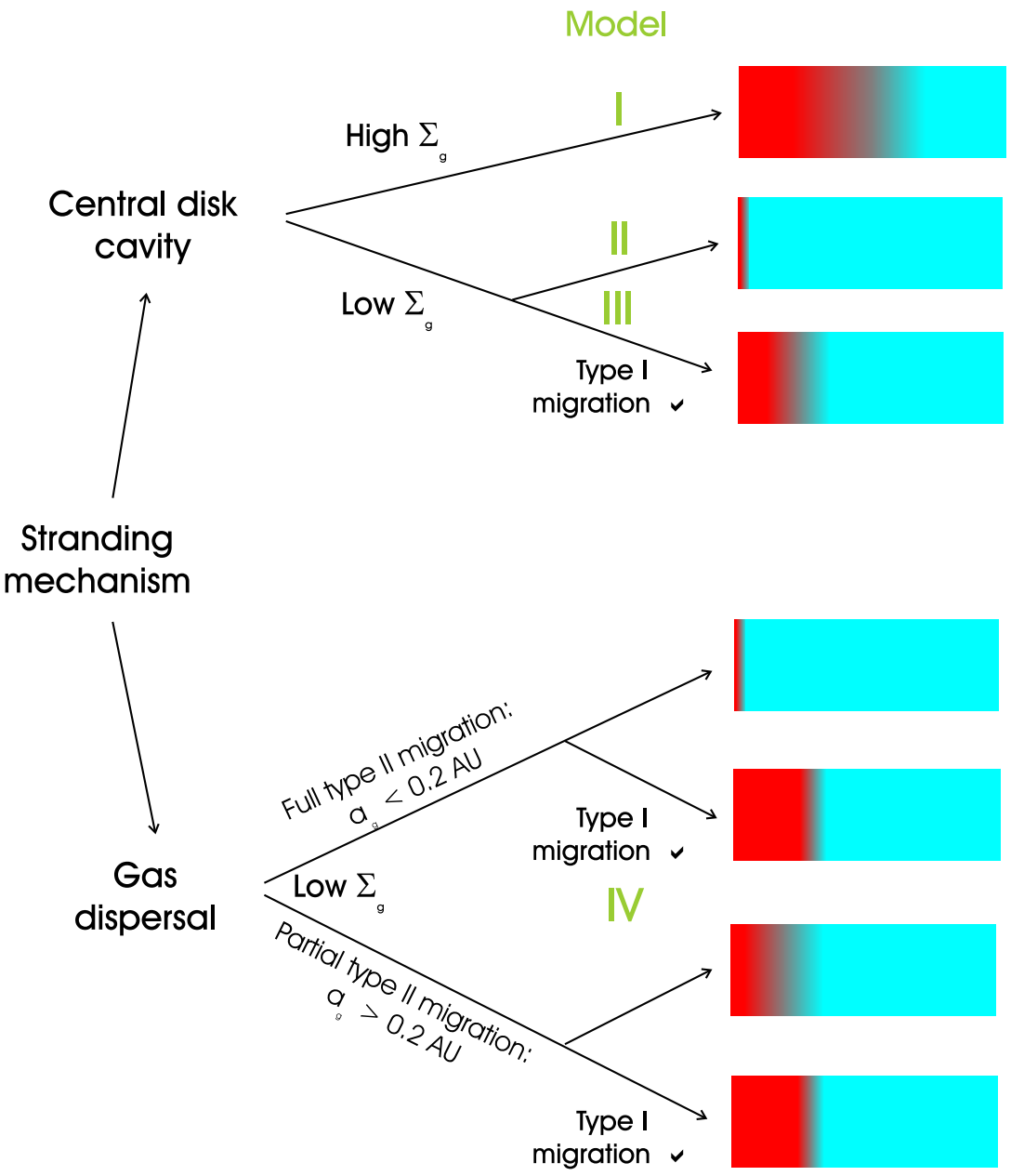

Figure 7.1: Partitioning of *surviving* solids disk material. Summary of averaged results from Models I – IV (excepting Scenario V, Model I). Red and blue represent disk fractions interior and exterior to $a_{\rm g}$ respectively. Blended colours represent overlap between scenarios.

giant planet migration on inner system terrestrial planet formation. It is the first theoretical test of the assumption that hot-Jupiter systems should lack terrestrial planets. *An important finding is that a giant planet does not clear all planetary building blocks from the zone swept by its migration.* Far from it: in every scenario of every model $> 50\%$ of the solids disk material originally interior to the giant planet is still present after the migration episode is complete. A rough average is $\sim 75\%$, and in one scenario 90% of the material survives. In every case enough material is scattered by the migrating giant planet to partially regenerate a solids disk external to the final position of the hot-Jupiter (amounting to 26% – 84% of the original disk mass) in which terrestrial planet formation can resume. This appears to be a robust finding, which has been confirmed by others (Raymond *et al.*, 2006; Mandell *et al.*, 2007), and is not negated by including the possibility of the action of strong type I migration on terrestrial protoplanets (Fogg and Nelson, 2007b).

A summary of the overall results of this research is shown in Fig. 7.1 which gives a qualitative impression of the partitioning of the surviving solids disk mass resulting from all four models which were presented in Chapters 3 – 6. The red in each horizontal bar represents the fraction of the remaining disk in the shepherded remnant interior to the stranding distance of the giant planet; the blue represents the fraction in the scattered disk exterior to the giant planet; and the blending of colours between the two gives a rough measure of the overlap between scenarios in each particular model. Generation of a substantial scattered disk in each case is an obvious feature of the data. However, survival of a shepherded interior disk remnant – especially one containing one or more large bodies – is much more model-dependent and strongly influenced by the strength of processes that act to damp the dynamics of both protoplanets and planetesimals.

If hot-Jupiters come to rest due to the presence of an ~ 0.1 AU gaseous inner disk cavity, then the migration episodes could take place within gas disks of varying densities. Although this stopping mechanism has not been consistently simulated here (unlike the gas dispersal mechanism of Model IV), Models I, II & III which halt the giant at 0.1 AU by prescription, and which model type II migration within gas disks of varying age and mass, come close to implicitly assuming the cavity migration halting mechanism. Hence, they are distinguished from Model IV in Fig. 7.1 on this basis, with the caveat that they do retain some gas interior to 0.1 AU (particularly in the case of Model I) which could affect some of the processes interior to the giant planet at the very end of the migration phase. In the case of a high $\Sigma_{\rm g}$ and a steep profile (Model I)[1], then hot-Earths and even hot-Neptunes are predicted to occur in

[1] It should be recalled that Model I is the least sophisticated of those presented in this thesis

orbits interior to the hot-Jupiter (Fig. 3.9). Only in the situation where the giant migrates down to $\lesssim$ 0.05 AU do these objects run a high risk of being driven into the central star (Fig. 3.11). In the case of a low $\Sigma_{\rm g}$ and a declining profile close to the central star (Model II), shepherding of material is weak, external scattering or accretion by the giant planet dominates, and no hot-Earths are found to survive at all (Fig. 4.10). Adding in the possible damping exerted on protoplanets through the action of type I migration (Model III) restores the finding of hot-Earth survival (Fig. 5.8), although these objects are typically found at first order resonances close to the giant planet and in more eccentric orbits than in Model I. If migrating giant planets halt through fortuitous disk dispersal (Model IV), then migration episodes inevitably occur in an environment of low $\Sigma_{\rm g}$, with stranding occurring at a range of distances from the central star. A variety of solids disk partitioning behaviour results, with interior planets being favored if the giant only partially traverses the confines of the original disk, or if strong type I migration is in force (Figs. 6.6 & 6.7).

The issue of whether the disk compaction mechanism of hot-Neptune or hot-Earth formation advanced in this thesis is valid, and occurs in nature, is still open. Only four observed systems, which contain both a hot-Neptune and a circumscribing giant planet, are relevant to this hypothesis (Fig. 1.4), and although results show some similarities with observations, there remain differences which the models do not account for. The four observed systems all contain more than one giant planet and their interior hot-Neptunes are all found further away from the inner giant than is typically found in the models, where the usual outcome is a hot-Earth captured at the 2:1 or 3:2 mean motion resonance. This is not an invariable result however as, in a minority of runs, hot-Earths are released from resonant locking with the giant planet during the dramatic terminal accretion phase of the compacted interior disk remnant through a combination of protoplanetary close encounters and giant impacts. One can still claim that the disk compaction hypothesis remains a plausible one, but it may not fully apply to the four systems cited. The models which generate hot-Earths tend to produce planets of lower mass than the minimum masses of observed examples, so it could be that objects which might provide better evidence for disk compaction await discovery in the future. The following predictions are a consequence of the results of the model as it stands:

1. Hot-Jupiters are accompanied by systems of terrestrial planets in higher orbits.

2. Hot-Jupiter systems have a good probability of hosting a terrestrial planet in the habitable zone; almost as high as observed in models where the inner system disk is undisturbed by giant planet migration. Given that there are $\sim 10^8$ hot-

Jupiter systems in the galaxy, 'rare Earths' are at least slightly less rare.

3. Terrestrial planets in hot-Jupiter systems are likely to be well endowed with volatiles, driven inward from the nebular snowline region by the migration of the giant planet.

4. Hot-Jupiters at $a_{\rm g} \gtrsim 0.05$ AU may also be accompanied by hot-Earths or hot-Neptunes in interior orbits, originating via accretion in a compacted disk remnant. These objects are expected to be in the Earth-mass range and are typically located close to first order resonances with the giant planet. Warm-Jupiters at $a_{\rm g} \gtrsim 0.2$ AU, in low eccentricity orbits, may be accompanied by interior multiple systems of hot-Earths.

5. Planned space-based observatories which are designed to search for potentially habitable terrestrial exoplanets and to detect biomarkers in their spectra (e.g. Darwin and TPF) will confirm or refute the above predictions in the coming decades.

7.2 Caveats

The point is made in the above Section that an assessment of the validity of predictions that arise from scientific hypotheses can benefit from a critical evaluation of the assumptions from which they are derived. How do the predictions arising from this work fare when this is done?

The models presented in this thesis have only explored a modest region of parameter space relevant to the problem, and have inevitably adopted assumptions that simplify or omit potentially important physical processes. Some of these caveats, and their possible implications, are discussed below.

7.2.1 Parameter variations

i) Nebular mass. All the models presented in this thesis have assumed a nebular mass equivalent to three times that of the minimum mass solar nebula model, which is implemented in Eqs. 2.6, 2.7, & 2.8 by setting $f_{\rm neb} = 3$. This is a reasonable value, given that $f_{\rm neb} = 1$ represents the bare minimum required to account for the solid matter contained in the planets of the solar system, and the theoretical necessity for a factor of several times this to account for the formation of a giant planet core before the loss of the nebular gas (Lissauer, 1987). Inferred masses of T-Tauri disks from observations point to a range of $f_{\rm neb} \sim 0.1$ – 30 (see the discussion in Ida and Lin,

2004a), with examples where $f_{\rm neb} > 1$ being commonplace. Although scaling the mass of the nebula by varying $f_{\rm neb}$ should result in a corresponding scaling of the mass of the resulting terrestrial planets, it is unlikely to dramatically change the conclusions of this thesis. A similar partitioning of the solids disk into shepherded and scattered fractions is observed in the model of Raymond *et al.* (2006) and Mandell *et al.* (2007) where $f_{\rm neb} = 2.2$. If $f_{\rm neb} \gg 3$, it is reasonable to speculate that the model might produce hot-Neptune type planets more readily. These might be more easily decoupled from interior first order resonances with the giant planet due to more energetic giant impacts at late times or stronger type I migration, perhaps producing better analogues of the observed hot-Neptunes illustrated in Fig. 1.4.

ii) Initial nebular surface density profile. In common with many other studies of terrestrial planet formation, the models presented in this thesis adopt an initial condition of a MMSN-type protoplanetary disk with an $r^{-1.5}$ surface density profile (Weidenschilling, 1977; Hayashi, 1981). Other disk models however predict that a shallower profile ($\Sigma \propto r^{-1}$) may be more realistic (e.g. Davis, 2005; Andrews and Williams, 2007). It is not expected that giant planet migration through a disk with a shallower initial profile would drastically change the conclusions of this thesis. Previous models that have explored this issue (e.g. Chambers and Cassen, 2002; Raymond *et al.*, 2005a; McNeil *et al.*, 2005) find that the architectures of their resulting terrestrial planetary systems depend only weakly on the slope of the initial surface density set up, with shallower gradients tending to result in more substantial planets forming further from the central star. If a giant planet were to migrate through such a disk, more mass would be encountered earlier in the migration, probably resulting in a more massive scattered disk and hence even more favorable prospects for external terrestrial planet formation.

iii) Gas disk viscosity and type II migration rate. The models presented in this thesis use an alpha disk model to simulate the evolution of the nebular gas and adopt an alpha viscosity parameter of $\alpha = 2 \times 10^{-3}$. Values of α between $10^{-4} - 10^{-2}$ have been inferred from observations of protostellar disks, but remain speculative (Papaloizou *et al.*, 2007). The effect of α in the models is to determine the type II migration rate and the question is whether a significant change in this rate might change the conclusions. The giant planet migration epoch takes place over 0.12 – 0.22 Myr in Models II & III and is extended up to 0.6 Myr in Model IV due to low gas density. No obvious effect on disk partitioning was noticed in the results over this range of timescales. In their simulations of Jupiter migrating through a mature inner solar system, Mandell

and Sigurdsson (2003) adopted migration times between 0.5 – 2.0 Myr and noted that a slower migration resulted in an increased tendency for planets to be ejected as they typically experienced a greater number of close encounters with the giant during scattering. However, they noted no discontinuous behaviour at slow migration rates that would invalidate the conclusions given here.

iv) Giant planet mass. All the models presented here adopt a giant planet mass of $0.5\ \mathrm{M_J}$. Whilst the giant planet can accrete solid matter as it migrates inward, it does not accumulate any more gas and so its mass changes by $\lesssim 5\%$ during a run. Hot-Jupiters, however, come in a variety of masses (see Fig. 1.2) and although their average $m \sin i$ is less than a Jupiter mass, more massive examples are known. The effect of increasing the mass of the migrating giant planet has not been explored here. One might expect that this would result in an enhanced and more widespread scattering of material into the external disk, and more accretion by the giant, but not that it would completely distort the aftermath of a migration episode. This assertion is supported by the subsequent work of Raymond *et al.* (2006) and Mandell *et al.* (2007) who computed similar scenarios involving a $1.0\ \mathrm{M_J}$ giant planet and obtained similar outcomes to those described here.

v) Giant planet radius. All the models presented here assume a giant planet density of $\rho_\mathrm{p} = 1.0\ \mathrm{g\ cm^{-3}}$ which gives a radius of $r_\mathrm{p} = 0.85\ \mathrm{R_J}$. This assumes a radius for the giant planet that is representative of a fully contracted state, which may not be realistic so soon after its formation. Giant planets of approximately Jovian mass contract to radii ~ 2 – $3\ \mathrm{R_J}$ during their rapid gas accretion phase (Papaloizou and Nelson, 2005), before cooling and contracting toward the Jovian radius over longer time scales. Adoption of a larger radius would result in greater accretion of solids by the giant, probably with gas–drag–sensitive planetesimals being preferentially accreted. However, this effect should be minor. The ratio of a planet's physical radius to that of its Hill sphere[2] is:

$$\frac{r_\mathrm{p}}{r_\mathrm{H}} = \left(\frac{9 M_*}{4 \pi \rho_\mathrm{p} a^3} \right)^{\frac{1}{3}}, \tag{7.1}$$

where a is the semi-major axis. In the model as it presently stands $r_\mathrm{p}/r_\mathrm{H} \approx 1.5 \times 10^{-3}$ at 5 AU and $r_\mathrm{p}/r_H \approx 0.075$ at 0.1 AU. Thus, doubling or tripling these ratios will not tip the balance overwhelmingly in favor of accretion at either end of the migration

[2]The square root of the ratio of accretion over scattering cross sections.

path.

vi) Solids disk inner boundary. The inner system solids disk adopted here begins with its inner boundary set at 0.4 AU. Its contents are then free to evolve inward during the maturation runs preceding the introduction of the giant at the start of a migration scenario. By this time, in low dissipation models (Model II and Model IV, Run Set **A**), dynamical spreading typically results in a modest inward movement of the disk edge to ~ 0.3 AU (see Fig. 2.2 & Fig. 6.4, upper panel) so that when the giant planet subsequently migrates down to 0.1 AU it passes through the entire inner disk annulus. This is not necessarily the case in high dissipation models (Models I, III and IV, Run Set **B**) where greater inward movement of the solids disk contents occurs during the maturation phase (see Figs. 3.1, 5.1 & 6.4, lower panel).

Thus, the question is raised as to whether the lack of interior hot-Earths resulting in Model II and Scenarios 1 & 2 of Model IV**A** is a realistic finding or an artifact of the initial position of the solids disk inner boundary. What if this boundary had been set at 0.1 AU instead? This would have provided an additional $\sim 3\ \mathrm{M}_{\oplus}$ of material from which potential interior planets could have been assembled (Eqs. 2.6 & 2.11). It cannot be ruled out therefore that some hot-Earths could grow and survive even in low dissipation settings such as Model II, especially if the giant planet stops short of their position. However, one would still expect them to be of lower mass and more prone to orbital destabilization than in high dissipation models where eccentricity damping is in play and where there has been much more extensive prior inward migration of solids.

7.2.2 Neglected physical processes

vii) Giant planet eccentricity evolution. The models assume that type II migration is associated with an eccentricity damping which maintains a near-circular orbit. However the question of whether a giant planet has its eccentricity damped or excited by the protoplanetary disk remains a point of ongoing debate (Papaloizou *et al.*, 2001; Goldreich and Sari, 2003; Ogilvie and Lubow, 2003; Moorhead and Adams, 2008). In the absence of eccentricity damping, interaction of the giant with the solids disk may cause modest excitation, but not at a level to significantly affect results. If the gas disk was to drive significant eccentricity increase then this would probably lead to a stronger interaction between the giant and the solids disk resulting in greater scattering and a more efficient clearing of material.

viii) Planetesimal size evolution. For computational simplicity the models presented here assume a uniform planetesimal population with radii of 10 km, which results in an identical effect of gas drag on any planetesimal at a particular orbital distance. In reality, but more challenging to adapt to a $N + N'$-type simulation, there would be a distribution of planetesimal sizes determined from a balance between their rates of accumulation and fragmentation, and hence a much more varied response of small objects to gas drag. In regions of the disk that are dynamically cold, the mean planetesimal size would grow via binary mergers, whilst in regions that are more dynamically excited, destructive collisions could result in the planetesimal population being ground down into smaller fragments. Fragmentation of the planetesimal population in the context of the oligarchic growth regime however is not necessarily an obstacle to planet formation and may actually assist planetary growth by supplying protoplanets with a more strongly damped feedstock, enhancing the effect of gravitational focussing (Chambers, 2006a, 2008). Simulations of accretion of terrestrial planets in dynamically cool disks, which include a fragmentation model, give results that are almost indistinguishable from the results of models where fragmentation is neglected (Alexander and Agnor, 1998; Leinhardt and Richardson, 2005). A particularly unfavorable environment for planetesimal survival in the simulations presented here is in the compacted region of the disk between the 4:3 and 2:1 resonances with the giant planet. In this region, planetesimal surface densities are enhanced (see the left hand panels in Figs. 3.8 & 4.9) and the population as a whole is strongly stirred generating eccentricities as high as 0.2 – 0.3 (e.g. Figs. 3.3, 4.5, 4.12 & 5.3). Random velocities of several km per second, far in excess of planetesimal escape velocities, are indicated and mutual planetesimal collisions would result in fragmentation. What this means for the model is unclear, but it is possible that the fragment population, which would be much more strongly affected by gas drag, would evolve inward rapidly, thereby escaping the dynamically excited zone. It could then be gathered efficiently by protoplanets and accreted. One might speculate that the overall effect of this process might be to reduce the planetesimal fraction of the external disk material, but not to reduce its overall mass as protoplanets should be scattered there with the same, or even greater, efficiency. This argument is weaker when type I migration is included. Supplying inner planets with an enhanced feedstock would not only boost their growth rates, but also their inward drift. It is shown in Chapter 5 how the influence of type I migration results in fewer protoplanets surviving in external orbits so boosting inward migration rates by enhancing mass growth would accentuate this trend. However, as accretion rates depend as $\dot{m}_{proto} \propto \Sigma_{\rm s}\Omega$ one would expect that the bulk of this additional growth would take place at late times when the giant planet has compacted

the shepherded fraction within a small orbital radius. It seems unlikely therefore that the additional dissipation resulting from planetesimal fragmentation would prevent entirely the scattering of some large bodies into the external disk.

ix) Supply of outer disk material. There would be a population of planetesimals and protoplanets exterior to the 5 AU initial position of the giant planet whose size distribution is unknown and is not accounted for in the models. Planetesimals with radii < 1 km would migrate in behind the gas giant due to gas drag, providing a source of material that may be accreted by outwardly scattered protoplanets that reside interior to 5 AU, and which may contribute to the damping of their inclination and eccentricity. Any late supply of larger bodies, following the giant planet inward due to type I migration (Thommes, 2005), would contribute to the protoplanetary population of the scattered disk boosting both its mass, maturity ($f_{\rm proto}$), and volatile content.

7.2.3 'Rare Earths' nevertheless?

Although this thesis argues that terrestrial planets are relatively commonplace in the habitable zones of hot-Jupiter systems, it is not necessarily implied that the habitability of such planets is usual also. One particular trend in the data describing the generated habitable planet candidates departs systematically from that of an idealized facsimile of the Earth.

x) Ocean planets. One effect of giant planet migration is to drive large quantities of icy material into the inner system, with the outcome that terrestrial planets that form in the aftermath are predicted to be richly endowed with volatiles and enveloped by global oceans. There is nothing about 100% ocean cover that necessarily rules out the presence of life. Indeed, life may have started in the Earth's oceans, and exploration beneath ocean-covered Europa's ice shell has long been regarded as a top priority by astrobiologists (Reynolds *et al.*, 1983, 1987). Ocean planets in the $\sim {\rm M}_\oplus$ range however have a problem not shared with Europa: if the depth of their oceans is $\gtrsim 100$ km, their floors are composed of high pressure phases of ice, rather than rock, with the ice-silicate interface (and much potentially crucial chemistry) sealed off beneath an icy mantle 100s or 1000s of km thick, depending on the planet's total mass and bulk water content (L*é*ger *et al.*, 2004). How this would effect the solute content of the oceans is unknown but one might speculate that some trace elements essential for terrestrial life might be lacking[3]. Meteoritic infall after planetary differentiation is complete would

[3]The elemental requirements of non-terrestrial life are another matter and unknown.

re-supply some rock-forming elements for dissolution into the ocean, but solid material that deposits on the ocean floor would be denser than the ice beneath and prone to removal by sinking into the mantle. A related problem deepens this uncertainty. Planets over-endowed with water might similarly possess massive atmospheres with unexpected compositions and properties. If ocean planets are more like thawed out versions of Titan, rather than water-rich Earths, then habitable zone calculations that rely on models of modest CO_2/H_2O atmospheres, coupled to a carbonate-silicate cycle and continental weathering (e.g. Kasting *et al.*, 1993; Selsis *et al.*, 2007; von Bloh *et al.*, 2007), may not be relevant.

If the water content of trans-snowline planetary building blocks is assumed to be $\sim 75\%$ ($\sim 1 - f_{\rm ice}^{-1}$), then the models presented here predict HZ planets composed of $\sim 20\%$ – 60% water. This is a vast inventory compared with the Earth's $\sim 0.1\%$ water. It is likely though that these figures are overestimated. If the snowline is further from the star than the 2.7 AU assumed in the MMSN Model, or if the giant planet forms closer to it, the material shepherded inward by type II migration will have a lower volatile content. In the models of Raymond *et al.* (2006) and Mandell *et al.* (2007), where the snowline is placed at 5 AU, HZ planets are produced with a water content of $\sim 10\%$ – a reduction from the above estimate, but still a factor of 20 greater than the typical outcome of $\sim 0.5\%$ water content when models are run without a migrating giant planet (Raymond *et al.*, 2004, 2007). However, all these models almost certainly overestimate the quantity of water retained by growing planets since loss of volatiles during accretion is not accounted for. Extensive depletion of both atmosphere and ocean could result from giant impacts late in formation (Genda and Abe, 2005; Asphaug *et al.*, 2006; Canup and Pierazzo, 2006) which could strip nascent ocean planets down to a more Earth-like remnant. All of the HZ planets generated by the models presented here undergo *at least* one giant impact at some point in their evolution, with a minority suffering a high velocity collision with a comparable sized object during the later stage of accretion within the scattered disk. Thus, whilst ocean planets in habitable zones are a robust prediction of the model, it is premature to say that they would invariably occur in nature and would inevitably be uninhabitable.

7.3 Afterword

Few of the dramas of nature are as epic as the birth and life of planets: worlds, oceans, atmospheres, even biospheres, all assembled ultimately through the action of physical law on tiny particles of dust – the smoke-like, radioactive, ejecta of exploded stars. It's a long story, and planetary formation theories remain too primitive to lay claim to a definitive explanation and full understanding of every stage. So it is with the work in this thesis. Its assumptions are open to change, and its physics to further supplementation and refinement. Its predictions await affirmation or refutation by future astronomers. This author looks to that future with hope, if not for confirmation, then certainly with the expectation of wonder at future discoveries. The one concrete fact to emerge over the past thirteen years is that, as far as the variety of planetary systems is concerned, the designs of nature are lavish rather than parsimonious.

> Moreover, there is no one thing in the whole sum which is produced unique, and grows up unique and alone, so as not to belong to some kind and to be one of many like it... Therefore, you must in like manner confess for sky and earth, for sun, moon, sea and all else that exists, that they are not unique, but rather of number innumerable;
>
> Lucretius, *De Rerum Natura*, 2, 1077-1088, c.60 BC.

References

Adachi I., Hayashi C., & Nakazawa K. 1976, *The gas drag effect on the elliptical motion of a solid body in the primordial solar nebula.*, Prog. Theor. Phys., **56**, 1756.

Adams F. C. & Laughlin G. 2003, *Migration and dynamical relaxation in crowded systems of giant planets*, Icarus, **163**, 290.

Agnor C. B. & Asphaug E. 2004, *Accretion efficiency during planetary collisions*, ApJ, **613**, L157.

Agnor C. B., Canup R. M., & Levison H. F. 1999, *On the character and consequences of large impacts in the late stage of terrestrial planet formation*, Icarus, **142**, 219.

Agnor C. B. & Ward W. R. 2002, *Damping of terrestrial-planet eccentricities by density-wave interactions with a remnant gas disk*, ApJ, **567**, 579.

Alexander R. D. & Agnor C. B. 1998, *N-Body simulations of late stage planetary formation with a simple fragmentation model*, Icarus, **132**, 113.

Alexander R. D., Clarke C. J., & Pringle J. E. 2006, *Photoevaporation of protoplanetary discs - II. Evolutionary models and observable properties*, MNRAS, **369**, 229.

Alibert Y., Mordasini C., Benz W., & Winisdoerffer C. 2005, *Models of giant planet formation with migration and disc evolution*, A&A, **434**, 343.

Andrews S. M. & Williams J. P. 2007, *High-resolution submillimeter constraints on circumstellar disk structure*, ApJ, **659**, 705.

Armitage P. J. 2003, *A reduced efficiency of terrestrial planet formation following giant planet migration*, ApJ, **582**, L47.

Armitage P. J. 2007, *Massive planet migration: theoretical predictions and comparison with observations*, ApJ, **665**, 1381.

Armitage P. J., Livio M., Lubow S. H., & Pringle J. 2002, *Predictions for the frequency and orbital radii of massive extrasolar planets*, MNRAS, **334**, 248.

Artymowicz P. 1993, *Disk-satellite interaction via density waves and the eccentricity evolution of bodies embedded in disks*, ApJ, **419**, 166.

Asphaug E., Agnor C. B., & Williams Q. 2006, *Hit-and-run planetary collisions*, Nature, **439**, 155.

Beauge C. & Aarseth S. J. 1990, *N-body simulations of planetary formation*, MNRAS, **245**, 30.

Bertout C. 1989, *T Tauri stars - wild as dust*, ARAA, **27**, 351.

Bodenheimer P., Hubickyj O., & Lissauer J. J. 2000, *Models of the in situ formation of detected extrasolar giant planets*, Icarus, **143**, 2.

Bodenheimer P. & Lin D. N. C. 2002, *Implications of extrasolar planets for understanding planet formation*, ARA&A, **30**, 113.

Boss A. P. 2000, *Possible rapid gas giant planet formation in the Solar Nebula and other protoplanetary disks*, ApJ, **536**, L101.

Bryden G., Chen X., Lin D. N. C., Nelson R. P., & Papaloizou J. C. B. 1999, *Tidally induced gap formation in protostellar disks: gap clearing and suppression of protoplanetary growth*, ApJ, **514**, 344.

Butler R. P., Vogt S. S., Marcy G. W., Fischer D. A., Wright J. T., Henry G. W., Laughlin G., & Lissauer J. J. 2004, *A Neptune-mass planet orbiting the nearby M dwarf GJ 436*, ApJ, **617**, L580.

Butler R. P., Wright J. T., Marcy G. W., Fischer D. A., Vogt S. S., Tinney C. G., Jones H. R. A., Carter B. D., Johnson J. A., McCarthy C., & Penny A. J. 2006, *Catalog of nearby exoplanets*, ApJ, **646**, 505.

Cameron A. G. W. 1963, *Interstellar Communication*. (W. A. Benjamin, Inc., New York).

Canup R. M. & Pierazzo E. 2006, *Retention of water during planet-scale collisions*, LPI, **37**, 2146.

Chambers J. E. 1999, *A hybrid symplectic integrator that permits close encounters between massive bodies*, MNRAS, **304**, 793.

Chambers J. E. 2001, *Making more terrestrial planets*, Icarus, **152**, 205.

Chambers J. E. 2006a, *A semi-analytic model for oligarchic growth*, Icarus, **180**, 496.

Chambers J. E. 2006b, *Planet formation with migration*, ApJ, **652**, L133.

Chambers J. E. 2008, *Oligarchic growth with migration and fragmentation*, Icarus, **198**, 256.

Chambers J. E. & Cassen P. 2002, *The effects of nebula surface density profile and giant-planet eccentricities on planetary accretion in the inner solar system*, M&PS, **37**, 1523.

Chambers J. E. & Migliorini F. 1997, *Mercury - a new software package for orbital integrations*, BAAS, **29**, 1024.

Chambers J. E. & Wetherill G. W. 1998, *Making the terrestrial planets: N-body integrations of planetary embryos in three dimensions*, Icarus, **136**, 304.

Chambers J. E. & Wetherill G. W. 2001, *Planets in the asteroid belt*, M&PS, **36**, 381.

Chatterjee S., Ford E. B., Matsumura S., & Rasio F. A. 2008, *Dynamical outcomes of planet-planet scattering*, ApJ, **686**, 580.

Clark S. 2008, *Are we alone in the dark?*, BBC Focus, **186**, 27.

Clarke C. J., Gendrin A., & Sotomayor M. 2001, *The dispersal of circumstellar discs: the role of the ultraviolet switch*, MNRAS, **328**, 485.

Cresswell P. & Nelson R. P. 2006, *On the evolution of multiple protoplanets embedded in a protostellar disc*, A&A, **450**, 833.

Cresswell P. & Nelson R. P. 2008, *Three-dimensional simulations of multiple protoplanets embedded in a protostellar disc*, A&A, **482**, 677.

Daisaka J. K., Tanaka H., & Ida S. 2006, *Orbital evolution and accretion of protoplanets tidally interacting with a gas disk*, Icarus, **185**, 492.

Davis S. S. 2005, *The surface density distribution in the Solar Nebula*, ApJ, **627**, L153.

Dick S. J. 1982, *Plurality of Worlds: the Origins of the Extraterrestrial Life Debate from Democritus to Kant*. (Cambridge U. Press).

Dick S. J. 1996, *The Biological Universe*. (Cambridge U. Press).

Dole S. H. 1964, *Habitable Planets for Man*. (Blaisdell Publishing Co., New York).

Drake M. J. & Righter K. 2002, *Determining the composition of the Earth*, Nature, **416**, 39.

Durisen R. H., Boss A. P., Mayer L., Nelson A. F., Quinn T., & Rice W. K. M. 2007. *Gravitational instabilities in gasous protoplanetary disks and implications for giant planet formation*, Reipurth B., Jewitt D., & Keil K., eds, *Protostars and Planets V*, p. 607. U. Arizona Press.

Durisen R. H., Cai K., Meja A. C., & Pickett M. K. 2005, *A hybrid scenario for gas giant planet formation in rings*, Icarus, **173**, 417.

Dvorak R., Pilat-Lohinger E., Schwarz R., & Freistette F. 2004, *Extrasolar Trojan planets close to habitable zones*, A&A, **426**, L37.

Erdi B. & Sandor Z. 2005, *Stability of co-orbital motion in exoplanetary systems*, CeMDA, **92**, 113.

Fischer D. A. & Valenti J. 2005, *The planet-metallicity correlation*, ApJ, **622**, 1002.

Fogg M. J. & Nelson R. P. 2005, *Oligarchic and giant impact growth of terrestrial planets in the presence of gas giant planet migration*, A&A, **441**, 791.

Fogg M. J. & Nelson R. P. 2006, *On the possibility of terrestrial planet formation in hot-Jupiter systems*, IJAsB, **5**, 199.

Fogg M. J. & Nelson R. P. 2007a, *On the formation of terrestrial planets in hot-Jupiter systems*, A&A, **461**, 1195.

Fogg M. J. & Nelson R. P. 2007b, *The effect of type I migration on the formation of terrestrial planets in hot-Jupiter systems*, A&A, **472**, 1003.

Fogg M. J. & Nelson R. P. 2008. *Can terrestrial planets form in hot-Jupiter systems?*, Fischer D. A., Rasio F., Thorsett S., & Wolszczan A., eds, *Extreme Solar Systems*, p. 525. ASP Conference Series, **398**.

Ford E. B., Havlickova M., & Rasio F. A. 2001, *Dynamical instabilities in extrasolar planetary systems containing two giant planets*, Icarus, **150**, 303.

Ford E. B., Rasio F. A., & Yu K. 2003. *Dynamical instabilities in extrasolar planetary systems*, Deming D. & Seager S., eds, *Scientific Frontiers in Research on Extrasolar Planets*, p. 181. ASP Conference Series, Vol. 294.

Genda H. & Abe Y. 2005, *Enhanced atmospheric loss on protoplanets at the giant impact phase in the presence of oceans*, Nature, **433**, 842.

Gillon M., Courbin F., Magain P., & Borguet B. 2005, *On the potential of extrasolar planet transit surveys*, A&A, **442**, 731.

Gillon M., Demory B. O., Barman T., Bonfils X., Mazeh T., Pont F., Udry S., Mayor M., & Queloz D. 2007, *Accurate Spitzer infrared radius measurement for the hot Neptune GJ 436b*, A&A, **471**, L51.

Goldreich P., Lithwick Y., & Sari R. 2004, *Final stages of planet formation*, ApJ, **614**, 497.

Goldreich P. & Sari R. 2003, *Eccentricity evolution for planets in gaseous disks*, ApJ, **585**, 1024.

Goldreich P. & Soter S. 1966, *Q in the Solar System*, Icarus, **5**, 375.

Goldreich P. & Tremaine S. 1980, *Disk-satellite interactions* , ApJ, **241**, 425.

Goldreich P. & Ward W. R. 1973, *The formation of planetesimals*, ApJ, **183**, 1051.

Greaves J. S. 2005, *Disks around stars and the growth of planetary systems*, Science, **307**, 68.

Grinspoon D. 2004, *Lonely Planets: The Natural Philosophy of Alien Life*. (Harper Collins, New York).

Haisch K. E., Lada E. A., & Lada C. J. 2001, *Disk frequencies and lifetimes in young clusters*, ApJ, **533**, L153.

Hayashi C. 1981, *Structure of the Solar Nebula, growth and decay of magnetic fields and effects of magnetic and turbulent viscosities on the nebula*, Prog. Theor. Phys. Suppl., **70**, 35.

Hayashi C., Nakazawa K., & Nakagawa Y. 1985. *Formation of the Solar System*, Black D. & Shapley Matthews M., eds, *Protostars and Planets II*, p. 1100. U. Arizona Press.

Hollenbach D., Johnstone D., Lizano S., & Shu F. 1994, *Photoevaporation of disks around massive stars and application to ultracompact H II regions*, ApJ, **428**, 654.

Hubickyj O., Bodenheimer P., & Lissauer J. J. 2005, *Accretion of the gaseous envelope of Jupiter around a 5 - 10 Earth-mass core*, Icarus, **179**, 415.

Ida S. & Lin D. N. C. 2004a, *Toward a deterministic model of planetary formation. I. A desert in the mass and semimajor axis distributions of extrasolar planets*, ApJ, **604**, 388.

Ida S. & Lin D. N. C. 2004b, *Toward a deterministic model of planetary formation. II. The formation and retention of gas giant planets around stars with a range of metallicities*, ApJ, **616**, 567.

Ida S. & Lin D. N. C. 2008, *Toward a deterministic model of planetary formation IV: effects of type-I migration*, ApJ, **673**, 487.

Irion R. 2005, *Extrasolar planets get smaller and (possibly) harder*, Science, **308**, 1727.

Ivanov P. B., Papaloizou J. C. B., & Polnarev A. G. 1999, *The evolution of a supermassive binary caused by an accretion disc*, MNRAS, **307**, 79.

Jones B. W., Sleep P. N., & Chambers J. E. 2001, *The stability of the orbits of terrestrial planets in the habitable zones of known exoplanetary systems*, A&A, **366**, 254.

Jones B. W., Sleep P. N., & Underwood D. R. 2006, *Which exoplanetary systems could harbour habitable planets?*, IJAsB, **5**, 251.

Jones B. W., Underwood D. R., & Sleep P. N. 2005, *Prospects for habitable "Earths" in known exoplanetary systems*, ApJ, **622**, 1091.

Juric M. & Tremaine S. 2008, *Dynamical origin of extrasolar planet eccentricity distribution*, ApJ, **686**, 603.

Kaltenegger L. & Fridlund M. 2005, *The Darwin mission: search for extra-solar planets*, Adv. Space Res., **36**, 1114.

Kasting J. F., Whitmire D. P., & Reynolds R. T. 1993, *Habitable zones around main sequence stars*, Icarus, **101**, 108.

Kleine T., Münker C., Mezger K., & Palme H. 2002, *Rapid accretion and early core formation on asteroids and the terrestrial planets from Hf-W chronometry*, Nature, **418**, 952.

Kokubo E. & Ida S. 1998, *Oligarchic growth of protoplanets*, Icarus, **131**, 171.

Kokubo E. & Ida S. 2000, *Formation of protoplanets from planetesimals in the Solar Nebula*, Icarus, **143**, 15.

Kominami J. & Ida S. 2002, *The effect of tidal interaction with a gas disk on formation of terrestrial planets*, Icarus, **157**, 43.

Kozai Y. 1962, *Secular perturbations of asteroids with high inclination and eccentricity*, AJ, **67**, 591.

Kuchner M. J. 2003, *Volatile-rich Earth-mass planets in the habitable zone*, ApJ, **596**, L105.

Kuchner M. J. & Lecar M. 2002, *Halting planet migration in the evacuated centers of protoplanetary Disks*, ApJ, **574**, L87.

Léger A., Selsis F., Sotin C., Guillot T., Despois D., Mawet D., Ollivier M., Labque A., Valette C., Brachet F., Chazelas B., & Lammer H. 2004, *A new family of planets? "Ocean-Planets"*, Icarus, **169**, 499.

Laughlin G., Bodenheimer P., & Adams F. C. 2004, *The core accretion model predicts few Jovian-mass planets orbiting red dwarfs*, ApJ, **612**, L73.

Lee M. H. & Peale S. J. 2002, *Dynamics and Origin of the 2:1 Orbital Resonances of the GJ 876 Planets*, ApJ, **567**, 569.

Leinhardt Z. M. & Richardson D. C. 2005, *Planetesimals to protoplanets. I. Effect of fragmentation on terrestrial planet formation*, ApJ, **625**, 427.

Lin D. N. C., Bodenheimer P., & Richardson D. C. 1996, *Orbital migration of the planetary companion of 51 Pegasi to its present location*, Nature, **308**, 606.

Lin D. N. C. & Papaloizou J. C. B. 1986, *On the tidal interaction between protoplanets and the protoplanetary disk. III - Orbital migration of protoplanets*, ApJ, **309**, 846L.

Lin D. N. C. & Papaloizou J. C. B. 1993. *On the tidal interaction between protostellar disks and companions*, Levy E. & Lunine J., eds, *Protostars and Planets III*, p. 749. U. Arizona Press.

Lineweaver C. H. 2001, *An estimate of the age distribution of terrestrial planets in the universe: quantifying metallicity as a selection effect*, Icarus, **151**, 307.

Lineweaver C. H., Fenner Y., & Gibson B. K. 2004, *The Galactic Habitable Zone and the age distribution of complex life in the Milky Way*, Science, **303**, 59.

Lineweaver C. H. & Grether D. 2003, *What fraction of Sun-like stars have planets?*, ApJ, **598**, 1350.

Lissauer J. J. 1987, *Timescales for planetary accretion and the structure of the protoplanetary disk*, Icarus, **69**, 249.

Lissauer J. J. & Stevenson D. J. 1993. *Growth of planets from planetesimals*, Levy E. H. & Lunine J. I., eds, *Protostars and Planets III*, p. 1061. U. Arizona Press.

Lissauer J. J. & Stevenson D. J. 2007. *Formation of giant planets*, Reipurth B., Jewitt D., & Keil K., eds, *Protostars and Planets V*, p. 591. U. Arizona Press.

Mandell A. M., Raymond S. N., & Sigurdsson S. 2007, *Formation of Earth-like planets during and after giant planet migration*, ApJ, **660**, 823.

Mandell A. M. & Sigurdsson S. 2003, *Survival of terrestrial planets in the presence of giant planet migration*, ApJ, **599**, L111.

Marcy G., Butler R. P., Fischer D., Vogt S., Wright J. T., Tinney C. G., & Jones H. R. A. 2005, *Observed properties of exoplanets: masses, orbits, and metallicities*, Prog. Theor. Phys. Suppl., **158**, 24.

Marzari F. & Weidenschilling S. J. 2002, *Eccentric extrasolar planets: the Jumping Jupiter model*, Icarus, **156**, 570.

Masset F. S., Morbidelli A., Crida A., & Ferreira J. 2006, *Disk surface density transitions as protoplanet traps*, ApJ, **642**, 478.

Masset F. S. & Papaloizou J. C. B. 2003, *Runaway migration and the formation of hot Jupiters*, ApJ, **588**, 494.

Matsuo T., Shibai H., Ootsubo T., & Tamura M. 2007, *Planetary formation scenarios revisited: core-accretion versus disk instability*, ApJ, **662**, 1282.

Mayer L., Quinn T., Wadsley J., & Stadel J. 2002, *Formation of giant planets by fragmentation of protoplanetary disks*, Science, **298**, 1756.

Mayor M. & Queloz C. 1995, *A Jupiter mass companion to a solar-type star*, Nature, **378**, 355.

McArthur B. E., Endl M., Cochran W. D., Benedict G. F., Fischer D. A., Marcy G. W., Butler R. P., Naef D., Mayor M., Queloz D., Udry S., & Harrison T. E. 2004, *Detection of a Neptune-mass planet in the ρ^1 Cancri system using the Hobby-Eberly telescope*, ApJ, **614**, L81.

McNeil D., Duncan M., & Levison H. F. 2005, *Effects of type I migration on terrestrial planet formation*, AJ, **130**, 2884.

Menou K. & Tabachnik S. 2003, *Dynamical habitability of known extrasolar planetary systems*, ApJ, **583**, 473.

Moorhead A. V. & Adams F. C. 2005, *Giant planet migration through the action of disk torques and planet planet scattering*, Icarus, **178**, 517.

Moorhead A. V. & Adams F. C. 2008, *Eccentricity evolution of giant planet orbits due to circumstellar disk torques*, Icarus, **193**, 475.

Morbidelli A., Chambers J., Lunine J. I., Petit J., Robert F., Valsecchi G., & Cyr K. 2000, *Source regions and time scales for the delivery of water to Earth*, M&PS, **35**, 1309.

Morbidelli A., Crida A., Masset F., & Nelson R. P. 2008, *Building giant-planet cores at a planet trap*, A&A, **478**, 929.

Morrison P., Billingham J., & Wolfe J. 1977, *The Search for Extraterrestrial Intelligence*. (NASA SP-419).

Murray C. D. & Dermott S. F. 1999, *Solar System Dynamics*. (Cambridge U. Press).

Nagasawa M., Thommes E. W., Kenyon S. J., Bromley B. C., & Lin D. 2007. *The diverse origins of terrestrial-planet systems*, Reipurth B., Jewitt D., & Keil K., eds, *Protostars and Planets V*, p. 639. U. Arizona Press.

Nelson R. P. 2005, *On the orbital evolution of low mass protoplanets in turbulent, magnetised disks*, A&A, **443**, 1067.

Nelson R. P. & Papaloizou J. C. B. 2004, *The interaction of giant planets with a disc with MHD turbulence - IV. Migration rates of embedded protoplanets*, MNRAS, **350**, 849.

Nelson R. P., Papaloizou J. C. B., Masset F., & Kley W. 2000, *The migration and growth of protoplanets in protostellar discs*, MNRAS, **318**, 18.

O'Brien D. P., Morbidelli A., & Levison H. F. 2006, *Terrestrial planet formation with strong dynamical friction*, Icarus, **184**, 39.

Ogilvie G. I. & Lubow S. H. 2003, *Saturation of the corotation resonance in a gaseous disk*, ApJ, **587**, 398.

Paardekooper S. J. & Mellema G. 2006, *Halting type I planet migration in non-isothermal disks*, A&A, **459**, L17.

Paardekooper S. J. & Mellema G. 2008, *Growing and moving low-mass planets in non-isothermal disks*, A&A, **478**, 245.

Papaloizou J. C. B. 2005, *Disk planet interactions and early evolution in young planetary systems*, CeMDA, **91**, 33.

Papaloizou J. C. B. 2007, *Protoplanet magnetosphere interactions*, A&A, **463**, 775.

Papaloizou J. C. B. & Larwood J. D. 2000, *On the orbital evolution and growth of protoplanets embedded in a gaseous disc*, MNRAS, **315**, 823.

Papaloizou J. C. B. & Nelson R. P. 2005, *Models of accreting gas giant protoplanets in protostellar disks*, A&A, **433**, 247.

Papaloizou J. C. B., Nelson R. P., Kley W., Masset F. S., & Artymowicz P. 2007. *Disk-planet interactions during planet formation*, Reipurth B., Jewitt D., & Keil K., eds, *Protostars and Planets V*, p. 655. U. Arizona Press.

Papaloizou J. C. B., Nelson R. P., & Masset F. 2001, *Orbital eccentricity growth through disc-companion tidal interaction*, A&A, **366**, 263.

Papaloizou J. C. B. & Terquem C. 1999, *Critical protoplanetary core masses in protoplanetary disks and the formation of short-period giant planets*, ApJ, **521**, 823.

Papaloizou J. C. B. & Terquem C. 2001, *Dynamical relaxation and massive extrasolar planets*, MNRAS, **325**, 221.

Pollack J. B., Hubickyj O., Bodenheimer P., Lissauer J. J., Podolak M., & Greenzweig Y. 1996, *Formation of the giant planets by concurrent accretion of solids and gas*, Icarus, **124**, 62.

Press W. H., Teukolsky S. A., Vetterling W. T., & Flannery B. P. 1992, *Numerical Recipies in Fortran, 2nd edn.* (Cambridge U. Press).

Pringle J. E. 1981, *Accretion discs in astrophysics*, ARAA, **19**, 137.

Quillen A. C. & Thorndike S. 2002, *Structure in the ϵ Eridani dusty disk caused by mean motion resonances with a 0.3 eccentricity planet at periastron*, AJ, **578**, L149.

Rafikov R. R. 2004, *Fast accretion of small planetesimals by protoplanetary cores*, AJ, **128**, 1348.

Rasio F. A. & Ford E. B. 1996, *Dynamical instabilities and the formation of extrasolar planetary systems*, Science, **274**, 954.

Rasio F. A., Tout C. A., Lubow S. H., & Livio M. 1996, *Tidal decay of close planetary orbits*, ApJ, **470**, 1187.

Raymond S. N., Barnes R., Armitage P. J., & Gorelick N. 2008, *Mean motion resonances from planet-planet scattering*, ApJ, in press.

Raymond S. N., Mandell A. M., & Sigurdsson S. 2006, *Exotic Earths: forming habitable worlds with giant planet migration*, Science, **313**, 5792.

Raymond S. N., Quinn T., & Lunine J. I. 2004, *Making other earths: dynamical simulations of terrestrial planet formation and water delivery*, Icarus, **168**, 1.

Raymond S. N., Quinn T., & Lunine J. I. 2005a, *Terrestrial planet formation in disks with varying surface density profiles*, ApJ, **632**, 670.

Raymond S. N., Quinn T., & Lunine J. I. 2005b, *The formation and habitability of terrestrial planets in the presence of close-in giant planets*, Icarus, **177**, 256.

Raymond S. N., Quinn T., & Lunine J. I. 2007, *High-resolution simulations of the final assembly of Earth-like planets. 2. Water delivery and planetary habitability*, AsBio, **7**, 66.

Reynolds R. T., McKay C. P., & Kasting J. F. 1987, *Europa, tidally heated oceans, and habitable zones around giant planets*, Adv. Space Res., **7**, 125.

Reynolds R. T., Squyres S., Colburn D. S., & McKay C. P. 1983, *On the habitability of Europa*, Icarus, **56**, 246.

Rivera E. J., Lissauer J. J., Butler R. P., Marcy G. W., Vogt S. S., Fischer D. A., Brown T. M., Laughlin G., & Henry G. W. 2005, *A $\sim$ 7.5 $M_\oplus$ planet orbiting the nearby star, GJ 876*, ApJ, **634**, 625.

Safronov V. S. 1969, *Evolution of the Protoplanetary Cloud and Formation of the Earth and Planets*. (Nauka, Moscow. (Translated in 1972 as NASA TTF-677.)).

Sagan C. 1980, *Cosmos*. (Macdonald & Co. (Publishers) Ltd., London & Sydney).

Saha P. & Tremaine S. 1992, *Symplectic integrators for solar system dynamics*, AJ, **104**, 1633.

Santos N. C., Bouchy F., Mayor M., Pepe (F.; Queloz) D., Udry S., Lovis C., Bazot M., Benz W., Bertaux J. L., Lo Curto G., Delfosse X., Mordasini C., Naef D., Sivan J. P., & Vauclair S. 2004, *The HARPS survey for southern extra-solar planets. II. A 14 Earth-masses exoplanet around μ Arae*, A&A, **426**, L19.

Santos N. C., Israelian G., Mayor M., Rebolo R., & Udry S. 2003, *Statistical properties of exoplanets. II. Metallicity, orbital parameters, and space velocities*, A&A, **398**, 363.

Selsis F., Kasting J. F., Levrard B., Paillet J., Ribas I., & Delfosse X. 2007, *Habitable planets around the star Gliese 581?*, A&A, **476**, 1373.

Shakura N. I. & Sunyaev R. A. 1973, *Black holes in binary systems. Observational appearance*, A&A, **24**, 337.

Shklovskii I. S. & Sagan C. 1966, *Intelligent Life in the Universe*. (Dell Publishing Company, New York).

Simon M. & Prato L. 1995, *Disk dissipation in single and binary young star systems in Taurus*, ApJ, **450**, 824.

Snellgrove M. D., Papaloizou J. C. B., & Nelson R. P. 2001, *On disc driven inward migration of resonantly coupled planets with application to the system around GJ876*, A&A, **374**, 1092.

Stewart I. 2008, *Earth: The Power of the Planet. Episode 3: Rare Earth*. (BBC Televison).

Sullivan W. & Carney D. 2007. *History of astrobiological ideas*, Sullivan W. T. & Baross J. A., eds, *Planets and Life: The Emerging Science of Astrobiology*, p. 9. Cambridge U. Press.

Syer D. & Clarke C. J. 1995, *Satellites in discs: regulating the accretion luminosity*, MNRAS, **277**, 758.

Takeuchi T., Miyama S., & Lin D. N. C. 1996, *Gap formation in protoplanetary disks*, ApJ, **460**, 832.

Tanaka H. & Ida S. 1999, *Growth of a migrating protoplanet*, Icarus, **139**, 350.

Tanaka H., Takeuchi T., & Ward W. R. 2002, *Three-dimensional interaction between a planet and an isothermal gaseous disk. I. Corotation and Lindblad torques and planet migration*, ApJ, **565**, 1257.

Tanaka H. & Ward W. R. 2004, *Three-dimensional interaction between a planet and an isothermal gaseous disk. II. Eccentricity waves and bending waves*, ApJ, **602**, 388.

Terquem C. & Papaloizou J. C. B. 2002, *Dynamical relaxation and the orbits of low-mass extrasolar planets*, MNRAS, **332**, L39.

Terquem C., Papaloizou J. C. B., Nelson R. P., & Lin D. N. C. 1998, *On the tidal interaction of a solar-type star with an orbiting companion: excitation of g-Mode oscillation and orbital evolution*, ApJ, **502**, 788.

Thommes E. W. 2005, *A safety net for fast migrators: interactions between gap-opening and sub-gap-opening bodies in a protoplanetary disk*, ApJ, **626**, 1033.

Thommes E. W., Duncan M. J., & Levison H. F. 2002, *The Formation of Uranus and Neptune among Jupiter and Saturn*, AJ, **123**, 2862.

Thommes E. W., Duncan M. J., & Levison H. F. 2003, *Oligarchic growth of giant planets*, Icarus, **161**, 431.

Thommes E. W. & Murray N. 2006, *Giant planet accretion and migration: surviving the type I regime*, ApJ, **644**, 1214.

Thommes E. W., Nilsson L., & Murray N. 2007, *Overcoming migration during giant planet formation*, ApJ, **656**, L25.

Trilling D. E., Benz W., Guillot T., Lunine J. I., Hubbard W. B., & Burrows A. 1998, *Orbital evolution and migration of giant planets: modeling extrasolar planets*, ApJ, **500**, 428.

Udry S., Bonfils X., Delfosse X., Forveille T., Mayor M., Perrier C., Bouchy F., Lovis C., Pepe F., Queloz D., & Bertaux J. L. 2007, *The HARPS search for southern extra-solar planets. XI. Super-Earths (5 and 8* $\mathrm{M}_{\oplus}$*) in a 3-planet system*, A&A, **496**, L43.

Udry S. & Santos N. C. 2007, *Statistical properties of exoplanets*, ARA&A, **45**, 397.

van der Kamp P. 1963, *Astrometric study of Barnard's star from plates taken with the 24-inch Sproul refractor*, AJ, **68**, 515.

Vogt S. S., Butler R. P., Marcy G. W., Fischer D. A., Henry G. W., Laughlin G., Wright J. T., & Johnson J. A. 2005, *Five new multicomponent planetary systems*, ApJ, **632**, 638.

von Bloh W., Bounama C., Cuntz M., & Franck S. 2007, *The habitability of super-Earths in Gliese 581*, A&A, **476**, 1365.

Ward P. D. & Brownlee D. 2000, *Rare Earth: Why Complex Life is Uncommon in the Universe*. (Copernicus Books, New York).

Ward W. R. 1997, *Protoplanet migration by nebula tides*, Icarus, **26**, 261.

Weidenschilling S. J. 1977, *The distribution of mass in the planetary system and solar nebula*, ApSS, **51**, 153.

Weidenschilling S. J. & Cuzzi J. N. 1993. *Formation of planetesimals in the solar nebula*, Levy E. & Lunine J., eds, *Protostars and Planets III*, p. 1031. U. Arizona Press.

Weidenschilling S. J. & Marzari F. 1996, *Gravitational scattering as a possible origin for giant planets at small stellar distances*, Nature, **384**, 619.

Wetherill G. W. & Stewart G. R. 1993, *Formation of planetary embryos - effects of fragmentation, low relative velocity, and independent variation of eccentricity and inclination*, Icarus, **106**, 190.

Wisdom M. & Holman J. 1991, *Symplectic maps for the n-body problem*, AJ, **102**, 1528.

Wolk S. J. & Walter F. M. 1996, *A search for protoplanetary disks around naked T Tauri stars*, AJ, **111**, 2066.

Wu Y., Murray N. W., & Ramsahai J. M. 2007, *Hot Jupiters in binary star systems*, ApJ, **670**, 820.

Wyatt M. C. & Dent W. R. F. 2002, *Collisional processes in extrasolar planetesimal discs - dust clumps in Fomalhaut's debris disc*, MNRAS, **334**, 589.

Yoshida H. 1993, *Recent progress in the theory and application of symplectic integrators*, CeMDA, **56**, 27.